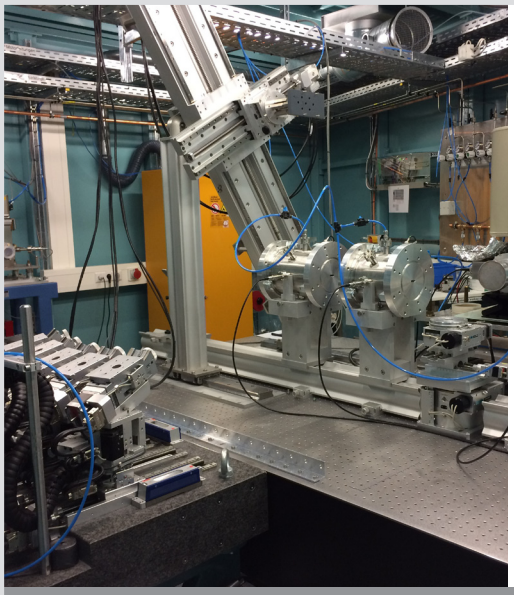
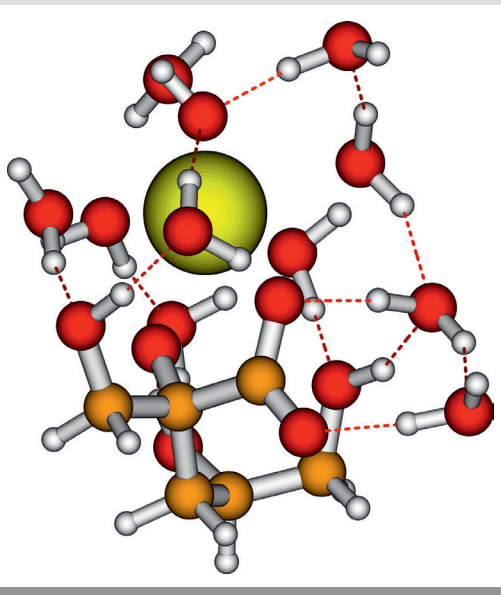


KIT SCIENTIFIC REPORTS 7743

Annual Report 2016

Institute for Nuclear Waste Disposal
Institut für Nukleare Entsorgung

H. Geckeis, M. Altmaier, S. Fanghänel (eds.)

KIT Scientific Publishing

H. Geckeis, M. Altmaier, S. Fanghänel (eds.)

Annual Report 2016

Institute for Nuclear Waste Disposal
Institut für Nukleare Entsorgung

Karlsruhe Institute of Technology
KIT SCIENTIFIC REPORTS 7743

Annual Report 2016

Institute for Nuclear Waste Disposal
Institut für Nukleare Entsorgung

by
H. Geckeis, M. Altmaier, S. Fanghänel (eds.)

KIT Scientific Publishing

Report-Nr. KIT-SR 7743

The Institute for Nuclear Waste Disposal, INE, (Institut für Nukleare Entsorgung) belongs to the KIT Energy Center. The KIT Energy Center with its 1100 employees is one of the largest energy research centers in Europe. It bundels the energy research activities of the KIT, the merger of the former Forschungszentrum Karlsruhe and Universität Karlsruhe and reknown cooperation partners. By this, it crosses the lines between disciplines and combines fundamental and applied research in all relevant energies for industry, household, service and mobility.
The involved institutes and research groups conduct the research work on their own authority. The joining of subjects, the interdisciplinary collaboration of scientists, and the common use of high-end devices and installations, develops a new quality of research and teaching. The KIT Energy Center develops solutions in energy technology from a single source and acts as a highly valuable consultancy institution for politics, business, and society in all questions of energy. (http://www.energy.kit.edu/)

Impressum

KIT Scientific Publishing

Karlsruher Institut für Technologie (KIT)
KIT Scientific Publishing
Straße am Forum 2
D-76131 Karlsruhe

www.ksp.kit.edu

Print on Demand 2017 – Gedruckt auf FSC-zertifiziertem Papier

ISSN 1869-9669
DOI 10.5445/KSP/1000073276

Foreword

Prof. Dr. Horst Geckeis

Director of the Institute for Nuclear Waste Disposal

2016 was another very important and successful year for the Institute for Nuclear Waste Disposal. INE completed the second year of the third Program oriented funding period (POF III) of the Helmholtz research program NUSAFE (Nuclear Waste Management, Safety and Radiation Research) and succeeded in passing significant milestones defined in the POF III research proposal. Research activities are strongly embedded into national and international collaborative projects and range from applied technology development e.g. for high-level radioactive waste vitrification and decommissioning of nuclear facilities to very fundamental science topics partly applying state-of-the-art spectroscopic techniques and theoretical approaches e.g. concerning the nature of actinide lanthanide binding to N-donor ligands and radionuclide behavior in cementitious systems. Research activities outside the nuclear topic related e.g. to the successful development of new monitoring approaches related to the minimization of induced seismicity in geothermal systems. INE-scientists are involved in teaching activities and the organization of international workshops and conferences on various topics related to our research. Numerous publications in peer-reviewed international journals and presentations at international conferences document their visibility.

Radionuclide speciation - As a major milestone in instrumentation development, in 2016 the new CAT-ACT hard X-ray beamline for CAT*alysis* and ACT*inide* research at ANKA became fully operational. After finishing the installation of beamline optic and infrastructure in 2015, the ACT experimental station of the new ANKA CAT-ACT wiggler beamline – jointly operated by KIT institutes ITCP/IKFT for CATalysis research and INE for ACTinide and radionuclide science – became fully operational towards the end of 2016. The new lab offers high flux synchrotron based speciation methods with monochromatic X-rays in a wide energy range encompassing the actinide M-edges and K-edges of the early lanthanide elements. The ACT station is equipped and licensed to handle radionuclide containing samples including highly radioactive waste forms with activities up to one million times the exemption limit inside a flexible containment concept. The multi crystal Johann-type high resolution X-ray emission spectrometer (HRXES) originally commissioned at the INE-Beamline has been transferred to the ACT station as core experimental infrastructure. As first of its kind this instrument allows advanced X-ray absorption and emission studies of solid and liquid radioactive sample systems (including in situ measurements) in the tender X-ray region with all beam paths enclosed by a gas-tight Helium environment.

Radiochemistry - KIT-INE has investigated the interaction of plutonium with Isosaccharinic acid within a research collaboration with Amphos21 (Spain), for the Swedish Waste Management Organization SKB. Isosaccharinic acid (ISA) is the main degradation product of cellulose materials which can be present in large amounts in low to intermediate level waste repositories. The studies target hyperalkaline pH conditions characteristic for a cementitious near field environment and redox neutral up to strongly reducing conditions. The results indicate that the trivalent and tetravalent plutonium oxidation states are relevant in both the aqueous and solid phase depending upon redox conditions. Systematic solubility studies performed with Pu in the presence of ISA show that the impact of ISA on Pu solubility is significantly lower than indicated by previous scoping experiments reported in literature. Based upon these studies, chemical models and thermodynamic data are derived, to be included in thermodynamic database projects.

Vitrification technology - The German-Chinese VPC (Vitrification Plant China) project has been established in November 2009 with the objective to construct an HLLW vitrification plant in the Sichuan province of China on the basis of the process technology developed by KIT-INE. From German side the project is executed by an industry consortium (STEAG Energy Services, WAK GmbH, Kraftanlagen Heidelberg GmbH) with KIT-INE as nominated subcontractor responsible for design of the core process technique and key components like the waste glass melter and for input of process-chemical and glass-chemical knowhow and expertise. This research topic has been completed in 2016 very successfully and respective activities are faded out.

DAEF - KIT-INE is founding member of the "Deutsche Arbeitsgemeinschaft für Endlagerforschung (DAEF)". As a major event, the second international conference on "Key Topics in Deep Geological Disposal – Challenges of a Site Selection Process: Society – Procedures – Safety", was organized in 2016 with INE being part of the local organizing team. The conference provided detailed information on the results of the work of the German commission on nuclear waste disposal ("Kommission Lagerung hoch radioaktiver Abfallstoffe") related to the design of a site selection process in Germany. In this respect, 2016 was a crucial year related to the provision of a basis for the siting process for a repository for heat generating radioactive waste in Germany: The commission has

set the framework and the criteria for the site selection process and the BGE ("Bundesgesellschaft für Endlagerung"), has been founded as the new implementing organization. The DAEF conference has covered all related topical issues and provided focused and dynamic presentations and discussions on research in different science disciplines including natural sciences, engineering, and social sciences relevant to the further development of nuclear waste disposal projects in Germany and internationally..

Finally, I would like to express my gratitude to our numerous partners, visitors and collaborators. Last, but not least, I extend a sincere thank you to the entire staff of INE for their dedication in both scientific activities and in administrative and technical support.

Table of contents

1 Introduction to the Institute for Nuclear Waste Disposal (INE)

The **Institute for Nuclear Waste Disposal** (INE), at the Karlsruhe Institute of Technology **KIT** performs R&D focusing on

(i) Long-term safety research for nuclear waste disposal (key focus of INE research),
(ii) Immobilization of high level radioactive waste (HLW),
(iii) Radiation protection
(iv) Decommissioning of nuclear facilities
(v) Geoenergy.

All R&D activities of KIT-INE are integrated into the program Nuclear Safety Research within the KIT-Energy Center and the program Nuclear Waste Management, Safety and Radiation Research (NUSAFE) within the Helmholtz Association. INE contributes to German provident research for the safety of nuclear waste disposal, which is in the responsibility of the Federal Government.

Following the decision taken by Germany to phase out the use of nuclear energy, the safe disposal of long-lived nuclear waste remains as a key topic of highest priority. Projections based on scheduled operation times for nuclear power plants (Amendment to German Atomic Energy Act, August 2011) in Germany indicate that about a total of 17,770 tons of spent nuclear fuel will be generated. About 6,670 tons have been shipped to France and the UK until 2005 for reprocessing, to recover plutonium and uranium. Consequently, two types of high level, heat producing radioactive waste have to be disposed of safely: spent fuel and vitrified high level waste from reprocessing (HLW glass). The disposal of low- and intermediate level waste present in much larger quantities likewise needs to be addressed.

Over the last decades, a consensus within the international scientific/technical community was established, clearly emphasizing that storage in deep geological formations is the safest way to dispose of high level, heat producing radioactive waste. Disposal concepts with strong inherent passive safety features ensure the effective protection of the population and the biosphere against radiation exposure over very long periods of time. The isolation and immobilization of nuclear waste in a repository is ensured by the appropriate combination of redundant barriers (multi-barrier system).

Long term safety research for nuclear waste disposal at KIT-INE establishes geochemical expertise and models to be used in the disposal Safety Case, focusing primarily on the detailed scientific description of aquatic radionuclide chemistry in the geochemical environment of a repository. Work concentrates on the disposal of spent fuel and HLW-glass in the relevant potential host rock formations currently considered: rock salt, clay and crystalline rock formations. Actinides and long-lived fission products play a central role, as they dominate HLW radiotoxicity over long periods of time. Long-live anionic fission products are likewise investigated as significant contributors to the maximum radiation dose projected for relevant scenarios.

Relevant long-term scenarios for nuclear repositories in deep geological formations have to take into account possible radionuclide transport via the groundwater pathway. Possible groundwater intrusion into emplacement caverns is assumed to cause waste form corrosion and eventually radionuclide release. Radionuclide mobility is then determined by the various geochemical reactions in complex aquatic systems: i.e. dissolution of the nuclear waste form (HLW glass, spent fuel), radiolysis phenomena, redox reactions, complexation with inorganic and organic ligands, colloid formation, surface reactions at mineral surfaces, precipitation of solid phases and solid solutions.

Prediction and quantification of all these processes require fundamental thermodynamic data and comprehensive process understanding at the molecular scale. Radionuclide concentrations in relevant aqueous systems typically lie in the nano-molar range, which is exceedingly small in relation to main groundwater components. Quantification of chemical reactions occurring in these systems require the application and development of advanced sophisticated methods and experimental approaches, to provide insight into the chemical speciation of radionuclides at trace concentrations. Innovative laser and X-ray spectroscopic techniques are continuously developed and applied to this end. A specialized working group performing state-of-art theoretical quantum chemical calculations for actinide chemistry support both interpretation of experimental results and optimized experiment design.

The long-term safety of a nuclear waste repository must be demonstrated by application of modelling tools on real natural systems over geological time scales. Geochemical models and thermodynamic databases are developed at INE as basis for the description of radionuclide geochemical behavior in complex natural aquatic systems. The prediction of radionuclide migration in the geosphere necessitates coupled modelling of geochemistry and transport. Transferability and applicability of model predictions are examined by designing dedicated laboratory experiments, field studies in underground laboratories and by studying natural analog systems. This strategy allows to identify and analyze key uncertainties and continuously optimize the developed models.

Within the R&D topic **immobilization of high-level radioactive waste**, INE contributes to the decommissioning of nuclear facilities. The core process technology for the vitrification plant (VEK) on the site of the former Karlsruhe Reprocessing Plant (KTE; located at KIT Campus North) has been developed by INE. INE was involved in functional testing of process systems, as well as in the performance of the cold test operation and played a leading role in the highly successful hot operation of the VEK plant. The vitrification technology developed at INE is highly competitive on an international level. This is evidenced by the strong interest of countries like China in establishing technology transfer. In 2016, this research topic has been completed very successfully and respective activities will fade out.

The R&D topic **radiation protection** at INE focuses on the assessment of radiation exposures on man by estimating doses either from external radiation fields or from incorporation of radionuclides. The strategy driving this work is to provide techniques and models for an individualized dosimetry, which goes beyond the current approach of applying reference models in dose assessments. Both the specific anatomical and physiological features of the exposed individual and the specific effective radiation fields are considered in the frame of an individualized dosimetry. Work is performed in close cooperation with the KIT safety management SUM.

The R&D topic **decommissioning of nuclear and conventional facilities** at INE expands the existing activities at the Institute of Technology and Management in Construction (KIT-TMB). Research in this field is focusing on a better understanding of the complete decommissioning process in Germany as well as on a global level.

The topic **geoenergy** is mainly focusing on geothermal energy research in fractured reservoir systems with special focus on Enhanced Geothermal Systems (EGS)

INE laboratories are equipped with all necessary infrastructures to perform radionuclide/actinide research, including hot cells, alpha glove boxes, inert gas alpha glove boxes and radionuclide laboratories. State-of-the-art analytical instruments and methods are applied for analysis and speciation of radionuclides and radioactive materials. Advanced spectroscopic tools exist for the sensitive detection and analysis of radionuclides. Trace element and isotope analysis is made by instrumental analytical techniques such as atomic absorption spectroscopy (AAS), ICP-atomic emission spectroscopy (ICP-AES) and ICP-mass spectrometry (Quadrupole-ICP-MS and high resolution ICP-MS). Methods available for surface sensitive analysis and characterization of solid samples include X-ray diffraction (XRD), atomic force microscopy (AFM) and laser-ablation coupled with ICP-MS. A modern X-ray photoelectron spectrometer (XPS) and an environmental scanning electron microscope (ESEM) are installed. INE has direct access to a TEM instrument on the KIT Campus North site (Institute for Applied Materials, IAM). Laser spectroscopic techniques are developed and applied for sensitive actinide and fission product speciation such as time-resolved laser fluorescence spectroscopy (TRLFS), laser-induced breakdown spectroscopy (LIBS) and Raman spectroscopy. Insight into structural and electronic properties of radionuclide species is obtained by X-ray absorption fine structure (XAFS) spectroscopy and related techniques available at the INE-Beamline and the ACT experimental station at the KIT synchrotron source ANKA. The ACT laboratory for radionuclide research at the new CAT-ACT beamline – a state-of the art facility jointly operated by INE and ITCP/IKFT – became fully operational in 2016. INE's ANKA beamlines, in close proximity to INE controlled area laboratories, represent in combination with the other analytical methods a unique experimental infrastructure, which both profits from and contributes to INE's leading expertise in the field of actinide chemistry and spectroscopy. A 400 MHz-NMR spectrometer adapted to measuring radioactive liquid samples adds to the analytical and speciation portfolio of INE. Quantum chemical calculations are performed on INE's computing cluster, which is equipped with 17 nodes and 76 processors. The INE CAD workstations enable construction and planning of hardware components, process layout and flow sheets. The institute workshop is equipped with modern machine tools to manufacture components for specific experimental and analytical devices in hot laboratories.

In 2016, the **Institute for Nuclear Waste Disposal** had around **100 employees** working in the seven departments, which reflect the R&D and organizational tasks of the institute (Fig. 1):

(i) Technical infrastructure / analytical chemistry
(ii) Safety of nuclear waste disposal
(iii) Radiochemistry
(iv) Radionuclide speciation
(v) Vitrification of high level waste
(vi) Geochemistry
(vii) Decommissioning of nuclear and conventional facilities.

Fig. 1: *Organizational chart of the Institute for Nuclear Waste Disposal (INE)*

2 Education and training

Teaching of students and promotion of young scientists is of fundamental importance to ensure high-level competence and to maintain a leading international position in the fields of nuclear and radiochemistry. INE scientists are strongly involved in teaching at KIT Campus South and the Universities of Heidelberg, Jena and Strasbourg as well as the Baden-Wuerttemberg Cooperative State University.

Prof. Dr. **Horst Geckeis**, director of INE, holds a professorship for radiochemistry at KIT Campus South, Department of Chemistry and Biosciences. He teaches fundamental and applied radiochemistry for chemistry students in bachelor and master courses. A radiochemistry module consisting of basic and advanced lectures on nuclear chemistry topics and laboratory courses has been set up for master students in Karlsruhe. In addition, Dr. **Marcus Altmaier**, head of the department radiochemistry, gives a lecture concerning the chemistry of f-elements.

Prof. Dr. **Sascha Gentes** head of the department decommissioning of nuclear and conventional facilities holds a professorship at the Institute for Technology and Management in Construction at the KIT-Department of Civil Engineering, Geo and Environmental Sciences and gives lectures in the field of decommissioning of nuclear facilities, environmentally-friendly Recycling and Disassembly of Buildings, Machinery and Process Engineering as well as construction technology.

Prof. Dr. **Petra Panak**, heading a working group on actinide speciation at INE, holds a professorship of radiochemistry at the University of Heidelberg. A basic course in radiochemistry is offered for bachelor and/or master students. An advanced course comprised of the chemistry of f-elements and medical applications of radionuclides is also offered. The advanced radiochemistry lectures are supplemented by scientific internships at the INE radioactive laboratories.

Around 30 students from Karlsruhe and Heidelberg participated in two 3-week radiochemistry laboratory courses in 2016 held at KIT Campus North in the FTU radiochemistry and hot laboratories at INE. Some students are intensifying their knowledge in nuclear/radiochemistry topics during scientific internships at INE. Obviously, students are very interested in nuclear chemistry topics and appreciate the various semester courses.

In 2016 Dr. **Tonya Vitova** gave lectures at the KIT Campus South, Department of Chemistry and Biosciences, in the field of instrumental analytics and Dr. **Eva Schill** and Dr. **Marika Vespa** at the Department of Civil Engineering, Geo and Environmental Sciences in the field of geophysics, general geology and analytical methods in applied mineralogy. Dr. **Volker Metz** gave lectures at the Department of Mechanical Engineering in the field of reactor physics.

Lectures and practical units taught by Prof. Dr. **Thorsten Schäfer**, Deputy Director of INE; in cooperation with Dr. **Frank Heberling**, Dr. **Florian Huber** and Dr. **Volker Metz** at KIT Campus South, Department of Civil Engineering, Geo and Environmental Sciences, focused in 2016 on "environmental geology: radio- & chemotoxic elements".

Dr. **Andreas Bauer** is lecturing Clay Mineralogy at the University of Jena. His lecture deals with the mineralogical characterization of these fine materials and the importance of quantifying surface reactions. In the second part of the lectures sound, practical advice on powder X-ray diffraction in general is provided, as well as a useful set of step-by step instructions for the novice.

Dr. **Andreas Geist** gave lectures at the École européenne de chimie, polymères et matériaux in Strasbourg concerning the Solvent Extraction of Metal Ions.

Moreover, INE was involved in many schools and workshops concerning the education and teaching of students and young scientists:

- Summer School EU project CAST „C-14 behavior under repository conditions", July 05 – 06, 2016
- Thul School in Actinide Chemistry, September 19 – 23, 2016

Through this close cooperation with universities, students are educated in the field of nuclear and actinide chemistry, which most universities can no longer offer. Hence, INE makes a vital contribution to the intermediate and long perspective of maintaining nuclear science competence. Moreover, INE is involved in the education of trainees (chemical lab technicians, industrial mechanics and product designers) as well as student internships like BORS and BOGY.

PhD students

In 2016, 17 PhD students worked at INE on their doctoral dissertations; two of them were awarded their doctorate. Topics of the theses are:

- Comparative NMR spectroscopic analysis of extracting agents for the separation of trivalent actinides
- Experimental and modelling studies of cement/clay interface process
- Advanced spectroscopic and microscopic structural investigations of nuclear waste glass forms
- Technetium interaction with inorganic ligands and retention processes in the sulfide system
- Solubility, speciation and thermodynamics of tetravalent and hexavalent Uranium

- Electromagnetical und Eigenpotential monitoring of fluid injections in crystalline rock
- Characterization of actinide species in systems relevant for safety assessment of a nuclear waste repository by high resolution X-ray emission/absorption spectroscopy
- Impact of anions on the retention of actinides on clay minerals under slightly alkaline to hyper alkaline pH conditions
- Bentonite erosion and colloid mediated radionuclide transport in advection controlled systems
- Development of methods for the individual dosimetry of the staff in disposal facilities
- Investigation of the solubility and complexation of Plutonium and Neptunium in highly reducing aquatic systems
- Impact of the flow channel geometry on the agglomeration of colloids and the reduction of permeability in altered granites of potential geothermic reservoir rocks
- Redox behavior, solubility and sorption of Pu(III/IV) in the presence of ISA
- Steel corrosion and actinides sorption by iron corrosion products under saline conditions
- Spectroscopic and thermodynamic investigations of the complexation of An(III) and Ln(III) with hydrophilic Bis-triazinylpyridines
- Investigation of the retention of actinides, lanthanides and long-lived fission products on stable solid phases within the system Mg – Na ± Cl ± CO_2 – H_2O
- Experimental investigation of the separation process of particle mixtures within a rod magnetic filter

3 National and international cooperation, conferences and workshops

3.1 National and international cooperation

INE R&D involves numerous national and international collaborations and projects. These are described in the following.

National

INE is involved in various bi- and multilateral collaborations with national research centers, universities and industrial partners on different topics. The projects are partly supported by the German Federal Ministry for Economics and Technology (BMWi), the Federal Ministry for Education and Research (BMBF), the Federal Ministry for the Environment, Nature Conservation, Building and Nuclear Safety (BMUB), the German Research Foundation (DFG) and the Helmholtz Association (HGF).

The **ThermAc** project aims at extending the chemical understanding and available thermodynamic database for actinides, long-lived fission products and relevant matrix elements in aquatic systems at elevated temperatures. To this end, a systematic use of estimation methods, new experimental investigations and quantum-chemistry-based information is intended. ThermAc has started in March 2015 and is projected for three years. The project is funded by the German Federal Ministry for Education and Research (BMBF) and is coordinated by KIT-INE. The ThermAc project is developed in order to improve the scientific basis for assessing nuclear waste disposal scenarios at elevated temperature conditions.

Within the **THEREDA** project, KIT-INE generates and evaluates thermodynamic data – complex formation constants, solubility data and modeling parameters for highly concentrated systems – for selected radionuclides from experiments and literature. The data are incorporated into a centrally managed and administered database of evaluated thermodynamic parameters after passing an evaluation process. This database is open for registered user. Thermodynamic data are required for environmental applications in general and radiochemical issues in particular. THEREDA is developed to be a national (reference) standard and will be the basis for performance assessment calculations for a national nuclear waste repository.

The **GRaZ** project deals with the migration of radionuclides in the near field of a repository for radioactive waste in clay formations with focus on the hyperalkaline water-cement-system. KIT-INE investigates the retention of actinides and lanthanides by clay minerals in presence of carbonate and silicate, cement phases and cement alteration phases. Furthermore, the influence of cement additives (e.g. plasticizer and superplasticizer) on the sorption of actinides is studied at high pH values. One important issue of the project is the thermodynamic modelling of experimental solubility, complexation, and sorption data. The project provides basic knowledge and thermodynamic data needed in the frame of a long-term safety analysis of different repository concepts.

The disassembly of the reactor pressure vessel and internals poses one of the most demanding challenges in the decommissioning of a nuclear power plant. For this purpose, a waterjet cutting technique (WASS) is used, employing a high-pressure water jet and a sharp-edged abrasive medium directed to the cutting material. Advantages of WASS among other conventional cutting techniques are the compact design of the setup, the ease of remote manipulation (also at difficult positions) and the “cold” operation under water, which also serves as shielding. However, this technique produces a considerable amount of expensive secondary waste, a water suspension containing small-grained radioactive metal cuttings and abrasive grains. The **MASK** project is initialized to overcome this limitation. Metal cuttings are separated by a magnetic filter in order to substantially minimize the radioactivity of the secondary waste.

The **KOLLORADO-e2** project focuses on the erosion stability of compacted bentonite (geotechnical barrier) as a function of the contact water chemistry/hydraulics and the formation of near-field colloids/nanoparticles as potential carriers for actinides/radionuclides. Both, a detailed experimental program quantifying the bentonite erosion and investigating the influence of surface roughness/charge heterogeneity on nanoparticle mobility and actinide bentonite nanoparticle sorption reversibility, as well as approaches to implement the acquired process understanding in reactive transport modelling codes comprise the project activities.

ENTRIA aims at evaluating criteria for the management of highly radioactive waste from the viewpoint of all involved academic disciplines such as natural sciences, engineering, law and social science. ENTRIA is addressing the three most important options in disposing highly radioactive waste: Final disposal in deep geological formations without any arrangements for retrieval (maintenance-free deep geological disposal); disposal in deep geological formations with arrangements for monitoring and retrieval; prolonged surface storage. A major goal of ENTRIA is the strong interaction between young and senior scientists of various disciplines (civil engineering, law, natural sciences, philosophy, and social sciences). Within the project, KIT-INE is responsible for work packages on developing radionuclide source terms and developing individual dosimetry for personnel with respect to the three options.

The collaborative project **EDUKEM** aims at an improved understanding of uranium chemistry in saline systems and establishing targeted experimental techniques. Work of KIT-INE within EUDKEM focusses on the aquatic chemistry and thermodynamics of hexavalent and tetravalent uranium in relevant saline solutions. Based upon new solubility studies, spectroscopic evidence and literature, a comprehensive description of U(IV) and U(VI) solubility and speciation in key saline systems relevant for nuclear waste disposal in salt-based repositories will be established.

The chemical and mechanical stability of metallic containers for radioactive waste play an important role in safety performance assessment. The goal of the project **KORSO** is to significantly improve the understanding of metallic corrosion in saline environments under conditions representative of disposal sites for heat generating waste. Partial reactions will be deciphered by applying electrochemical methods, and formed corrosion products will be characterized by applying complementary microscopic and spectroscopic techniques. Investigations of the retention of radionuclide by synthetic corrosion products by combining spectroscopic and chemical methods constitute another emphasis of the project. The ultimate goal is to significantly reduce uncertainties concerning the interaction mechanism(s) between radionuclides and corrosion products and thereby improve the confidence in the long-term prediction of radionuclide mobility.

The Helmholtz young investigators group (HYIG) **"Advanced synchrotron-based systematic investigations of actinide (An) and lanthanide (Ln) systems to understand and predict their reactivity"** systematically investigates the electronic and coordination structures of actinide (An) and chemical homologue lanthanide (Ln) systems with novel synchrotron-based high energy resolution X-ray emission/absorption/inelastic scattering techniques. The experimental results are supported by theoretical calculations and simulations with quantum chemical codes. These investigations improve the understanding of An/Ln reactivity in repository systems and waste matrices on a molecular scale and thereby support the reliability of safety case evaluation of the repository long term safety. The elucidation of electronic and coordination structures of An/Ln systems provide basic insight into structure-reactivity relationships of actinide elements, which is a present scientific frontier.

In the framework of measures for retrieval of radioactive waste and decommissioning of the **Asse II salt mine**, provisions for emergency preparedness are taken. Therefore, the operator of Asse II, the Federal Office for Radiation Protection (BfS), drilled an exploration drilling in the overlaying sedimentary rocks of the salt diapir and coordinates studies with respect to the near-field of the radioactive waste. KIT-INE contributes both to the studies on samples of the overlaying sediments as well as to studies on geo-engineered barriers in the near field of the radioactive waste. Drill cores and pore water samples of the exploration borehole, comprising Triassic shell limestone (Muschelkalk), Bunter sandstone (Buntsandstein) and sulfate-rich cap rock samples, were geochemically and mineralogically characterized. The sample characterization data provide a basis for interpretation for forthcoming radionuclide sorption studies with selected drill core samples and pore water simulates. With respect to the near field KIT-INE compiles the present state of knowledge on geochemical processes in the waste emplacement rooms.

International

The international Colloid Formation and Migration (**CFM**) project focuses on the stability of the bentonite buffer/backfill in contact with water conducting features and the influence of colloids on radionuclide migration in crystalline host rocks coordinated by NAGRA (National Cooperative for the Disposal of Radioactive Waste, Switzerland). The project uses the experimental set-up in the controlled zone at the Grimsel Test Site (Switzerland). Additional partners involved are from Japan (JAEA, AIST, CRIEPI), South Korea (KAERI), Finland (POSIVA Oy and Helsinki University), Switzerland (NAGRA, PSI-LES), Spain (CIEMAT), Sweden (SKB, KTH), United Kingdom (NDA RWMD) and United States (LANL). INE plays a decisive role in the laboratory program and is also mainly carrying out the field activities.

Within the framework of the strategy of the German Federal Government for the internationalization of science and research to foster the bilateral cooperation with Korea in the area of science and technology (WTZ) KIT-INE has started a two year project from 1.10.2014 entitled "Molecular-scale investigation of interaction mechanisms between uranium and iron-bearing minerals under diverse geochemical conditions of groundwater (**BioFeRad**)" with KAIST (Korean Advanced Institute of Science and Technology), group of Prof. Woojin Lee including student exchange and two bilateral workshops.

EURATOM FP7 and Horizon 2020

ASGARD is a EURATOM FP7 Large Scale Integrated Project focusing on advanced/novel nuclear fuels fabrication and their respective reprocessing issues. ASGARD seeks integration between reactor, fuel and recycling communities, which today is lacking. In some cases, this results in discrepancies between the reactor design on one hand, and the technological feasibility of fabricating, dissolving and reprocessing the selected fuel on the other hand. ASGARD is an integrated effort of 16 institutions from 9 European countries. It is coordinated by Chalmers Technical University.

SACSESS is a EURATOM FP7 Collaborative Project dealing with safety aspects of hydrometallurgical and pyrometallurgial actinide separation processes developed in previous EURATOM projects. SACSESS provides a structured framework to enhance the fuel cycle safety associated to P&T. In addition, safety studies are performed to identify weak points to be further studied. These data are used to

optimize flow sheets and process operation conditions. 26 Partners from 10 countries (plus JRC-ITU and Japan) contribute to SACSESS. The project is coordinated by CEA; KIT is in charge of the hydrometallurgy domain.

The separation of rare earth elements (REE) from secondary sources such as mine tailings is studied in the ERA-MIN project **ENVIREE**. The project is coordinated by CHALMERS (Sweden). Eleven partners form eight counties contribute to the following areas: assessment of sources, development of innovative, efficient and environmentally benign leaching and separation methods, life cycle assessment and economic feasibility studies.

Recent safety assessments of nuclear waste repositories in crystalline formations have shown that the formation and stability of colloids may have a direct impact on the overall performance of the repository. The main aim of the 7th framework collaborative project **BELBaR** is to increase the mechanistic understanding of the processes that control bentonite erosion, clay colloid stability, and ability to transport radionuclides. The final outcome is to examine how colloids and related phenomena can be considered in the long-term safety case and to make recommendations on the quantitative and qualitative approaches that a safety case could pursue to adequately address this potentially very significant issue. BELBaR coordinated by SKB consists of a consortium of 14 partners from Sweden, Finland, Spain, Czech Republic, Great Britain, Russia and Germany with KIT-INE leading WP3 on "Colloid radionuclide & host rock interaction".

The Collaborative Project **CAST** aims to develop understanding of the generation and release of C-14 from radioactive waste materials under conditions of underground geological repositories. KIT-INE contributes with experimental studies to work packages "Steels" and "Zircaloy" as well as to the work package "Dissemination of knowledge". Within the two experimental work packages, KIT-INE conducts studies with highly active stainless steel and Zircaloy-4 samples in the shielded box-line of KIT-INE.

KIT-INE contributes actively to international organizations, such as the Thermodynamic Database Project of the Nuclear Energy Agency (NEA).

Cebama is a collaborative project investigating cement-based materials, properties, evolution and barrier functions within the European Commission Horizon 2020 frame. Scientific and technical research in Cebama is largely independent of specific disposal concepts and addresses different types of host rocks, as well as bentonite. Cebama is not focusing on one specific cementitious material, but aims at studying a variety of important cement-based materials in order to provide insight on general processes and phenomena. Cebama is coordinated by KIT-INE.

The Coordination and Support Action **Graduate and Executive Nuclear Training and Lifelong Education (GENTLE)** focuses on education of undergraduate and graduate students of European academic institutions by means of student research experiences in nuclear laboratories and intersemester courses. Scientists of universities and major research institutions of ten European countries participate in this Education and Training action. Within GENTLE, KIT-INE supervised students of European universities, who conducted research projects at the KIT-INE laboratories.

The goal of the H2020 project **DEEPEGS** is to demonstrate the feasibility of enhanced geothermal systems (EGS) for delivering energy from renewable resources in Europe. Testing of stimulating technologies for EGS in deep wells in different geologies will deliver new innovative solutions and models for wider deployments of EGS reservoirs across Europe. DEEPEGS will demonstrate advanced technologies for widespread exploitation of high enthalpy heat (i) beneath existing hydrothermal field at Reykjanes (volcanic environment) with temperature up to 550°C and (ii) very deep hydrothermal reservoirs in France with temperatures up to 220°C. The focus on business cases will demonstrate advances in bringing EGS derived energy (TRL6-7) to market exploitation. We seek to understand and address social concerns about EGS deployments. We will through risk analysis and hazard mitigation plans ensure that relevant understanding and minimization of the risks will be implemented as part of the RTD business case development.

The **GEMex** project is a EU-Mexico joint effort in development of Enhanced Geothermal Systems (EGS) and Superhot Geothermal Systems (SHGS) at Acoculco and Los Humeros that bases on three pillars:

1 – Resource assessment of these geothermal sites by understanding the tectonic evolution, fracture distribution and hydrogeology and predicting in-situ stresses and temperatures at depth.

2 – Reservoir characterization including novel geophysical and geological methods to be advanced for the specific condition. Accompanying high-pressure/ high-temperature laboratory experiments will provide the input parameters.

3 – Concepts for site development will include definition of drill paths, a design for well completion including suitable material selection, and optimum stimulation and operation procedures for safe and economic exploitation. In these steps, we will address issues of public acceptance and outreach as well as the monitoring and control of environmental impact.

3.2 Second conference on ‚Key Topics in Deep Geological Disposal – Challenges of a Site Selection Process: Society – Procedures – Safety‘

Following the previous conference in 2014 the second international conference ***Key Topics in Deep Geological Disposal – Challenges of a Site Selection Process: Society – Procedures – Safety*** was held between 26th and 28th September 2016 at the Gürzenich conference center in Cologne, Germany. The conference was jointly organized by the members of the German association for repository research (DAEF) representing leading research organizations active in radioactive waste disposal research. The aim of this association is to contribute to the safe disposal of radioactive waste, to improve the scientific basis and to offer respective fact based information.

The conference set a focus on the following topics:

- International experiences in designing and implementing siting processes – mastering social and technical challenges
- Development and application of science based site selection criteria
- Scientific aspects of the nuclear waste disposal safety case

Moreover, detailed information on the results of the work of the German commission on nuclear waste disposal (“Kommission Lagerung hoch radioaktiver Abfallstoffe”) related to the design of a site selection process in Germany was provided.

The interdisciplinary approach with various disciplines such as natural sciences, engineering, and social sciences represented an ideal platform for a fruitful scientific exchange and a valuable instrument for further improving multilateral co-operation for mutual benefit.

The excellent scientific work of young scientist was awarded with three poster prices.

4 Fundamental studies: Process understanding on a molecular scale

Fundamental studies on radionuclide chemistry and geochemistry are performed at KIT-INE in order to develop detailed scientific understanding on a molecular scale and ensure the reliable quantitative prediction of key processes in aquatic chemistry. Aiming at a comprehensive assessment of radionuclide behavior and mobility in aquatic systems relevant for the Nuclear Waste Disposal Safety Case, experimental studies with actinides and long-lived fission products are performed. The investigated aqueous systems range from dilute solutions to highly saline salt brine systems and establish essential site-independent data and scientific process understanding. Work is focusing both on detailed experimental investigations using the unique facilities available at KIT-INE, and subsequently developing reliable chemical models and consistent thermodynamic data. This combined approach allows a systematic and reliable evaluation of key processes such as radionuclide solubility, radionuclide speciation, radionuclide retention and transport processes in relevant near- and far-field scenarios.

The work summarized in this section is related to the (i) chemistry and thermodynamics of actinides and fission products in aqueous solution, (ii) radionuclide sorption on mineral phases, and (iii) retention of radionuclides by secondary phase formation. The studies aim at identifying relevant radionuclide retention/retardation mechanisms on a molecular level and their robust thermodynamic quantification in support of the Nuclear Waste Disposal Safety Case. The fundamental studies on aqueous radionuclide chemistry described in Chapter 4 are using radionuclide speciation methods developed at KIT-INE (see Chapter 8), and support the applied studies performed at KIT-INE (see Chapter 5).

4.1 Chemistry and thermodynamics of actinides and fission products in aqueous solution

N. Adam, M. Altmaier, A. Baumann, M. Böttle, N. Cevirim, K. Dardenne, F. Endrizzi, D. Fellhauer, D. R. Fröhlich, X. Gaona, J.-Y. Lee, P.J. Panak, R. Polly, J. Rothe, J. Schepperle, A. Skerencak-Frech, A. Tasi, M. Trumm, E. Yalcintas

In co-operation with:

J. Bruno[a], E. Colàs[a], M. Grivé[a], A. Johnsen[b], K. Källström[c]

[a] Amphos[21] Consulting S.L., Passeig Garcia i Faria, 49-51, 1-1a, 08019 Barcelona, Spain; [b] Penn State University, Radiation Science and Engineering Center, 101 Breazeale Nuclear Reactor, University Park, PA 16802, USA; [c] Svensk Kärnbränslehantering AB, Avd. Låg-och medelaktivt avfall, Box 250, 101 24 Stockholm, Sweden

Introduction

Aquatic chemistry and thermodynamics of actinides and fission products is a multifold and scientifically challenging field of inorganic chemistry. The research activities developed at KIT-INE within this field mainly focus on systems relevant for nuclear waste disposal, and aim at contributing to the Safety Case and Performance Assessment of repositories designed for the disposal of such wastes. This section highlights the fundamental and applied research performed at KIT-INE in 2016 within this topic.

In the context of aquatic chemistry and thermodynamics, KIT-INE contributes to several national projects with focus on the interdisciplinary analyses of disposal options for radioactive waste (ENTRIA, funded by BMBF), providing support and expert judgement to BfS with regard to geochemical processes of relevance in the Asse II salt mine, or participating in the development of the national thermodynamic reference database for actinides and fission products (THEREDA project). The leading role of KIT-INE in this field is further reflected in key contributions to highly relevant international projects, such as the OECD NEA-TDB thermodynamic series, the IUPAC Subcommittee on Solubility and Equilibrium Data, or the update of the Plutonium Handbook edited by the American Nuclear Society, among others.

Tc(IV) solubility and carbonate complexation in alkaline, dilute to concentrated saline systems

Technetium-99 is one of the main fission products of ^{235}U and ^{239}Pu produced in nuclear reactors. Due to its long half-life ($2.1 \cdot 10^5$ a) and redox-sensitive character, ^{99}Tc is a very relevant radionuclide in the Safety Assessment of nuclear waste repositories. Tc(VII) is the prevailing oxidation state under oxidizing and redox-neutral conditions and exists as soluble and mobile TcO_4^-. On the contrary, Tc(IV) forms sparingly soluble hydrous oxides ($TcO_2 \cdot xH_2O(s)$) under reducing conditions as those expected in deep underground repositories. Carbonate is an important component in the pore water of certain host-rocks, and is known to form strong complexes with metal cations, potentially contributing to the mobilization of radionuclides. In this context, an appropriate understanding of Tc(IV) solubility and aqueous speciation in alkaline car-

bonate-containing solutions provides relevant inputs for assessing the behavior of Tc in underground repositories for radioactive waste disposal.

The solubility of Tc(IV) was investigated in carbonate-containing solutions of varying ionic strength (I = 0.5 - 5.0 M) and at different pH_m (-log $[H^+]$ = 8.5 - 14.5). The experiments were split in three independent series: (i) constant ionic strength I = 5.0 M ($NaCl$-$NaHCO_3$-Na_2CO_3) with total carbonate concentration ($C_{tot} = [HCO_3^-] + [CO_3^{2-}]$) 0.01 M ≤ C_{tot} ≤ 0.5 M and 8.5 ≤ pH_m ≤ 12.0, (ii) constant C_{tot} = 0.05 and 0.1 M with 0.5 M ≤ I ≤ 5.0 M ($NaCl$-$NaHCO_3$-Na_2CO_3) and 8.5 ≤ pH_m ≤ 12.0, (iii) constant C_{tot} = 0.1, 0.5 and 1.0 M with 0.01 M ≤ [NaOH] ≤ 0.6 M (in the absence of NaCl). $SnCl_2$ was used as reducing agent to ensure that Tc both as solid and in solution remains in oxidation state +IV. [Tc], pH_m and E_h were monitored at regular time intervals. The redox state of Tc in the aqueous phase was investigated for selected samples by XANES/EXAFS spectroscopy and solvent extraction with TPPC. Density functional theory (DFT) calculations were performed to identify the most stable structure of the Tc(IV)-CO_3 complexes forming in alkaline pH conditions.

A strong effect of carbonate was observed in all investigated samples, leading to up to 3 orders of magnitude greater solubility than in carbonate-free systems (see Figure 1).

XANES and solvent extraction confirmed that Tc(IV) prevails in the aqueous phase of the investigated systems, and thus that the increase in solubility is not caused by the oxidation to Tc(VII). Solubility data collected at 9 ≤ pH_m ≤ 12 are properly explained with the equilibrium reaction $TcO_2{\cdot}0.6H_2O(s) + CO_3^{2-} + 0.4\ H_2O(l) + H^+ \Leftrightarrow TcCO_3(OH)_3^-$, although thermodynamic data selected in the NEA-TDB for this complex significantly underestimates the experimental results obtained in the present study [1].

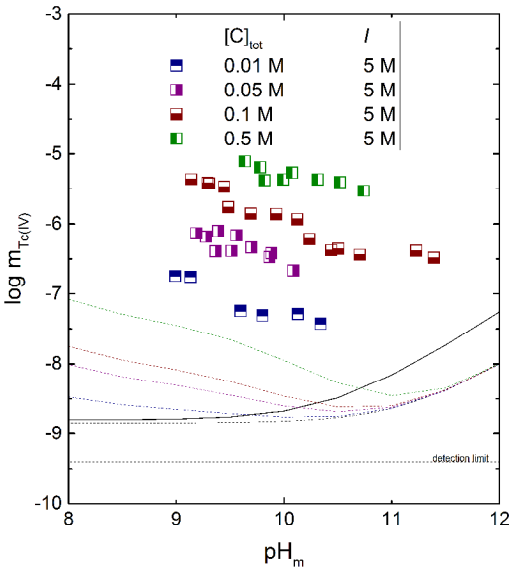

Fig. 1: *Experimental solubility data of Tc(IV) in carbonate systems with I = 5 M (symbols), and calculated solubility using thermodynamic and activity models reported in [1–3] (dashed lines).*

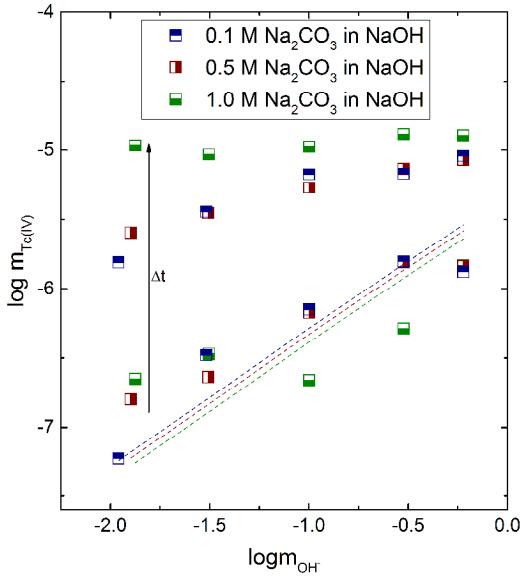

Fig. 2: *Experimental solubility data of Tc(IV) in carbonate systems (symbols), and calculated solubility using thermodynamic and activity models reported in [1–3] (dashed lines).*

Above $pH_m \approx 12$, the increased Tc(IV) solubility with respect to carbonate-free systems may hint to the formation of the so far unreported complex $TcCO_3(OH)_4^{2-}$ (see Figure 2), although further experimental evidences are needed to confirm this hypothesis. DFT calculations point to the stabilization of hydrated carbonate hydroxo complexes ($TcCO_3(OH)_x^{2-x}$) over oxo-hydroxo complexes ($TcOCO_3(OH)_y^{y-}$) containing the moiety TcO^{2+}. The systematic and very comprehensive solubility dataset obtained for Tc(IV) in alkaline carbonate-containing solutions allows deriving accurate chemical, thermodynamic and activity (SIT) models for the system Tc^{4+}-H^+-Na^+-CO_3^{2-}-HCO_3^--OH^--Cl^--$H_2O(l)$. These models are highly relevant in geochemical calculations and for the estimation of reliable Tc(IV) source term concentrations in the context of safety assessments for nuclear waste repositories.

U(IV) hydrolysis and carbonate complexation in dilute to concentrated salt systems

Uranium is the main element in the nuclear fuel cycle and, consequently, contributes with the largest inventory to radioactive waste. U(VI) is the most stable oxidation state of uranium under anoxic and oxidizing conditions, whereas U(IV) prevails in strongly reducing environments, forming the sparingly soluble UO_2(am,hyd) in the absence of complexing ligands. The predominance of the latter oxidation state is expected in underground repositories, where very reducing conditions are expected due to the anoxic corrosion of steel. The geochemical boundary conditions of aqueous solutions potentially contacting nuclear waste may contain low to high concentrations of dissolved salts (I = 0.1 M - 15 M) as well as strong complexing ligands like CO_3^{2-}, which can significantly alter the

chemical behavior of uranium and therefore impact its retention/migration processes. In this framework, an appropriate understanding of the solubility, hydrolysis and carbonate complexation of U(IV) in dilute to concentrated saline systems is a relevant contribution to the Performance Assessment of repositories for nuclear waste.

The solubility of uranium was investigated in 0.1, 0.5, 2.0, 5.0 M NaCl-NaOH solutions at $1 \leq pH_m \leq 14.5$ using an undersaturation approach. The solubility of U(IV) in the presence of carbonate was investigated as a function of carbonate concentration (C_{tot} = 0.01 M - 1.5 M), ionic strength (C_{tot} = 0.1 M - 0.3 M, I = 0.5 M - 4.0 M (NaCl-$NaHCO_3$-Na_2CO_3)) and hydroxide concentration (C_{tot} = 0.1, 0.01 M ≤ [NaOH] ≤ 0.6 M). All experiments were performed in Ar gloveboxes at T = (22 ± 2)°C. Reducing conditions were chemically controlled with Sn(II) resulting in (pe + pH_m) ≈ 2. Approximately 5 mg of U(IV) was added to each sample. [U], pH_m and E_h values were monitored at regular time intervals. Thermodynamic equilibrium was assumed after repeated measurements with constant [U] and pH_m. After attaining equilibrium conditions, solid phases of selected batch experiments were characterized by XANES/EXAFS analyses.

Figure 3 shows the solubility of UO_2(am,hyd) in the absence of carbonate. Two distinct regions can be identified: I. steep decrease of [U] at $pH_m \leq 3$, which is attributed to the predominance in solution of $U(OH)_x^{4-x}$ cationic hydrolysis species with $x \leq 3$. The solubility in this pH-region shows the same trend but falls well below the solubility curve of UO_2(am,hyd) calculated using thermodynamic data reported in [1] and [4], indicating a higher degree of crystallinity of the solid phase used in the present study; II. all [U] measured above $pH_m \approx 3$ and up to $pH_m = 14.5$ are at the detection limit of ICP-MS (10^{-9} to 10^{-8} M, depending upon salt concentration and dilution factor).

The present observations give no indication for the formation of $U^{IV}(OH)_5^-$ and $U^{IV}(OH)_6^{2-}$ hydrolysis

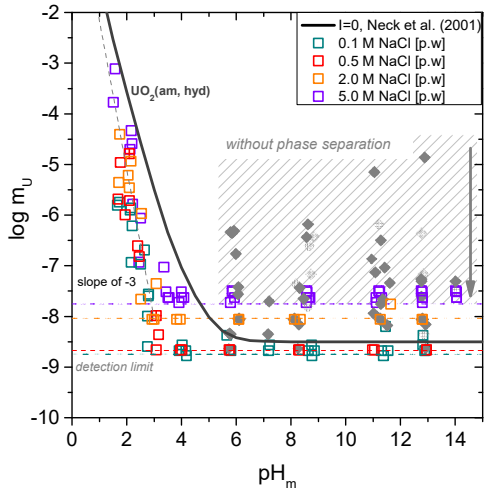

Fig. 3: *Solubility of U(IV) in 0.1, 0.5, 2.0, and 5.0 M NaCl solutions. Solid line corresponds to the solubility curve of UO_2(am, hyd) calculated for I = 0 using thermodynamic data reported in [1, 4].*

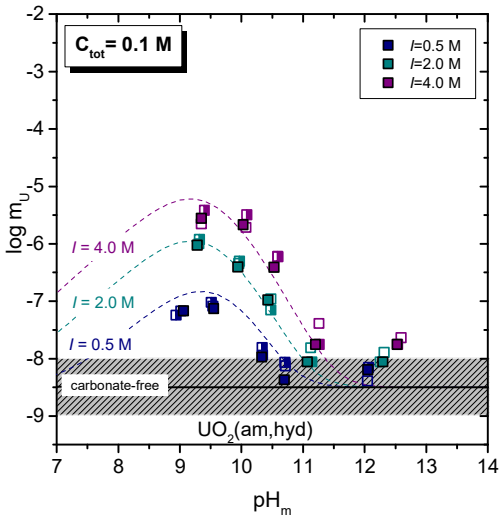

Fig. 4: *Solubility of U(IV) in 0.5, 2.0 and 5.0 M NaCl–$NaHCO_3$–Na_2CO_3 solutions with C_{tot} = 0.1 M. Dashed lines correspond to UO_2(am,hyd) solubility considering the formation of species $U(OH)_2(CO_3)_3^{4-}$.*

species within the investigated boundary conditions. Increased [U] were measured for samples in region II without phase separation, indicating the presence of U(IV) intrinsic colloids. The U(IV) colloidal fraction decreased with time, eventually reaching the detection limit of ICP-MS after $t \approx 205$ days.

Figure 4 shows the solubility of UO_2(am,hyd) in 0.5, 2.0 and 4.0 M NaCl-$NaHCO_3$-Na_2CO_3 solutions with C_{tot} = 0.1 M. Solubility data at $8.5 \leq pH_m \leq 11$ in carbonate solutions is up to three orders of magnitude higher than carbonate-free systems. Changes in the solubility suggest the formation of ternary U(IV)-OH-CO_3 species in this pH region. No effect of carbonate on the solubility is observed at $pH_m \geq 12$, expectedly due to the strong hydrolysis of U(IV). Figure 4 shows also preliminary chemical, thermodynamic and activity models derived in the present work for the system U^{4+}-Na^+-H^+-Cl^--HCO_3^--CO_3^{2-}-OH^--H_2O(l). Solubility data above $pH_m \approx 8.5$ can be properly explained by defining $U(OH)_2(CO_3)_3^{4-}$ and $U(OH)_4$(aq) as the predominant aqueous species in equilibrium with UO_2(am,hyd).

Solubility and redox behavior of Pu in the presence of ISA and Ca under alkaline, reducing conditions

The final repository for short-lived low- and intermediate-level (L/ILW) nuclear waste in Sweden (SFR) is located in a crystalline host rock formation near Forsmark. Groundwater is expected to slowly intrude from the surrounding rock and saturate the repository in the post-operational phase. Cementitious materials present in SFR will buffer the pH in the alkaline range ($10 \leq pH \leq 13.3$) over a very long time-scale, whereas strongly reducing conditions are expected to develop as a result of the anaerobic corrosion of the steel containers.

Residual amounts of plutonium present in the inventory of SFR contribute to the long-term radiological

risk potentially arising from the waste due to the long half-life of ^{239}Pu ($t_{½}$ ^{239}Pu = $2.41 \cdot 10^4$ a) [5]. In reducing aqueous environments, the formation of Pu(III) and Pu(IV) is expected [6]. However, uncertainties in the available thermodynamic data lead to a rather ill-defined redox transition border, especially under alkaline to hyperalkaline conditions [1, 6]. Cellulose is disposed of in large quantities along with L/ILW in SFR [5]. Iso-saccharinic acid (ISA) is the main degradation product of cellulose under hyperalkaline pH conditions defined by cementitious systems [7]. The strong complexation of ISA with An(III) and An(IV) [8] together with the large inventory of this organic ligand present in SFR requires dedicated research efforts with focus on the Pu-ISA-cement system, for which almost no experimental studies are available in the literature.

All experiments were conducted in Ar glove boxes at $T = (22 \pm 2)$°C with O_2 concentration below 2 ppm. Independent undersaturation solubility experiments were prepared with 0.2 - 2 mg (per batch sample) of a well-characterized, aged ^{242}Pu(IV)O_2(am,hyd) solid phase. Redox conditions were either buffered with 2 mM hydroquinone (HQ) at (pe + pH_m) ~ 10 or with Sn(II) at (pe + pH_m) ~ 1.5. Three series of solubility experiments were performed at $8 \le pH_m \le 13$: i. absence of ISA, ii. presence of ISA with 10^{-6} m ≤ $m(ISA)_{tot} \le 0.1$ m, and iii. presence of ISA and Ca(II) with 10^{-6} m ≤ $m(ISA)_{tot} \le 0.1$ m and $3 \cdot 10^{-4}$ m ≤ $m(Ca)_{tot} \le 0.02$ m. Solid phases retrieved from selected batch samples were characterized by XPS, *in-situ* XRD and Pu L_{III} edge XANES/EXAFS at the INE-Beamline for Actinide Research at ANKA synchrotron facility.

Pu(III/IV)-ISA system. A pronounced increase of Pu(IV) solubility (compared to ISA-free systems) by up to 2.5 $\log_{10}$-units was observed in the presence of ISA and absence of Ca(II) (see Figure 5). In HQ systems, slope analysis of solubility data in combination with solid phase characterization and DFT calculations resulted in chemical and thermodynamic models including the predominance of $Pu(OH)_3ISA_{-H}^-$ and $Pu(OH)_3ISA_{-2H}^{2-}$ complexes below and above $pH_m \approx 12$, respectively (with ISA_{-H} and ISA_{-2H} corresponding to ISA molecules where 1 and 2 alcohols groups are deprotonated). The significantly higher $m(Pu)_{tot}$ measured in Sn(II) systems with $pH_m < 12$ indicated the formation of Pu(III)-ISA complexes under these boundary conditions. Above this pH_m, solubility data in HQ and Sn(II) systems were virtually identical indicating that the same equilibrium reaction (*e.g.* Pu(IV)(s) ⇔ Pu(IV)-ISA(aq)) controlled the solubility in both systems.

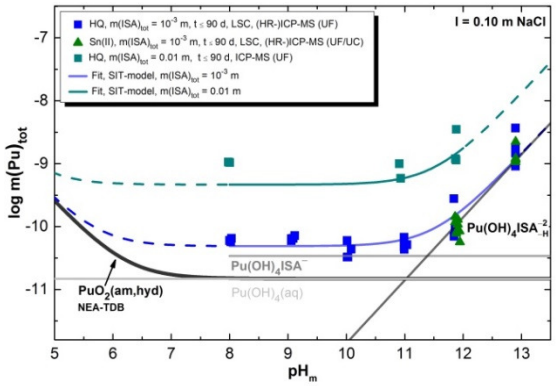

Fig. 5: *Plutonium concentration in equilibrium with PuO_2(am,hyd) in redox buffered systems (■: hydroquinone; ▲:$SnCl_2$) at constant $m(ISA)_{tot}$ (0.01 m and 10^{-3} m). Solid lines correspond to the calculated solubility of PuO_2(am,hyd) in the absence of ISA: black line [6] and at constant $m(ISA)_{tot}$ = 0.01 m: dark green lines and 10^{-3} m: blue lines, using the thermodynamic model derived in this work.*

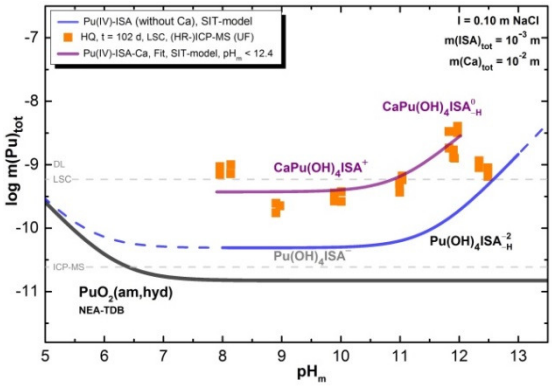

Fig. 6: *Plutonium concentration in equilibrium with PuO_2(am,hyd) for HQ-buffered systems (■) at constant $m(ISA)_{tot}$ (10^{-3} m) and $m(Ca)_{tot}$ (0.01 m). Solid lines correspond to the calculated solubility of PuO_2(am,hyd) in the absence of ISA: black line [6]; with constant $m(ISA)_{tot}$ = 10^{-3} m: blue lines; and with constant $m(ISA)_{tot}$ = 10^{-3} m and $m(Ca)_{tot}$ = 0.01 m concentrations: purple line, using the thermodynamic model derived in this work.*

Ca(II)-Pu(III/IV)-ISA system. The presence of Ca(II) and ISA further enhanced the solubility of Pu in HQ-buffered systems (compared to Ca(II)-free systems), indicating the formation of quaternary Ca(II)-Pu(IV)-OH-ISA aqueous complexes (Figure 6). Chemical and thermodynamic models were derived for this system based on the slope analysis of solubility data and solid phase characterization, and included the formation of the quaternary complexes $CaPu(OH)_3ISA_{-H}^+$ and $CaPu(OH)_3ISA_{-2H}$(aq) below and above $pH_m \approx 11$, respectively. The proposed model overestimates the experimentally measured solubility at $pH_m \ge 12.5$ and $m(ISA)_{tot} \ge 0.01$ m, possibly due to the formation of a yet undefined Ca(II)-Pu(IV)-ISA solid phase. On the contrary, data collected in Sn(II)-buffered solubility experiments do not support the existence of analogous Pu(III)-bearing quaternary species with Ca(II) ions. The chemical and thermodynamic models derived in this work for the system Pu^{3+}-Pu^{4+}-Ca^{2+}-H^+–Na^+-ISA^--Cl^--OH^--H_2O(l) can be implemented in geochemical models/calculations, and provide relevant data for the safety analysis of repositories for the disposal of L/ILW.

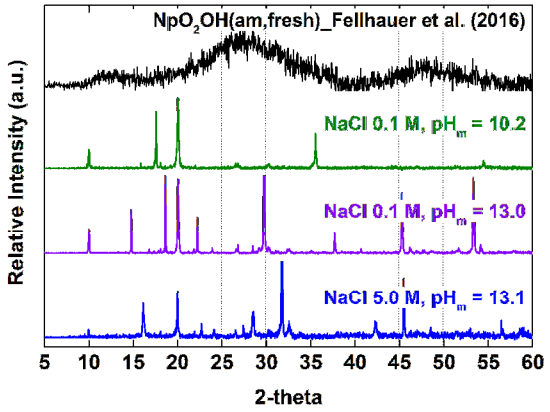

Fig. 7: *XRD patterns of Np(V) solid phases tempered at T = 80°C for 30 days in 0.1 and 5.0 M NaCl solutions. XRD diffractrogram reported in Fellhauer et al. (2016) [9] for NpO_2(am,fresh) is appended for comparison.*

Actinide solution chemistry at elevated temperatures

Temperature is one of the parameters that will vary during the different phases of operation of a high level radioactive waste (HLW) repository. Elevated temperature conditions (up to 200°C depending on hostrock system and repository concept) will affect actinide chemistry in the near-field of a HLW repository. In the context of the ThermAc project funded by BMBF, experiments on the solubility and the stability of solid phases of different actinides in aqueous solutions (NaCl, $MgCl_2$, $CaCl_2$) at T = 25 - 80°C were performed by KIT-INE.

The effect of temperature on Np(V) solid phase formation was investigated to obtain insights about the thermodynamic stability of Np(V) solid phases, assess the role of kinetics in solid phase transformations and evaluate possible redox processes occurring at elevated temperatures. About 5 mg of NpO_2OH(am,fresh) were equilibrated with 20 ml of various background electrolytes (0.1 and 5.0 M NaCl; 0.02, 0.15, and 3.5 M $CaCl_2$; 0.01 and 2.0 M $MgCl_2$) under Ar atmosphere. Initial pH_m values in the solutions were between 6 and 13. Samples were tempered at T = (80 ± 5)°C for 30 days in airtight autoclaves. After cooling down to ambient temperature, Np solid phases were washed with ethanol for further analyses by means of powder X-ray diffraction (XRD), scanning electron microscopy combined with energy-dispersive X-ray spectroscopy (SEM-EDS), and quantitative analysis methods (ICP-MS/OES).

Apparent changes in color of Np(V) solids from initial green to either bluish-green, black, or violet, respectively, along with a considerable decrease in Np(V) solubility were observed in most of the tempered samples, unambiguously indicating the transformation of initial NpO_2OH(am,fresh) solid phases. Furthermore, a significant decrease of pH_m values occurred which could be elucidated by the transformation into further hydrolyzed solid Np(V) phases. Figure 7 represent the powder XRD patterns obtained for NaCl samples. In contrast to the initial amorphous NpO_2OH(am,fresh) [9], Np(V) solid phases tempered in alkaline NaCl solutions show characteristic XRD peaks indicating the formation of (micro)crystalline compounds.

The transformation of the initial Np(V) solid phase was also observed in $CaCl_2$ solutions. While a (micro)crystalline compound formed at weakly alkaline conditions, XRD patterns obtained for hyper-alkaline samples show the presence of rather poorly crystallized products, similar to $CaNpO_2(OH)_{2.6}Cl_{0.4}\cdot 2H_2O$(s) [9]. Although none of the collected diffractograms matched with that of crystalline NpO_2, the possibility of temperature induced redox transformations as reported in [10] will be further assessed by XANES/EXAFS at the INE-Beamline at ANKA synchrotron facility.

The result of the present work contributes to a better understanding of the solubility behavior and solid phase speciation of actinide elements, and provides relevant process understanding for the reliable Safety Assessment of high-level waste repositories in deep-geological formations.

Complexation of Cm(III) with malonate

Small organic molecules are present naturally in ground waters or can be formed due to degradation of macromolecular organic matter (e.g. humic/fulvic acids). The complexation of actinides with small organic ligands is a topic of fundamental scientific interest and a potentially relevant geochemical process and may influence the migration behavior of actinides in a potential host-rock of a nuclear waste repository. Detailed thermodynamic data at ambient and elevated temperatures as well as structural information of the different complexes are necessary for an in-depth understanding of the complexation mechanism on the molecular level.

In the present work, the complexation of Cm(III) with malonate is investigated by time resolved laser fluorescence spectroscopy as function of $[Mal^{2-}]_{tot}$, I_m(NaCl) and T = 20 - 90°C, and evaluated using the specific ion interaction theory (SIT) as performed for

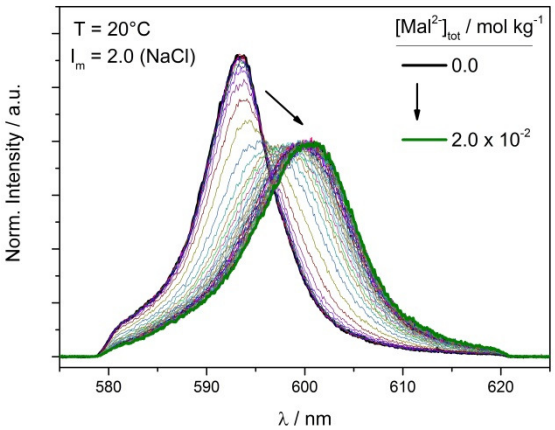

Fig. 8: *Emission spectra of Cm(III) (10^{-8} m) as function of $[Mal^{2-}]_{tot}$. T = 20 °C, I_m = 2.0 m (NaCl).*

comparable ligand systems [11-12]. Furthermore, the structures of the respective complexes are determined by quantum chemical calculations.

The evolution of the fluorescence spectrum of Cm(III) with the total concentration of malonate is shown in Figure 8. The emission band of the Cm^{3+} aquoion (593.8 nm) is clearly shifted towards 601 nm with increasing $[Mal^{2-}]_{tot}$. This is attributed to the successive shift of the Cm(III) speciation towards complexed species. Using the SIT, the log K^0_n(T) of the $[Cm(Mal)_n]^{3-2n}$ complexes (n = 1, 2) were determined for the entire temperature range. The log K^0_3(T) was determined only for $T \geq 40$ °C. The results show a general increase of the constants with the temperature by about 0.25 - 0.50 orders of magnitude.

The stability constants are linearly correlated with the reciprocal temperature. Thus, their temperature dependency is fitted by the integrated Van't Hoff equation, yielding the respective thermodynamic functions $\Delta_r H^0_m$ and $\Delta_r S^0_m$ of the complexes. The results show a small and almost constant reaction enthalpy around 10 kJ·mol^{-1} for each stepwise formation of the three complexes. The reaction entropies however decrease successively for each complexation step from 130 to 60 J·mol^{-1}K^{-1}.

This effect is explained by analyzing the calculated structures of the different Cm(III) malonate species. For each complex, every combination of end-on (non-chelating) and side-on (chelating) coordination is calculated and the respective binding energies (BE) are compared. The lowest BE are found for the structures with only side-on coordinated ligands, showing that malonate prefers a chelating binding mode to Cm(III) via two oxygen atoms, one of each carboxylic group. This is in agreement with the analogues ligands oxalate and succinate [11-12]. Contrary to these two ligands however, for malonate the difference between the BEs of the all side-on structures to the mixed structure with one ligand in end-on coordination are quite small. The reason is that the length of the carbon chain of malonate enables the ligand to form hydrogen bonds to inner-sphere water molecules of Cm(III) via the free carboxyl group when in end-on coordination. This stabilizes the end-on coordination of malonate to some extent and lowers the respective BEs. To illustrate this effect, the structure of $[Cm(Mal)_{2,side}(Mal)_{end}]^{3-}$ complex is given in Figure 9.

The present work gives detailed insights into the complexation of Cm(III) with malonate, showing how structural properties of the ligand influences the coordination on the molecular level, which in turn affects the thermodynamics of complexation on the macroscopic scale. The results contribute to an in-depth understanding of the interaction of aliphatic dicarboxylic ligands with trivalent actinides in aqueous solution.

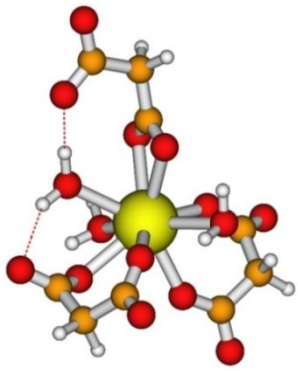

Fig. 9: *Molecular structures of $[Cm(Mal)_3]^{3-}$ with two ligands coordinated side-on and one ligand end-on.*

References

[1] Guillaumont, G., et al., *Chemical Thermodynamics Vol. 5*, Elsevier, Amsterdam, (2003).

[2] Yalcintas, E., et al., Dalton Transactions, **45**, 8916–8936, (2016).

[3] Alliot, I., et al., Environ. Sci. Technol., **43**, 9174–9182, (2009).

[4] Neck, V., et al., Radiochim. Acta, **89**, 1-16, (2001).

[5] Almkvist, L. and Gordon, A., *Low and intermediate level waste in SFR 1. Reference waste inventory 2007*. SKB R-07-17, Svensk Kärnbränslehantering AB, (2007).

[6] Neck, V., et al., C. R. Chimie, **10**, 959-977, (2007).

[7] Glaus M.A., et al., Environ. Sci. Technol., **42**, 2906-11, (2008).

[8] Gaona, X., et al., J Contam Hydrol, **102**, 217-27, (2008).

[9] Fellhauer, D., et al., Radiochim. Acta, **104**, 381-397, (2016).

[10] Roberts, K. E., et al., Radiochim. Acta, **91**, 87-397, (2003)

[11] Skerencak-Frech, A. et al., Inorg. Chem., **54**, 1860-1868, (2015).

[12] Fröhlich, D.R., et al, Inorg. Chem., **55**, 4504-4511, (2016).

4.2 Sorption on mineral surfaces

4.2.1 Electrokinetics of dioctahedral smectites and europium interaction at low pH

J. Lützenkirchen, Th. Schäfer

In co-operation with:

L. Delavernhe[a], *K. Emmerich* [a]

[a] Competence Center for Material Moisture (CMM), Karlsruhe Institute of Technology (KIT), Hermann-von-Helmholtz-Platz 1, D-76344 Eggenstein-Leopoldshafen, Germany

Introduction

The charging of clay minerals is complex since it involves interactions of solutes with various crystal planes that have different properties. Amphoteric sites at the edges induce pH-dependent charges and basal surfaces involve a negative permanent charge resulting from the isomorphous substitutions within the tetrahedral and octahedral sheets [1]. In the present study, the electrophoretic mobility has been investigated as a function of pH on four Na-saturated dioctahedral smectites < 0.2 µm separated from blended bentonites and their related reduced-charge materials (RCM) previously characterized [2]. The blended bentonites selected were Calcigel® (Bavaria, Germany), Volclay® (Wyoming, USA), the Cabo de Gata bentonite (Almería, Spain) and the bentonite P provided by Süd-Chemie AG (Germany) thereafter called BC, BV, BS and BP respectively. In addition, interaction with dissolved europium at low pH has been studied in comparison with other trivalent or divalent and monovalent cations. Clay concentrations were 1 g/l in all cases.

Mobilities in the absence and presence of Europium at low pH

As expected, the electrophoretic mobility of the dioctahedral smectites were negative and almost constant over the pH range of 2 to 10 (Figure 1 shows the results for the BV samples). However, the smectite from Wyoming (USA) (BV) characterized by the lowest layer charge of 0.26 eq/f.u and the largest mean layer diameter of 277 nm showed the highest mobility.

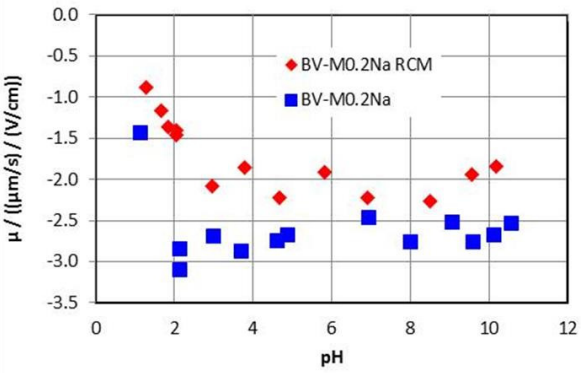

Fig. 1: *Electrophoretic mobility of samples BV-M0.2Na RCM and BV-M0.2Na as a function of pH in 2 mM monovalent salt.*

The RCM materials characterized by collapsed interlayers and consequently a higher contribution from the edge surfaces showed a slightly lower mobility and a decrease of mobility at pH < 2 for the BV sample as observed by others [3].

The ion-exchange that is responsible for the uptake of metal cations at low pH can be conveniently tested by adding solutions of the metal ion of interest. The low pH conditions (in the following the pH is set to about pH 2) have the advantages that (i) stock solutions of the metal ions can be easily prepared at the low pH (no or limited hydrolysis, no interference from any potential complexing anion), (ii) the metal ion concentration can be increased to nearly any concentration of interest, and (iii) the pH is strongly buffered and does not change significantly. However, contact times of clay at low pH have to be limited to prevent side reactions due to dissolution. In some cases, a clay sample was left at low pH for extended times (i.e. longer than the duration of the experiments the results of which are shown), but in none of these investigation changes of the mobility were observed. Thus, dissolution of the clay and subsequent re-adsorption of e.g. dissolved aluminum is not interfering in the reported results.

Addition of europium leads to mobilities that are close to zero for Europium concentrations above 5 mM (Figure 2). There is as would be expected scatter in the mobilities. Some of the data points have been repeated using a separate cell, the same sample aliquot, a new sample aliquot and combinations thereof. The largest errors quantified from these data are about 0.5 µm/s/(V/cm).

Overall, no significant difference between the clays (including the other three samples investigated for which the experimental data is not shown) with respect to europium interaction at this low pH occurs. With respect to the results in Figure 1, it can also be stated that there is no difference between the dioctahedral smectites and the reduced-charge samples. Finally, there is no significant over-charging of the clays, considering the experimental uncertainties, i.e.

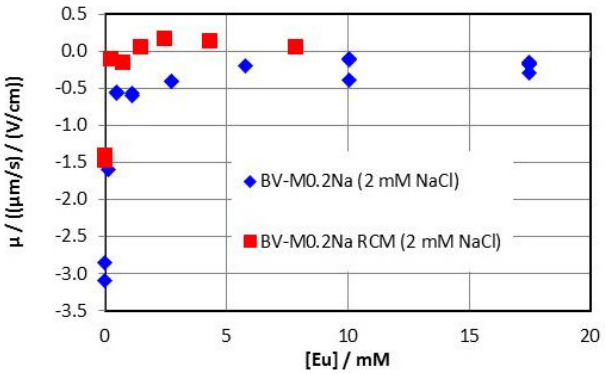

Fig. 2: *Electrophoretic mobility of samples BV-M0.2Na RCM and BV-M0.2Na as a function of Europium concentration at pH about 2 in 2 mM monovalent salt.*

the data suggest that the negative charge of the clays is just neutralized.

With some of the clays a separate set of experiments has been carried out to study whether the nature of the trivalent ion has an influence on the behavior. Figures 3 A and B show that with trivalent cations that are more strongly hydrolyzing than europium the same behavior is retrieved. Changing the charge of the ion, however, results in clear differences. Thus, in the presence of sodium, the BS-M0.2Na clay remains negatively charged up to at least 200 mM (Figure 3 C). In the case of BC-M0.2Na RCM, addition of Barium also results in a negative surface in the concentration range studied (Figure 3 D). Relating the curves for the differently charged ions, the sequence is obvious: The higher the charge, the closer to zero the electrokinetic mobility becomes.

Conclusions

The electrokinetic data show that the studied clay samples cannot be significantly overcharged, i.e. within the concentration ranges studied, even the trivalent cations do not cause significant positive mobilities. The interaction with the trivalent cations appears to be non-specific and all the trivalent cations cause neutralization of the electrokinetic surface charge. From comparison with cations of lower charge, it becomes clear that they are not able to cause complete neutralization of the electrokinetic charge.

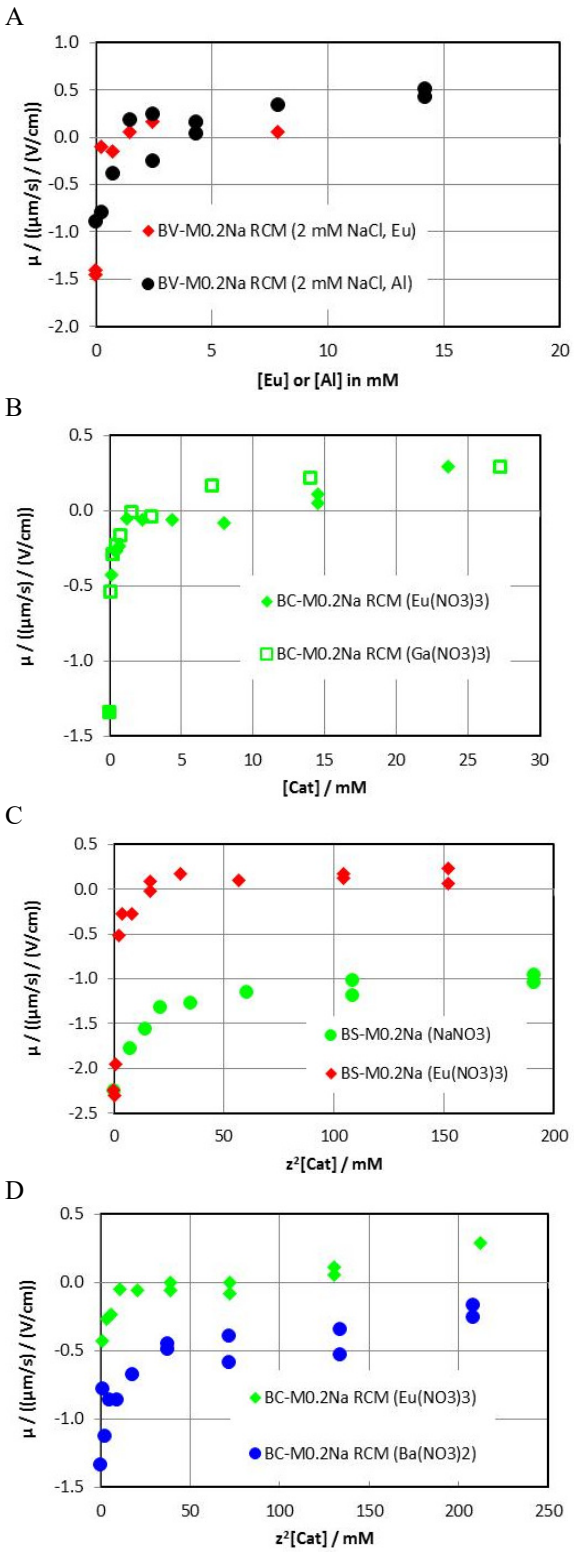

Fig. 3: *Electrophoretic mobility of selected samples at pH about 2 starting from 2 mM monovalent salt as a function of concentration (A, B) or "effective" concentration (C,D). A and B: Effect of nature of trivalent cation. C and D: Effect of ion charge.*

References

[1] Leroy, P., Tournassat, C., Bernard, O., Devau, N., Azaroual, M., 2015. The electrophoretic mobility of montmorillonite. Zeta potential and surface conductivity effects. J. Colloid Interface Sci. 451, 21-39.

[2] Thomas, F., Michot, L.J., Vantelon, D., Montargès, E., Prélot, B., Cruchaudet, M., Delon, J.F., 1999. Layer charge and electrophoretic mobility of smectites. Colloids and Surfaces A: Physicochemical and Engineering Aspects 159, 351-358.

[3] Delavernhe, L., Steudel, A., Darbha, G.K., Schäfer, T., Schuhmann, R., Wöll, C., Geckeis, H., Emmerich, K., 2015. Influence of mineralogical and morphological properties on the cation exchange behavior of dioctahedral smectites. Colloids and Surfaces A: Physicochemical and Engineering Aspects 481, 591-599.

4.2.2 Influence of carbonate and gluconate on the Eu(III) and Cm(III) sorption onto clay minerals

F. Rieder, Th. Rabung, H. Geckeis, Th. Schäfer

Introduction

Trivalent actinides generally show a strong interaction with clay mineral surfaces in terms of sorption reactions [1]. This strong retention was demonstrated recently also for highly saline conditions [2]. A significant decline in sorption is, however, to be expected in presence of organic complexing ligands, either naturally occurring like e.g. humic acids [3] or originating from the waste form or the concrete used as construction material. Among other relevant complexing ligands, gluconate as a representative of α–hydroxo carboxylic acids and an analogue to isosaccharinic acid (main product of cellulose degradation) and an important cement additive, might significantly decrease the sorption of trivalent actinides. In a recent study related to the impact of gluconate on the sorption of ^{63}Ni onto TiO_2, a decrease in sorption was observed at pH > 8, which was significantly enhanced in $CaCl_2$ containing aqueous solutions [4]. Such insufficiently understood findings prompted us to address this topic in more detail.

Sorption of europium in presence of carbonate or gluconate onto clay minerals

Only a few detailed studies are available in the literature dealing with the influence of carbonate as an omnipresent and strongly complexing groundwater ligand on actinide sorption onto clay minerals [4] and virtually no published data are available for higher ionic strength conditions, which is relevant for some nuclear waste disposal safety case studies. In order to assess the strong radionuclide retention capacity of clay minerals either in bentonite barriers or claystone host rocks of nuclear waste repositories, the potential impact of strong complexing anionic ligands on sorption must be quantified. For a sound mechanistic understanding and a reliable prediction of the metal ion sorption under relevant conditions a sufficient number of experimental data under variation of sensitive parameters (e.g. pH, ligand concentration, variation of background electrolyte concentration and composition etc.) is essential. Spectroscopic techniques such as the time resolved laser fluorescence spectroscopy (TRLFS) by using Cm provide a powerful tool to get direct information on the complexation in solution and on the mineral surface complexation by identifying different species. By combining all available information reliable thermodynamic models can be derived or validated.

In the present work batch sorption experiments in presence of carbonate or gluconate were performed with Illite du Puy (Na-IdP-2), montmorillonite (Na-SWy-2) and a synthetic iron free montmorillonite (IFM) [5], using a solid to liquid ratio of 1 g/L and different NaCl background electrolytes concentrations (0.1, 1, 3 M). For the gluconate system experiments were done additionally also in $CaCl_2$ background electrolyte solutions (0.06, 0.6, 2 M). The radionuclide concentration was limited to $2 \cdot 10^{-8}$ M ^{152}Eu (carrier free) for batch experiments and $1 \cdot 10^{-7}$ M ^{248}Cm for TRLFS. In case of the gluconate studies all experiments were performed under argon atmosphere with $1 \cdot 10^{-2}$ M sodium or calcium gluconate, depending on the background electrolyte. Experiments with carbonate were performed in equilibria with different CO_2 containing atmospheres by selecting $p_{CO2}=10^{-3.3}$ (atmospheric conditions; partial pressure slightly higher compared to the obsolete standard value of $p_{CO2}=10^{-3.5}$, in consideration of the increasing global CO_2 content of the atmosphere) and 10^{-2} bar (1% CO_2 in a glove box; higher carbonate contents are expected for deep repository conditions). To guarantee equilibrium conditions with the gas phase, calculated (using the geochemical code PHREEQC and the databases THEREDA or the PSI/Nagra Chemical Thermodynamic Database) amounts of bicarbonate, carbonate and hydroxide ions were added to the solutions to achieve fixed pH values under equilibrium conditions. For TRLFS measurements with Cm in carbonate containing systems a reduced solid to liquid ratio of 0.25 g/L for measurements in suspension and 1 g/L for measurements of wet pastes were selected. Besides TRLFS spectra also fluorescence lifetime measurements have been performed.

A strong reduction of Eu (III) / Cm(III) retention

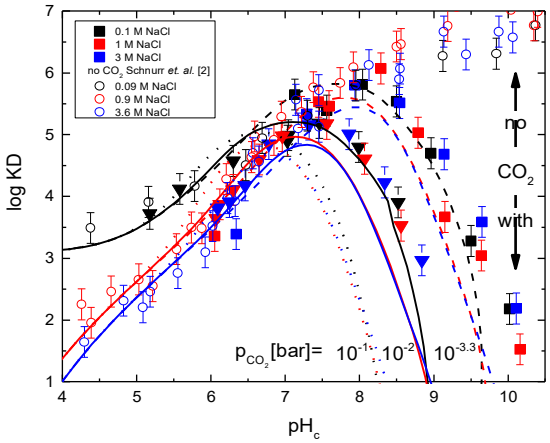

Fig. 1: *Sorption of Eu(III) onto Illite, from low to high salinity in absence (open symbols [2]) and presence of carbonate (closed symbols, this work) at different p_{CO2} values. Drawn, dashed and dotted lines represent calculated sorption data acc. to the 2 SPNE/CE model combined with the Pitzer approach for elevated ionic strength conditions.*

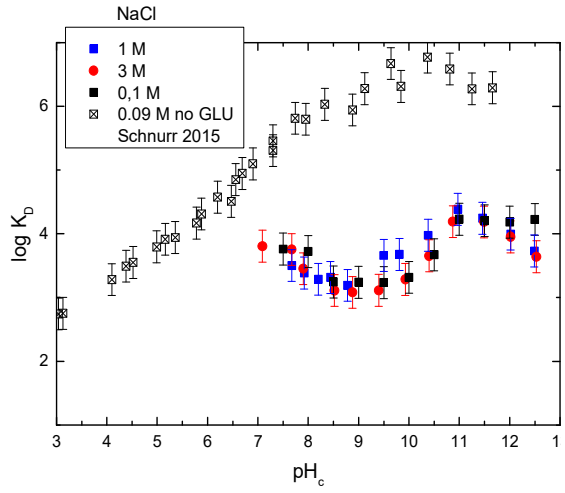

Fig. 2: *Sorption of Eu(III) onto Illite, from low to high salinity in absence (open symbols [2]) and presence of 0.01 M gluconate (closed symbols, this work) at different* p_{CO2} *value.*

with increasing p_{CO2} for pH > 7.5 is obvious in agreement with previous studies (Figure 1). Compared to carbonate free conditions K_D values were up to 3 orders of magnitude lower at pH ~ 9.5. No significant effect of increasing the NaCl background electrolyte concentration could be detected. The modelling of experimental data using the 2 SPNE/CE model [1] combined with the Pitzer approach to take ion-ion interactions in solution into account is in good agreement with the experimental findings. TRLFS spectra and lifetime measurements clearly point to the presence of different carbonate containing surface sorbed Cm(III) species. According to previous studies model calculations were performed using two ternary carbonate-Eu/Cm(III)-surface species (in agreement with TRLFS observations) with a slight increase of respective log K values (e.g. Illite: ≡SOEuCO_3 with log K = 10.4, and ≡SOEu(OH)CO_3^- with log K = 1.8). Virtually no ionic strength effect is visible for experimental data in the pH range > 8, where carbonate influences sorption. Model calculations, however, predict a slightly decreasing sorption at increasing ionic strength. Yet, the agreement of model calculations and experiment is still good.

First experimental results for studies with gluconate indicate a significant reduced Eu(III) sorption in the alkaline pH range consistent with previous findings obtained for ^{63}Ni and rutile. However, experiments are still ongoing and yet incomplete. Additional studies will be performed and finally complemented with establishing a geochemical sorption model to describe experimental findings.

Conclusions

The presence of competing ligands like carbonate or gluconate shows a major effect on the sorption behavior of trivalent lanthanides and actinides. First Eu(III) sorption experiments in presence of a relatively high gluconate concentration show a significantly reduced retention over the whole pH-range covered in this study. Sorption experiments in presence of carbonate were performed in equilibrium with different CO_2 containing atmospheres. This generates a pH dependent increase of carbonate concentrations, which results in strongly decreasing K_D-values with increasing pH.

References

[1] M. H. Bradbury, Baeyens, B., Geckeis, H., Rabung, T., *Geochimica Et Cosmochimica Acta* **2005**, *69*, 5403-5412.

[2] A. Schnurr, R. Marsac, T. Rabung, J. Lutzenkirchen, H. Geckeis, *Geochimica et Cosmochimica Acta* **2015**, *151*, 192-202.

[3] T. Rabung, H. Geckeis, J. I. Kim, H. P. Beck, *Radiochim. Acta* **1998**, *82*, 243.

[4] M. M. Fernandes, B. Baeyens, M. H. Bradbury, *Radiochimica Acta* **2008**, *96*, 691-697; bM. M. Fernandes, T. Stumpf, B. Baeyens, C. Walther, M. H. Bradbury, *Environmental Science & Technology* **2010**, *44*, 921-927; cM. Marques Fernandes, N. Vér, B. Baeyens, *Applied Geochemistry* **2015**, *59*, 189-199.

[5] M. Reinholdt, J. Miehe-Brendle, L. Delmotte, M. H. Tuilier, R. le Dred, R. Cortes, A. M. Flank, *Eur. J. Inorg. Chem.* **2001**, *11*, 2831.

4.3 Retention of radionuclides by secondary phase formation

F. Heberling, N. Finck, Z. Nie, C. Garcia, T. Hippel, P. Lindqvist-Reis, K. Dardenne

In co-operation with:

N. Bogachev[a]

[a] Saint Petersburg State University, Saint Petersburg, Russia

Introduction

During the (geo)chemical evolution of a nuclear waste repository, ground water may migrate through the geological and geotechnical barriers and reach the technical barrier encapsulating the nuclear waste. In aqueous environments, various secondary phases may form as alteration or corrosion products of materials from the multi-barrier system or the waste matrix itself. Steel canisters and the waste glass are expected to corrode/alter over extended periods of time in contact with ground water and various Fe-bearing secondary phases will form, such as for example iron (hydr)oxides and iron containing clay minerals. Calcite on the other hand is expected to form as an alteration product of concrete based materials and also may be present as a constituent of possible host rock formations (e.g. argillites).

Secondary phases have the potential to scavenge radionuclides (RNs) and to retard their migration to the biosphere. Various molecular scale retention processes, from surface adsorption to structural incorporation have been reported. Especially structural incorporation, i.e. solid-solution formation, is argued to lead to a significant retention of the RNs in the near field of a repository. However, despite the abundance of solid-solutions found in natural systems, reliable thermodynamic and kinetic models to predict their formation are hardly available.

The group working on secondary phases at INE aims at developing quantitative thermodynamic models based on a molecular scale process understanding, by combining information from specific laboratory experiments with information from advanced spectroscopic, microscopic, and diffraction techniques as well as computational studies. Thus, we investigate the structural incorporation of RNs into various secondary phases expected to form in the multi-barrier system around potential nuclear waste repositories. Detailed below are two examples: Ln/An(III) uptake by calcite and a study characterizing structural iron in clay minerals.

Eu^{3+} incorporation into calcite

Eu^{3+}, Cm^{3+}, and Am^{3+} uptake by calcite is a subject of investigations by the KIT-INE secondary phases group since several years. Besides the relevance of this system for the potential retention of long-lived trivalent actinide elements in the multi-barrier system, especially Eu^{3+} and Cm^{3+} in calcite provide ideal substrates for investigations with time resolved luminescence spectroscopy. Especially since we have the possibility to perform site-selective, direct excitation measurements at low temperature (< 20 K) (e.g. [1]) detailed information on the incorporation species has been obtained. First studies relied on calcite syntheses in Mixed Flow Reactors (MFR) at steady state conditions. Marques et al. (2008) [2] investigated the influence of the available surface area in the MFR and the background electrolyte cations (Na^+, K^+), which are available to provide charge compensation in the potential incorporation mechanism where two Ca^{2+} ions in calcite are replaced by one Eu^{3+} and one Na^+/K^+. In contrast to Na^+, the larger K^+ ion is incompatible with the calcite structure and distorts the local structure upon charge compensation. Marques et al. report three incorporation species A, B, and C.

Species C is identified as a well-ordered incorporation species. The corresponding $^7F_0 \rightarrow {}^5D_0$ transition is excited at 579.5 nm. The twofold crystal field splitting of the $^5D_0 \rightarrow {}^7F_1$ transition and the threefold splitting of the $^5D_0 \rightarrow {}^7F_2$ transition, detected for the sample synthesized in the presence of Na^+, are in line with Eu^{3+} occupying a Ca^{2+} site in the calcite structure (D_{3d} symmetry). For the sample synthesized in the presence of K^+, Marques et al. report threefold splitting of the $^5D_0 \rightarrow {}^7F_1$ band and a fivefold splitting of the $^5D_0 \rightarrow {}^7F_2$ band, due to a lowering of the symmetry of the local structural environment of Eu^{3+} in calcite due to charge compensation by the large K^+ cation. Species C has a long fluorescence lifetime (> 3 ms), indicating no coordinating water [3].

Species B is another incorporation species, as identified by the long fluorescence lifetime (> 3 ms, [3]). Species B is characterized by a low-symmetry coordination environment, compared to species C as indicated by the full crystal field splitting of the $^5D_0 \rightarrow {}^7F_1$ and $^5D_0 \rightarrow {}^7F_2$ bands. Species B is excited at 578.4 nm. It has a very characteristic $^5D_0 \rightarrow {}^7F_2$ transition spectrum with a sharp emission peak around 619 nm. A fact not mentioned by Marques et al, but obvious from their spectra is, that the formation of species B seems to be enhanced in the presence of K^+ compared to the synthesis in the presence of Na^+.

Species A is excited at 578.1 nm, it has a substantially lower fluorescence lifetime (0.46 ms) compared to species B and C. This lifetime would be in line with one or two water molecules coordinated to the Eu^{3+} ion [3]. The ratio between species B and C on the one hand side and species A on the other hand side increased strongly upon a decrease of the reactive

surface area in the MFR. Thus, species A is interpreted as a surface species.
In a follow up study calcite was synthesized by recrystallization of metastable vaterite to the more stable polymorph calcite [4]. Here an additional transition species, which we will denote as species D here, was introduced. Species D was detected at early stages of calcite formation. It has a fluorescence lifetime of 1.1 ms, corresponding to 0.3 coordinating water molecules.

In a later study, Hofmann et al. reported on the effect of NO_3^- on Eu^{3+} incorporation into calcite [10]. Besides Eu doped calcite synthesized in MFR experiments Hofmann et al. report results of batch sorption experiments. Compared to the previous studies, Eu containing calcite synthesized in the presence of $NaNO_3$ in the MFR or in batch sorption experiments (in the presence of $NaNO_3$ or $NaClO_4$) show no well-defined species with sharp absorption peaks. Instead, excitation spectra are characterized by broad peaks, which shift slightly depending on the background electrolyte anion or the addition order of NO_3^- and Eu^{3+}.

In a most recent study Hellebrandt et al. report on calcite recrystallization in the presence of Eu^{3+} [5]. For short reaction times and low reactive surface areas they find broad peaks in excitation spectra similar to Hofmann et al.. For longer reaction times and small calcite particles with large reactive surface areas sharper bands are reported. Among these, species B is reproduced quite clearly and an additional species with similarities to species D is reported.

Here we report on Eu^{3+} incorporation into calcite upon recrystallization of calcite and aragonite. Aragonite is a less stable polymorph of $CaCO_3$ at standard conditions compared to calcite. Thus, aragonite dissolves in aqueous solution to transforms to the more stable calcite. In the pure calcite system, rough irregular calcite particles transform via dissolution-reprecipitation processes to more stable idiomorphic calcite crystals [6].

Experimental details

We performed calcite recrystallization experiments in a kinetic series in 0.01 M NaCl solution at 5 µM initial Eu^{3+} concentration, and in a second and third experimental series in various background electrolytes ($NaBrO_3$, $NaClO_4$, NaI, NaBr, NaCl, $NaNO_3$, and KCl) at 0.1 M concentration and 1 µM initial Eu^{3+} concentration. The aragonite-calcite recrystallization study was a long-term experiment in 0.1 M NaCl solution at 0.76 µM initial Eu^{3+} concentration. For the calcite recrystallization experiments in the presence of various background electrolyte anions and the kinetic series, we follow the course of recrystallization by ^{45}Ca exchange measurements as previously described [6]. The solid / liquid ratio is 2 g/L in the calcite recrystallization experiments, and 20 g/L in the aragonite experiment.

Spectroscopy is performed using a Dye Laser (Radiant Dyes Laser) pumped by the second harmonic (532 nm) a Nd:YAG Laser (Continuum). The used dye, Pyrromethene 597, allows to adjust the excitation wavelength in a range from 582 nm to 575 nm, the range relevant for direct excitation of the Eu^{3+} $^7F_0 \rightarrow {}^5D_0$ transition. The sample is cooled to 4 - 6 K in a He-cryostat (CryoVac) at ~10^{-8} mbar. Luminescence is recorded on an intensified CCD camera coupled to an Andor spectrometer employing a 1200 lines/mm grating. The full setup is controlled by a homemade Labview software.

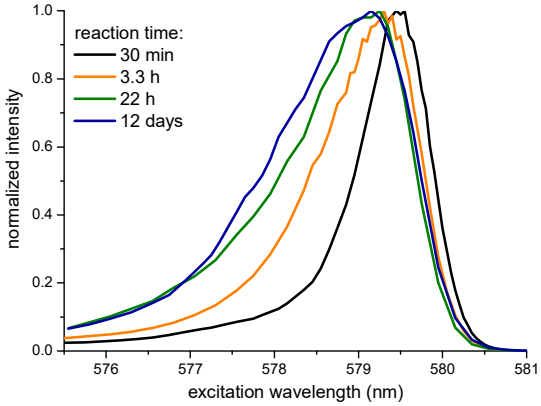

Fig. 1: *TRLFS excitation spectra of Eu^{3+} in Calcite recrystallized in the presence of 0.01 M NaCl. Spectra are recorded after various reaction times.*

Results

Spectra measured on samples from the kinetic experiment are shown in Figure 1. The excitation spectra show a continuous trend towards excitation at lower wavelength with increasing reaction time. Luminescence spectra recorded at various excitation wavelength (not shown here) demonstrate that except for the first sampling time (30 min) the Eu species in the various samples are very similar. According to ICP-MS Eu^{3+} concentration, and LSC ^{45}Ca concentration measurements (results not shown), the Eu^{3+} uptake in the system is very fast, while ^{45}Ca uptake is sequentially increasing over the 14 days' reaction period. For the sample taken after 30 min this means that Eu^{3+} is obviously already bound to the surface, while calcite transformation has not yet started. This nicely explains the clearly different spectroscopic signature of the sample taken after 30 min. At later stages ^{45}Ca data indicate a sequential increase from 1.5% and 7.5% calcite recrystallization, which would correspond to 5 to 28 monolayers. This continuous recrystallization, which is not accompanied with a measurable decrease in Eu^{3+} solution concentration, does not lead to substantial changes in the emission spectra.

Results of the second experimental series are shown in Fig. 2. In this experimental series, the influence of the background electrolyte anion is investigated. The initial Eu^{3+} concentration is lower than in the previous series (1 µM instead of 5 µM). Spectra are recorded after 14 days of reaction time. At that time 16% of calcite recrystallized. The overall reaction progress does not vary significantly with the background electrolyte.

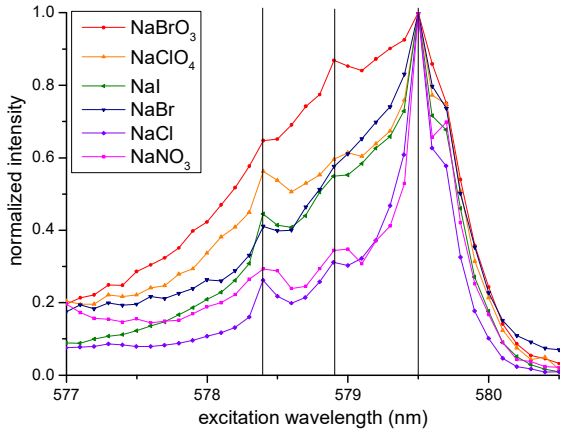

Fig. 2: *TRLFS excitation spectra of Eu^{3+} in calcite, recrystallized in various background electrolytes. Vertical lines highlight the peak positions assigned to species B (578.4 nm), D (578.9 nm), and C (579.5 nm).*

As shown in Fig. 2, we observe the formation of more well defined species with sharp peaks at 578.4 nm, 578.9 nm, and 579.5 nm compared to the spectra in Fig 1. It is interesting to note that despite very similar overall recrystallization rates, the degree to which distinct well-defined Eu^{3+} incorporation species form, seems to vary with the background electrolyte anion. Thus, as previously described [7], the background electrolyte anions must in a way affect interfacial kinetics. Still we consider it more important to point out the similarities between the samples. Emission spectra (not shown) after excitation at 578.4 nm clearly show a sharp peak close to 619 nm, characteristic for the previously described species B [2]. After excitation at 578.9 nm luminescence shows similarities to spectra in the previous experimental series, and to species D [4]. The $^5D_0 \rightarrow {}^7F_2$ emission after excitation at 579.5 nm nicely exhibits threefold splitting, characteristic for the previously described species C [2].

In a third experimental series, we investigated the influence of the background electrolyte *cation*. Fig. 3 shows the corresponding $^5D_0 \rightarrow {}^7F_1$ and $^5D_0 \rightarrow {}^7F_2$ emission spectra recorded after excitation at 578.4 nm (species B) and 579.5 nm (species C) for two samples prepared in the presence of NaCl and KCl, respectively. Thus, we reproduce the effects discussed above with respect to the work by Marques et al.: the formation of species B (characteristic sharp F_2 emission peak around 619 nm) is more pronounced in the KCl system, while the centro-symmetric species C (twofold split F_1 band, and threefold split F_2 band) forms only in the presence of Na^+, and becomes distorted if only K^+ is available for charge compensation.

Results of the long-term aragonite to calcite recrystallization experiment are shown in Fig. 4. After 400 days' recrystallization, all aragonite had transformed to calcite according to powder XRD. No additional mineral phase was detected. The initially measured excitation spectrum exhibits only one sharp peak at 579.50 nm, which perfectly corresponds to species C, also regarding the emission spectrum. A more detailed measurement, however, revealed that there are two peaks, one at 579.50 nm, and one extremely sharp and intense peak at 579.58 nm, in the following denoted as species C'. According to the fluorescence lifetime (1.8 ms, < 0 coordinating water molecules [3]), species C' seems to be an incorporated Eu-species.

Demixing and formation of a separate Eu-phase cannot be ruled out completely. However, on the basis of XRD results and the fact that a pure Eu-phase would be expected to exhibit an even shorter fluorescence lifetime due to concentration quenching, this explanation seems unlikely. The observed crystal

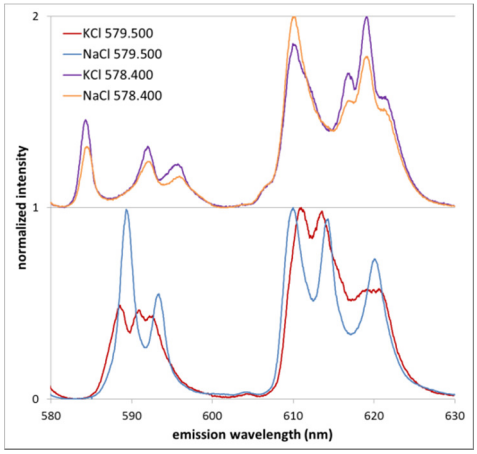

Fig. 3: *TRLFS emission spectra of Eu^{3+} in calcite, recrystallized in presence of NaCl and KCl, respectively. Luminescence is recorded after excitation at 578.40 nm and 579.50 nm as indicated in the Figure legend. $^5D_0$-$^7F_1$ emission corresponds to peaks between 585 nm and 600 nm, $^5D_0$-$^7F_2$ emission corresponds to peaks between 606 nm and 630 nm. Note the small peak around 604 nm, a vibronic sideband caused by coordinating carbonate ligands.*

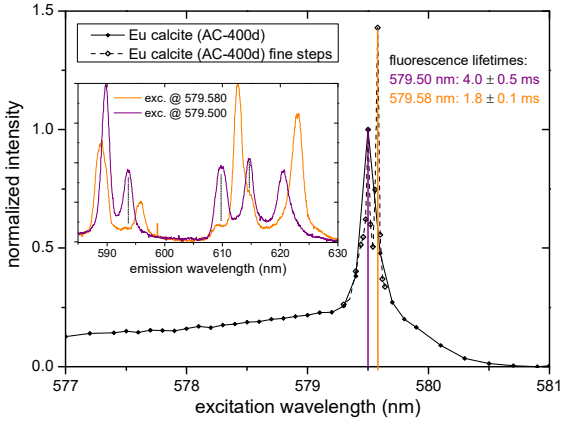

Fig. 4: *Spectra recorded on the Eu-doped calcite sample obtained from the long-term aragonite to calcite recrystallization experiment after 400 days, denoted AC-400d. The main graph shows excitation spectra measured with different step sizes. Note that the intensity of the detailed spectrum was adjusted to match the main peak of the spectrum measured with coarse steps. The insert shows corresponding emission spectra after excitation at the two peak maxima at 579.50 nm and 579.58 nm.*

Tab. 1: *Eu-species identified in calcite*

	Species B	Species D	Species C	Species C'
excitation wavelength	578.40 nm	~ 579 nm	579.50 nm	579.58 nm
lifetimes (ms)	(0.9 ± 0.1) 4 ± 1	0.7 ± 0.2 2.1 ± 0.4	(1.2 ± 0.2) 3.6 ± 0.6	- 1.8 ± 0.1
interpretation	low symmetry incorporation species	disordered surface or near surface incorporation species	centro-symmetric incorporation species, coupled substitution (2 Ca ↔ Na/K+Eu)	locally ordered version of species C?

field splitting (twofold split F_1 band, and twofold split F_2 band) would be in line with a local D_3 symmetry and has been previously reported for Eu in a distorted perovskite structure [8]. The intensity ratio between F_1 and F_2 band suggests that species C, with the more intense magnetic dipole transition (F_1), is centro-symmetric, while species C', with a more intense electric dipole transition (F_2) is not [8]. One tentative explanation for species C' might be, that after the very slow formation of the Eu-calcite in this experiment local ordering occurs around the Eu-incorporation species. Such an ordering effect has previously been proposed by a theoretical study, suggesting that the relevant $EuNa(CO_3)_2$ endmember, which might be used in a thermodynamic model to describe the formation of species C, should have a dolomite like ordered structure [9]. Whether the proposed ordering may explain the observed crystal field splitting remains, however, to be clarified.

In summary, we identified four Eu species in calcite (neglecting for now the initial species identified in the kinetic experiment). The characteristics of these species are listed in Table 1. In our opinion it is possible to integrate our new results with previous findings and to develop a comprehensive mechanistic picture of Eu^{3+} incorporation into calcite. We suggest that Eu^{3+} interaction starts with the formation of a broad distribution of surface or near surface incorporation species (species D). Depending on time, interfacial kinetics (background electrolyte), Eu^{3+} concentration and solid/liquid ratio (i.e. Eu^{3+} surface coverage) species D evolves towards more well defined species: a sharper band of species D itself (cf. Fig. 2 and [4, 5]) and incorporation species B and C. Species D, but also species B seem to have a transitional character. Upon very slow calcite precipitation (aragonite to calcite transformation) we observe solely the formation of Species C, maybe accompanied by local ordering (Species C'). Note that after recrystallization experiments we hardly ever observe mono-exponential fluorescence decay behavior. We interpret the short-lived components of species B and C as overlap with species D.

Previously reported Species A seems to reflect special conditions in coprecipitation experiments at moderate supersaturation (SI(calcite) between 0.6 (vaterite–calcite recrystallization [4]) and ~1 (MFR [2, 10])) and low Eu^{3+} surface coverage. In MFR experiments at elevated Eu^{3+} concentration (results not shown) we observe the formation of Eu-species with broad excitation peaks, similar to Fig. 1 and similar to the nitrate experiments by Hofmann et al.. Thus, we tend to interpret the formation of well-defined species rather as being related to Eu^{3+} surface coverage and interfacial kinetics. We cannot reproduce the previously reported special effect of nitrate (cf Fig. 2). Concerning the effect of Na^+ vs. K^+, we confirm that species C is likely the result of coupled substitution (2 Ca ↔ Na/K+Eu). However, we consider the statement that Eu^{3+} incorporation in calcite is favored in the presence of Na^+ a misinterpretation (especially emphasized in [11]). There seems to be a slight shift from species C to species B in the presence of K^+. According to results reported by Marques et al. the overall Eu^{3+} uptake in calcite is, however, even slightly higher in the presence of K^+ compared to coprecipitation in the presence of Na^+.

Finally, our results indicate that over geologic periods of time species C will be the relevant incorporation species. In natural systems, usually sufficient Na^+ should be available to provide charge compensation. Especially if it should be possible to confirm the local ordering of species C and the consequent formation of species C', we are confident that it will be possible to develop a thermodynamic model for this long-term incorporation process based on DFT double-defect calculations [9] and few additional experiments. On the other hand, concerning the short-term effects observed in sorption and coprecipitation experiments, it will remain a major challenge to develop a comprehensive quantitative model recovering the various species in the various experiments (cf. also [12]).

X-ray spectroscopic investigations on structural iron in clay minerals

The encapsulation of nuclear waste in thick-walled cast-iron containers will result in an iron inventory exceeding by far that of e.g., uranium. The presence of high iron inventories may ultimately result in corrosion/alteration products containing structural iron. Specifically, structural iron in clay minerals can have a significant impact on the redox- and sorption capacity of clay minerals. Studies aiming at investigating the chemical status of structural iron in various mineral phases have been initiated in the group. Below are preliminary results obtained for structural iron present in two clay minerals: hectorite, a magnesian smectite frequently detected in glass corrosion experiments (e.g., [13]), and nontronite which is a smectite of high iron content.

Experimental details

Hectorite ($Na_{0.33}[Li_{0.33}Mg_{2.67}Si_4O_{10}(OH)_2]$) and nontronite ($Na_{0.5}[Fe_{3.0}Si_{3.5}Al_{0.5}O_{10}(OH)_2]$) were purchased from the Source Clay Repository, purified and the fraction < 0.1 µm separated by sedimentation and centrifugation techniques. XRD and FTIR data

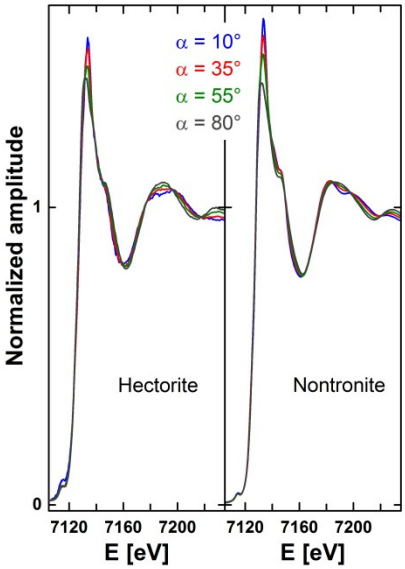

Fig. 5: *Experimental polarized XANES of hectorite (left) and nontronite (right).*

indicated the absence of any impurities. Both smectites were prepared as highly textured sample and the Fe local environment probed by polarized X-ray absorption spectroscopy at the INE beamline [14] at the synchrotron light source ANKA. Data were recorded considering various angles between the electric field of the X-ray beam and the clay layer plane (α = 10, 35, 55, 80°).

Results and interpretation

XANES can be used as fingerprint of the local chemical environment. The experimental XANES of hectorite differ from that of nontronite (Fig. 5) notably in the shape of the white line and in the first resonance centered at ~7200 eV, hinting at distinct short range environments. Both sets of polarized XANES exhibit clear angular dependences indicating that Fe is located in an anisotropic environment, and the decreasing amplitude with increasing angle α hints at an in-plane orientation of neighboring shells.

Both sets of polarized EXAFS spectra (Figure 6) exhibit significant angular dependences and contain several isosbestic points over the whole *k*-range. The spectra of hectorite differ from that of nontronite mostly in terms of position of the oscillation maxima, such as for example in the range $7 < k < 9$ Å^{-1}. Such frequencies as well as the change in oscillation maxima with increasing angle indicate the presence of backscattering shells located at different crystallographic positions within the structure.

The Fourier transforms (FT) also exhibit significant angular dependences (Figure 7). While the amplitude of the first contribution at $R + \Delta R$ ~1.7 Å decreases slightly, the increase in amplitude of the second FT peak of hectorite is remarkable. For nontronite, the amplitude of the first FT peak decreases and the amplitude of the second peak decreases while shifted to larger distances. This behavior indicates the presence of at least two atomic shells with distinct

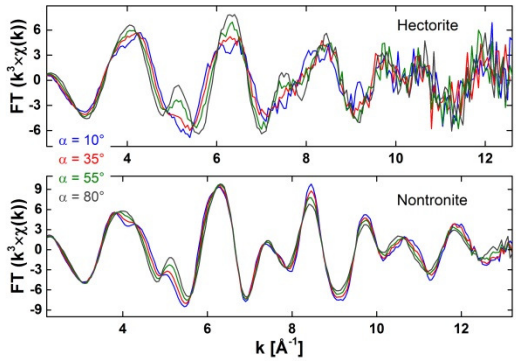

Fig. 6: *Experimental polarized EXAFS spectra of hectorite and nontronite.*

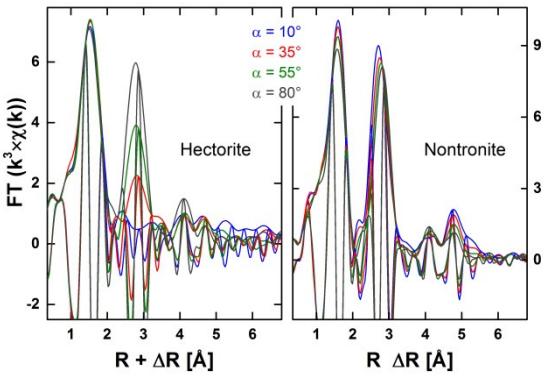

Fig. 7: *Experimental polarized Fourier transforms of spectra for hectorite (left) and nontronite (right).*

orientation, e.g., in-plane and out-of-plane orientation. For both smectites, the first FT peak is attributed to the first oxygen shell, preliminary fit results indicate the presence of 6 O atoms at ~2.00 Å. These fit results and the decrease in apparent coordination number with increasing angle are consistent with octahedral Fe^{3+} ions [15]. The next FT peak is due to contributions from neighboring octahedral and tetrahedral atoms. According to P-EXAFS, contributions in hectorite are significantly different from that in nontronite. Preliminary fit results indicate the presence of ~2 octahedral Mg and 4 tetrahedral Si atoms in hectorite. The low number of detected octahedral cations can originate either from a local dioctahedral environment or from an increased number of neighboring Li [16], an element too light to be detected by EXAFS spectroscopy. For nontronite, the detection of 3 octahedral Fe and 4 tetrahedral Si atoms agrees with earlier findings from Manceau et al. [15].

Further studies will focus on the characterization of structural iron as a function chemical composition of the octahedral and tetrahedral sheets.

References

[1] Lindqvist-Reis, P. et al., J. Phys. Chem. B, 110, (11), 5279-5285 (2006).
[2] Marques Fernandes, M. et al., J. Coll. Interface Sci., 321, 323-331 (2008).
[3] Kimura, T. et al., J. Alloys Comp., 213, 313-317 (1994).

[4] Schmidt, M. et al., J. Coll. Interface Sci., 351, (1), 50-56 (2010).
[5] Hellebrandt, S. et al., Sci. Rep., 6 (2016).
[6] Heberling, F. et al., Environ. Sci. Technol., 50, (21), 11735-11741 (2016).
[7] Ruiz-Agudo, E. et al., Geochim. Cosmochim. Acta, 75, (13), 3803-3814 (2011).
[8] Blasse, G. et al., J. Phys. Chem. Solids, 27, (10), 1587-1592 (1966).
[9] Vinograd, V. et al., Geochim. Cosmochim. Acta, 73, (13), A1386-A1386 (2009).
[10] Hofmann, S. et al., Geochim. Cosmochim. Acta, 125, 528-538 (2014).
[11] Schmidt, M. et al., Angew. Chem. Int. Edit., 47, (31), 5846-5850 (2008).
[12] Curti, E. et al., Geochim. Cosmochim. Acta, 69, (7), 1721-1737 (2005).
[13] Thien, B. et al., Appl. Clay Sci., 49, (3), 135-141 (2010).
[14] Rothe, J. et al., Rev. Sci. Instrum., 83, (4), 043105 (2012).
[15] Manceau, A. et al., Phys. Chem. Miner., 25, (5), 347-365 (1998).
[16] Finck, N. et al., Phys. Chem. Miner., 42, (10), 847-859 (2015).

5 Applied studies: Radionuclide behavior in the multi-barrier system

Long-term safety of a deep geological repository for nuclear waste depends on a multi-barrier system which consists of technical and geo-technical barriers such as the waste form, the canister, backfilling and sealing of the mined openings as well as on the natural barrier function of the host rock. At KIT-INE, a series of applied studies on subsystems of various multi-barrier systems are performed, which cover a variety of components with specific characteristics and properties. Investigations presented in the first sub-chapter cover the experimental quantification of radionuclide release from spent nuclear fuel under strongly reducing conditions and the determination of the chemical form of C-14 present in irradiated steel sampled from a fuel rod segment. In the following, we describe activities on preservation of know-how with respect to results of R&D in the field of radioactive waste management performed at the former Research Centre Karlsruhe / Kernforschungszentrum Karlsruhe. The third sub-chapter deals with formation of colloids and impact of colloids on radionuclide migration in various technical, geo-technical and geological barriers of a multi-barrier system. We report on results of experimental studies on long-term Lu incorporation into iron-(hydr)oxides phases, characterization of natural organic matter and interaction of natural organic colloids with radionuclides, erosion of compacted bentonite erosion and formation of bentonitic colloids, bentonitic colloids radionuclide sorption, and interactions of synthetic colloids with mineral surfaces. In addition to these experimental studies, modelling studies on coupled processes in the near-field of geological repositories are conducted. In the final sub-chapter, modelling studies on coupled processes at the concrete / clay interface with respect to a repository in an argillaceous host rock and the effect of fracture geometry on bentonite erosion with respect to a repository in a crystalline host rock are described.

5.1 Highly radioactive waste forms

E. González-Robles, M. Herm, N. Müller, M. Böttle, E. Bohnert, B. Kienzler, V. Metz

In collaboration with:

R. Dagan[a], D. Papaioannou[b]

[a] Karlsruhe Institute of Technology, Institute for Neutron Physics and Reactor Technology, Karlsruhe, Germany; [b] European Commission, Joint Research Centre, Karlsruhe, Germany

Matrix dissolution of spent nuclear fuel under H_2 overpressure in bicarbonate water

Introduction

In case of container failure in a deep geological repository for spent nuclear fuel (SNF), intruding water possibly gets into contact with the waste. Besides anaerobic corrosion of the container material and consecutive production of hydrogen, radionuclides will be released into the groundwater [1,2].

Initially a fast radionuclide release is expected to occur, which will include the release of fission gases and volatile radionuclides segregated at the gap between fuel and cladding, at fuel fractures and at grain boundaries. Simultaneously to the fast leaching of the so-called instant release fraction, a relatively slow dissolution of the fuel matrix will begin, resulting in the release of matrix-bound radionuclides. The matrix dissolution is a long-term process, which will continue after the fast leaching processes will have been ceased.

Dissolution of the fuel matrix will be affected both by the presence of molecular hydrogen and by water radiolysis. The later will result in the production of oxidizing radiolysis products (e.g. OH radicals and H_2O_2) in the micrometer scale vicinity of the fuel surface that might enhance the matrix dissolution, even if reducing conditions are expected to prevail within the near-field of the deep geological repository. The present study focuses on the impact of H_2 overpressure on the release of uranium and other matrix-bound radionuclides, in particular actinides. Therefore, the dissolution behavior of an irradiated UO_2 fuel with an average burn-up of 50.4 MWd/kg_{HM} was studied under deep geological repository conditions with a simulated near neutral pH groundwater and H_2 overpressure.

Spent nuclear fuel samples

The studied SNF samples were taken from the SBS1108 N0204 fuel rod segment, which was irradiated in the pressurized water reactor of the Gösgen nuclear power plant in Switzerland.

The irradiation was carried out in four cycles for a period of time of 1226 days with an average linear power rate of 260 W/cm and achieving an average burn-up of 50.4 GWd/t_{HM}. The fuel rod segment was discharged the 27th of May 1989 that implies a cooling time of 24 years before characterization and cutting of the segment.

Characteristic data of the studied SBS1108 N0204 fuel rod segment are given in [3,4]. Based on results of a puncturing test of the fuel rod segment, the fission gas release into the plenum of the segment was previously calculated to be 8.35% [4,5].

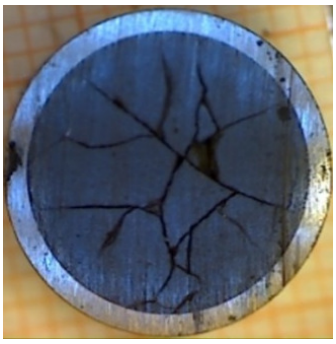

Fig. 1: *Bottom side of the cladded pellet used in the first SNF dissolution experiment.*

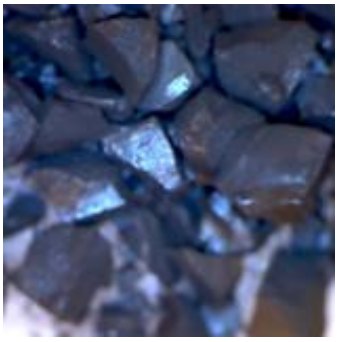

Fig. 2: *Fragments obtained from the decladding of a pellet used in the second SNF dissolution experiment.*

Sample preparation

Two cladded fuel pellets were cut from the fuel rod segment and were used in two leaching experiments. The complete sampling process is described elsewhere [4, 6].

The first leaching experiment was performed with a cladded pellet, whereas the second experiment was performed with SNF fragments. Therefore, the second pellet was decladded in order to get fragments and to separate the fuel from the Zircaloy (the cladding was not used during the leaching experiment).

Prior to the start of the experiments, both SNF samples were weighed. In the case of the cladded pellet, the length and diameter of the sample were measured too. The weight of the cladded pellet was (7.77 ± 0.01) g, the length (9.85 ± 0.01) mm with and external and internal diameter of (10.75 ± 0.01) and (9.35 ± 0.01) mm, respectively. The weight of the fuel without cladding was calculated to be (6.97 ± 0.01) g, taking into account the internal diameter) and the length of the fuel pellet. In case of the fragments, their total weight was (5.69 ± 0.01) g and the average size was determined to be 1 mm.

Images of the cladded pellet and the fragments used during the leaching experiments are given in figures 1 and 2.

Experimental set-up of leaching experiments

Both tests were conducted as static leaching experiments in 250 mL stainless steel Ti-lined VA autoclaves (Berghof Company, Eningen, Germany).

The composition of the bicarbonate leaching solution used in each of the experiments was as following: 19 mM NaCl + 1 mM $NaHCO_3$ with a pH of (8.9 ± 0.2) and $Eh_{(vs\ SHE)}$ of (-116.3 ± 50) mV.

The leachant for the two experiments was prepared in a glove-box under Ar atmosphere. The experiments themselves were carried out in an Ar / H_2 atmosphere with a total pressure of (40 ± 1) bar, with a partial pressure of H_2 of (3.2 ± 0.1) bar, at room temperature.

In the case of the experiment with the cladded pellet, the sample was mounted in a Ti sample holder to ensure the contact of the top and bottom surfaces of the pellet with the solution, whereas the fragments were kept in a glass basket.

Once the samples were placed into the autoclaves, they were closed and flushed with Ar to avoid any possible presence of air.

Afterwards, a pre-leaching test with duration of 1 day was performed by filling each autoclave with (220 ± 1) mL of the bicarbonate leaching solution mentioned above. This pre-leaching step was performed in order to reduce the amount of Cs in solution and to remove any pre-oxidation layer potentially present at the surface of the SNF samples. After the pre-leaching, a gas sample was collected and the solution was completely purged. Then each autoclave was again replenished with (220 ± 1) mL of bicarbonate solution as described above.

Gaseous (50 ± 1) mL and liquid (15 ± 1) mL samples were taken at certain time steps. After the sampling, the gas volume of the autoclaves was purged with Ar, and the initial conditions (40 bar of Ar + H_2 mixture) were again established. The solution was not renewed after sampling, thus the remaining leachant volume was reduced at each sampling step.

From the liquid samples obtained during each campaign different aliquots were prepared to determine the amount of ^{237}Np, ^{238}U, ^{239}Pu, ^{243}Am and ^{244}Cm as following: A (5.0 ± 0.1) mL aliquot was acidified and, subsequently, ammonium molybdate phosphate (AMP) was added to remove Cs by precipitation giving as a result a free Cs solution with a lower activity than the original one.

From this aliquot, (2.5 ± 0.1) mL were analyzed by means of Inductively Coupled Plasma Mass Spectrometry (ELAN 6100 Perkin Elmer Inc, Waltham, USA) to quantify ^{237}Np, ^{238}U, ^{239}Pu, ^{243}Am and ^{244}Cm dissolved in solution.

The pH and Eh of the samples were measured at the end of the four experiments to avoid possible air intrusion that in the case of the Eh measurement would have given unrealistic values. The device and the procedure followed is the same as stated in [7].

At the end of each experiment the pH was (8.7 ± 0.5) and the $Eh_{(vs\ SHE)}$ was (-518 ± 50) mV for the pellet and (-418 ± 50) mV for the fragments.

Results and Discussion

Aqueous concentrations of ^{237}Np, ^{238}U, ^{239}Pu, ^{243}Am and ^{244}Cm in both SNF dissolution experiments are shown in figures 3 and 4.

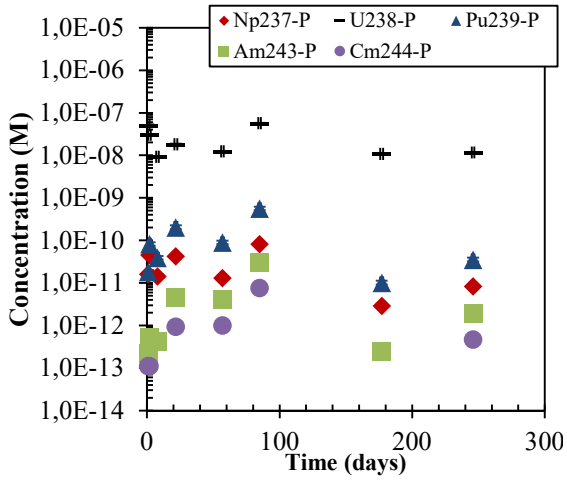

Fig. 3: *Aqueous concentrations of ^{237}Np, ^{238}U, ^{239}Pu, ^{243}Am and ^{244}Cm as a function of time in the dissolution experiment performed with a cladded SNF pellet.*

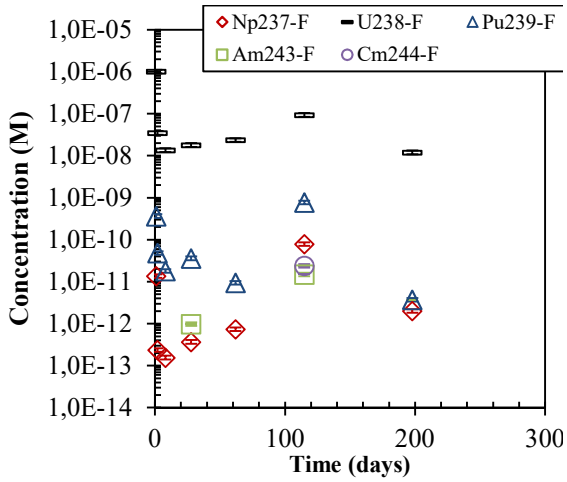

Fig. 4: *Aqueous concentrations of ^{237}Np, ^{238}U, ^{239}Pu, ^{243}Am and ^{244}Cm as a function of time in the dissolution experiment performed with SNF fragments.*

In order to interpret the measured radionuclide concentrations, thermodynamic calculations were performed using the PHREEQC program [8] and the ThermoChimie database [9]. These calculations were performed taking into account the measured pH, (8.7 ± 0.5) in both experiments, and the $Eh_{(vs\ SHE)}$, (-518 ± 50) mV for the experiment with the cladded pellet and (-418 ± 50) mV for the experiment with the fragments measured in solution at the end of both experiments.

As can be seen in figures 1 and 2, after a relatively high initial release the concentrations of ^{238}U decreases until approaching a virtually constant value at $1x10^{-8}$ M in both experiments. At the experimental pH and redox conditions, uranium is expected to be present as aqueous U(IV) species with low solubility controlled by a U(IV) solid in the long run. However, the relatively high initial release may be associated to the presence of oxidized layers on surfaces of the samples that release U(VI) to the solution.

According to the thermodynamic calculation U will be present in solution as $U(OH)_4(aq)$ as the predominant aqueous uranium specie and $UO_2{:}xH_2O(s)$ as the solubility controlling solid phase. The steady state reached in both experiments indicates that the uranium is not being released anymore from the SNF to the solution, this observation is related to the presence of H_2 in the system that will consume oxidants generated by water radiolysis, which could oxidize U(IV) on the SNF surface to more soluble U(VI) species. This effect has already been proposed by other authors [10-13].

In case of ^{237}Np, the concentration in both experiments was found stable at around $1x10^{-12}$ M. Similar to uranium, neptunium is a redox sensitive element. According to thermodynamic calculations, the predominant aqueous specie in solution is $Np(OH)_4$ in equilibrium with $NpO_2{:}xH_2O(s)$ as solid phase.

The concentration in solution of ^{239}Pu in both experiments does not exhibit an initial higher release. The concentration of plutonium in solution scattered in both experiments but apparently reached a steady state at about $1x10^{-11}$ M. Under these conditions, Pu is expected to be present in solution as Pu(III) with $Pu(CO_3)_3^{-3}$, $Pu(CO_3)_2^-$ and $Pu(CO_3)^+$ as the main aqueous species; the solid phase controlling the solubility is PuO_2.

Finally, the concentration of ^{243}Am and ^{244}Cm in the experiment performed with a cladded SNF pellet scattered from $1x10^{-13}$ M to $1x10^{-11}$ M around an average value of $1x10^{-12}$ M. In case of the experiment performed with SNF fragments aqueous concentration of ^{243}Am and ^{244}Cm could not be detected, because their concentrations were under the detection limit of the ICP-MS. According to our thermodynamic calculations, Am and Cm is expected to be present in solution as $Am(CO_3)_2^-$, $Am(CO_3)^+$, $Cm(CO_3)_2^-$, $Cm(CO_3)^+$ in equilibria with their respective solid phases $Am_2O_3(s)$ and $C\ m_2O_3(s)$.

Quantification and speciation of ^{14}C from irradiated metals

Introduction

The activation product ^{14}C is produced by neutron capture reactions during reactor operation from precursor elements (^{14}N, ^{17}O, and ^{13}C) present as impurities in metallic parts of nuclear fuel assemblies.

In safety analysis of deep geological repositories for spent nuclear fuel, ^{14}C must be considered due to its long half-life (~5730 years) and assumed mobility after release from the waste. Corrosion of the emplaced steel components of fuel assemblies possibly releases ^{14}C bearing volatile and/or dissolved compounds. Organic ^{14}C bearing compounds reveal a high mobility either in the aqueous or in the gaseous phase whereas volatile/dissolved inorganic ^{14}C bearing compounds are affected by various retention processes in the near-field of a repository.

In this study, the inventory of ^{14}C present in irradiated stainless steel is determined. Furthermore, the

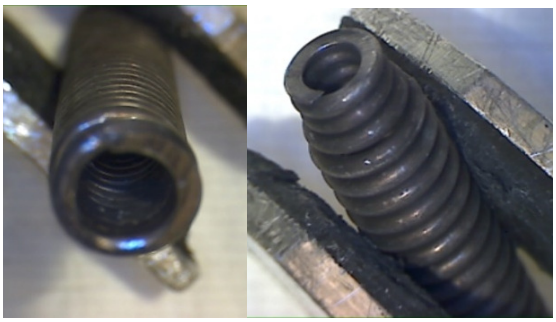

Fig. 5: *Images of the irradiated stainless steel plenum spring.*

chemical form of ^{14}C released from the steel is analyzed. Experimentally measured radionuclide contents are compared to theoretically predicted inventories of the irradiated steel, obtained by means of Monte Carlo N-Particle calculations (MCNP-X).

Stainless steel sample origin, irradiation characteristics, and subsample preparation

The studied stainless steel spring was sampled from the plenum of fuel rod segment N0204 of the fuel rod SBS1108. The characteristics of the irradiation of the fuel rod were described in the previous section.

Images of the 10.422 g heavy plenum stainless steel spring are given in figure 5. The plenum spring is made of X7CrNiAl17.7, and had a dose rate of ~1600 mSv/h in contact.

Subsamples for dissolution experiments were dry cut using an IsoMet® Low Speed Saw (11-1180, Buehler Ltd.) equipped with an IsoMet® diamond wafering blade (11-4254, Buehler Ltd.). Cutting was performed very slow (5 - 10 hours per sample) to prevent overheating of the material. Three subsamples with masses ranging from (47 ± 0.2) mg to (356 ± 0.2) mg were prepared by remote handling in a shielded box. Masses and dose rates were measured using an analytical balance and a dose rate meter. Dose rate of the subsamples was typically less than 230 mSv/h. Due to the high dose rate of the subsamples, also dissolution experiments had to be performed in a shielded box.

Dissolution of irradiated stainless steel subsamples

A stainless-steel specimen was placed in an autoclave equipped with a PTFE liner and a double-ended gas-collecting cylinder. The autoclave was flushed with argon for about 20 minutes. A mixture of 150 mL 24% H_2SO_4 + 3% HF was added through a tube using a syringe. After the addition, all valves in the lid of the autoclave were closed. The sample was digested within a day. However, to ensure complete digestion, sampling of the gaseous and aqueous phase was performed on the following day. Photos of the experimental set-up are shown in figure 6.

The evacuated gas-collecting cylinder was opened and the gas phase collected within two minutes. Finally, the autoclave was opened and the digestion liquor was sampled. The gas-collecting cylinder was removed from the shielded box and the collected gas phase was analyzed by means of a multipurpose mass spectrometer with customized gas inlet systems (GAM 400, InProcess Instruments). Aliquots of the digestion liquor (after dilution due to dose rate) as well as the remaining gas phase in the gas collecting cylinder were also analyzed for ^{14}C in the extraction and analysis system installed in a glove box, as described in detail elsewhere [14]

Activation calculation for stainless steel radionuclide inventory prediction

The activation of the stainless-steel plenum spring was calculated by means of MCNP-X with its burn-up and activation module CINDER [15]. The nuclear data library used was the ENDF/B-VII database [16]. The simulation is based on a fuel subassembly of the PWR Gösgen core in which the fuel rod segment SBS1108-N0204 was inserted. Since the MCNP-X transport code evaluates the neutron flux of the subassembly, the input parameters include geometrical shape, material composition, and irradiation characteristics etc. of the subassembly. The obtained zone and energy dependent fluxes are forwarded to CINDER allowing for enhanced accuracy of the reaction rates evaluations upon which the activity of the relevant nuclides is determined. The properties of the plenum spring (mass, density, and dimensions) were accounted for in such a way it will include as much as possible all heterogeneity effects around the fuel rod segment. Thereby, the local neutron flux within the plenum could be simulated more accurately.

Since the exact composition of the stainless-steel spring is not available, nominal chemical composition data was used for simulation of the neutron flux and consequently for the activation calculation.

Results of experimental inventory analysis of irradiated stainless steel and chemical form of ^{14}C released from the studied material

Mean values of the experimentally determined ^{14}C inventory of the irradiated stainless steel plenum

Fig. 6: *Autoclave for dissolution experiments, loaded with a steel specimen, inside a shielded box. The gas-collecting cylinder is not yet connected to the autoclave.*

Tab. 1: *Mean value of the experimentally determined inventory of ^{14}C in comparison with results from the activation calculation performed in this study.*

	experimental [Bq/g]	calculated [Bq/g]	ratio
^{14}C	$2.7(\pm0.3)\times10^{5}$	$8.5(\pm0.9)\times10^{4}$	3.2

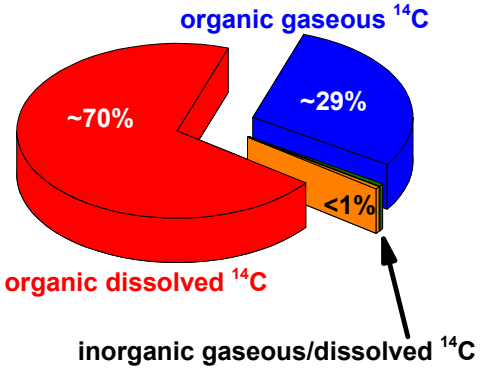

Fig. 7: *Distribution of inorganic and organic ^{14}C bearing compounds in the gaseous and aqueous phase.*

spring are summarized in Table 1. The experimentally determined ^{14}C inventory is further compared to theoretically predicted inventory obtained by MCNP calculations. Experimental and calculated results agree within a factor of about three. Given the limited knowledge of the nitrogen impurity in the irradiated steel and the great uncertainty of nitrogen contents in stainless steel in general (from 0.04 to 0.1 in weight % [17]), the experimental results obtained in the digestion experiments for ^{14}C is in good agreement with the calculated value. Experimental ^{14}C inventory in irradiated stainless steel, recently assessed by [17], exceeds the calculated value by a factor of four. It is noticeable that in both studies the experimentally determined inventory exceeds the calculated inventory by similar factors.

Moreover, about 99% of the ^{14}C is found as gaseous or dissolved organic ^{14}C bearing compounds after release from steel. These results are in accordance with results obtained on the chemical form of ^{14}C after release from irradiated Zircaloy-4 cladding [14]. The partitioning of ^{14}C bearing compounds in inorganic and organic fractions and their distribution in the gaseous and aqueous phase is provided in figure 7.

About (70 ± 10)% of the ^{14}C inventory present in irradiated stainless steel is released as dissolved organic ^{14}C bearing compounds in the acidic digestion liquor. About (29 ± 10)% of the ^{14}C inventory is released as gaseous ^{14}C bearing compounds during dissolution into the gas phase. Almost no inorganic ^{14}C bearing compounds (< 1%) are found in all experiments neither in the gaseous nor in the aqueous phase.

References

[1] Johnson, L., Ferry, C., Poinssot C., Lovera, P. *J. Nucl. Mater.*, 346, 56-65(2005).

[2] 24. Metz, V., Geckeis, H., González-Robles, E., Loida, A., Bube, C., Kienzler, B., *Radiochimica Acta.,* 100, 699-713 (2012).

[3] Metz, V., González-Robles, E., Kienzler, B., KIT Scientific Reports, Karlsruhe KIT-SR 7676, 55-60 (2014).

[4] González-Robles, E., Wegen, D. H., Metz, V, Herm, M., Papaioannou, D., Bohnert, E, Gretter, R., Müller, N., Nasyrow, R., der Weerd, W., Wiss, T., Kienzler, B. *J. Nucl. Mater.,* 479, 67-75 (2016).

[5] González-Robles, E., Wegen, D. H., Bohnert, E, Papaioannou, D., Müller, N., Nasyrow, R., Kienzler, B., Metz, V. *Mat. Res. Soc. Symp. Proc.,* 1665, 283-289 (2014).

[6] Wegen, D.H., Papaioannou, D., Gretter, R., Nasyrow, R., Rondinella, V.V., Glatz, J.-P. KIT-SR 7639, 193-199 (2013).

[7] Loida, A., Gens, R., Metz, V., Lemmens, K., Cachoir, C., Mennecart, T., Kienzler, B. *Mat. Res. Soc. Symp. Proc.,* 1193, 597-604 (2009).

[8] Parkhurst, D.L. and Appelo, C.A.J. U.S. Geological Survey Techniques and Methods, book 6, chap. A43, (2013).

[9] Giffaut, E., Grivé, M., Blanc, P., Vieillard, P., Colàs, E., Gailhanou, H., Gaboreau, S., Marty, N., Madé, B., Duro, L. (2014).. *Appl. Geochem.,* 4, 225-236 (2014).

[10] Spahiu, K., Werme, L., Eklund, U.-B. *Radiochim. Acta*, 88, 507-511(2000).

[11] Röllin, S., Spahiu, K., Eklund, U.-B. *J. Nucl. Mater.*, 297, 231–243(2001).

[12] Loida, A., Metz, V., Kienzler, B., Geckeis, H. *J. Nucl. Mater.*, 346, 24–31(2005).

[13] Fors, P., Carbol, P., Van Winckel, S., Spahiu, K. *J. Nucl. Mater.*, 394, 1-8 (2009).

[14] Herm, M. PhD thesis. Karlsruhe Institute of Technology (KIT), Karlsruhe, 2015.

[15] Pelowitz, D.B. LA-CP-11-00438 (2011).

[16] Chadwick, M.B., Herman, M., Oblozinsky, P., Dunn, M.E., Danon, Y., Kahler, A.C., Smith, D.L., Pritychenko, B., Arbanas, G., Arcilla, R., Brewer, R., Brown, D.A., Capote, R., Carlson, A.D., Cho, Y.S., Derrien, H., Guber, K., Hale, G.M., Hoblit, S., Holloway, S., Johnson, T.D., Kawano, T., Kiedrowski, B.C., Kim, H., Kunieda, S., Larson, N.M., Leal, L., Lestone, J.P., Little, R.C., McCutchan, E.A., MacFarlane, R.E., MacInnes, M., Mattoon, C.M., McKnight, R.D., Mughabghab, S.F., Nobre, G.P.A., Palmiotti, G., Palumbo, A., Pigni, M.T., Pronyaev, V.G., Sayer, R.O., Sonzogni, A.A., Summers, N.C., Talou, P., Thompson, I.J., Trkov, A., Vogt, R.L., van der Marck, S.C., Wallner, A., White, M.C., Wiarda, D., Young, P.G. Nucl. Data Sheets, 112, 2887-2996 (2011).

[17] Schumann, D., Stowasser, T., Volmert, B., Günther-Leopold, I., Linder, H.P., Wieland, E. *Anal. Chem.*, 86, 5448-5454 (2014).

Acknowledgement

The research was partially funded by the European Union's Seventh Framework Program for research, technological development and demonstration under grant agreement no. 604479, the CAST project.

5.2 Preservation of know-how on R&D activities in the field of radioactive waste management

B. Kienzler

Since 1976, when the fourth modification of the German atomic law (ATG) passed the Bundestag, the polluter-pays principle was fully accepted. Scientists, engineers and politicians assumed that the questions concerning the disposal of nuclear waste could be resolved within one generation, which means that those who benefitted from nuclear power should pay for the back-end. Over time, societal, political and scientific views to the problem of nuclear waste disposal changed significantly. Finally, the report of the "Kommission Lagerung hoch radioaktiver Abfallstoffe" [1] proposed a way forward which requires preservation of knowledge and know-how for many decades. For this reason, an attempt was made to view and summarize the results of R&D performed at the former Kernforschungszentrum Karlsruhe (KfK) / Nuclear Research Centre Karlsruhe. Many of the R&D outcomes were not published in regular journals, but in conference proceedings, internal reports and other hidden documents. The studies covered following aspects:

- R&D activities in the field of nuclear waste management and disposal at the Kernforschungszentrum Karlsruhe [2, 3]. The retrospective analysis of nuclear waste management research programs clearly points to the close relationship of research priorities with changes in societal and political perception of nuclear energy and nuclear waste issues.
- A re-evaluation of results of corrosion studies for disposal casks. In this study, the corrosive mass losses of different metallic and ceramic materials under saline conditions were summarized [4]. This report is based on numerous publications but also on the availability of the database of more than 7000 experimental data sets including details of the various long-term experiments. Most of the immersion test were performed at temperatures above 90°C up to more than 600 days.
- Treatment of liquid highly radioactive wastes, discussing the vitrification processes and other options. The report covers the R&D performed in Germany, Europe, USA, Russia and Australia and the discussions and decisions leading to the selection of borosilicate glass. The vitrification process developed by INE resulted in the single stage directly heated ceramic melter technology which was implemented and successfully operated in the VEK plant for the solidification of the high-level waste from the WAK [5]. Comparisons with other solidification processes (phosphate glass, glass ceramics or Synrock) are shown, as well as the international methods for comparing the quality of the waste products.
- Organic matrices for solidification of low/intermediate level waste streams. This waste stream was generated in Germany: 2% of the wastes in the Asse II salt mine consist of bituminized waste forms. Additionally, 185 tons of solidified organic waste forms are waiting to be disposed. The report provides an overview of the use of organic matrices, such as bitumen, polyethylene, and other plastics in various fields of nuclear technology, the process technologies and provides characteristic mechanical, chemical and radiological data as well as data on leaching behavior of these waste forms [6].

References

[1] Kommission Lagerung hoch radioaktiver Abfallstoffe, Abschlussbericht: Verantwortung für die Zukunft: Ein faires und transparentes Verfahren für die Auswahl eines nationalen Endlager-standortes. K-Drs 268, 2016.

[2] B. Kienzler, 50 Jahre Forschungs- und Entwicklungsarbeiten zur Endlagerung im KIT. Karlsruhe Institute of Technology, KIT SR 7723, 2017.

[3] B. Kienzler and H. Geckeis, 50 years of research and development for nuclear waste disposal at KIT, presented at the 2nd Conference on Key Topics in Deep Geological Disposal, Cologne, 26 – 28 September, 2016.

[4] B. Kienzler, F&E-Arbeiten zur Korrosion von Endlager-Behälterwerkstoffen im INE (SR 7729, 2017).

[5] B. Kienzler, Flüssige hochradioaktiver Abfälle: Verglasung und andere Optionen. (SR 7730., 2017).

[6] B. Kienzler, Schwach- und mittelradioaktive Abfälle: Organische Matrices. (SR 7731, 2017).

5.3 Colloid impact on radionuclide migration

M. Bouby, K. Dardenne, G. Darbha, N. Finck, F. Geyer, S. Heck, F. Huber, U. Kaplan, C. Marquardt, R. Polly, F. Quinto, Th. Rabung, F. Rinderknecht, Th. Schäfer, D. Schild, M. Stoll, T. Yokosawa

In co-operation with:

S. Brassines[a], M.A. Denecke[b], J. Haigh, E. Prestat[c]

[a]ONDRAF/NIRAS, Bruxelles, Belgium; [b]Dalton Nuclear Institute, University of Manchester, United Kingdom; [c]School of Materials, University of Manchester, United Kingdom

Introduction

Aquatic colloids / nanoparticles (NPs), *i.e.* nanoscopic solids of organic or inorganic nature in the size range from ~1 nm up to ~1 µm remaining suspended in water [1], are known to be ubiquitous in natural groundwater (up to 10^6 part./mL in surface fresh waters). They are continuously generated by multiple physico-chemical processes (inter alia erosion, nucleation / precipitation, …) [2]. Naturally occurring nano suspended material (organic detritus, iron and aluminosilicate oxi/hydroxide…), residues and transformation products of alteration and corrosion processes of the multi barrier system (i.e. waste matrix, geotechnical and geological barriers) may potentially contribute to the migration of radionuclides towards the biosphere [3,4].

Long-term safety being a pre-requisite to any deep geological nuclear waste repository (DGR), performance assessment has to consider which parameters to take into account for reliable predictions. To state if the presence of colloids is one of them and to define the boundary conditions for the colloid relevance are our objective.

Our current activities deal with 1) the detection and the identification of the relevant NPs forming or existing in repository specific areas, 2) the control of their stability as a function of geochemical parameters, 3) the thermodynamics and kinetics description of their interaction with radionuclides, 4) the elucidation of their interaction with mineral surfaces and 5) the quantification of the colloid mobility. To do that, from the near-field to the far-field, we are combining laboratory and in-situ migration experiments which need the use and development of highly sensitive and sophisticated analytical techniques. The final goal is to implement our experimental data into reactive transport modelling codes (see following subchapter).

Our work is conducted with the support and in close collaboration with international nuclear waste management agencies (ONDRAF / NIRAS, Belgium; NAGRA, Switzerland), in the framework of several projects like the BMWi project HATT-2 (duration 2012 - 2013), the European FP7 CP-Belbar project and BMWi project KOLLORADO-e (durations 2013-2016) closely related to the international Colloid Formation and Migration (CFM) project performed in the Grimsel Test Site (GTS) in the frame of the investigation Phase VI.

According to the waste matrix (in particular HLW glass), steel container, backfill material (e.g. compacted bentonite) and the host rock selected (i.e. argillaceous, crystalline or saline host rocks) various colloids/nanoparticles might form and play a role which have to be examined individually. This year, in the present report we highlight some specific studies related to that question.

Long-term Lu incorporation into iron (hydr)oxide phases

Iron (hydr)oxides, widespread in nature, can play an important role in the bioavailability and migration of pollutants, such as heavy metal ions or radionuclides. Ferrihydrite and its transformation products (hematite and goethite) are commonly found in nature. In DGR sites, iron (hydr)oxides are also expected to form upon steel canister corrosion and can thus serve as sinks for radionuclides, either by surface adsorption and/or by structural incorporation. In this study, 2-line ferrihydrite was freshly synthesized, Lu(III) used as homologue for trivalent actinides was added to the suspension which was then aged for 12 years under ambient conditions in the dark. Previous characterization started by applying transmission electron microscopy (TEM) with high efficiency energy dispersive X-ray spectroscopy (EDX) and probe-side aberration corrected high-angle annular dark field STEM (HAADF-STEM) on the individual hematite NPs and

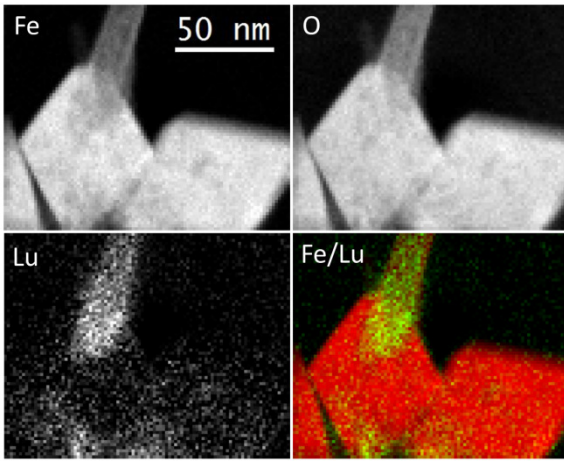

Fig. 1: *EDX spectrum images of hematite particles and goethite needle. Fe and Lu distributions in the overlapped image (Fe/Lu) are indicated by red and light green, respectively.*

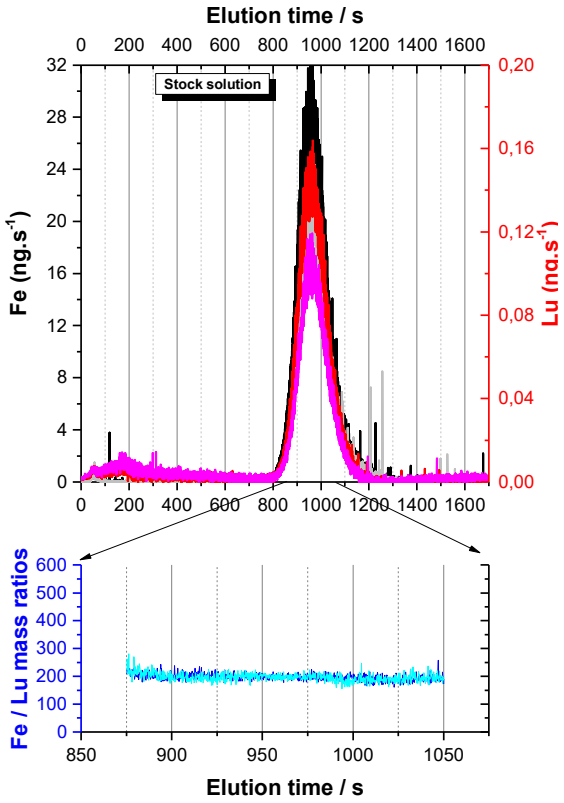

Fig. 2: *AsFlFFF-ICP-MS data, Fe- and Lu-ICP-MS fractograms, two successive injections of the stock suspension.*

the goethite needles grown on them (Fig. 1, [5]).

It was completed by using extended X-ray absorption fine structure (EXAFS) spectroscopy and Asymmetric Flow Field-Flow Fractionation (AsFlFFF) coupled to UV-Vis. and ICP-MS techniques [6] while modeling was done by density functional calculations (DFT) [5]. AsFlFFF/UV-vis./ICP-MS results confirm the size obtained previously [5] and indicate a clear correlation between the Fe and Lu signals which strongly hinted to a structural incorporation (Fig. 2).

EXAFS was used to further characterize the binding mode and to identify the host phase. The results do not evidence any surface adsorption or incorporation within hematite, but rather that Lu very likely substitutes for Fe within goethite. Consequently, a very consistent picture is obtained by the complementary use of different analytical techniques strongly suggesting that Lu atoms mainly associated with the goethite NPs, where they are occupying (substituting) Fe sites. Results from DFT calculations indicate that Lu incorporation within the goethite or hematite structures are almost equally likely, suggesting that experimental conditions may play an important role.

Accordingly, demonstration has now been done of the possible sequestration over years of trivalent element. In case of effective mobilization, these NPs might transport radionuclides towards the biosphere. Their potential role has thus to be considered.

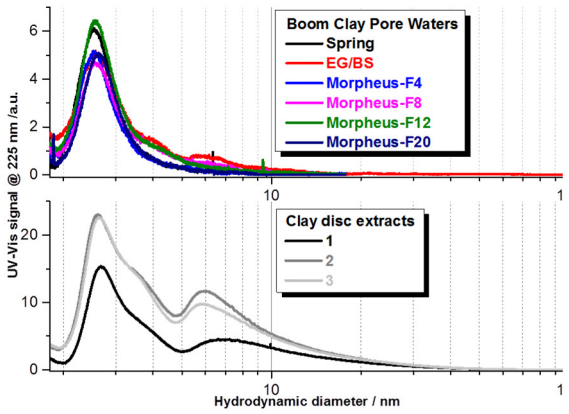

Fig. 3: *UV-fractograms converted in hydrodynamic diameter according to a calibration of the system performed by using PSS standards and carboxylated polystyrene nanoparticles.*

Characterization of natural organic matter derived from different layers within the Boom Clay formation and their radionuclide interaction

In Belgium, deep geological disposal of nuclear waste is envisaged by ONDRAF/NIRAS in poorly indurated clay formations like the Boom Clay (BC) or Ypresian clays (http://www.ondraf-plandechets.be). These host rocks have favorable intrinsic properties promoting the retention of radionuclides (low hydraulic conductivity, reducing redox capacity, slightly alkaline character, high specific surface area, cationic exchange capacity and plasticity). Organic material (OM) is present in 1 to 5% wt in BC [7]. To complement the Belgian research program conducted so far, our program work focuses on the determination and characterization of the mobile size fraction of dissolved organic matter (DOM) currently present and to be expected within the lifespan of the repository (i.e., taking into account the possible geochemical evolution). Here we report on the size distribution and natural metal association determination of 1) current BC pore water DOM and 2) DOM released from solid clay samples. The pore waters and solid clay samples comes from the HADES underground research laboratory (URL) (Mol, Belgium) and are representative of different horizons of the Boom Clay formation under present-day conditions (i.e., 15 mM $NaHCO_3$), see [8] for details.

Highly sensitive and complementary analytical, imaging and spectroscopic techniques have been used on the original samples or their isolated size fractions, see [8] for details.

The data presented first are those obtained by using the AsFlFFF/UV-Vis./ICP-MS. The present results show a relative OM size homogeneity (Fig. 3): Small size OM fractions (< 10 nm) are found in all natural pore waters and in the leached samples but with various relative quantities.

In the BC pore waters, several elements like Mg, Al, Fe, Mn, Sr, Y and a part of the lanthanides (Lns) and actinides (Ans, e.g. U, Th) are associated with the OM. In the leached extract, the Lns and Ans are mainly detected in bigger sized fractions (4 - 30 nm), the nature of which remains to be identified.

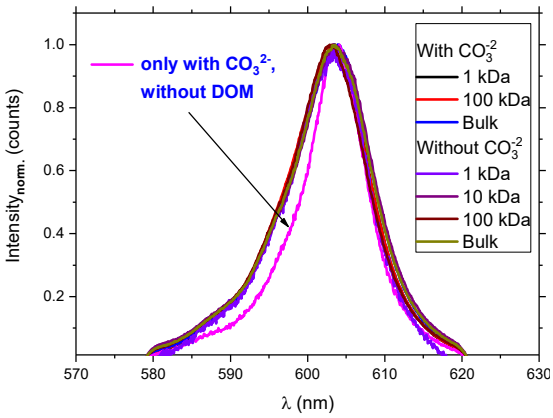

Fig. 4: *Compilation of the Cm(III) fluorescence spectra in the EG/BS sample in the presence and absence of carbonate recorded by the "indirect excitation" method. The spectra are scaled to the same peak height. The spectra obtained in the absence of DOM is also added.*

Complexation properties have been examined by using the time resolved laser induced fluorescence spectroscopy (TRLFS) applied to Cm(III) ions as representative of trivalent actinides. The two pore waters investigated (Morpheus-F20 and EG/BS) contain two types of strongly complexing ligands: DOM and carbonates. Indirect excitation measurements allow to elucidate the Cm(III) speciation. It is concluded that the Cm(III)-DOM complexes are the dominant species and no ternary complexes (e.g. Cm(III)-carbonato-DOM) are formed. In addition, it can be concluded after examination of specific DOM size fractions isolated by ultrafiltration, that their binding properties are identical or at least very similar, as illustrated exemplary Fig. 4 for one of the BC pore water investigated (EG/BS).

To better characterize and understand the behavior of the BC OM, one has now to concentrate on its origin, on the long-term stability of the leached or fractionated BC OM and on the reversibility of the metal ion complexation process.

Experiments on compacted bentonite erosion and colloid formation at the bentonite pore water interface

In present DGR concepts, low permeability swelling clay material is surrounding the HLW products. Besides acting as a transport vehicle for contaminants, colloid release / bentonite buffer erosion is an issue with respect to the long-term integrity of the geotechnical barrier. Bentonite erosion experiments have been an important component within the Kollorado-e [9] and BelBar projects (http://skb.se/belbar). Erosion processes have been simulated under dynamic but rather stagnant flow conditions simulating repository post-closure conditions. To better understand the FEBEX and MX-80 bentonite erosion behavior, systematic variation of the compaction density, chemistry of the contact water (ionic strength (IS), pH value, cation composition), contact surface and angle, and type of bentonite (raw material or homo-ionic Na/Ca form) was performed. Results were compared with modeling approaches. Experiments performed in the laboratory with two different setups [10,11] evidence the erosion (clay colloid detachment) whatever the clay composition. For the raw material, three phases can be identified: 1-washing of loosely bound particles, 2-dissolution of accessory minerals and 3-erosion. Remarkably, comparable colloid concentrations (< 2 mg/L) and erosion rates have been reported. The erosion rate for natural FEBEX bentonite in Grimsel ground water is 71.0 ± 20.1 g/m²/y and for natural MX-80 bentonite in a synthetic low glacial melt ground water is 51 ± 7 g/m²/y. More details in [10,11]. In the so-called Long Term In-situ Test (LIT) performed at the GTS, a bentonite source was emplaced in a water conducting feature. After 1 year, colloid concentrations < 1 mg/L have been reported in the effluent samples. These values are consistent with those obtained in the laboratory. Experiments are still on-going.

Colloid stability under specific conditions

Once produced, bentonite clay colloids have to be stable under relevant geochemical conditions to play a role. Numerous experiments have been carried out on that topic over the past years and research programs (CFM&Kollorado, Kollorado-2, Kollorado-e, BelBar). The stability has been proven in NaCl media, up to 0.1 M, whatever the bentonite material considered as clay colloidal source. On the opposite, the presence of divalent cations destabilizes the clay colloids. While numerous studies have been conducted over a rather short time period (fast coagulation) only few are reported over period of more than 1 year [12]. In that case, agglomeration has been reported even under geochemical conditions where colloids are supposed to be highly stabilized. To confirm this observation, a systematic study has been initiated in the frame of the BelBar project. Clay colloid suspensions have been prepared at different concentrations, at two pHs (~6 and 8.4), in various electrolytes at fixed ionic strength (10^{-3} M), in presence or not of organic matter (i.e. fulvic acids (FA)). The few samples tested after 4 years aging confirm previous results with a gradual agglomeration. A complete analysis is planned in 2018.

In the frame of the BMWi HATT-2 project [13], the stability of FA has been tested in very high ionic strength media simulating saline solutions eventually present in rock salts formations. The results demonstrate the high stability of this small sized organic matter up to 5 M IS NaCl and 3 M IS $CaCl_2$/$MgCl_2$, i.e. the FAs remain suspended (less than 10% variation of the dissolved organic concentration (DOC) reported). In addition, conformational changes have been evidenced leading to an increase of their size but their mobility might be preserved.

Concerning the BC OM previously characterized (see above), an increase of salinity evidences a dissociation and a coagulation of the different fractions. The largest sizes fractions tend to coagulate under

high IS. On the opposite, the smallest sized fractions dissociate for IS > 0.5 M. As usually observed, divalent cations such as Ca^{2+} have a more pronounced effect than monovalent cation such as Na^{+}.

Colloids interaction with mineral surface

While adsorption of colloids on rock surfaces has been attributed to electrostatic interactions, contradictory results evidenced colloidal adsorption even under unfavorable (repulsive) conditions. Migration processes have thus to be investigated in more details by looking at the deposition of colloids onto mineral surfaces. In a recent study [14], the impact of gravity, collector surface roughness and fracture orientation on colloid retention kinetics in an artificial fracture has been examined. It appears clearly that the behavior of bigger sized colloids (1000 nm carboxylated polystyrene nanoparticles) is dominated by the gravity and not affected by the mineral surface (granodiorite from Grimsel, Switzerland) roughness. On the opposite, smaller sized nanoparticles (25 nm carboxylated polystyrene nanoparticles) are not subject to sedimentation under the present experimental conditions (pH 5, 1 mM NaCl IS, 7 mL/h laminar flow) but impacted by surface inhomogeneities such as surface roughness.

Bentonite colloids-radionuclides sorption and reversibility

Radionuclides sorption and reversibility studies are on-going, under realistic conditions (pore water and glacial melt water) and long contact time periods (more than 5 years). The aim is to determine radionuclides kinetics rates which are necessary to simulate the field and laboratory experiments when inserted into transport codes. The role played by organic matter or fracture filling material (FFM, consisting mainly of fault gouge) is scrutinized. Batch radionuclides sorption / desorption studies on fault gouge material from Grimsel Test Site have been conducted (PhD work of F. Rinderknecht, 2017). Sorption kinetics rates have been derived by fitting when possible. ^{242}Pu shows the fastest kinetics closely followed by ^{243}Am and ^{233}U, while ^{237}Np present a lower rate of one order of magnitude. No fitting was possible for ^{99}Tc due to its weak interaction with FFM. Kinetics rates for desorption have been fitted using both 1-rate and 2-rate exponential equation approach revealing a simple sorption / desorption process (for ^{242}Pu and ^{243}Am) or a more complex coupled sorption / reduction process (for ^{237}Np).

For in-situ experiment performed at the GTS, the application and further development of Accelerator Mass Spectrometry (AMS) [15] offered new opportunity. AMS does not provide direct information on the association of actinides with colloids and neither on their speciation, however due to its extreme sensitivity, it has enabled to study the long term release and retention of the actinide tracers within the system of groundwater – bentonite colloids – fault gouge minerals at the GTS. Recent investigations consisted in sampling the tailing of the breakthrough

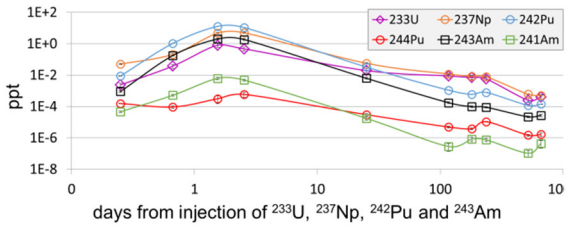

Fig. 5: *Concentrations expressed in ppt of ^{233}U (violet rhombuses), ^{237}Np (orange circles), ^{242}Pu (blue circles), ^{244}Pu (red circles), ^{243}Am (black squares) and ^{241}Am (green squares) determined with AMS in selected samples of CFM run 13-05.*

curve over a period of eight months and more which definitely provided additional details on the sorption / desorption processes / kinetics of the fault gouge. Both in the *in situ* test CFM run 12-02 and CFM run 13-05, AMS has been employed as analytical technique complementary to SF ICP-MS in order to investigate ultra trace levels of actinide nuclides in the Grimsel groundwater samples. In fact, as depicted in Fig. 5, concentrations of ^{233}U, ^{237}Np, ^{242}Pu, ^{244}Pu, ^{243}Am and ^{241}Am have been determined down to values of ca. 1 x 10^{-7} ppt in samples collected in the tailing of the breakthrough curve of run 13-05. Details on the analytical method as well as the outcome of the study are given in references [15] and [16].

References

[1] Honeyman, B.D., Nature, 397, 23-24, (1999)

[2] Stumm, W. et al., Aquatic Chemistry: chemical equilibria and rates in natural waters, 3rd. Ed., John Wiley & Sons, USA, 1996.

[3] Kim, J.I., Radiochim. Acta, 52/53, 71-81 (1991)

[4] Schäfer, Th. Et al., Appl.Geochem, 27, 390-403, (2012)

[5] Yokosawa, T. et al., Fate of Lu(III) sorbed on 2-line ferrihydrite at pH 5.7 and aged for 12 years at room temperature. II: Insights from STEM-EDXS and DFT calculations (to be submitted to JCIS, 2017).

[6] Finck, N. et al., Fate of Lu(III) sorbed on 2-line ferrihydrite at pH 5.7 and aged for 12 years at room temperature. I: Insights from ICP-OES, XRD, ESEM, AsFlFFF/ICP-MS and EXAFS spectroscopy (to be submitted to JCIS, 2017).

[7] Bruggeman, C. et al., Boom clay natural organic matter. Status report 2011, SCK.CEN-ER206, External report, 2012

[8] Kaplan, U. et al., KIT-internal report 04/2016, 20004085

[9] Huber, F. et al. Project Kollorado-e final report, DOI: 10.5445/IR/1000059756

[10] Rinderknecht, F. et al., Bentonite erosion and colloid mediated transport of radionuclides in advection controlled systems (to be submitted to Applied Clay Science, 2017)

[11] M. Bouby et al., Colloid generation from compacted raw or homo-ionic MX80 bentonite in a low ionic strength carbonated synthetic

(ground)water under quasi stagnant flow conditions: Erosion rates and propagation front determination (to be submitted to Applied Clay Science, 2017)
[12] Bouby, M. et al., Geochim. Cosmochim. Acta, 75, 3866-3880, (2011)
[13] Marquardt, C. et al., HATT-2 final report, in print (2017)
[14] Stoll, M. et al., J. Coll. Int. Sci, 475, 171-183, (2016)
[15] Quinto, F. et al., Anal. Chem, 87, 5766-5773, (2015)
[16] Quinto, F. et al.; (to be submitted to Anal. Chem, 2017).

5.4 Reactive transport modeling

V. Montoya, F. Huber, D. Leone, N. Ait Mouheb, M. Trumm, T. Schäfer, V. Metz

Introduction

Advanced numerical methods are needed to quantitatively assess and predict radionuclide migration and geochemical evolution of different systems of interest for nuclear waste disposal by reactive transport modelling approaches. Quantitative calculations of radionuclide release and migration are necessary to evaluate the safety functions of the different engineered barriers and geometry included in a geological disposal concept.

The understanding of the evolution of a deep repository system over geological time scales requires a detailed knowledge of a series of highly complex coupled processes. By using small-scale laboratory experiments, under well-defined boundary conditions, numerical modelling can provide information to help in the repository design and predict future radionuclide migration in case of an incident in the post-closure phase

Research activities on reactive transport modelling during 2016 have been focused on coupled advective or diffusive transport processes with different chemical reactions (sorption, precipitation, aqueous speciation, kinetics). As a site for high level waste (HLW) disposal has not yet been selected in Germany, research in the reactive transport field deal with all relevant host rock types (rock salt, clay and crystalline rock) in close cooperation and interaction with strong national and international academic partners as well as waste management organizations.

At this moment, there are different systems under study in a laboratory scale where reactive transport modelling is applied:

- Diffusion and sorption of radionuclides in illite and montmorillonite.
- Diffusion in the interface low pH cement / clay system (EU Horizon2020 CEBAMA project) and study of the change in the pore structure.
- Diffusion and precipitation in sea sand and clay.
- Migration of redox sensitive radionuclides in fractured crystalline rock.

Other system where transport processes are modelled also includes:

- Modelling the effect of fracture geometry on the bentonite erosion.
- Simulation of colloid transport in artificial and real gap geometries.

This kind of calculations in the laboratory scale can provide the scientific basis for the performance assessment of various repository design options. Additionally, reactive transport modelling tools have also been used to predict radionuclides release / retention under various geochemical boundary conditions in the near-field of a generic repository scenarios in an argillaceous host rock (ENTRIA project).

The reactive transport simulations described previously, have been conducted with different codes depending on the studied system: PHREEQC v. 3 [1] and COMSOL Multiphysics ® 5.0 [2]. Additionally, the interface iCP [3] has been used and tested taking advantage that KIT-INE is part of the Consortium where this tool has been developed. One of the advantages of using these codes is that all of them are in continuous development. This interface provides a numerical platform that can efficiently simulate a wide number of multiphysics problems coupled to geochemistry (i.e. liquid flow, solute and heat transport, elastic and plastic mechanical deformations and geochemical reactions).

Modelling of coupled processes at the low pH cement / clay interface

This work is included in a PhD in the framework of the EU Horizon2020 CEBAMA project and includes experimental and modelling studies of interface processes between a low pH cement (50% CEM I 52.5N + 50 silica fume) and a MX-80 bentonite pore water and assess the specific impact on HTO, $^{36}Cl^-$, $^{129}I^-$ and Be migration. The modelling work supports the interpretation of the experimental results and help to identify possible missing parameters and enhance the process understanding.

The reactive transport model consists of a one dimensional (1D) fully water saturated isothermal (298 K) problem representing a laboratory through diffusion experiment of HTO, Be(II) $^{36}Cl^-$, and $^{129}I^-$ across the interface bentonite pore water/low pH cement. Geometrical and initial transport parameters including the discretization of the system have been implemented (see Figure 1). The mesh size and the time steps have been selected to ensure a satisfactory compromise between computation time and sufficient spatial resolution of the expected geochemical and transport processes, especially at the interface between the bentonite pore water and the low pH cement hydrated phases. A constant and no-flux bound-

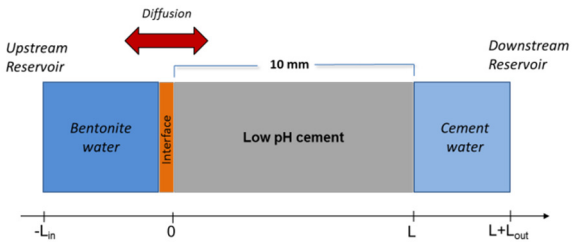

Fig. 1: *Schematic representation of the diffusion experiments*

ary condition has been imposed on the extremities of the upstream and downstream reservoir, respectively.

Considering the very low permeability of cement mass transport will be considered diffusion driven only, following Fick's law.

$$J = -D\frac{\partial C}{\partial x}$$

where J is the substance flux [kg/m^2·s]; ∂C/∂x is the concentration gradient [kg/m^4]; and D is the diffusion coefficient [m^2/s]. In the absence of data concerning the effective diffusion in low pH cements, a value of 10^{-10} m^2/s was selected. The effective diffusion coefficient was then related to the porosity evolution according to the Archie's law. Initial porosity of the cement has been determined experimentally by mercury intrusion porosimetry (MIP). Additionally, porosity changes due to mineral precipitation/dissolution and feedback on the effective diffusion coefficient are also taken into account in the model considering the molar volumes of the different solids formed or dissolved. Electrostatic surface interactions are not included, although they may influence the transport of the anionic tracers $^{36}Cl^-$, $^{129}I^-$ and $Be(OH)_3^-$ [4].

The system studied is implemented in the code PHREEQC v.3 [1] which can take into account geochemical and physical parameter variations due to mineralogical evolution as a function of time. The initial mineralogical composition of the cement hydrated phases considered is representative of a low pH cement (pH ~ 11.0) with 93 wt-% being form by C-S-H phases with a Ca:Si ratio of 0.8. Mineralogical composition has been determined experimentally with a combination of different techniques (X-ray diffraction (XRD), thermogravimetric - differential thermal analysis (TG-DTA), ^{29}Si and ^{27}Al Magic angle spinning nuclear magnetic resonance (^{29}Si and ^{27}Al MAS NMR) and scanning electron Microscopy - energy dispersive X-ray spectroscopy (SEM-EDX) At this moment, it has not been possible to experimentally identify the solid phase containing iron and for this reason we have assumed that iron phases are in the form of Fe-ettringite. The initial pore water composition of the low pH cement is defined in equilibrium with the hydrated solid phases present in the system and in agreement with the measured concentrations. The pore water composition of the clay is representative of the MX-80 bentonite described in the literature [5] and has been synthetized and measured in the laboratory.

Chemical reactions at equilibrium and kinetically controlled have been simulated using the thermodynamic database Cemdata07 available in PHREEQC format [6]. Debye-Hückel equation, valid for the ionic strength of the studied system (< 0.3 M) is preferred to save computational time. Cemdata07 includes hydrates commonly encountered in Portland cement systems in the temperature range 0 - 100°C. Rate equations of precipitation/dissolution of secondary / primary phases are provided directly in the input files of PHREEQC. Kinetic parameters for C-S-H phases and ettringite have been selected from [7, 8].

In the present status, sorption of the tracers in the cement matrix is not included in the model, sorption reactions of $^{36}Cl^-$ and $^{129}I^-$ and Be into the low pH cement matrix will be considered by a thermodynamic mechanistic sorption model to be implemented in PHREEQC. The recent review of Ochs et al. (2016), [9] will be considered to select the most appropriate sorption parameters, as well as the data generated in this PhD work with batch experiments.

The simulations were carried out for different contact times (14 min, 5 and 30 days) predicting that the low pH cement will be damaged in contact with the bentonite pore water, having a degraded area of ~2 mm after one month of alteration. The alteration on the low pH cement is mainly due to the partial dissolution of C-S-H phases resulting in an increase of the porosity. The carbonation is linked to the precipitation of calcite and thus the decalcification of C-S-H phases. Magnesium enrichment in the decalcification area has been reported in the literature [10, 11]. In our system, brucite is undersaturated and attempts to model the magnesium perturbation using available thermodynamic data suggested the formation of hydrotalcite. However, the recent determination of the solubility data for M-S-H phases will make it possible to account for the potential formation of M-S-H phases [11] and will be considered in the future. Finally, no attempts have been done to model the iron evolution and the diffusion of HTO in the system will reach the steady state after 5 days of interaction.

Modelling the effect of fracture geometry on bentonite erosion

The effect of fracture geometry on bentonite erosion has been studied by means of numerical simulations. The 2D model for the sodium bentonite erosion used in this work was developed and applied by Neretnieks, Liu and Moreno [12,13,14]. For a thorough discussion on the governing equations describing the bentonite expansion and erosion the reader is referred to the literature given above. The model is applicable for simplified chemical system where bentonite is represented by a sodium montmorillonite and only monovalent cations (1-100 mM) are present in the groundwater. Figure 2 gives an overview of the model geometry and boundary conditions for the flow and mass transport. The model is implemented in the finite element code COMSOL Multiphysics V5.2 [2].

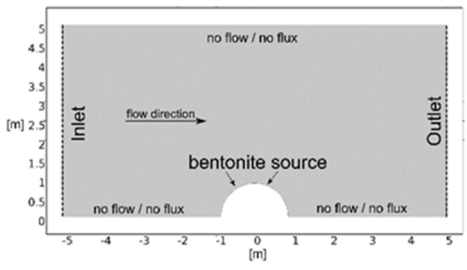

Fig. 2: *Model geometry and boundary conditions*

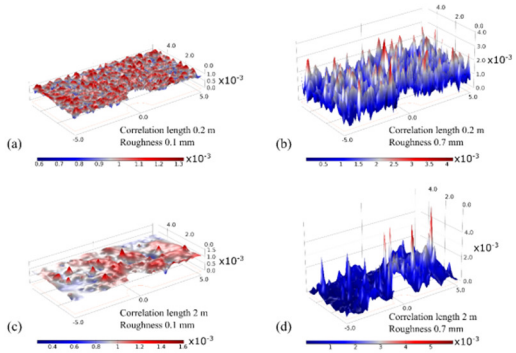

Fig. 3: *Aperture fields for a correlation length of 0.2 m for STD of 0.1 mm (a) and 0.7 mm (b) and a correlation length of 2 m for STD of 0.1 mm (c) and 0.7 mm (d). Please note that a superelevation factor of 1200 was used.*

A triangular mesh with 13362 elements is used for the numerical simulation.

So far, the model considered only a parallel plate fracture with a constant aperture (1 mm). To examine the effect of heterogeneous fracture geometry random normal aperture distributions with correlation lengths of both 0.2 m and 2 m and a mean aperture of 1 mm have been generated for different standard deviations (STD; equivalent to surface roughness of 0.1 mm, 0.3 mm, 0.5 mm and 0.7 mm). Based on these aperture distributions hydraulic conductivity fields were calculated with the Cubic Law [15] and subsequently used in the Darcy equation to calculate the fracture flow fields. A two-way coupling between the flow and the bentonite erosion process is considered.

A range of mean fracture flow velocities was covered in the study (1×10^{-5} m/s, 1×10^{-6} m/s and 1×10^{-7} m/s, respectively). Generally speaking, the heterogeneous aperture fields induce flow channeling and

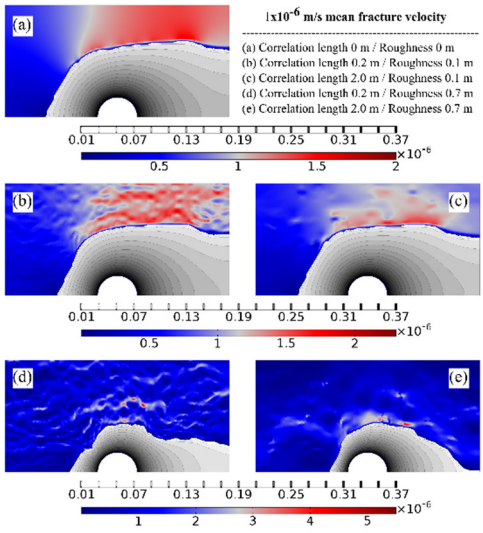

Fig. 4: *Bentonite erosion patterns (greyish areas) and flow fields (red-blue colorbar) for STDs of (a) 0 mm, (b) 0.1 mm CL 0.2 m, (c) 0.1 mm CL 2 m, (d) 0.7 mm CL 0.2 m, (e) 0.7 mm CL 2 m for 1×10^{5}m/s.*

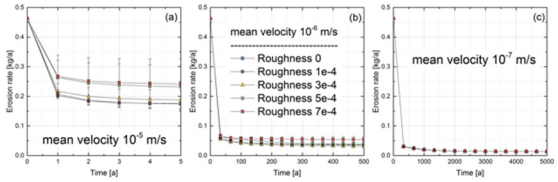

Fig. 5: *Calculated erosion rates for the CL of 2 m*

therefore locally varying shear forces which lead to irregular bentonite expansion and erosion patterns. Figure 4 shows results for the bentonite erosion for a mean fracture flow velocity of 1×10^{-6} m/s. The extent of swelling into the fracture decreases for increasing roughness due to higher flow velocities/shear forces.

Figure 5 shows simulated erosion rates [kg/a] for the 2-m correlation length aperture fields. With respect to the two different aperture correlation lengths used, no dependency on the erosion rate results was found. In case of the highest mean flow velocity (1×10^{-5} m/s), a clear trend is visible. That is, the erosion rates correlate significantly with increasing roughness ($\geq 3\times10^{-4}$ m). The highest mean erosion rates (~0.24 kg/a) are ~40% higher than the erosion rate for the homogeneous case (~0.17 kg/a). Even extreme values of ~0.33 kg/a were calculated yielding an increase of up to ~95 %. For decreasing mean flow velocities, the impact of fracture geometry on the erosion rates starts to decrease. Only 33% increase in erosion rates are found for the 1×10^{-6} m/s case.

For 1×10^{-7} m/s mean velocity no impact of roughness was found (0.013 kg/a; increase of < 1% only). Here, the variability in shear forces due to the heterogeneous flow field are not high enough to lead to an increase in erosion rate. The results obtained verify the importance of fracture heterogeneity on the bentonite erosion for mean velocities higher than ~1×10^{-7} m/s.

References

[1] Nardi A., et al. (2014) *Computers & Geosciences,* **69,** 10-21.

[2] COMSOL (2014) COMSOL-Multiphysics. Version 5.0, www.comsol.com

[3] Parkhurst and Appelo (2013) C. A. J. U.S. Geological Survey Techniques and Methods, 2013, book 6, chap. A43, 497 p.

[4] Chagneau, A., et al. (2015). *Env. Sci. & Tech. Letters*, **2**, 139–143.

[5] Wersin, P. (2003). *Journal of Contaminant Hydrology,* **61,** 405-422.

[6] Lothenbach, B. and Winnefeld, F (2006) *Cement and Concrete Research* **36**–2, 209–226.

[7] Marty, N. et al (2015). *Applied Geochemistry*, **55**, 108-118.

[8] Baur, I., et al. (2004). *Cement and Concrete Research,* **34**, 341–348

[9] Ochs, et al. (2016). Springer International Publishing Switzerland.

[10] Jenni, A. et al. (2014) *Phys. Chem. Earth A/B/C* **70–71**, 71–83.

[11] Dauzeres, A. et al. (2016) *Cem. Concr. Res.*, **79** 137–150

[12] Neretnieks, I., et al. (2009) SKB Technical report TR-09-35. Svensk Kärnbränslehantering AB, Stockholm, Sweden.
[13] Moreno, L., et al. (2011) *Physics and Chemistry of the Earth, Parts A/B/C* **36**, 1600-1606.
[14] Liu, L., et al. (2009) *Langmuir* **25**, 679-687.
[15] Witherspoon, P.A., et al. (1980). *Water Resources Research* **16**, 1016-1024.

6 Solvent extraction chemistry

Solvent extraction is a widely-used technique for separating and purifying ionic species. Solvent extraction is applied on an industrial level e.g. in the reprocessing of spent nuclear fuels by the PUREX process and in the large-scale copper production by the solvent extraction/electro-winning technique.
We develop and study solvent extraction systems both in the nuclear and the non-nuclear context. Within the nuclear context, we have been focusing on solvent extraction systems for actinide separations, most notably for separating trivalent actinides, An(III), from the chemically similar lanthanides, Ln(III). From the early 1990's with Z. Kolarik's contribution to an FP3 EURATOM project [1], these studies have continuously been performed in the framework of EURATOM research programs, the most recent being SACSESS [2]. A common denominator throughout these projects is the use of heterocyclic nitrogen donor complexing agents. Such compounds exhibit high selectivity for An(III) over Ln(III), with molecules based on the BT(B)P (bis-triazinyl-(bi)-pyridine) core being among the most efficient.
Non-nuclear applications are related to the recycling of critical metals such as rare earth elements (REE) and refractory metals. With this topic being a comparatively recent addition to our portfolio, we have started work on REE separations using commercial extracting agents. Currently we are contributing to the ERA-MIN project, ENVIREE (environmentally friendly and efficient methods for extraction REE from secondary sources) [3].

6.1 Complexation of Cm(III) and Eu(III) with PTD

C. Wagner, U. Müllich, A. Geist, P. J. Panak

In co-operation with:

E. Mossini[a], E. Macerata[a], M. Mariani[a], A. Arduini[b], A. Casnati[b]

[a] Politecnico di Milano, Italy; [b] Università di Parma, Italy

Over the years, we have developed and studied solvent extraction systems capable of separating trivalent actinides, An(III), from chemically similar lanthanides, Ln(III). The chemistry applied is based on the use of polydentate nitrogen donor heterocycles such as 2,6-(bis-1,2,4-triazin-3-yl)pyridines (BTP) and 6,6'-(bis-1,2,4-triazin-3-yl)-2,2'-bipyridines (BTBP) [4]. Initially such compounds were used as lipophilic extracting agents, selectively extracting An(III) from aqueous solutions containing HNO_3.

More recently, water soluble derivatives were developed and tested. For example, SO_3-Ph-BTP (Fig. 1 top) selectively back-extracts An(III) from an organic phase loaded with An(III) and Ln(III) while Ln(III) remain in the organic phase [5,6]. Successful lab-scale process tests have been performed using this compound [7, 8].

Unfortunately, the presence of Sulphur poses issues with the management of secondary waste. Preferably, all chemicals used should be composed of only C, H, O and N atoms, making them combustible to gaseous products.

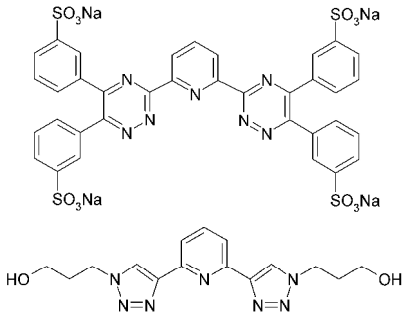

Fig. 1: *Top, SO_3-Ph-BTP; bottom, PTD.*

Addressing this issue, PTD (Fig. 1 bottom) has recently been synthesized and evaluated by our colleagues from Università di Parma and Politecnico di Milano. This compound is a CHON alternative to SO_3-Ph-BTP. It appeared that a solvent extraction system using PTD to strip An(III) from a TODGA organic phase loaded with An(III) and Ln(III) [9] is slightly less selective than the SO_3-Ph-BTP/TODGA system [5].

To understand this difference and explore possible ways of improvement, the complexation of Cm(III) and Eu(III) with PTD was studied by TRLFS [10].

This study concluded that PTD is not intrinsically less selective than SO_3-Ph-BTP; the stability constants of the 1:3 Cm(III) complexes are approximately two orders of magnitude higher than those of the Eu(III) complexes, for both ligands. However, PTD is a weaker and more easily protonated ligand, as inferred from the Cm(III) 1:3 complex stability constants (corrected for ligand protonation) and pK_a values (see Table 1).

Tab. 1: *Cm(III) 1:3 complex stability constants (corrected for ligand protonation) and pKa values for PTD and SO_3-Ph-BTP.*

Ligand	lg β_3 (Cm)	pK_a
PTD	9.9 ± 0.3	2.1 [9]
SO_3-Ph-BTP	12.2 ± 0.3 [6]	0.5 [11]

As a consequence, PTD does not exclusively form the 1:3 complexes under conditions applicable to the PTD/TODGA solvent extraction system, i.e. at a PTD concentration of 80 mmol/L in approx. 0.5 mol/L HNO_3. Indeed, a mixture of Cm(III) 1:2 and 1:3 complexes in a concentration ratio of approx. 1:4 is present, as probed by TRLFS. This significant fraction of the Cm(III) 1:2 complex is responsible for the system's lower selectivity.

Building on the otherwise excellent properties of PTD [9], future work aims at finding PTD derivatives which form more stable metal ion complexes and/or are less prone to protonation.

6.2 Am(III)/Cm(III) separations column experiments

C. Wagner, A. Geist, P. J. Panak

In co-operation with:

R. Malmbeck[a]

[a]European Commission, DG Joint Research Centre-JRC, Directorate G – Nuclear Safety & Security, Karlsruhe, Germany

A solvent extraction system consisting of TODGA as organic phase extracting agent and SO_3-Ph-BTBP as aqueous phase complexing agent allows for the separation of Am(III) from Cm(III) and Ln(III) [11] (in contrast to systems using SO_3-Ph-BTP [5] or PTD [9] which do not differentiate Am(III) and Cm(III), thus co-separating them from Ln(III)).

With the SO_3-Ph-BTBP/TODGA system, a separation factor of 2.5 - 3 for Cm(III) over Am(III) is achieved. Even with such a comparatively low selectivity, efficient separation is possible using multi-stage counter-current equipment.

We investigated the performance of the SO_3-Ph-BTBP/TODGA system in a solid liquid setup. The TODGA based Eichrom® DGA resin was used as the stationary phase and a solution of SO_3-Ph-BTBP in HNO_3 is the mobile phase. Am(III) and Cm(III) distribution ratios were determined for varied SO_3-Ph-BTBP and HNO_3 concentrations in batch experiments, the aqueous phase speciation was studied by TRLFS, and finally a column experiment was performed.

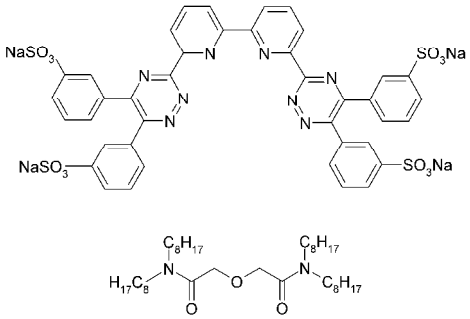

***Fig. 2**: Top, SO_3-Ph-BTBP; bottom, TODGA.*

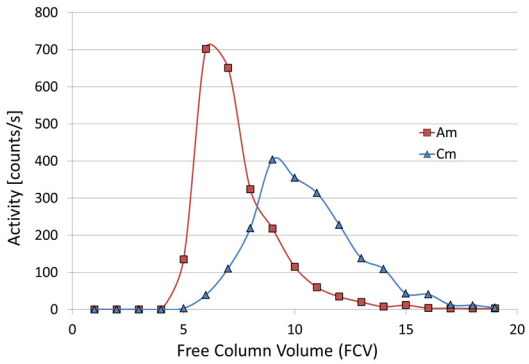

***Fig. 3**: Elution of Am(III) and Cm(III) from an Eichrom® DGA column by a solution of 5 mmol/L SO_3-Ph-BTBP in 0.15 mol/L HNO_3. FCV, 0.25 mL; Flow rate, 0.22 mL/min.*

Batch extraction experiments showed the SO_3-Ph-BTBP/ Eichrom® DGA system to perform similar to the SO_3-Ph-BTBP/TODGA liquid-liquid system [12]. Distribution ratios increase with increasing HNO_3 concentration and decrease with increasing SO_3-Ph-BTBP concentration. The separation factor for Am(III) over Cm(III) remains in the range of 2.5 - 3.5 throughout the experimental conditions applied.

The influence of the SO_3-Ph-BTBP concentration on the distribution ratios insinuates the formation of Cm(III)/SO_3-Ph-BTBP 1:1 complexes. This was already observed with the respective liquid-liquid extraction system [12], for which however the presence of 1:2 complexes was unambiguously determined by TRLFS [12]. Consequently, the aqueous phase from a SO_3-Ph-BTBP/ Eichrom® DGA experiment was investigated by TRLFS. In accordance with the liquid-liquid system, the exclusive formation of the Cm(III) 1:2 complex was proven.

Finally, a column experiment was run, eluting Am(III) and Cm(III) from a column packed with Eichrom® DGA resin, particle size 50 - 100 µm (ID = 4 mm, L = 40 mm). Elution was performed by passing a solution of 5 mmol/L SO_3-Ph-BTBP in 0.15 mol/L HNO_3 at a gravitational flow rate of approximately 0.2 mL/min.

As evident from Figure 3, Am(III) was preferentially eluted. Unfortunately, baseline separation was not achieved for the experimental conditions applied.

While the result from this first run is encouraging, optimization is required to achieve better separation between Am(III) and Cm(III). This may be achieved by using a longer column and/or finer material (which however will require the stationary phase being pumped). Also, running the column at an elevated temperature is expected to have a positive impact.

6.3 REE separation

A. Geist

The extraction of trivalent lanthanide ions by acidic organophosphorus extracting agents such as di(2-ethylhexyl)phosphoric acid (D2EHPA) is usually described by the following equilibrium, considering the dimerization of D2EHPA in non-polar diluents.

$$Ln^{3+} + 3\ (HL)_2 \rightleftharpoons Ln(LHL)_3 + 3\ H^+ \qquad (1)$$

Applying a concentration-based equilibrium model, a slope of 3 is expected for plotting $\lg D_{Ln(III)}$ over p*H*. However, slopes of approximately 3.5 are observed when extracting from HNO_3. This discrepancy is caused by the ionic interaction between Ln^{3+} and NO_3^-. The Specific Ion Interaction Theory (SIT) [13] is one way to account for this interaction.

We have previously been using SIT based equilibrium models for describing solvent extraction systems used for actinide separations. Consequently, such a model was tested for the extraction of Eu(III) into D2EHPA. This model calculates equilibrium distribution ratios as a function of initial concentrations. Activities are used in the aqueous phase, concentrations are used in the organic phase. Ion interaction coefficients of $\varepsilon(H^+, NO_3^-) = 0.07$ and $\varepsilon(Eu^{3+}, NO_3^-) = 0.27$ and an extraction constant of $K = 1500$ are used.

Figure 4 compares experimental and calculated Eu(III) distribution ratios as a function of initial HNO_3 concentration. Excellent agreement is achieved throughout; the small deviations at 0.03 and 2 mol/L HNO_3 are due to experimental uncertainties frequently observed for distribution ratios below 0.001 or above 1000.

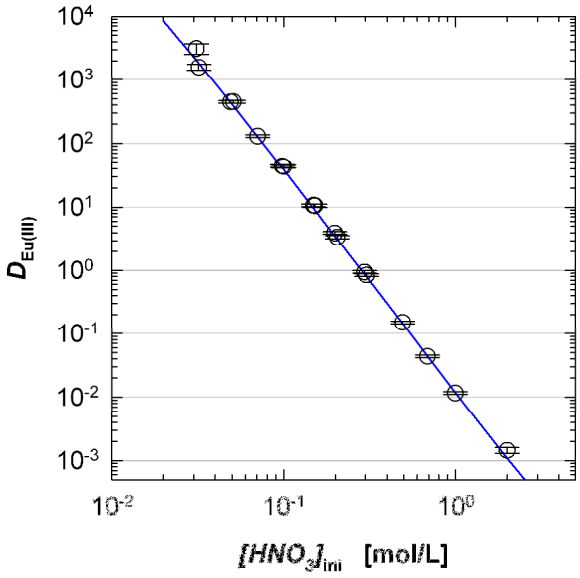

Fig. 4: *Extraction of Eu(III) from HNO_3 into D2EHPA. Organic phase, 0.1 mol/L D2EHPA in kerosene. Aqueous phase, 2 kBq/mL ^{152}Eu(III) + 50 mg/L Eu((III) in HNO_3. A/O = 1, T = 20 °C.*

Again, SIT was shown to be useful for describing solvent extraction systems. Further experiments to validate the model under loading conditions (i.e. for metal ion concentrations that result in a significant consumption of the extracting agent) are foreseen.

References

[1] Kolarik, Z.; Schuler, R.; Müllich, U. EUR 16958, European Commission, Luxembourg: 1996.

[2] www.sacsess.eu

[3] www.enviree.eu

[4] Panak, P. J.; Geist, A., *Chem. Rev.* **2013,** *113* (2), 1199–1236.

[5] Geist, A.; Müllich, U.; Magnusson, D.; Kaden, P.; Modolo, G.; Wilden, A.; Zevaco, T., *Solvent Extr. Ion Exch.* **2012,** *30,* 433–444.

[6] Ruff, C. M.; Müllich, U.; Geist, A.; Panak, P. J., *Dalton Trans.* **2012,** *41,* 14594–14602.

[7] Wilden, A.; Modolo, G.; Kaufholz, P.; Sadowski, F.; Lange, S.; Sypula, M.; Magnusson, D.; Müllich, U.; Geist, A.; Bosbach, D., *Solvent Extr. Ion Exch.* **2015,** *33,* 91–108.

[8] Carrott, M.; Bell, K.; Brown, J.; Geist, A.; Gregson, C.; Hérès, X.; Maher, C.; Malmbeck, R.; Mason, C.; Modolo, G.; Müllich, U.; Sarsfield, M.; Wilden, A.; Taylor, R., *Solvent Extr. Ion Exch.* **2014,** *32,* 447–467.

[9] Macerata, E.; Mossini, E.; Scaravaggi, S.; Mariani, M.; Mele, A.; Panzeri, W.; Boubals, N.; Berthon, L.; Charbonnel, M.-C.; Sansone, F.; Arduini, A.; Casnati, A., *J. Amer. Chem. Soc.* **2016,** *138* (23), 7232–7235.

[10] Wagner, C.; Mossini, E.; Macerata, E.; Mariani, M.; Arduini, A.; Casnati, A.; Geist, A.; Panak, P. J., *Inorg. Chem.* **2017,** *56* (4), 2135–2144.

[11] Wagner, C.; Müllich, U.; Geist, A.; Panak, P. J., *Solvent Extr. Ion Exch.* **2016,** *34* (2), 103–113.

[12] Wagner, C.; Müllich, U.; Geist, A.; Panak, P. J., *Dalton Trans.* **2015,** *44* (39), 17143–17151.

[13] Ciavatta, L., *Ann. Chim. (Rome)* **1980,** *70*, 551–562.

7 Department of decommissioning of nuclear facilities

M. Brandauer, N. Gabor, E. Zellmann, K. Findling, S. Gentes [a]

[a] Department of Deconstruction and Decommissioning of Conventional and Nuclear Buildings, Institute for Technology and Management in Construction (TMB), Karlsruhe Institute of Technology (KIT)

Overview

The integration of the decommissioning department into the program-oriented funding research of the Helmholtz Association in 2015 allows a focused addressing of this important issue between research on the reactor safety and the disposal of nuclear waste.

The shut-down of eight active German nuclear power plants in 2011 and the subsequential shut-down of the remaining facilities up to 2022 will lead to a big challenge of parallel decommissioning of a large quantity of large scale facilities in a very short time frame. The starting point will be in 2017, where most of the facilities of 2011 will finally acquire the license for finally proceeding with the decommissioning of their facility.

Considering this development, activities within the established decommissioning center of the KIT in 2015 have been further extended to an international level by establishing the "Decommissioning Cluster" in February 2016. This endeavor has gathered five big entities in the region to a joint venture with regard to harmonizing and strengthening E&T, R&D as well as maintaining competences in the field of decommissioning. The partners of this new group are the Duale Hochschule Baden-Württemberg (DHBW), the Paul Scherrer Institut (PSI), the University of Stuttgart, the Joint Research Center (JRC) of the European Commission, and the KIT (see Fig. 1).

The set-up, coordination and continuous strengthening of this cooperation is being supported by the Ministry of Science, Research and the Arts (MWK) of the State of Baden-Wuerttemberg since December of 2016.

The great need of focusing on the decommissioning of nuclear facilities is, however, not limited to the German nuclear phase-out. The European Commission assumes that by 2025 approx. one third of the 145 nuclear facilities currently in use will be put out of service [2], apart from estimates of almost 300 nuclear power plants going into decommissioning by 2030. For this reason, the European Commission has created the ELINDER initiative (European Learning Initiatives for Nuclear Decommissioning and Environmental Remediation). On 2nd of December 2016, fifteen partners have signed a memorandum of understanding to establish a European decommissioning training and education program, allowing a standardization and improvement of the education system in this field on a European level.

***Fig. 1**: Partners of the "Decommissioning Cluster" [1].*

Other activities of the program comprise the further intensification of international partner relations, such as with the Fukui University in Japan. As a coordinated effort, an international symposium was organized in Osaka in October 2016, followed by a two-day student workshop about the decommissioning of Fukushima at the University of Fukui, moderated and taught by Dr. Larry Boing from the Argonne National Laboratory and Mr. Martin Brandauer from KIT.

In December 2016, Dr.-Ing. Patrick Kern defended his doctoral thesis. His work contributes significantly to the development of automatized robotic systems for the characterization and decontamination of concrete surfaces. Dr. Kern has extensively studied the behavior of vacuum suction plates and provided a first-of-a-kind model for the prediction of force transfer of these units both in normal as well as tangential direction [3]. His findings will provide a substantial contribution to future systems in this field, since suction plates allow a flexible and reliable fixation of systems and components without significant changes to the surface to be treated (like e.g. bolting).

Further major topics will be addressed in more detail below.

Knowledge database for the decommissioning of nuclear facilities

In order to successfully handle decommissioning projects, comprehensive data and information is vital; e.g. to establish state-of-the-art decommissioning processes, define future R&D in the field, develop improvements on technical and management issues, both on a national and international level. For this reason, a comprehensive decommissioning database based on a team collaboration platform by Atlassian Inc. has been set up in 2016 and implemented in 2017. The software selected gathers information of different types e.g. papers, articles, other databases, books, news, etc. (Fig. 2).

Hence, the purposes of the database are:

- Fast and easy information access with links to detailed content

- Data and document storage
- Illustration of the current decommissioning status of nuclear facilities, decommissioning knowledge and technologies
- Information compilation
- Identification of relevant characteristic values for nuclear decommissioning projects and procedures and further development of decommissioning technologies
- Creation of a basis for future research, standardization and optimization procedures

The key advantages of the Atlassian system software *Confluence* are the user friendly, intuitive interface which is based on a Wikipedia format (Fig. 3), the data entry and upload possibilities, the openness of the system for further processing, and evaluation tools. The integration of tables, documents, and links makes it a powerful tool for combining management aspects with technical procedures and therefore providing an overall overview of and interconnection with information needed for the planned R&D in decommissioning of nuclear facilities.

For this information compilation, a top-down structure has been set up as can be seen in Fig. 4. This structure shows an overview of the topics analyzed in depth in the database.

By 2018, it is planned to further collect, handle, and process different relevant information within the database, to create tools for the analysis and processing of recent, ongoing and completed decommissioning procedures. The tools will further allow the identification of relevant characteristic values for nuclear decommissioning procedures and development of decommissioning technologies.

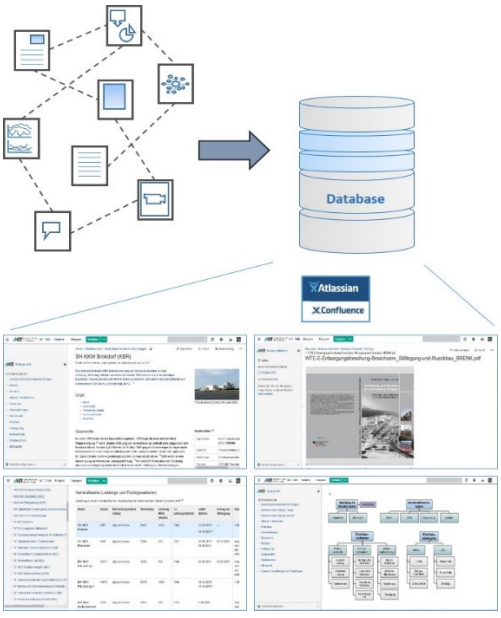

Fig. 2: *Illustration of information gathering and processing with the Atlassian database system.*

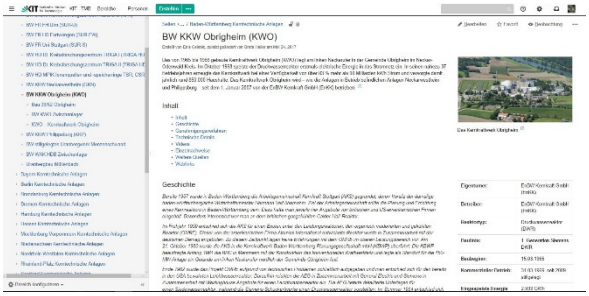

Fig 3: *Example page of the database.*

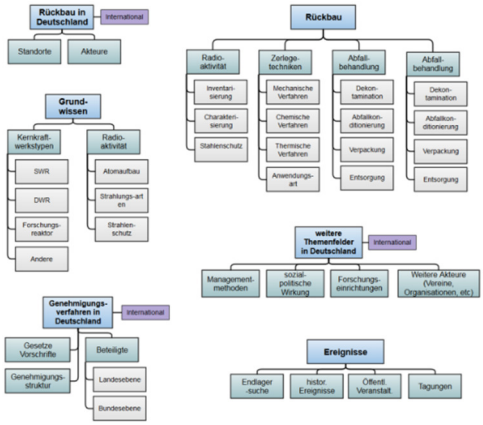

Fig. 4: *Structure of topics pursued in the database.*

Development of a system for the surface decontamination of reinforced concrete structures

One of the decontamination challenges of concrete structures is the deep decontamination of cracks, fractures, and the removal of steel fixtures (e.g. anchor plates, dowels, etc.). This procedure requires the application of a tool, which can not only remove a deep layer of concrete but also deal with the reinforcement within the structure while generating a smooth enough surface to allow the subsequent measurement of contamination. The different properties of the materials (i.e. concrete and steel) make it very challenging to design a tool that can deal with a ductile and a brittle material at the same time. State-of-the-art decontamination tools for this application are usually relying on the usage of two different set of tools for each of the components.

In a joint effort, a novel patented tool is being developed by the Karlsruhe Institute of Technology (including this working group and the chair of mobile machinery), the Institute of Production Engineering and Machine Tools (IFW) at Leibniz University Hannover, Kraftanlagen Heidelberg GmbH, and Herrenknecht AG. The system allows the removal of highly reinforced concrete, the removal and transportation of debris, as well as suitable storage and packaging of the debris for the nuclear repository. These efforts are being sponsored by the Federal Ministry of Education and Research through the project

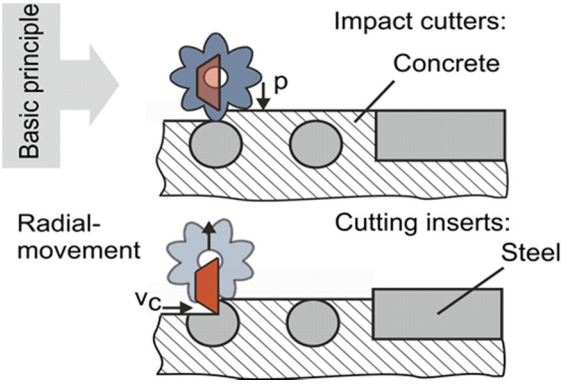

Fig. 5: *Operating principle of the tool [4].*

02S9093C „Definierter Abtrag hocharmierter Stahlbetonstrukturen (DefAhS) “.

Prior to the system development, a survey of the requirements has been carried out with the following results: a surface removal up to a depth of 5 mm (90% of the cases), and a depth removal up to 300 mm (10%). The system will have a modular design with a machining system and a corresponding carrier device, both designed to fit through a standard door opening of 1x2 m. It will allow the machining of walls, ceilings, wall projections and wall openings with slide adjustments, achieving similar efficiency (0.1 m³/h) and life time of the cutters and inserts (up to 3h) of established technologies. A detection and control system has been integrated into the tool to identify the required machining parameters per material properties (concrete or steel) [4].

To fulfil the requirements for machining concrete and steel, the system uses a hybrid-removal procedure. The concrete is crushed by impact cutters with floating bearing to uncover steel installations and reinforcement rods. Due to the ductile properties of the uncovered steel inlays, the impact cutters are bounced back. Cutting inserts have been placed 6 mm radially inwards to allow milling of these ductile materials, reducing the cutting speed of the tool accordingly. The approach design of the tool can be seen in Fig. 5.

These two kinds of tools are installed on modules, which are attached to a drum (see Fig. 6). Each module is equipped with a shaft mounting and the impact cutters. On top of this part of the module, seven cutting inserts are fixed with a certain offset.

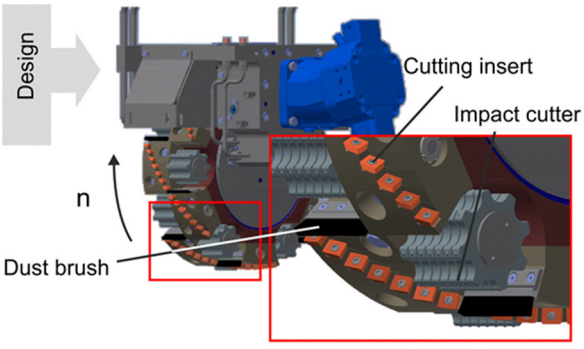

Fig. 6: *Design principle of the tool [4].*

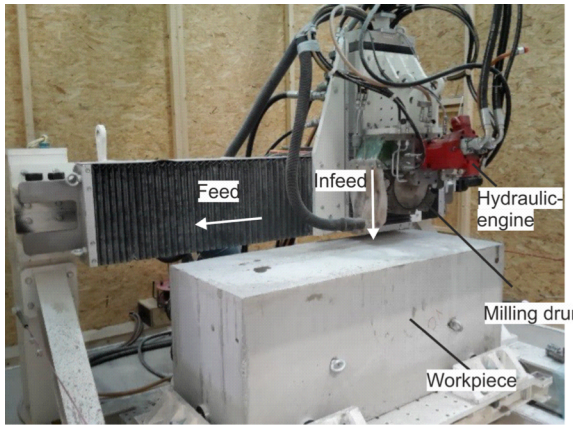

Fig. 7: *Test rig for experimental analysis [4].*

The hydraulic engine with an offset gearbox and centrally placed bearings allows the drum to rotate freely up to the specified depth of 30 mm (see Fig. 6).

To remove the debris produced during machining, brushes are placed on each side of the modules behind the impact cutter. With these, the debris is removed from the machining area and conveyed to the suction system behind the drum. The suction system also holds the detection sensors for the speed control of the unit.

For the experimental evaluation of the newly developed tool, the set-up has been carried out in the workshop of the Institute for Technology and Management in Construction (TMB) at the KIT (see Fig. 7).

Here, the preliminary technical feasibility of the novel tool will be tested. Following this, experimental tests to determine the necessary process forces for the milling tool and the wear behavior of different carbide cutting materials for various parameters will be tested. Based on these results, the optimum cutting material will be selected and the operating points for the milling tool will be determined.

Treatment of secondary waste from the water abrasive cutting technique

For the treatment and disposal of the secondary waste caused by the application of the water abrasive suspension cutting, two research approaches have been followed in previous years. On the one hand, research has been undertaken to treat the secondary waste by a novel physical separation method of the radioactive particles contained in the mixture. The second approach analyzed the possibility of admixing the secondary waste into the concrete which is used to fill-up KONRAD containers.

The first approach involves the significant reduction of the radiological inventory and hence improves the safety in the handling, conditioning and disposal of the material. With the possibility of systematically disposing of this fraction, the usage of the remaining material for the concrete mixture is enabled while avoiding unforeseen agglomeration of highly activated particles. The combination of both approaches

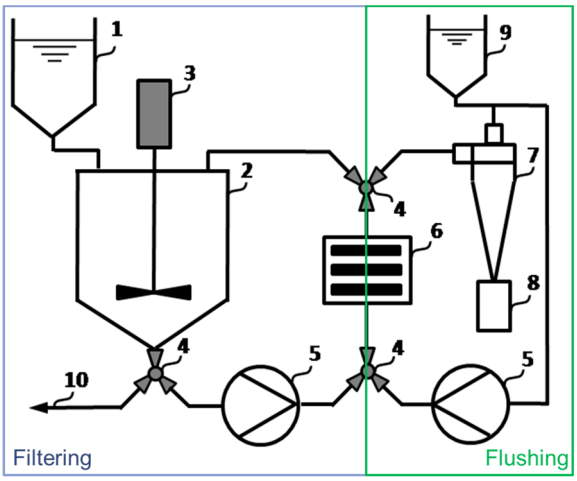

Fig. 8: *Applied process chain of the preliminary test rig [5].*

allows the treatment of this radioactive waste, which, up to date, had to be disposed of in a final repository.

The process chain of the separation system can be seen in Fig. 8.

In order to develop a prototype separation system with components that might be applicable for the usage with activated waste, a big effort has been made to develop a test rig, which is as insusceptible towards malfunction as possible. Furthermore, to reduce costs, only commercially available components have been used while taking considering a possible decontamination of the components in the later application.

In order to profit from the water's shielding effect and to also track possible leakage in the system, the abrasive and steel mixture from the water suspension cutting is suspended using a slurry feed tank (**2**). With membrane pumps (**5**) the suspension is pumped through a magnetic filter (**6**) in a closed loop for the magnetic separation of the steel fraction. A magnet filter has been chosen for this application and can be seen in the following Fig. 9. The magnet rods used in the system do not require additional power supply and provide easily accessible surfaces for later decontamination. The four permanent magnet rods (**1**) of the filter are inserted through the front of the unit into casing tubes (**2**) which seal the chamber of the filter off. Therefore, the suspension can be filtered in a leakage-free environment. By inserting or withdrawing the magnet rods, the magnetic filtering can be turned on and off.

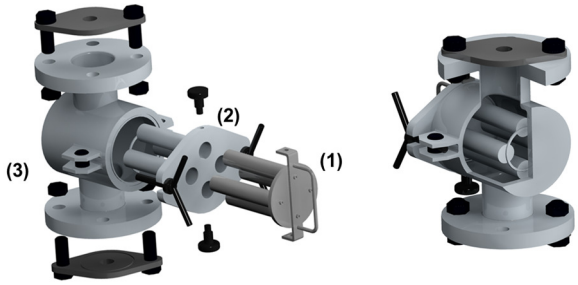

Fig. 9: *Magnet rod filter used in the separation system [5].*

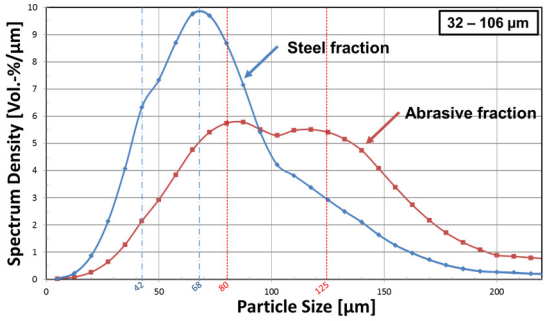

Fig. 10: *Different size distribution of the fractions in the mixture in the size of 32 – 106 µm [5].*

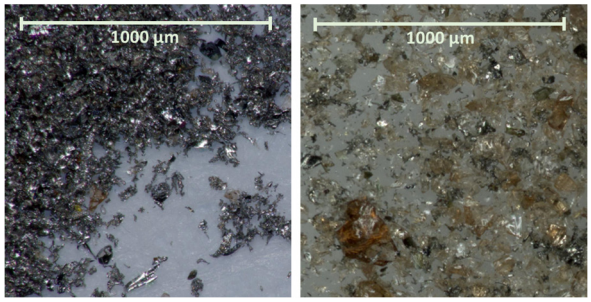

Fig. 11: *Different consistency of separated fraction dependent on operation parameters of the system [5].*

The magnetic filtering loop of the separation system is operated with this filter for a predefined time. After this filtering loop, the magnet rods of the filter are removed and a second loop is used to flush the filter using fresh water. The separated steel particles (activated fraction) are drained out of the system by a hydro cyclone (**7**) and collected into a depository container (**8**). The remaining equipment for the separation system is a prior feed tank (**1**), the drivetrain and corresponding agitator (**3**) of the slurry feed tank, a fresh water supply (**9**) and 2/3-way valves (**10**) to operate both closed loops sequentially.

The experimental investigation of this system has shown very different results in the properties of the flushed fraction depending on the operation parameters of the system (flow rate, particle loading or filtering time). In Fig. 10 two exemplary fractions of very different consistency are shown. Depending on the set of parameters, the separated fraction is either mostly composed of steel particles (left of Fig. 10) or a mixture of steel particles with a large quantity of abrasive particles (right of the same figure).

To allow the characterization of these obtained fractions, a detailed characterization of the original mixture after the cutting has been carried out [5]. For this reason, the mixture has been classified by size and in addition sorted by magnetic susceptibility. These fractions have been analyzed as to their particle size distribution. This has been carried out by a system set up at the Institute for Technology and Management in Construction (TMB) using an absorbance measurement technique. These analyses have shown that the steel fraction within the mixture has a far smaller

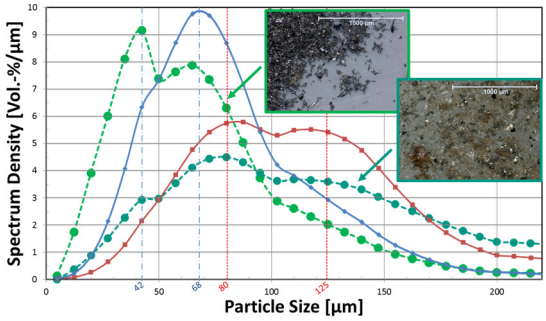

Fig. 12: *Different size distribution of the fractions compared to fraction of the experimental analysis [5].*

particle size compared to the abrasive particles. There is a clear difference in particle size distribution of the finest fractions of steel particles and abrasive particles, as can be seen in Fig. 11.

With these findings (for details please refer to [5]) a clear assignment of the separated fraction can be achieved by the particle size distribution of the analyzed sample. This association becomes clearer when combining the results of the particle size distribution of the two samples of Fig. 10 with those shown in Fig. 11. This can be seen in Fig. 12.

In the comparison of Fig. 12 the difference between the particle size distribution of the different samples is explicit. These findings allow a new and simple characterization of the separated fractions of the developed separation system, i.e. a qualitative evaluation of the achieved results. Therefore, this analysis permits a quick estimation of the fractions gained during the separation without having to rely on extensive and time consuming chemical analysis. With further efforts, this evaluation process can be included in the separation system, making the online evaluation possible.

With this method, the separation process will be further analyzed using variations of the system parameters flow rate and particle loading and filtering time to achieve a good estimation of the best operating parameter for the magnetic separation of particle mixtures using a magnet rod filter. This is the basis of ongoing research for the treatment of secondary waste of the water abrasive suspension cutting in the nuclear decommissioning field.

These results have been achieved within the framework of project 02S8871 and the follow-up project 15 S 9225A&B, both funded by the German Federal Ministry of Education and Research.

References

[1] W. Tromm and M. Brandauer, “Aufbau eines Clusters Rückbau für den Rückbau kerntechnischer Anlagen,” Annual Meeting on Nuclear Technology (AMNT), Berlin, 2017.

[2] W. Irrek, K. Müller, D. Fouquet, and A. P. Froggatt, “Comparison among different decommissioning funds methodologies for nuclear installations,” Wuppertal Institut für Klima, Umwelt, Energie GmbH on behalf of the European Commission Directorate-General Energy and Transport, H2, 2007.

[3] P. Kern, “Elastomerreibung und Kraftübertragung beim Abscheren von aktiv betriebenen Vakuumgreifern auf rauen Oberflächen,” Dissertation, KIT, Karlsruhe, 2016.

[4] P. B. Denkena, T. Grove, U. Hess, P. M. Geimer, D. Engelmann, P. S. Gentes, S. Kaiser, T. Edelmann, F. Cousseau, J. Braun, and M. Kisling, “Development of a tool system for the surface decontamination of reinforced concrete structures,” 13. Internationales Symposium “Konditionierung radioaktiver Betriebs- und Stilllegungsabfälle” einschließlich 13. Statusbericht des BMBF “Stilllegung und Rückbau kerntechnischer Anlagen” 22.-24. März, 2017.

[5] M. Brandauer, J. Starflinger, S. Gentes, R. Langlois, and K. Waters, “Magnet Rod Filter Analysis for the Treatment of Radioactive Waste from the Abrasive Water Jet Cutting,” Physical Separation ‘17, Minerals Engineering International (MEI), Falmouth, UK, 2017, 2017.

8 Development of actinide speciation methods

Maintaining a state-of-the-art portfolio of advanced surface science and spectroscopy methods at INE is an important R&D activity, as these methods are crucial tools for advancing our understanding of actinide and radionuclide (geo)chemistry or the behavior of nuclear waste forms during prolonged interim storage. Radionuclide speciation methods available at INE radiochemical laboratories and the KIT synchrotron radiation facility ANKA are continuously adapted to serve the requirements of the INE in house R&D program. Access to this unique instrumentation is as well provided to INE's national and international partners in the frame of cooperation agreements or joint research projects. As a major milestone in instrumentation development, in 2016 the new CAT-ACT hard X-ray beamline for CAT*alysis* and ACT*inide* research at ANKA became fully operational. The new ACT lab for synchrotron based radionuclide speciation studies - operated by INE in addition to the existing INE-Beamline - was fully equipped and licensed to handle radioisotopes with activities up to one million times the European exemption limit. The multi analyzer-crystal (MAC) X-ray emission spectrometer previously commissioned at the INE-Beamline was moved to the ACT station, where it has already shown to provide unprecedented insight into electronic and bonding characteristics of radionuclides in highly active nuclear materials, e.g., with the characterization of Pu oxidation states in borosilicate glasses by high resolution Pu M_5-edge XANES spectroscopy. The portfolio of laser based speciation techniques at INE comprises different optical and non-optical methods: LIBD, TRLFS, LIBS, and LA-ICP-MS (the latter in collaboration with JRC-ITU). Currently, an ambitious program to upgrade all existing systems and to improve their performance is under way. In this context, a new mobile setup for TRLFS-based U(VI) speciation studies was built and successfully commissioned in 2016. Processes determining radionuclide retention or release from nuclear waste matrices are generally controlled by surface reactions. Applying angle-dependent photoelectron spectroscopy (ADXPS), formation of an U_4O_9 (U(IV,V)) surface oxide underneath a thin (~0.5 nm) hydroxylated layer was observed on a sintered and annealed UO_2 pellet exposed for 15 months to ambient conditions. Nuclear magnetic resonance spectroscopy (NMR) gives direct insight into metal-ligand bonding phenomena relevant for complex formation and selectivity studies in the field of actinide / lanthanide separation chemistry. In 2016, a combined NMR and Cm-TRLFS investigation allowed to explain the unexpected extraction kinetics of a new bis-pyrazolyl pyridine (C4-BPP) ligand observed in initial actinide extraction studies. A method more recently established at INE is accelerator mass spectrometry (AMS). AMS is presently one of the most sensitive analytical techniques with an overall sensitivity of ~10^4 atoms in a sample. The analytical capability to determine concentrations of actinides and long lived fission products (like ^{99}Tc) in natural samples at ultra-trace levels (fg/g and ag/g) is of great relevance both for environmental studies and for in situ tracer tests or diffusion experiments as, e.g., in the frame of the CFM project at the Grimsel test site. Many of the in-house research activities at INE benefit from strong support by quantum chemical calculations, providing molecular structures or thermodynamic data. The systems under investigation vary from small complexes in solution to crystals or interfaces. New algorithms and the constantly improving hardware allow to get continuously closer to a detailed description of radionuclide systems at the level of electronic structures, thus directly complementing experimental results.

8.1 R&D projects conducted at the INE-Beamline for actinide research and the new CAT-ACT beamline at ANKA

S. Bahl, A. Bauer, E. Bohnert, K. Dardenne, E. González-Robles, M. Herm, V. Krepper, V. Metz, I. Pidchenko, J. Rothe, M. Vespa, T. Vitova

In co-operation with:

J.-D. Grunwaldt[a], H. Lichtenberg[a], T. Prüßmann[b], A. Zimina[b], T. Spangenberg[c], R. Steininger[c], S. Mangold[c], S. Peuget[d], J. Delrieu[d], C. Jégou[d]

Karlsruhe Institute of Technology, [a]Institute for Chemical Technology and Polymer Chemistry (ITCP), [b]Institute for Catalysis Research and Technology (IKFT); Karlsruhe Institute of Technology, [c]Institute for Photon Science and Synchrotron Radiation (IPS); [d]Institut de Chimie Séparative de Marcoule, CEA Valrhô Marcoule, UMR 5257, BP 17171, 30207 Bagnols-sur-Cèze, France

Introduction

Synchrotron radiation (SR) based speciation techniques have become key methods in basic and applied radionuclide research. This development is primarily driven by the need to secure molecular-scale understanding for (geo-)chemical processes determining the mobility of long-lived radionuclides possibly released from a projected disposal site for highly active, heat producing nuclear waste (HAW). Presently, final disposal in deep bedrock repositories is deemed as the preferred option for the management of spent nuclear fuel (SNF) and high level waste (HLW) glass used for conditioning of highly radioactive residues from nuclear fuel reprocessing. Solving the nuclear disposal safety case requires the assessment of an envisaged

disposal site on geological time scales, where speciation techniques like XAS (X-ray Absorption Spectroscopy) and XES (X-ray Emission Spectroscopy) provide necessary input parameters to model the geochemical behavior of radionuclides. More recently, as well attempts to directly characterize HAW matrices by XAFS techniques came into focus, mainly due to the necessity to assess effects of an extended interim storage period preceding deep geological disposal, e.g., embrittlement of fuel pin claddings.

The INE-Beamline for radionuclide science [1] at the KIT synchrotron source ANKA became fully operational in 2005 as a flexible experimental station for X-ray based radionuclide speciation investigations. One decade later, the commissioning of the new hard X-ray beamline 'CAT-ACT' for CATalysis and ACTinide research at ANKA has been completed [2] and the ACT lab for synchrotron based radionuclide speciation studies fully equipped and licensed to handle radioisotopes with activities up to one million times the exemption limit. The multi analyzer-crystal (MAC) X-ray emission spectrometer previously commissioned at INE-Beamline will serve as core component of the experimental infrastructure at the ACT lab. The INE-Beamline and the ACT experimental station are the only facilities of their kind in Europe offering direct access to radiochemistry laboratories operating a shielded box-line in close proximity to the synchrotron light source on the same research campus.

INE-Beamline user operation in 2016

After conversion of ANKA from a LK-II national user facility to a LK-I KIT internal research infrastructure in 2015, beamline operation had to be rearranged in 2016 to suit new boundary conditions, first of all a markedly reduced availability of beamtime shifts. Future ANKA operation under the auspices of the newly founded KIT Institute for Accelerator Physics and Technology (IBPT) foresees a combined use of the ANKA storage ring as SR source and testbed for the development of accelerator technology - including insertion devices, electron beam sources and beam diagnostic tools. As a consequence of ANKA restructuring beamtime distribution is no longer based on a peer review proposal process, but on in house needs within the KIT and HGF research programs and individual agreements between beamline operators and external cooperation partners.

For 2016, a total of 73 days of standard SR operation days had been initially projected (compared to 126 days in 2014) – 19 days (about 25%) of those were lost due to storage ring and beam quality failure. The remaining days were spent for INE in-house research (35%), beamline development and maintenance (10%) and external beamtime projects (30%). Nevertheless, still a total of 20 in house and external projects were successfully carried out at the beamline. For the first time, in 2016 limited user operation was also offered at the new ACT endstation after completion of the experimental setup (cf. the following section). As in previous years, INE in house projects in 2016 covered the investigation of a broad range of materials containing actinides (*An*), fission products or their chemical homologues in the context of nuclear waste disposal safety research or basic actinide chemistry. These studies comprised the investigation of Np(V) complexation by chloride, µ-focus investigations of irradiated SNF cladding fragments (described in more detail below), the effect of chemical pressure on the local structure of Eu^{3+} in $M(OH)_3$ (M = La, Y), in-situ XRD and XAFS investigations of Pu(III/IV)-ISA complexation, the redox behavior of U(VI/IV) in acidic to hyper-alkaline conditions, the solubility of U(IV) under reducing conditions in the absence and presence of carbonate or XANES measurements to identify the redox-state and speciation of As in geothermal scaling samples containing radioactive Pb-210. Several further projects received beamtime as pilot experiments during commissioning of the XAFS detection systems in the ACT laboratory, e.g., a XAS study of the co-adsorption of Se(IV) and Sr(II) on goethite. Some of these studies are presented in more detail elsewhere in this annual report. A study focusing on the advanced high resolution X-ray emission techniques (HRXES) in the tender X-ray regime (actinide M-edges) - now possible at the ACT station – is highlighted in the last section below.

HGF external scientists from the German and international research institutions listed below conducted research at the INE-Beamline in 2016:

- FZ Jülich / IEK-6, Germany
- Heidelberg University, Germany
- CEA Cadarache, France
- JRC Karlsruhe, European Commission

As in the preceding years a considerable share of INE in house beamtime was spent for experiments conducted by master and graduate students in the frame of their thesis projects.

Commissioning of the ACT experimental station and upgrades at the INE-Beamline

To secure reliable beamline operation for in house and cooperation partner requirements and to exploit

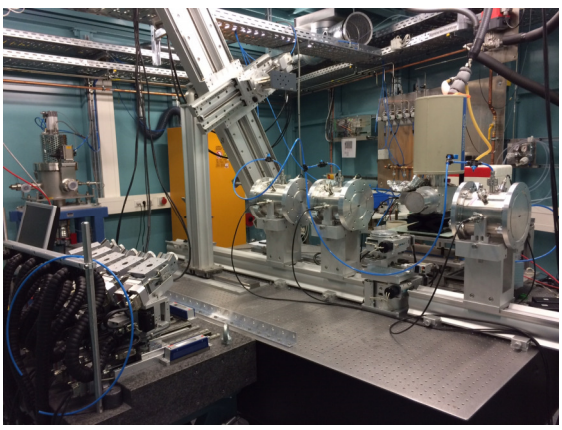

Fig. 1: *XAFS and XES detection setup at the ACT experimental station.*

limited ANKA SR operation at utmost efficiency, maintenance and consequent infrastructure upgrading are mandatory at both beamline facilities in INE's responsibility. The year 2016 was characterized by the challenge to replace major components at INE-Beamline and to setup an entirely new XAFS data acquisition system at the ACT experimental station – including capabilities for high resolution X-ray emission spectroscopy (HRXES), standard X-ray transmission and X-ray fluorescence (XRF) detection. Exchangeability of components and control software macros was intended to keep maintenance efforts at a reasonable level.

After installation of the 2.1×1.4 m^2 optical table (Newport, France), the main components of the Johann-type MAC spectrometer (analyzer crystal and detector stages) were craned into the ACT hutch and precisely aligned to a permanent position relative to the X-ray focus inside the hutch defined by the toroidal second mirror of the CAT-ACT optic. The crystal and detector positioning system was extended by a 4 axis (x,y,z,φ) sample positioning stage (Huber Diffraktionstechnik, Germany). For standard XAFS data acquisition, an optical bench based on X-95 profile rails holding three ionization chambers for parallel absorption and reference sample measurements (Poikat, Germany) was installed. The 5-pixel LEGe solid state fluorescence detector (Canberra, Belgium) – previously operated at INE-Beamline – was finally moved to ACT, as it permits detection of high energy photons up to the Kα lines of the early lanthanides accessible at the new beamline. The whole setup is depicted in Fig. 1.

Although CAT-ACT with its 2.5 T superconducting wiggler source is optimized for hard X-ray operation, the achievable low spectral limit of ~3.4 keV in the tender X-ray regime permits highly efficient absorption and emission spectroscopy at the *An* M edges (the U M4-edge, e.g., is at 3.73 keV). To avoid scattering and absorption in air, at these energies all beam paths can be kept in He atmosphere by installation of a temporary gas tight structure consisting of a rigid plexiglass frame bolted to the experiment table, which spans two flexible bags surrounding the analyzer crystals and the detector which are movable along vertical Rowland circles. Commissioning of the ACT station was completed after final tests of the ventilation system, providing about -20 Pa lower pressure inside the experiment hutch which can be designated as a temporary controlled area. A license for handling doubly contained samples with radionuclide activities up to one million times the exemption limit (with the exception of 200 mg each for the fissile isotopes U-235 and Pu-239 and 10^5 times the exemption limit for Pa-231) is provided, following the same safety concept previously implemented at the INE-Beamline.

The LEGe detector dismounted at the INE-Beamline was replaced by a thermoelectrically cooled 4-pixel Vortex ME4-multichannel system (Hitachi High-Technologies Science America, USA), which can be read-out in parallel with the existing Vortex-60VX manufactured by the same company. At both experimental stations, state-of-the-art digital X-ray pulse processors (XIA xMap DXP, USA) have been commissioned and integrated into the SPEC-based data acquisition system. Furthermore, at INE-Beamline the ageing DCM Bragg-axis servo motor controller was replaced by a state-of-the-art system (Newport XPS, France), which allows for angle encoder controlled closed loop positioning with a resolution of 1E-4 degree/step.

XAS, µ-XAS and µ-XRF investigation of an irradiated SNF cladding ring segment

In the light of a yet unclear timeframe for the necessary site selection, construction and licensing procedure before a final HAW repository becomes operational in Germany, a significant prolongation of SNF interim storage above surface (> 40 a) has to be considered. In this context, the possibly limited integrity of fuel pins - affecting SNF transportability and conditioning prior to final disposal - is of major concern. Hence, a better understanding of the effects of thermal, mechanical and radiological stress on fuel pin claddings is mandatory. Research at INE focuses on Zircaloy-4 – a cladding material commonly used in PWR fuel rod assemblies – both with respect to the formation of activation nuclides (cf. chapter 5.1) during reactor operation and the possible hull material corrosion induced by blueish-black deposits of volatile fission products observed on the inner cladding surface. In 2016 Zircaloy-4 cladding ring segments

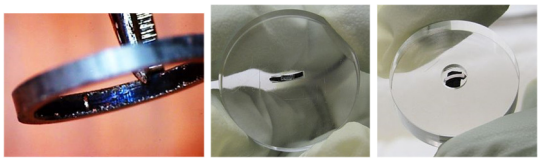

Fig. 2: *Zircaloy-4 cladding ring cut from fuel rod plenum section (left) with blueish deposit on inner surface; ring fragments mounted to expose inner surface (middle) and cross-section (right hand side image).*

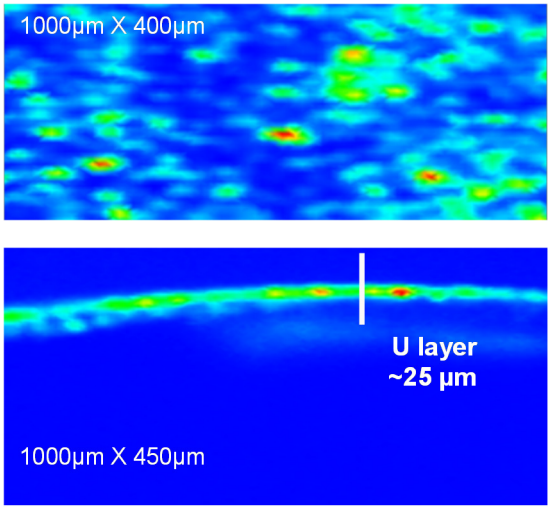

Fig. 3: *U Lα fluorescence images of (top) the inner cladding surface and (bottom) the ring cross section.*

Tab. 1: *Fabrication characteristics of Pu doped borosilicate glasses; R = m(Si_3N_4)/m(PuO_2).*

Sample	Melting temperature (°C)	m(PuO_2) (wt%)	Atmosphere	Crucible material	R
G1	1200	0.85	Ar	Pt	0
G2	1400	2.0	Ar	Pt	0.37
G3	1400	4.0	Ar	Pt	0.56
G4	1400	8.0	Ar	Pt	0.73

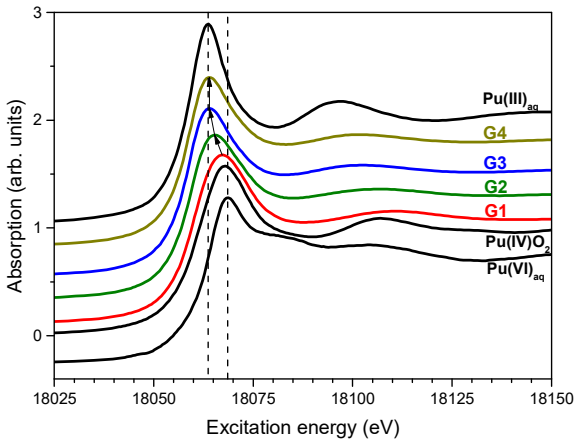

Fig. 4: *Pu L_3 edge XANES spectra of the G1-G4 glasses and the Pu(III)$_{aq}$, Pu(IV)O_2, Pu(VI)$_{aq}$ references.*

for investigation by SR-based methods were sampled from the plenum section of a fuel rod irradiated in the Swiss PWR Gösgen (average burn-up: 50.4 GWd/tHM). These measurements represent to our knowledge the first attempts ever made to characterize cladding materials from irradiated fuel with XAS and XRF techniques at a SR beamline facility. Two mm-sized cladding fragments cut from a hull material ring (contact dose rate ~30 µSv/h) were sealed in acryl glass sample holders allowing for exposure of the inner surface or the cross section towards the incident beam (cf. Fig. 2) and transferred to the INE-Beamline. U L3 bulk XAS and µ-XAS measurements for elements identified in µ-XRF distribution maps with a lateral resolution of better than 20 µm were performed for both samples in fluorescence detection mode. Excitation energies were kept below the Zr K-edge (17.998 keV) to avoid saturation of the Vortex fluorescence detector.

Surprisingly, uranium was detected as most abundant element (besides Zr which was not excited) omnipresent on the inner cladding surface – mostly concentrated in hot spots of a few tens of µm diameter (Fig. 3, top). As this part of the fuel hull was not in contact with UO_2 pellets during fuel burnup in the reactor, it has to be assumed that most of the uranium was originally deposited by abrasion during manufacturing of the fuel rods. The µ-XRF scan of the cladding ring segment cross section in Fig. 3 (bottom) exposes a marked uranium layer of about 25 µm thickness following the curvature of the inner surface (note that the blue zero-intensity area below this curve depicted in Fig. 3 represents the acryl glass backside of the sample containment, while the blue zone above corresponds to the zirconium alloy). µ-focus U L3 XANES spectra obtained from the cross-section layer and bulk U L3 XANES spectra obtained from the inner surface (beam dimension ~600 µm × 300 µm) exhibit the typical $U^{IV}O_2$ fluorite-type signature, yet with a significantly increased white line intensity – likely a particle size effect pointing to the presence of small UO_2 entities at the inner cladding surface. Preliminary U L3 EXAFS analysis does not provide clear evidence for U-Zr backscattering, thus U does not seem to be incorporated in the Zircaloy-4 matrix, but rather dispersed as oxide nanoparticles in groves or small cracks. Besides uranium, a multitude of elements was detectable on the inner cladding surface, some of them probably deposited as volatile fission products (e.g., Hg, Rb, Ba, Ti), while some (Fe, Cu, Ni) were detected as metallic particles, probably originating from sawing and sample conditioning. Unambiguous detection of cesium and iodine, both by excitation at their L3 absorption edges at 5.012 keV and 4.557 keV, respectively, was not possible due to reabsorption of their soft fluorescence photons in the UO_2 matrix or the sample containment. Future attempts will focus on the detection of these elements which are of special relevance as possibly mobile and bioavailable fission nuclides by hard X-ray K-edge measurements (Cs(0) 1s: 35.985 keV, I(0) 1s: 33.169 keV) at the ACT station.

Comparison of Pu L3-XANES with M5 HR-XANES for characterization of Pu oxidation states in borosilicate glasses

Tailored glass compositions and vitrification processes leading to desired oxidation states of the *An* elements require sensitive characterization methods. One of the widely-used tools for determination of the oxidation states of the *An* elements is the *An* L_3 edge XANES technique. However, due to the large core-hole lifetime broadening contributing to the *An* L_3 edge XANES (e.g., Pu $2p_{3/2}$: 7.8 eV), the spectrum is insensitive to the presence of minor amounts of *An* oxidation states. Deschanels *et al.* studied the Pu solubility in borosilicate glass and prepared several homogeneous glasses with increasing Pu content (0.85 - 8 wt% PuO_2) and variable amount of reducing agent (cf. Table 1). [3] They characterized the Pu oxidation state by the Pu L_3 edge XANES technique and reported stabilization of Pu in its tetra- and trivalent oxidation states. We have reexamined the oxidation states of Pu in the same glass samples applying the more advanced Pu M_5 edge high energy resolution XANES (HR-XANES) method. The *An* $M_{4,5}$ HR-XANES technique recently emerged as a valuable direct probe of the *An* 5f valence orbitals, which are largely responsible for the chemical bonding in the *An* compounds [4]. It was demonstrated that the spectra are very sensitive to the *An* oxidation states and allow, e.g., to distinguish between U(IV), U(V) and U(VI) species when mixed in the same material - not easily

possible with other spectroscopy techniques [5]. This method probes the bulk of the material (1 µm penetration depth) and does not require vacuum conditions as, e.g., the laboratory based surface sensitive X-ray photoelectron spectroscopy (1 - 10 nm penetration depth). Due to the drastically reduced core-hole lifetime broadening (0.5 eV) contributing to the spectrum compared to the Pu L_3 absorption edge (7.8 eV) and the improved experimental energy resolution, the spectral resolution is significantly enhanced, providing more reliable access to the *An* oxidation states.

Here we provide new insight into the redox behavior of Pu, which controls its solubility in glass matrices. The Pu oxidation states are correlated to the applied vitrification conditions and the added amount of reducing agent. The first application of the Pu M_5 edge HR-XANES technique for oxidation state characterization of Pu with the specific example of Pu incorporated into borosilicate glasses is reported. We demonstrate the need for development and application of such advanced methods for investigations of complex nuclear waste matrices.

The Pu doped borosilicate glasses were synthesized in the Atalante laboratories of the Commissariat à l'énergie atomique et aux énergies alternatives (CEA) Marcoule Centre, France. The chemical compositions of the Pu doped borosilicate glasses and the preliminary structural analyses can be found in the publication by Deschanels et al. [3]. The investigations discussed below are performed within the frame of the TALISMAN project TALI-C03-01 in collaboration with Sylvain Peuget, CEA Marcoule Centre.

Pu L_3 edge XANES: Fig. 4 depicts the Pu L_3 edge XANES spectra of the Pu doped G1-G4 glass samples and the $Pu(III)_{aq}$, $Pu(IV)O_2$, $Pu(VI)_{aq}$ reference materials. The experiments were performed at the INE-Beamline. The Pu L_3 edge XANES spectra mainly describe dipole allowed electronic transitions from 2p to unoccupied 6d orbitals ($2p_{3/2} \rightarrow 6d$). The energy positions of the abrupt increase in absorption (absorption edge) and the most intense absorption resonance (white line, WL) typically shift to higher energies by reduction of the electronic density in the vicinity of the Pu atom nucleus; this energy shift of the spectrum is commonly used for oxidation state analysis. However, the spectra can also shift due to changes in the short and long-range atomic environment around the absorbing atom. A well-known challenge is to differentiate between Pu(IV) and Pu(VI), where the latter tends to form short trans-dioxo bonds with lengths of 1.75 Å (Pu-yl, plutonyl) in both solid and liquid states. Due to the strong covalence of the plutonyl bond, there is an accumulation of electronic charge on the Pu atoms. As a result, the 2p core-hole is well screened and the WL positions of the Pu(VI) and the Pu(IV) spectra can coincide (cf. Fig. 4). Note that the Pu L_3 edge XANES of Pu(V) trans-dioxo species (axial bond length around 1.94 Å) is even shifted to lower energies compared to the spectrum of Pu(IV).

A trend indicated with solid black arrows can be observed in the spectra. The energy position of the WL of the G1 spectrum is slightly shifted to lower energies compared to the WL of the Pu(IV) reference spectrum, suggesting contribution of Pu(III) in the G1 sample. For R values < 0.73 (G1-G3), mixtures of most likely tri- and tetravalent Pu are formed. The energy positions of the WLs of the G4 (R = 0.73) and the Pu(III) spectra coincide, affirming the efficient reduction of Pu(IV) to Pu(III) in the G4 glass caused by the reducing agent Si_3N_4.

These results are in good agreement with the report of Deschanels *et al.*, who also applied the Pu L_3 edge XANES technique to investigate the Pu oxidation states in the glasses G1-G3. [3] However, these analyses cannot exclude potential stabilization of minor amounts of higher Pu oxidation states.

Pu M_5 edge HR-XANES: Fig. 5 depicts the Pu M_5 edge HR-XANES spectra of the G1-G4 glass samples and the $Pu(III)_{aq}$, $Pu(IV)O_2$, $Pu(VI)_{aq}$ reference materials. These experiments were performed at the INE-Beamline, whereas the spectra depicted in Fig. 6 were recorded at the new ACT experimental station. The

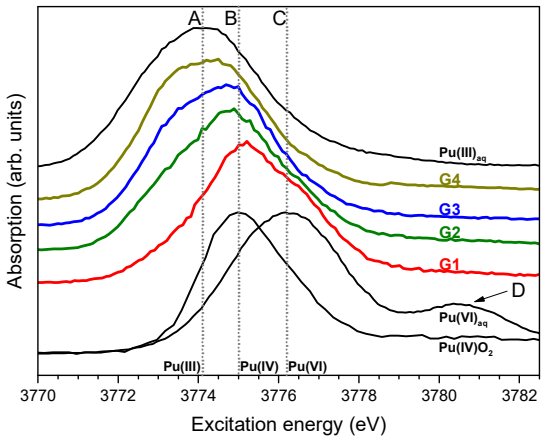

Fig. 5: *Pu M_5 edge HR-XANES spectra of the G1-G4 glasses, $Pu(IV)O_2$ reference and the $Pu(III)_{aq}$, $Pu(VI)_{aq}$ references recorded with medium and low experimental energy resolution, respectively.*

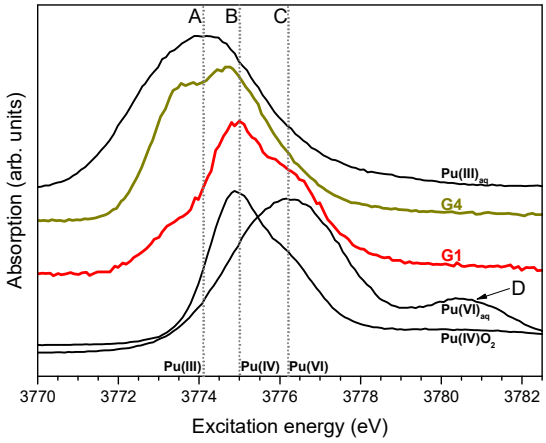

Fig. 6: *Pu M_5 edge HR-XANES spectra of the G1, G4 glasses, $Pu(IV)O_2$ reference and the $Pu(III)_{aq}$, $Pu(VI)_{aq}$ references recorded with high and low experimental energy resolution, respectively.*

MAC spectrometer described above was used for both experiments. Due to the higher photon flux at the CAT-ACT beamline, it was possible to achieve higher experimental resolution, the beam size was confined to 500 × 500 μm^2 size by applying a pinhole in front of the sample and additional masks giving access only to the central section of the five Si(220) analyzer crystals.

The Pu M_5 edge HR-XANES spectra describe the dipole allowed transitions of 3d electrons to 5f unoccupied orbitals ($3d_{3/2} \rightarrow 5f$), which contain most of the *An* valence electrons participating in the chemical bonding. The valence electronic configuration of metallic Pu is $7s^25f^6$. In contrast to the Pu L_3 edge XANES spectra, the Pu M_5 edge HR-XANES reference spectra clearly shift to higher energies in the order Pu(III), Pu(IV), Pu(VI); Pu(V) is difficult to stabilize, therefore no reference spectrum is presented. The spectra of the $Pu(III)_{aq}$ and $Pu(VI)_{aq}$ references were recorded with lower experimental energy resolution. This results in a larger broadening of the spectra. Considering the PuO_2 spectra measured with variable experimental energy resolutions a shift towards lower energies of up to 0.1 eV can be expected for $Pu(III)_{aq}$ and $Pu(VI)_{aq}$ spectra if measured with a resolution comparable to the glass spectra.

The G1 and the Pu(IV) spectra have very similar energy positions (cf. Fig. 5, line B), which is a strong indication that Pu(IV) is the main species in the G1 sample. The G2-G4 spectra are shifted to lower energies with increasing R; the spectrum of G4 peaks at about the energy position of line A (3774.1 eV) marking the most intense absorption resonance of the Pu(III) reference spectrum. This general trend suggests a reduction of the Pu oxidation state going from G1 to G4 in agreement with the Pu L_3 edge results. However, the G1-G4 spectra have asymmetric shapes. There are shoulders on the low (3774.1 eV) and high energy (3776.5 eV) sides of the G1 spectrum, which increase and decrease in intensity, respectively, going from the G1 to the G4 spectrum. These additional spectral features point to mixtures of Pu(III) (line A), Pu(IV) (line B) and a higher oxidation state of Pu. We infer that this spectral contribution is likely due to the presence of Pu(VI) (line C). Note that the shoulder positioned next to line C on the high-energy side of the main peaks of the G1 and G2 spectra (3776.5 eV) nearly coincides with the main peak of the Pu(VI) reference. Pu(V) is less probable but it might be potentially stabilized in the glass matrix as well, therefore we cannot completely exclude its presence.

The G1, G4 and PuO_2 spectra recorded with even higher experimental energy resolution are depicted in Fig. 6. The shoulder C is well pronounced in the G1 spectrum, affirming the formation of Pu species with higher than +IV oxidation state. The low energy shoulder corresponding to minor contribution of Pu(III) is now clearly distinguishable in the G1 spectrum. The high-energy resolution enables also distinct detection of Pu(III) and Pu(IV) in the G4 glass. The spectrum demonstrates formation of similar amounts of Pu(III) and Pu(IV).

The post-edge feature D in the Pu(VI) reference spectrum is characteristic for plutonyl [4,6] and describes transitions to the sigma antibonding (σ^*) molecular orbital. [6]. A similar peak was reported recently also for uranyl by Vitova *et al*. [4]. As feature D is not present in the spectra of G1 and G2, we conclude that the potential Pu(VI) species does not form a plutonyl type of bonding. It is more likely that the Pu-O distances are elongated and Pu is coordinated by a more symmetric set of O atoms than in the plutonyl case, i.e., in a plutonate structure.

In summary, the Pu M5 edge HR-XANES method is clearly capable of detecting Pu(III), Pu(IV) and Pu(VI) being simultaneously present in a nuclear glass sample. Quantitative analyses of the Pu species with different oxidization states are possible when spectra of appropriate reference materials are recorded under the same experimental conditions. Our study demonstrates that this characterization method can be used for monitoring the redox conditions in vitrification processes upon reductant addition. A clear correlation of Pu oxidation state distribution and added amount of the reductant is revealed. For complete reduction of Pu to the trivalent state in glass with similar chemical composition it would be necessary to adjust R to a value higher than 0.73. This will most likely further increase the Pu loading in the glass.

We also clearly detected for the first time the formation of Pu(VI) species in glasses synthesized upon addition of a Pu nitric acid solution to the glass melt. Further experiments are needed to verify if Pu(VI) yields higher solubility as compared to Pu(III). In case of an analogy of Pu(VI) and U(VI) behavior in borosilicate glasses, a solubility limit around 40 wt% would be expected. This might open new possibilities to increase Pu solubility in vitrification processes.

References

[1] Rothe, J. et al., *Rev. Sci. Instrum.*, **83**: 043105 (2012).

[2] Zimina, A. et al., *J. Phys.: Conf. Series*, **712**: 012019 (2016).

[3] Deschanels, X. et al., *Prog. Nucl. Ener.*, **49**: 623 (2007).

[4] Vitova, T. et al., *Inorg. Chem.*, **54**: 174 (2008).

[5] Pidchenko, I. et al., *Environ. Sci. & Technol.*, **51**: 2217 (2017).

[6] Vitova, T. et al., in print, *Nature Comm.* (2017).

8.2 Laser spectroscopy

C. Garcia, R. Götz, T. Hippel, C. Koke, V. Krepper, P. Lindqvist-Reis

Introduction

Laser based spectroscopy techniques are very useful in the nuclear waste disposal field because of their ability to provide speciation information at trace levels or detection of colloidal species with highest sensitivity. Nowadays there are several laser based speciation methods used at INE – including LIBD, TRLFS, LIBS or LA-ICP-MS (the latter in collaboration with JRC Karlsruhe), mostly for studies in the context of the migration behavior of different actinide (An) species (or chemically homologue lanthanides (Ln)) after their hypothetical release from a nuclear waste repository. In order to broaden the TRLFS speciation capabilities at INE, new instrumental set-ups and upgrades of already existing instrumentation have been carried out in 2016. The design of a cell for high temperature/high pressure TRLFS measurements previously developed at INE has been improved to extend its applicability to high pH solutions or highly corrosive media. Additionally, a new portable set-up for luminescence measurements of uranyl species at ambient, high and low temperature has been designed and constructed, offering the capability to be coupled to different detection systems.

Development of a high-temperature/high-pressure cell for TRLFS measurements

Understanding An behavior in (geo)chemical systems is essential when assessing the safety of an envisaged nuclear waste repository. Hydrolysis or complexation mechanisms of these elements in aquifers possibly neighboring the repository site have been extensively studied during the past decades. Radionuclide (RN) migration or retention behavior in the multi-barrier system isolating the repository from the biosphere are not only influenced by the (geo)chemical environment, but also by thermal or pressure conditions given at or near the repository [1,2].

TRLFS is a laser based technique routinely used for An and Ln speciation studies. Although most of the experiments are performed at ambient temperature/pressure conditions, one needs to consider that the temperature in some parts of the repository after waste emplacement and closure might exceed 90°C due to the persistent radioactive decay heat. Nevertheless, a rather limited number of studies has been published in the past with the focus on possible effects of elevated temperatures on An/Ln complexation behavior [3-5]. With the aim to carry out systematic high-temperature experiments on radioactive solutions, about a decade ago a high-pressure cell for TRLFS and XAFS speciation studies was developed and successfully employed at INE (Fig. 1(a)) [6-8]. In this first design all parts of the cell (main body, windows (alternately quartz or beryllium), O-rings and PEEK fittings) are in direct contact with the sample solution. A special Ti/Pd alloy for the main body and Kalrez® O-rings for window sealing – parts exposed to the highest temperatures during operation – were chosen for their high corrosion resistance. Those parts not exposed to high temperatures are made of PEEK. Quartz windows are embedded into the Ti/Pd body to easily couple a fiber optic bundle for delivery of the excitation laser beam and collection of the optical fluorescence. In case of XAFS measurements at the INE-Beamline, two of the quartz windows are replaced by metallic beryllium windows coated with Kapton® tape. The possibility to increase the working pressure up to 13 - 15 bar facilitates to suppress the formation of bubbles when analyzing samples at $T > 100°C$. With this original cell design, a regular filling requires sample volumes above 2 ml.

Although the original cell was working very reliably, some specific drawbacks exist. When analyzing highly corrosive media, persistent contamination of the cell body or even structural damages were detected. Due to these limitations and the high costs of the cell body material, the original cell was only used for specific analytical tasks with less corrosive samples and for combined TRLFS and XAFS studies.

In the last two years, an improved cell design has been conceived, built and recently successfully tested (Fig. 1(b)) in order to overcome the aforementioned drawbacks. The new cell design resembles an autoclave comprising a stainless-steel body with an interior holder for standard Suprasil® spectroscopy cuvettes. The holder can be moved up and down, allowing the adjustment of the cuvette height to the beam path – a very important feature when analyzing small sample volumes. Additionally, the cuvette holder can be easily exchanged to adapt to different cuvette geometries. As in the previous design, the new cell possesses four quartz windows allowing for a similar

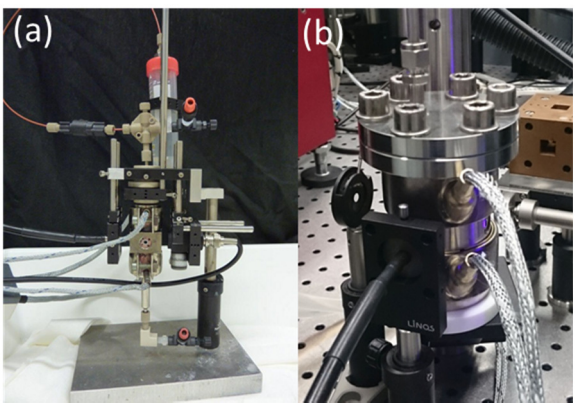

Fig. 1: *(a) Original high-temperature TRLFS cell built at INE. (b) Advanced cell design (cf. text for details).*

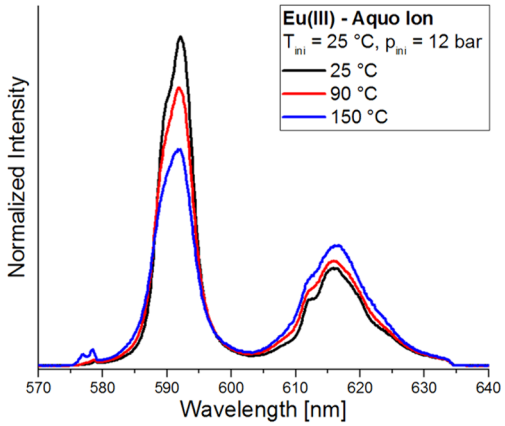

Fig. 2: *TRLFS of Eu(III) aquo ion measured with the new cell at 25, 90 and 150°C. Initial pressure: 12 bar; pressure at 150°C: ~20 bar.*

fiber optic coupling. The main advantages of the new design are: easy decontamination of cuvette and cell body, reduced sample volume, the possibility to use similar media for high-temperature and room temperature measurements, exclusion of sample induced cell damage and reduction of material costs.

As a result of preliminary tests, the cell has been proven to be airtight at 30 bars for almost 5 days with the maximum applied pressure being 66 bar. The first TRLFS signals measured for an aqueous sample containing the Eu(III) aquo ion at temperatures up to 150°C are plotted in Fig. 2. This experiment demonstrates that the new cell design is well applicable for An/Ln high-temperature speciation investigations. For these measurements the 3rd harmonic of a Nd:Yag Laser at 355 nm was used to pump a dye Laser, using Exalite 398 as a dye and an excitation wavelength of 394 nm. The fluorescence emission was dispersed with a polychromator and detected by using an intensified CCD camera. The new cell, with some small modifications, will be also available in the future for XAFS measurements at the INE-BL and ACT experimental stations at ANKA.

Development of a TRLFS set-up for U(VI) speciation studies

Uranium (U) is by far the most abundant radioactive element in nuclear wastes originating from various steps of nuclear power generation (including uranium mining, fuel fabrication or spent fuel disposal). U contaminants in the environment may be present in different chemical forms depending on the actual (geo)chemical conditions. Changes of the oxidation state will affect U solubility in aqueous solution and its sorption properties on mineral surfaces. Under oxidizing conditions U predominantly exists as U(VI) species, which is highly water soluble in form of the linear trans-dioxo uranyl cation (UO_2^{2+}).

TRLFS has been used for many years to follow uranyl migration in environmental compartments at rather low U concentrations [9-10]. Here the position of the emission bands in uranyl luminescence spectra and the radiative lifetimes provide useful speciation information. Dedicated to this analytical purpose, a new portable luminescence excitation set-up has been designed and built at INE in 2016 (Fig. 3). The system will be applied to characterize UO_2^{2+} aqueous species or for uranyl analyses in soils or solid mineral phases (e.g., to follow carbonate induced dissolution of uranium containing precipitates possibly forming near a nuclear waste repository). Depending on the ligand system, uranyl luminescence emission at room temperature is very weak (e.g., for pure uranyl carbonate complexes), but easier to detect at liquid helium temperature [11]. To overcome this limitation and to offer high flexibility when simulating repository conditions, the new set-up allows analyses at ambient as well as at high and low temperatures.

The excitation source is a Nd:Yag laser (SpitLight Compact 100, InnoLas Laser) equipped with crystals for the 4th harmonic generation (266 nm), providing energies up to 30 mJ/pulse with 7 ns pulse duration and 10 Hz repetition rate. Excitation at this wavelength induces the typical green emission of the $(UO_2)^{2+}$ cation due to deactivation of a formally triplet ligand-to-metal charge transfer (LMCT) excited state. The laser has been installed in a carbon fiber reinforced optical bench from CarbonVision GmbH (300 mm × 900 mm). The bench is integrated into an aluminum rack with wheels. The entire instrument is movable and can be attached to different detection set-ups. In the optical set-up two dichroic mirrors positioned in a 90° configuration relative to the laser beam enable easy and fast alignment and increase the rigidity of the optical system. The beam energy is measured with a thermopile sensor (Newport Corpo-

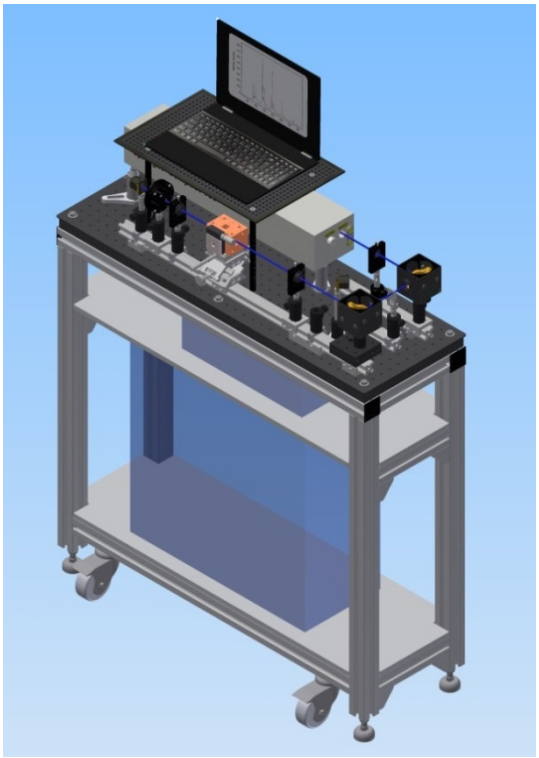

Fig. 3: *New portable laser excitation setup for TRLFS speciation studies.*

ration) by using a beam splitter between the two dichroic mirrors. Its value can be fixed between 0.5 and 10 mJ/pulse depending on the sample. Additional optical elements have been introduced in the set-up to reduce the primary inner filter effect (PIFE) and to avoid second order diffraction of the laser stray light at 532 nm.

For the analysis of liquid samples at room temperature the laser passes through a quartz cuvette (Helma) introduced in a home-built copper holder mounted on the optical bench and equipped with a mini stirrer. The luminescence propagating in a perpendicular direction to the laser beam is collected by a customized bundle-type fiber optic connected to the copper holder. The output of the fiber optic can be easily fed into different detection systems. During initial tests of the set-up it was coupled to the variable entrance slit of a Czerny-Turner Shamrock SR 303i spectrometer (Andor Technology) with a triple grating turret (400, 1200 and 2400 l/mm gratings) using an intensified CCD camera (Andor iStar) for luminescence detection. Time resolution is achieved by synchronizing the data acquisition by the CCD camera with the sync output signal delivered by the laser system. The time interval between the trigger signal of the laser and data acquisition by the camera is adjusted by an external digital delay generator (Stanford Research Systems). The delay values can be optimized depending on the lifetime of the analyzed species. For species with short luminescence lifetimes the delay inherent to the laser electronics as well as the insertion delay time of the CCD must be taken into account. The capability of the system to detect short lifetime species has been demonstrated by analyzing a cerium chloride ($CeCl_3 \cdot 7H_2O$) sample, obtaining a lifetime of 24.5 ns. Note that Cerium luminescence can be as well excited at a laser wavelength of 266 nm (the $CeCl_3$ crystal structure is of the UCl_3 structure type).

For TRLFS measurements at low temperature, one of the mirrors has been mounted on a kinematic magnetic base (Newport) to allow its easy removal and reinsertion into the beam path with high reproducibility. The portable laser table is fixed next to the He cryostat (CryVac). The samples introduced in the custom-made vacuum chamber of the cryostat with a capacity for two sample cuvettes can be cooled down to 4 K. Operation of the cryostat and the vacuum system are controlled by a home-made LabView program. The low-temperature sample luminescence is collected at an angle of 45° relative to the exciting laser beam by an optical fiber bundle connected to an x/y alignment stage coupled to the cryostat chamber. Detection of low-temperature TRLFS spectra is normally performed with the spectrometer/camera system described above. The luminescence of a $Cs[UO_2(NO_3)_3]$ crystal sample measured with the new set-up at room temperature is shown in Fig. 4 (a). When analyzing the same sample in the cryostat at liquid helium temperature (4 K) and with a 2400 l/mm grating, the electronic-vibrational spectra of the uranyl species in the crystal are easily discernible (Fig. 4 (b)) [12]. The good spectral resolution allows to investigate the effect of the crystal lattice on the vibrational structure of the spectra.

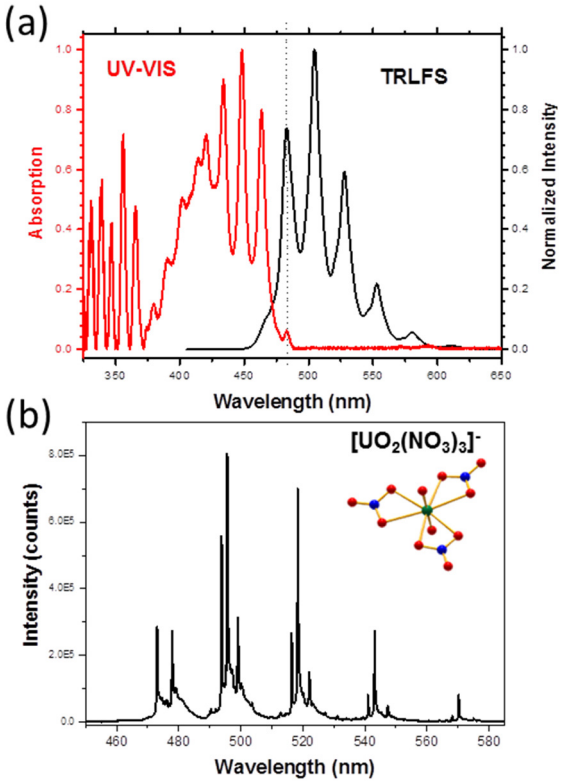

Fig. 4: *TRLFS spectra of $Cs[UO_2(NO_3)_3]$ measured with the new set-up (a) at room temperature and (b) at 4 K. For comparison purposes the UV-VIS spectra of the same sample is shown in graph (a).*

References

[1] J.R. Haas et al., *Geochimica et Cosmochimica Acta*, **59**, 4329-4350 (1995).

[2] L. Rao, *Chemical Society Reviews*, **36**, 881-892 (2007).

[3] T. Kimura et al., *Radiochimica Acta*, **90**, 715-719 (2002).

[4] A. Kirishima et al., *Journal of Alloys and Compounds*, **374**, 277-282 (2004).

[5] L. Rao et al., *Inorganic Chemistry*, **48**, 964-970 (2009)

[6] P. Lindqvist-Reis et al., *Journal* of *Physical Chemistry B*, **109**, 3077-3083 (2005).

[7] A. Skerencak et al., *Radiochimica Acta*, **97**, 385-393 (2009).

[8] A. Skerencak-Frech et al., *Inorganic Chemistry*, **53**, 1062-1069 (2014).

[9] G. Meinrath, *Journal of Radioanalytical and Nuclear Chemistry*, **224**, 119-126 (1997).

[10] G. Geipel, *Coordination Chemistry Reviews*, **250**, 844-854 (2006).

[11] Z. Wang et al., *Environmental Science & Technology*, **38**, 5591-5597 (2004).

[12] L.V. Volod'ko et al. *Journal of Applied Spectroscopy,* **20,** 480-483 (1974).

8.3 Microscopy and surface analytics

T. Yokosawa, K. Hinz, W. Tobie, M. Plaschke, M. Brandauer, E. Soballa, D. Schild, H. Geckeis

In co-operation with:

C.-O. Kraußª, A. Henekaª, S. Gentesª

ª Department of Deconstruction and Decommissioning of Conventional and Nuclear Buildings, Institute for Technology and Management in Construction (TMB), Karlsruhe Institute of Technology (KIT)

Introduction

Nuclear waste forms and brines at a deep underground repository may contain borate. In case water ingress and failure of the nuclear waste containers, the chemical state of released radionuclides affects their ability to migrate. Secondary phase formation can attenuate migration of highly mobile Np(V). New solids of Np-borate formed in diluted brines are analyzed by electron microscopy and spectroscopy.

Oxidation of spent nuclear fuel towards U_3O_8 in case of cladding failure during intermediate long-term storage is accompanied by an increase in volume of 31% which disintegrates pellets. The initial oxidation of an UO_2 pellet surface at the atmosphere is studied by angle-dependent XPS.

Interaction of abrasive particles with steel during water abrasive suspension cutting is characterized by SEM-EDX. This cutting technique is beneficial if applied to activated components with internal stress such as in the deconstruction of nuclear reactor pressure vessels and internals.

Investigation of Neptunium-borate by SEM, XPS, and TEM

In this study, the interaction of highly mobile Np(V) with borate in diluted NaCl and $MgCl_2$ solutions was analyzed by solubility experiments with solid amorphous NpO_2OH. Np(V)-borate complexes have a minor impact on the solubility of Np(V) at near-neutral to weakly alkaline pH. In dilute NaCl (0.1 M) or $MgCl_2$ (0.25 M) solutions with 0.16 M B and $pH_m < 9$, however, the Np(V) solubility is lowered by 3 to 4 orders of magnitude after 270 days of experiment. The color of the solid phase changed from greenish to light grey [1]. The solids were washed with ethanol prior to characterization by XRD, XPS, SEM-EDX, and TEM.

SEM images of the newly formed Np(V)-borate solid phases recorded by a FEI Quanta 650 FEG instrument are shown in Fig. 1. The sample equilibrated in 0.1 M NaCl is composed of thin (~20 nm) hexagonal platelets with a size of about 500 nm, whereas the platelets of the sample equilibrated in 0.25 M $MgCl_2$ appear less crystallized. SEM-EDX of the Np(V) secondary phases detects O, Na, Mg, and Np, XPS

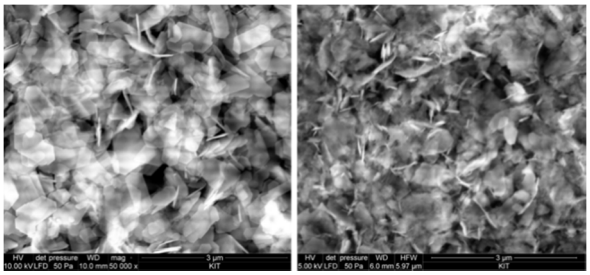

Fig. 1: *SEM images of Np(V)-borate phases formed in solutions of 0.1 M NaCl (left) or 0.25 M $MgCl_2$ (right).*

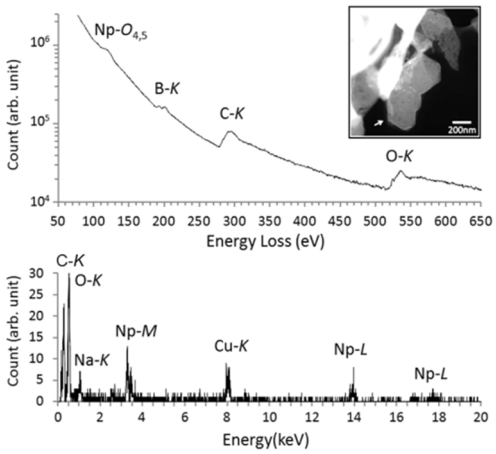

Fig. 2: *EELS (top) and TEM-EDX (bottom) of Np(V)-borate phase formed in 0.1 M NaCl solution.*

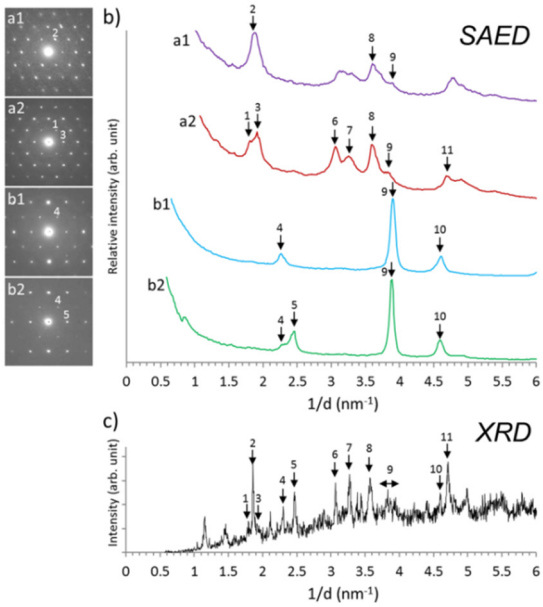

Fig. 3: *SAED patterns of various particles of Np(V)-borate formed in 0.1 M NaCl solution. Diffractograms obtained by rotational averaging of the SAED patterns are compared to powder XRD data.*

additionally shows presence of B, whereas Cl is not detected. The EDX detector was not able to detect boron. Atomic concentrations are determined by XPS survey spectra. Narrow scans of elemental lines indicate Np(V) and a single B species. The stoichiometry of the solid phases deduced from XPS data is supposed to be neptunyl-pentaborate – $NpO_2[B_5O_6(OH)_4]\cdot 2NaOH$ in case of NaCl solution and $(NpO_2)_2[B_5O_6(OH)_4]_2\cdot 3Mg(OH)_2$ in case of $MgCl_2$ solution, respectively.

TEM measurements are performed by employing a FEI Tecnai G2 F20 X-TWIN operated at 200 kV, located at IAM-WBM-FML (KIT). EELS and EDX spectra (Fig. 2) of the sample equilibrated in 0.1 M NaCl show the presence of Np, B, O, and Na, consistent with the result obtained by XPS. Since powder XRD diffractograms obtained for the newly formed solid phase with crystalline character gave no positive match with any of the existing borate entries in the JCPDS database, selected area electron diffraction (SAED) was applied (Fig. 3). Comparing the SAED radial profiles to the XRD profile, diffraction peaks indicated by 1, 2,.. and 11 observed in the radial profiles and in the XRD profile show a good match at the peak positions, although there are some diffraction peaks in the XRD profile which were not observed by SAED in this study. Thus, it was revealed by SAED that the sample of 0.1 M NaCl contains several (at least four) phases which show different SAED patterns from each other, causing difficulty in performing the phase identification by XRD.

Oxidation of UO_2 pellet exposed to atmosphere

Exposure of UO_2 to the atmosphere results in fast formation of UO_{2+x} ($x < 0.25$) at the surface via diffusion of oxygen. U_4O_9 is formed which transforms to U_3O_7 during ongoing oxidation. Subsequent nucleation and growth yields U_3O_8 which is the most abundant form of uranium found in nature. Further oxidation to UO_3 is very slow. The oxidation from UO_2 to U_3O_8 is accompanied by an increase in volume by 31% which will disintegrate UO_2 pellets [2]. There is a still ongoing discussion about how this oxidation proceeds, either via U(IV,VI)-oxides or if U(V) is involved, e.g., U_4O_9 is represented by $(UO_2)_3\cdot UO_3$ or $(UO_2)_2\cdot U_2O_5$. In nature, wyartite $CaU^{(V)}(UO_2)_2O_4(CO_3)(OH)\cdot 7H_2O$, which is a natural alteration product of uraninite, was the first mineral identified to contain U(V) [3]. The presence of U(V) in U_3O_8 was predicted theoretically [4]. U(V) in U_4O_9 and U_3O_8 ($U_2O_5\cdot UO_3$) was observed by use of HERFD-XANES [5].

In this study, an ULVAC-PHI VersaProbe II X-ray photoelectron spectrometer was used for analyses of the outermost surface of a polished sintered UO_2 pellet exposed to the atmosphere during 15 months at room temperature after H_2 annealing. Angle-dependent XPS (ADXPS) was applied by recording narrow scans of elemental lines at various angles between pellet surface normal and analyzer axis in order to probe different depths. Monochromatic Al K_α X-ray excitation and pass energy of the analyzer of 23.5 eV was used. The acceptance angle into the analyzer was 0.1 sr. U 4f and C 1s spectra are similar at all measured angles, whereas O 1s spectra differ (Figs. 4, 5). The U 4f elemental lines are composed of two main components of similar intensity. In Figure 4 the U $4f_{7/2}$ lines are additionally deconvolved applying the maximum entropy method [6] to a virtual pass energy of 2.95 eV of the analyzer by (PHI-ULVAC software MultiPak Ver.7.1). The U $4f_{7/2}$ binding energies (380.0 eV and 380.8 eV) and binding energy separations between main line and associated shake-up satellite (6.6 eV and

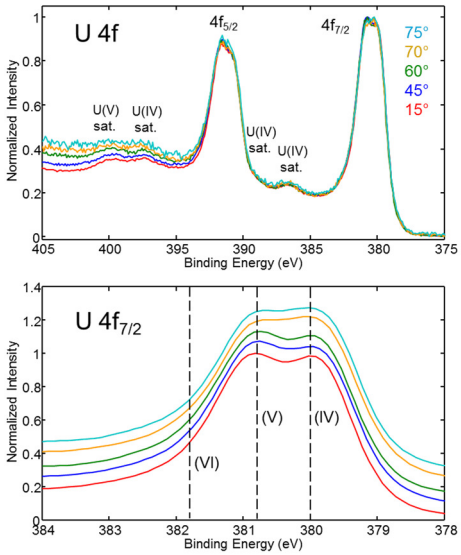

Fig. 4: *ADXPS narrow scans of U 4f elemental lines of oxidized UO_2 pellet recorded at various angles between surface normal and analyzer. Enhanced view of U $4f_{7/2}$ shows the result of deconvolution (stack plot). Binding energies typical for the valence states of U are indicated.*

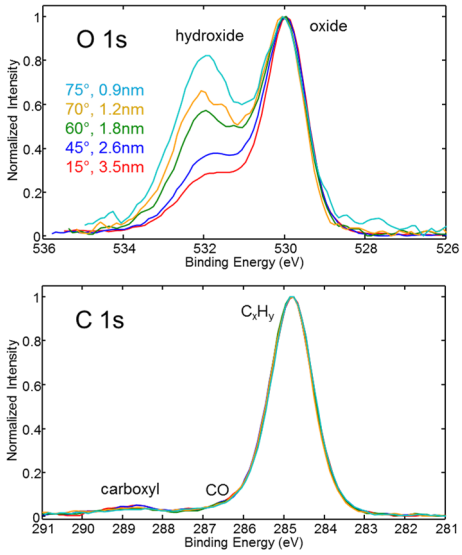

Fig. 5: *ADXPS narrow scans of O 1s and C 1s elemental lines of oxidized UO_2 pellet recorded at different angles between surface normal and analyzer. Depths of information (95% of signal) are calculated for different angles.*

8.1 eV, respectively) are characteristic for U(IV) and U(V) [7]. Similar abundances of U(IV) and U(V) point to the existence of U_4O_9 at the pellet surface. The portion of U(VI) is less than 7% as revealed by a curve-fit. O 1s spectra show two components, the binding energy of the component at 530.0 eV is characteristic for oxide; the component at 532.0 eV is assigned to hydroxide. According to analyses of uranium minerals [8] the binding energy of the hydroxide portion is typical for OH in the equatorial plane of uranyl polyhedrons.

Probing different depths by ADXPS shows enhanced abundance of hydroxide at the outermost surface of the pellet. A homogeneous layer model consisting of an adventitious hydrocarbon layer at the outermost surface, a hydroxylated layer, and U_4O_9 beneath is employed to estimate the extent of hydroxide formation. Since the adventitious hydrocarbon layer does not contain significant amounts of oxygen (only in traces of carboxylic and COH groups), Strohmeier´s equation [9] and C2 equation for electron effective attenuation lengths [10] are employed for calculation of the thickness of hydroxylated layer by use of curve-fits to O 1s spectra. The thickness of the hydroxylated layer is about 0.5 nm, calculated at 45° between surface normal and analyzer axis. Since the results for the thickness vary at various angles by about 10%, a gradient of the hydroxide concentration is likely, similar to results by Marchetti [11], who immersed UO_2 in ^{18}O labelled water and applied SIMS depth profiling. The thickness of the adventitious hydrocarbon layer is calculated to 0.8 nm by comparison of the C 1s intensity with that of low density-polyethylene as a model substance for adventitious hydrocarbon.

The result of this study shows that (a) valence state identification of uranium is feasible by XPS with monochromatic X-ray excitation, (b) a hydroxylated layer with U(IV,V)-oxide U_4O_9 beneath is formed at ambient conditions, (c) the hydroxylated layer is not carbonated at the experimental conditions applied.

MASK project: SEM analyses

The objective of the BMBF project MASK is the magnet separation of granular mixtures of waterjet cutting to minimize secondary waste in the decommissioning of nuclear facilities. The dissection of the reactor pressure vessel and internals may be performed by cutting with a high-pressure waterjet with admixture of abrasive grains. To reduce the radioactivity of the used solid material which is composed of about 98 wt% abrasive grains and 2 wt% radioactive steel cuttings, magnet separation is applied to the suspension. SEM imaging of separated abrasive grains show in some cases steel adherences and void filling (Fig. 6). The steel adherences originate from impact of abrasive particles onto steel. In addition, fractures occur in the vicinity of impact areas at abrasive grains causing fragmentation. Closer analyses of the steel adherences show signs of solidified melts of steel and abrasive material (Fig. 7). The abrasive grains are sharp-edged almandine, $Fe_3Al_2(SiO_4)_3$, a mineral with a density of 4.2 g/cm^3, hardness of 7.5 - 8.5 on Mohs scale, and melting point of (1250 - 1315)°C. Stainless steel has a density of 8 g/cm^3 and a melting point of (1325 - 1530)°C depending on the specific alloy. The velocity of the waterjet is about 580 m/s, a typical abrasive grain has thus a kinetic energy of ~3 mJ. During impact of an abrasive grain onto steel the kinetic energy is dissipated within the contact time of 1 to 3 ns. Radiative heat transfer proportional to T^4 limits the temperature rise but it is still high enough to melt almandine and steel. However, the images indicate that intermixing of the materials during the melting process does not take place. Presently, the adherences of steel to abrasive grains limit the magnetic separation process and an additional treatment step is needed to improve the separation grade.

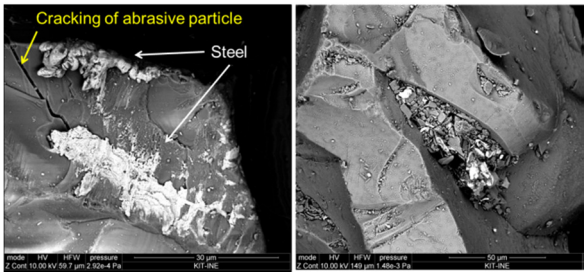

Fig. 6: *Backscattered electron images. Left image: edge of an abrasive particle (grey) with steel adherence (light) and crack formation, horizontal field width of image: 60 µm. Right image: filling of void at an abrasive particle; horizontal field width of image: 149 µm.*

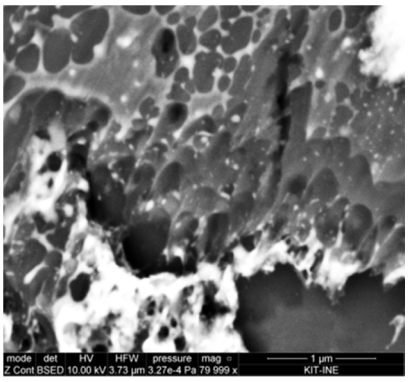

Fig. 7: *Backscattered electron image of steel adherence to an abrasive particle showing evidence of solidified melt of steel and abrasive material. Horizontal field width of image: 3.73 µm.*

References

[1] Hinz, K., *PhD thesis,* Karlsruhe Institute of Technology (2015).

[2] McEachern, R.J. et al., *J. Nucl. Mat.* **254**, 87-121 (1998).

[3] Burns, P.C., et al., *Am. Mineral.* **84**, 1456-1460 (1999).

[4] Yun, Y., et al., *Phys. Rev. B* **83**, 075109 (2011).

[5] Kvashnina, K.O., et al., *Phys. Rev. Lett.* **111**, 253002 (2013).

[6] Jansson, P.A. (ed.), *Deconvolution of Images and Spectra.* Academic Press, London (1997).
[7] Ilton, E.S., et al., *Surf. Interface Anal.* **43**, 1549-1560 (2011).
[8] Schindler, M., et al., *Geochim. Cosmochim. Ac.* **73**, 2488-2509 (2009).
[9] Strohmeier, B.R., *Surf. Interface. Anal.* **15**, 51-56 (1990).
[10] Cumpson, P.J., et al., *Surf. Interface Anal.* **25**, 430-446 (1997).
[11] Marchetti, I., *PhD thesis,* Ruprechts Karls University Heidelberg, 61 (2013).

8.4 Structural investigations on radioactive materials in solution by NMR-Spectroscopy

Ch. Adam, Ch. Wagner, A. Skerencak-Frech, P. Weßling, A. Geist, P. J. Panak

In co-operation with:

L. Medyk[a], J. Korzekwa[b], A. Scheurer[b], K. Meyer[b], A. Wilden[c], G. Modolo[c]

[a] Ecole Nationale Supérieure de Chimie de Montpellier; France; [b] Department of Chemistry and Pharmacy, Chair of Inorganic and General Chemistry, Friedrich-Alexander-University Erlangen-Nürnberg, Germany; [c] Forschungszentrum Jülich GmbH, Institut für Energie- und Klimaforschung (IEK-6), Nukleare Entsorgung und Reaktorsicherheit, 52425 Jülich, Germany

Introduction

Originally derived from the bis-triazinyl pyridine (BTP) motif, bis-pyrazolyl pyridine (BPP) type ligands have the ability to achieve the separation of trivalent actinides (An) from lanthanides (Ln) in liquid-liquid extraction processes [1-2]. The preferred complexation of An(III) ions in the presence of chemically highly similar Ln(III) ions also poses an intriguing research topic, as it includes the understanding of structure and bonding in *f*-element complexes. In-depth knowledge of the underlying mechanisms is not only desirable from a scientific point of view, but could also enable the rational design of improved tailored extractants.

The substituents on the triazine rings in BTPs and the pyrazolyle rings in BPP ligands are of crucial importance for the solubility in organic or aqueous media. They also influence the extraction behavior, stability against hydrolysis and radiolysis, and the selectivity of the ligands. However, this influence has so far not been studied in a systematic manner. Previous efforts in our group contain a comparative study of *n*-propyl- and *iso*-propyl substituted BTP ligands [3-4] and studies of C5-BPP (1) complexes with Ln(III) and Am(III) ions [5-6]. Recently, the aliphatic *neo*-pentyl side chains of C5-BPP were exchanged to *tert*-butyl substituents in C4-BPP (2) at FAU Erlangen-Nürnberg.

As both molecules are very similar in structure, resembling properties in terms of complex stability and formation were expected. However, initial extraction studies performed at FZJ-IEK-6 showed inexplicable extraction kinetics, which prompted us to perform a thorough investigation of the lanthanide and actinide C4-BPP complexes. For this, we employed a combination of further extraction studies, Nuclear Magnetic Resonance (NMR) and Time-Resolved Laser Fluorescence Spectroscopy (TRLFS).

TRLFS studies

The complexation of Cm(III) and Eu(III) with C4-BPP was studied with TRLFS. Cm(III) and Eu(III) are used as representatives of the trivalent actinides and lanthanides because of their excellent fluorescence properties which allow spectroscopic investigations at very low metal concentrations. Conditions of the experiments were chosen as for previous studies on C5-BPP [2] to allow for maximum comparability of the results. With TRLFS the speciation of the Cm(III) and Eu(III) C4-BPP complexes as well as the thermodynamic parameters of the complexation reaction are determined.

Fig. 1: *Structures of the C5-BPP (1) and C4-BPP (2) ligands.*

The complexation of Eu(III) with C4-BPP was studied in dependence of the ligand concentration ($c(Eu^{3+})_{ini} = 1 \cdot 10^{-5}$ mol·L^{-1}, c(C4-BPP) = 0-1.01·10^{-2} mol·L^{-1}). The fluorescence spectra of the pure components (Eu(III) aquo, 1:1, 1:2 and 1:3 Eu(III) C4-BPP complexes) were used to determine the fractions of these species by peak deconvolution of the emission spectra. In the ligand concentration range of up to 10^{-2} mol·L^{-1} only the 1:1 ($\log K'_1 = 6.2$) and 1:2 ($\log K'_2 = 4.1$) Eu(III) C4-BPP complexes are formed. No evidence for 1:3 complexes have been found in the TRLFS experiments. Considering the complex stability constants, which are comparable to the Cm(III) complexation of C5-BPP (*cf.* Table 1; complex stability constants for Eu(III) complexes are not available in literature), where 1:3 complexes were found, this result seems surprising. First temperature-dependent TRLFS measurements to determine the thermodynamic parameters of the complexation show that the first complexation step is exothermic, while the formation of the 1:2 complex is endothermic. If the third complexation step is even more endothermic, this might explain the observed complexation behavior.

The complexation of Cm(III) with C4-BPP in dependence of the ligand concentration was also studied using TRLFS. While 1:1 and 1:2 complexes are formed during the titration, evidence for a 1:3 com-

Tab. 1: *Conditional complex stability constants for the Cm(III) complex species of C4-BPP and C5-BPP [2].*

Species	log K' C4-BPP	log K' C5-BPP
1:1	7.0	6.9
1:2	2.6	4.3
1:3	---	3.6

plex was only found in a batch experiment at decidedly higher ligand-to-metal ratios.

The comparison of the conditional complex formation constants with those of the Cm(III) C5-BPP complexes (Table 1) shows that the 1:1 complexes have almost the same stability constants, while the C4-BPP 1:2 complex is 1.3 orders of magnitude less stable. We assume that this is an effect of the greater sterical hindrance in the C4-BPP complexes: the bulky *tert*-butyl groups are closer to the aromatic ligand core, and with the absence of the methylene group in the side chain the molecule loses its flexibility. This leads to an increased ligand-ligand repulsion in the first coordination sphere of the metal ion.

NMR studies

In continuation of the TRLFS experiments, NMR titration experiments with the C4-BPP ligand were performed. As NMR is an inherently less sensitive method, higher metal and ligand concentrations are required. A solution of $Lu(OTf)_3$ in deuterated methanol ($c(Lu^{3+})_{ini}$ = 10 mmol·L^{-1}) was titrated with a concentrated ligand solution in deuterated methanol. Lu(III) was chosen as it is diamagnetic and does not perturb the chemical shifts by paramagnetic chemical shifts [7]. The results of the titration are shown in Figure 2 for the resonance signals of the *tert*-butyl groups of the ligand molecules. The resonance signals show a clear shift dependence on the coordination number, as the number of molecules in the complex influences the local symmetry and electronic structure. The composition of the individual complex species was identified by diffusion-ordered NMR spectroscopy [8-9] which links the observed NMR signals to the diffusion coefficient and thus molecular weight of the molecule. In the concentration range used for NMR experiments it was clearly shown that the 1:3 complex is preferably formed for a range of lanthanide ions (Ln(III) = La, Sm, Eu, Yb, Lu and Y) and that it is the dominating complex species for stoichiometric 1:3 compositions of ligand and metal ion. Furthermore, the existence of the 1:3 complexes has been proven by HR-ESI mass spectrometry.

Temperature-dependent NMR measurements in a temperature range from 185 K to 335 K were performed to gain insight into the magnetic behavior of complexes of the paramagnetic ions Eu(III), Sm(III) and Yb(III). In the diamagnetic reference compounds Lu(III) and La(III) a dependence of the complex speciation on the temperature was observed (Figure 3). While at low temperatures the 1:3 complex is the dominating species, the fraction of this complex decreases with rising temperature in favor of the free ligand and the 1:2 complex. This result is in line with observations from TRLFS spectroscopy. High temperatures favor the endothermic formation of the 1:2 complex. While the formation of a probably even more endothermic 1:3 complex should in principle be favored as well, an increased molecular motion of the bulky ligand molecules within the sterically crowded first coordination sphere effectively hinders the formation of this complex species.

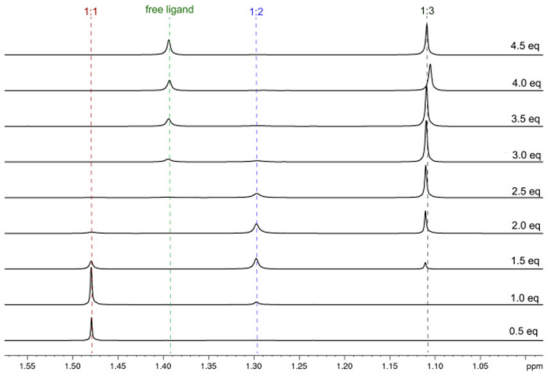

Fig. 2: *Resonance signals of the tBu groups of C4-BPP in $Lu(C4\text{-}BPP)_x(OTf)_3$ complexes in a NMR titration.*

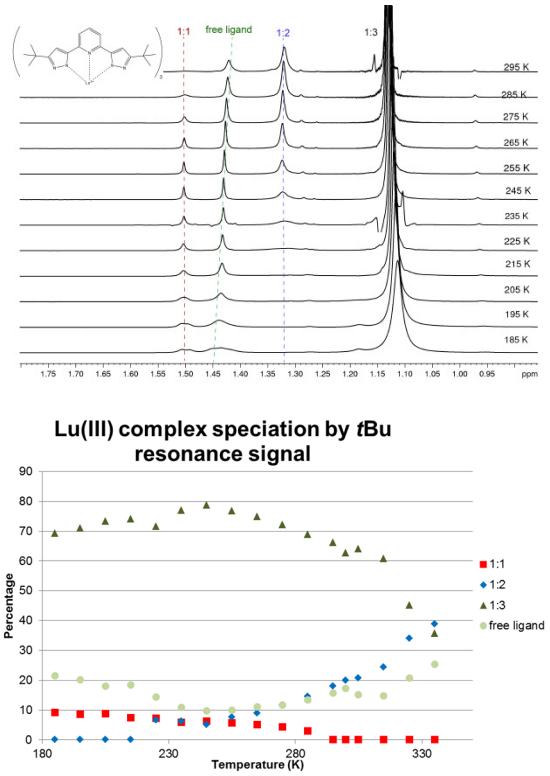

Fig. 3: *Top: Temperature-dependent ^1H direct excitation spectra of the tBu signals in different Lu(III) complex species of C4-BPP. The spectra exhibit a clear dependence of the speciation on the temperature. Bottom: Resulting speciation diagram.*

We also synthesized the Am(III) complex as a representative of An(III) complexes. It turned out that in contrast to expectations from C5-BPP, C4-BPP does not readily form complexes with Am(III). The NMR spectra of a titration of one equivalent of $Am(OTf)_3$ with up to 8 equivalents of ligand are shown in Figure 4. The free ligand increases during the titration and always remains the dominating species while the share of the different complexes is always below 10% for each complex species. Furthermore, after waiting for 48 hours after the last titration step we found that the relative shares of the complexes had changed. This

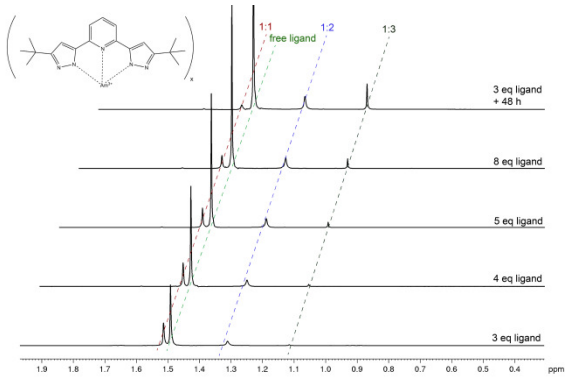

Fig. 4: *Spectra of the* t*Bu region of a titration of an Am(OTf)₃ solution with C4-BPP. The free ligand is the dominating species. The slow kinetics of the complexation reaction are shown by comparison to the topmost spectrum, acquired after a waiting period of 48 h.*

indicates that the C4-BPP complexation with Am(III) has slow kinetics.

We were also able to acquire $^{1}H,^{15}N$-gHMQC correlation spectra from the mixture of complex species, even without ^{15}N enrichment. This had previously been needed for the C5-BPP ligand. These spectra show that upon coordination to the Am(III) the resonance signal of the coordinating nitrogen atom N_8 is shifted upfield to 13 ppm in the 1:1 complex and -4 ppm in the 1:3 complex. In the paramagnetic Lu(III) complex, this signal is found at 265 ppm. A paramagnetic chemical shift of this magnitude has been observed previously in the *n*PrBTP [3,5], *i*PrBTP [4] and C5-BPP [5-6] complexes. This shift is interpreted as being mainly a Fermi contact shift (FCS), *i.e.* a paramagnetic chemical shift that originates from the actual transfer of unpaired electron spin density from the metal ion onto the ligand nuclei [7]. This argument is furthermore supported by the comparably small change of the chemical shift upon the structural rearrangement by the complexation of two additional ligand molecules to form the 1:3 complex. The second contributor to the paramagnetic chemical shift (pseudo contact shift, PCS) depends very strongly on the geometrical relation between metal ion and ligand nuclei. If the paramagnetic chemical shift was mainly PCS, a stronger chemical shift dependence on the coordination number would be found.

The comparability of the chemical shifts originating from the complexation of the Am(III) for C4-BPP and C5-BPP show that the bonding situation in complexes of both ligands is fairly similar. This in turn is a clear indication that the better complexation of Am(III) by C5-BPP is not due to electronic or bonding differences, but is a direct consequence of the greater steric hindrance in the first coordination sphere.

The slow complexation kinetics found in NMR experiments also helped to explain the extraction behavior of the C4-BPP. In the first extraction tests, the contact time of the aqueous and organic phase containing the extractant was too short and the samples were not in equilibrium. The NMR results prompted new extraction tests at FZJ with longer contact times. In these experiments, the contact time was prolonged and an extraction curve complying to expectations was obtained.

Conclusion and Outlook

The case of C4-BPP exemplifies how a minor modification on the ligand periphery of an established extraction ligand (C5-BPP) produces a major influence on the speciation of the formed complexes, the coordination kinetics and ligand selectivity. While C5-BPP forms stable complexes with Ln(III) and Am(III) ions, An(III) coordination is disfavored for C4-BPP. This is obvious by a low ratio of 1:3 complexes observed by NMR spectroscopy, as well as lower complex stability constants in TRLFS experiments. By NMR spectroscopy important insights into the bonding situation of the C4-BPP complexes were obtained. Our results highlight once more that the combination of TRLFS and NMR for Ln(III) and An(III) complexation studies is highly valuable.

Acknowledgements

Most NMR and TRLFS results were obtained during an internship of L. Medyk at KIT-INE, which was funded by the GENTLE (Graduate and Executive Nuclear Training and Lifelong Education) project in the 7th Framework program of the European Commission.

We like to thank Dr. Jürgen H. Gross, Doris Lang and Norbert Nieth (Institute of Organic Chemistry, Mass Spectroscopy Laboratory, Heidelberg University) for the ESI MS measurements.

References

[1] Bremer, A. Geist, P. J. Panak, *Radiochim. Acta* **2013**, *101*, 285-291.

[2] A. Bremer, C. M. Ruff, D. Girnt, U. Müllich, J. Rothe, P. W. Roesky, P. J. Panak, A. Karpov, T. J. J. Müller, M. A. Denecke, A. Geist, *Inorg. Chem.* **2012**, *51*, 5199-5207.

[3] C. Adam, P. Kaden, B. B. Beele, U. Müllich, S. Trumm, A. Geist, P. J. Panak, M. A. Denecke, *Dalton Trans.* **2013**, *42*, 14068-14074.

[4] C. Adam, V. Rohde, U. Müllich, P. Kaden, A. Geist, P. J. Panak, H. Geckeis, *Procedia Chemistry* **2016**, *21*, 38-45.

[5] C. Adam, Ph. D. thesis, Ruprecht-Karls-University (Heidelberg), **2016**.

[6] C. Adam, B. B. Beele, A. Geist, U. Müllich, P. Kaden, P. J. Panak, *Chemical Science* **2015**, *6*, 1548-1561.

[7] C. Piguet, C. F. G. C. Geraldes, in *Handbook on the Physics and Chemistry of Rare Earths, Vol. Volume 33* (Eds.: J. K.A. Gschneidner, J. C. G. Bünzli, V. K. Pecharsky), Elsevier, **2003**, pp. 353-463.

[8] M. D. Pelta, G. A. Morris, M. J. Stchedroff, S. J. Hammond, *Magn. Reson. Chem.* **2002**, *40*, S147-S152.

[9] C. S. Johnson Jr, *Prog. Nucl. Magn. Reson. Spectrosc.* **1999**, *34*, 203-256.

8.5 AMS

F. Quinto, F. Geyer, M. Plaschke, T. Schäfer, C. Walschburger, H. Geckeis

In co-operation with:

T. Faestermann[a], J. M. Gómez Guzmán[a], K. Hain[a], G. Korschinek[a], P. Ludwig[a], P. Steier[b]

[a] Physik Department, Technische Universität München, James-Franck-Straße 1, D-85748 Garching, Germany; [b] VERA Laboratory, Faculty of Physics, University of Vienna, Währinger Straße 17, A-1090 Vienna, Austria.

Introduction

The analytical capability of determining actinides (An) and long lived fission products, like ^{99}Tc, in natural samples at ultra-trace levels (fg/g and ag/g) is of great relevance both for environmental studies and for *in situ* tracer tests and diffusion experiments aiming to evaluate the safety of the geological disposal of nuclear waste. With the multi-actinides analysis and accelerator mass spectrometry (AMS) at the VERA Laboratory (University of Vienna) we have investigated the long-term migration behavior of actinides at the fg/g and ag/g levels in a water conducting granodiorite fracture in the frame of the CFM Project run 12-02 [1] and 13-05 [2].

Similarly, at the AMS facility of the Technical University of Munich (TUM) in Garching, with the Gas-Filled Analyzing Magnet System (GAMS) [3], the concentration of ^{99}Tc in samples belonging to the **L**ong-Term **I**n situ **T**est (LIT) has been determined at the fg/g levels. In order to investigate both the actinides and ^{99}Tc at ultra-trace levels given a limited groundwater sample volume of ca. 3 ml, we are testing an analytical procedure allowing for the separation of the group of An and Ru from Tc. In the actual report, we present the recent outcomes achieved with AMS in the frame of the CFM run 13-05 and the first results on the determination of ^{99}Tc with AMS and its chemical separation from the actinides.

In the frame of a joint GENTLE project with HZDR, we adapted the multi-actinides analysis approach with AMS to more complex sample matrices than groundwater, e.g., soil, sediments or clay deposits. For that purpose, a chemical procedure consisting in the group separation of the actinides with the DIPEX® extractant (Eichrom) was successfully tested.

Investigation on ^{241}Am and ^{244}Pu in samples of CFM run 13-05

The injected tracers ^{233}U, ^{237}Np, ^{242}Pu and ^{243}Am were determined with AMS over six orders of magnitude: from the maximum value of the ^{242}Pu concentration equal to $(3.71 \pm 0.04) \times 10^{10}$ atoms/g (ca. 15 pg/g) to the minimum value of the ^{243}Am concentration of $(6.2 \pm 0.6) \times 10^{4}$ atoms/g (ca. 0.025 fg/g) as shown in Figure 1. The first four samples collected between 0.01 d (14 min) and 0.4 d (9 hours) represent the levels of the investigated actinide nuclides in the groundwater before the arrival of the migration front.

In order to explain the origin of this unexpected signal, we have considered the hypothesis of a background from the previous *in situ* tracer experiments. In fact, ^{237}Np, ^{242}Pu and ^{243}Am were injected as tracers in the granodiorite fracture in the frame of both the CFM run 12-02 and the CRR run 1, while ^{237}Np, ^{233}U, ^{241}Am and ^{244}Pu were employed in the CRR run 2 [4]. The only two An nuclides exclusive of such previous experiments and not employed in CFM run 13-05, were ^{241}Am and ^{244}Pu. Therefore, we have performed a further determination with AMS of the concentration of masses 241 u and 244 u in a group of chosen samples of run 13-05. Such masses are present also as minor nuclides in the ^{242}Pu and ^{243}Am solutions used for the composition of the injection cocktail. The atomic ratios of mass 241/^{243}Am and mass 244/^{242}Pu in the injection cocktail determined with SF-ICPMS, are equal to $(2.6 \pm 0.6) \times 10^{-3}$ and $(3 \pm 4) \times 10^{-5}$, respectively. As it can be seen in Figure 2, the corresponding atomic ratios measured in the samples of run 13-05 are significantly higher than those of the injection cocktail both before and after the peak of the breakthrough curve, while they are consistent with the values of the injection cocktail in correspondence to the peak (Figure 1 and Figure 2). Considering such results, we can conclude that there are two sources of masses 241 u and 244 u in the samples: one is likely to be the injection cocktail itself, which becomes dominant with the arrival of the peak of the breakthrough curve; the second source could be identified as a signal superimposed by the isotopic signature of previous *in situ* tracers tests.

The amount of An left in the fracture after the CRR tests [4] can be roughly estimated as follows: 5.2×10^{14} (^{233}U), 1.2×10^{16} (^{237}Np), 1.2×10^{13} (^{241}Am), 4.2×10^{14} (^{242}Pu), 2.0×10^{14} (^{243}Am) and 5.7×10^{13} (^{244}Pu) atoms. Considering the series of *in situ* tests performed at the GTS in the period between the CRR tests and the CFM run 13-05, we estimate a total volume of groundwater passing through the fracture equal to ca. 1.1×10^{5} L. In a simple hypothesis in which the total number of An atoms left in the fracture before the starting of CFM run 13-05 is entirely released into the aforementioned volume of groundwater, concentrations equal to ca. 5×10^{6} (^{233}U), 1×10^{8} (^{237}Np), 1×10^{5} (^{241}Am), 4×10^{6} (^{242}Pu), 2×10^{6} (^{243}Am) and 5×10^{5} (^{244}Pu) atoms/ml are estimated. Clearly, such scenario does not reflect the complexity of the sorption/desorption dynamics of the various An in the

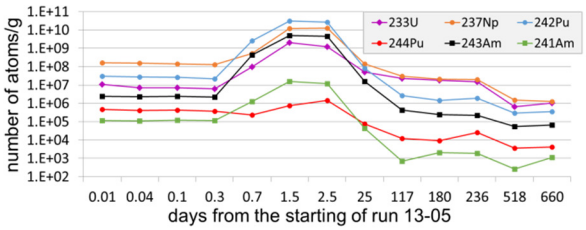

Fig. 1: *Concentrations expressed in atoms/g of ^{233}U (violet rhombuses), ^{237}Np (orange circles), ^{242}Pu (blue circles), ^{244}Pu (red circles), ^{243}Am (black squares) and ^{241}Am (green squares) determined with AMS in chosen samples of CFM run 13-05.*

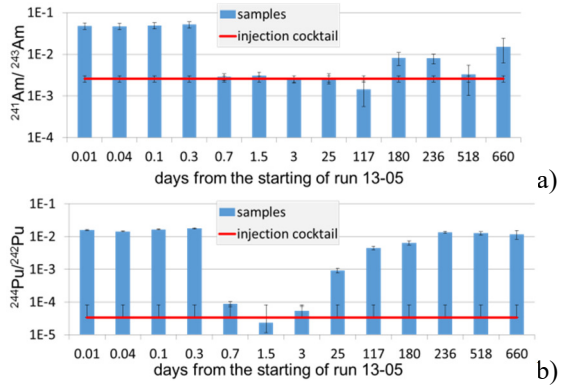

Fig. 2: *Atomic ratio between mass 241 u and ^{243}Am (a), mass 244 u and ^{242}Pu (b) determined with AMS in eleven chosen samples of run 13-05 and in two samples collected after 518 and 660 d from the starting of the experiment; the corresponding atomic ratios in the injection cocktail are depicted as red line.*

system of groundwater - bentonite colloids - fault gouge minerals at the GTS. However, with the sensitivity of AMS we can determine the aforementioned estimated levels which may give us the opportunity to extend the present and upcoming *in situ* studies of the An long-term behavior to longer time spans, e.g. a decade or more [2].

Determination of ^{99}Tc and the actinides at ultra-trace levels in environmental samples

At the 14 MV Tandem AMS facility of TUM, the GAMS is used in order to suppress atomic isobaric interferences [3], which in the case of ^{99}Tc are represented mainly by ^{99}Ru. With this setup, concentration of ^{99}Tc in four investigated LIT samples have been determined in the range of 7 and 250 fg/g.

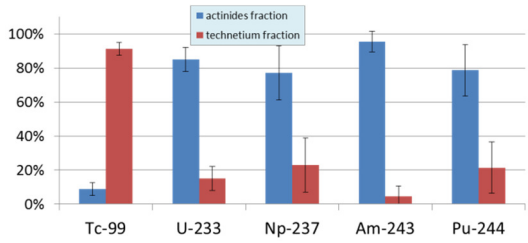

Fig. 3: *Recovery of ^{99}Tc, ^{233}U, ^{237}Np, ^{243}Am and ^{244}Pu in the Tc (red bars) and An fraction (blue bars), determined with ICPMS.*

In order to determine both the actinides and ^{99}Tc in the LIT samples with small volumes we are testing an analytical procedure allowing for the ultra-trace determination of the actinides and ^{99}Tc in the same sample employing TEVA® Resin. Six samples containing ca. 60 ppt each of ^{99}Tc and ca. 2 ppt each of ^{233}U, ^{237}Np, ^{244}Pu and ^{243}Am were prepared and adjusted to 0.2 M HCl. With such loading solution, the An pass through the chromatographic column and are separated as a group from Tc. After a further washing with 0.2 M HCl, Tc is eluted with a 8 M HNO_3 solution. In this way, two fractions are obtained: the first one containing the An as a group as well as the matrix elements and the second one containing the Tc fraction. Figure 3 depicts the recovery of ^{99}Tc, ^{233}U, ^{237}Np, ^{244}Pu and ^{243}Am in the An and Tc fraction, respectively, obtained with ICPMS.

The separation of the group of An from Tc is successful with ca. 91% of ^{99}Tc recovered in the Tc fraction and ca. 85%, 77%, 79% and 96% of ^{233}U, ^{237}Np, ^{244}Pu and ^{243}Am, respectively, recovered in the An fraction.

For the investigation of the LIT specimens as well as of natural waters, the samples will be appropriately spiked with tracers before the chemical separation with TEVA® Resin, after which the An and Tc fractions will be further processed for AMS analysis.

References

[1] Quinto, F. et al.; *Anal Chem* **2015**, *87*, 5766-5773.

[2] Quinto, F. et al.; *Anal. Chem,* (2017) to be submitted.

[3] Fimiani, L. et al.; *Phys Rev Lett* **2016**, *116*, 151104.

[4] Geckeis, H. et al; *Radiochimica Acta* **2004**, 765.

8.6 Computational chemistry

R. Polly, M. Trumm, B. Schimmelpfennig

In co-operation with:

A. Tasi, X. Gaona, I. Pidchenko, T. Vitova, C. Adam, M. Maiwald, P. J. Panak, A. Skerencak-Frech, A. Geist

Introduction

Computational Chemistry using ab initio, first principle and classical mechanics methods at KIT-INE provides valuable insights on a molecular scale, assisting and complementing experimental investigations in the field of safety research for nuclear waste disposal. There is a wide range of application for Computational Chemistry at KIT-INE: from providing structures of complex chemical systems including actinides in solution, at surfaces or solid phases, thermodynamic data or reproducing the actual experimental spectra for EXAFS or XANES, to perform simulations and visualization of complex chemical reactions. Hence, the considered systems vary from molecular species in the gas phase over small complexes in solution to bulk phases or mineral/liquid interfaces.

New theoretical methods and the constantly improving hardware allow a steady improvement of the description of actinide systems at the electronic structure level. These improvements also increase the accuracy and reliability of quantum chemistry as a predictive tool.

Quantum chemical considerations of incorporation of U^{5+} into magnetite

Uranium is the main constituent of spent nuclear fuel, but it can be also found in high quantities at contaminated sites. Developing the Safety Case for the disposal of radioactive waste requires mechanistic understanding of the interaction of the waste products with repository components. In case of water accessing the waste, corroding iron container materials will react with radionuclides and potentially represent a very relevant reactive barrier retaining pollutants release in the repository near field. Of particular interest is the detailed understanding of actinide interactions with iron (Fe) oxides, e.g. magnetite (Fe_3O_4) considered as corrosion products of Fe based container materials.

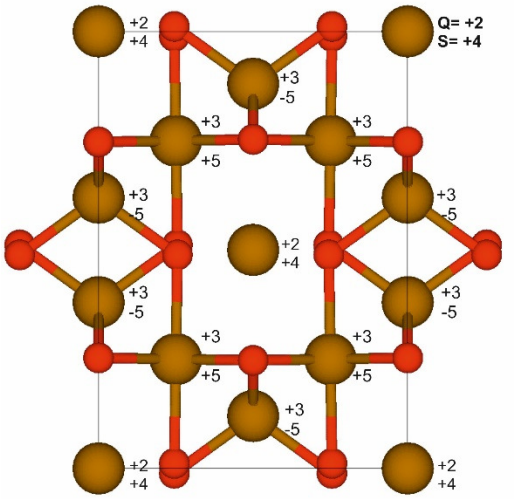

Fig. 1: *Unit cell of magnetite showing the charge (Q) and the spin (S) of the $Fe^{2+,3+}$ ions at the tetrahedral and octahedral sites, respectively.*

Pidchenko et al. [1] showed that U(V) incorporated in octahedral magnetite sites remains under ambient conditions as shown for magnetite nanoparticles containing 1000 ppm uranium. This study was strongly supported by the density functional theory (DFT) calculations described here.

The theoretical consideration of the incorporation of U^{5+} into magnetite poses several challenges for the calculations since we have to deal with a variety of open shell systems (Fe^{3+}: $3d^5$, Fe^{2+}: $3d^6$, U^{6+}: $5f^1$) simultaneously. CASSCF calculations showed that these ions have a single reference ground state in the octahedral oxygen environment and thus can theoreti-

Tab 1: *Unit cell and structural parameters of magnetite.*

Functional	a,b	C	Fe-O	Fe-Fe
Experiment				
	594	840	189, 206	297, 348
DFT				
PBE	590, 588	834	187, 205	295, 346
GGA	588, 587	834	187, 205	294, 346
DFT+U				
PPB	600, 597	853	189, 192, 203, 210, 215	300, 349
GGA	600, 596	853	190, 192, 205, 210, 215	299, 350

Tab. 2: *Magnetic properties of magnetite.*

Functional	Fe^{2+}/oct	Fe^{3+}/oct	Fe^{3+}/tet
Experiment			
	-	-	-3.82μ_B
DFT			
PBE	3.57μ_B	3.57μ_B	-3.49μ_B
GGA	3.55μ_B	3.55μ_B	-3.46μ_B
DFT+U			
PPB	3.67 μ_B	4.18 μ_B	-4.07 μ_B
GGA	3.66 μ_B	4.15 μ_B	-4.05 μ_B
Hybrid functionals			
HSE03	3.64 μ_B	4.12 μ_B	-4.06 μ_B
HSE06	3.64 μ_B	4.13 μ_B	-4.05 μ_B
PBE0	3.64 μ_B	4.15 μ_B	-4.06 μ_B
B3LYP	3.44 μ_B	3.87 μ_B	-3.96 μ_B
HF	3.80 μ_B	4.62 μ_B	-4.61 μ_B

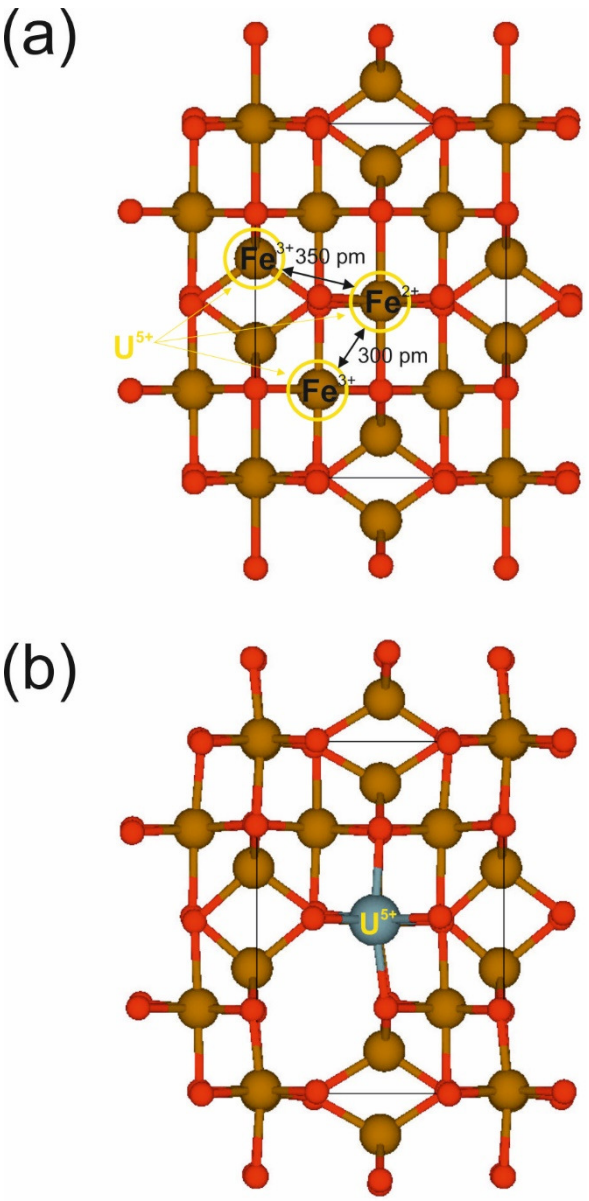

Fig. 2: *Incorporation scheme of U^{5+} into magnetite.*

cally be dealt with using first principle density functional theory (DFT).

The most relevant results for the DFT calculations on pure magnetite are presented in Table 1 and 2.

The results of the structural and magnetic properties presented in Table 1 and 2 clearly show that DFT is a suitable tool to tackle pure magnetite and the study of the incorporation of U^{5+} can be carried out based on these results and with this theoretical approach.
We investigated the incorporation of U^{5+} into magnetite using the following scheme

$$Fe^{2+}+Fe^{3+}\rightarrow U^{5+}+\square \qquad (1).$$

Hence U^{5+} and one vacancy (□) replace one Fe^{2+} and one Fe^{3+} in magnetite as shown in Figure 2 a and b. The results of the DFT calculations agree very well with the experimental results of Pidchenko *et al.* [1] (see Table 3) and allow to identify the incorporation site by comparison with the experimental results.

The best agreement between the EXAFS results and the DFT calculations are for the incorporation of U^{5+} into an octahedral Fe^{2+} site (Fe^{2+}/U^{5+} (oct)) or into an octahedral Fe^{3+} site (Fe^{3+}/U^{5+} (oct)). All other results show a less satisfying agreement with the EXAFS results and have a higher electronic energy. Hence can be excluded by these two arguments.

Furthermore, the results show that an incorporation of U^{6+} following the scheme

$$Fe^{3+}+Fe^{3+}\rightarrow U^{6+}+\square \qquad (2)$$

is less likely because the corresponding structures do not agree with the experimental findings and the much higher electronic energy.

With these calculations, we strongly support the experimental EXAFS study. The theoretical results allow an assignment of the observed structures to an incorporation scheme and thus greatly enhance the available experimental knowledge by theoretical data.

Pu(IV)-isosacharinate complexes

D-Isosaccharinic acid (HISA) is a poly-hydroxo carboxylic acid expected in repositories for low and intermediate level waste as a degradation product of cellulosic materials in cementitious, alkaline environments [2]. Due to the large inventory of cellulose in some repository concepts and the strong complexing capacity of HISA towards hard Lewis cations, an accurate knowledge of the interaction of HISA with actinides is needed in the safety assessment of such repositories.

Solubility experiments with $Pu(IV)O_2$(am,hyd) performed in the presence of HISA under alkaline, reducing conditions showed the predominance of two Pu(IV)-ISA species in solution. Slope analysis of the solubility data provides an unequivocal insight on the charge of these species (–1 and –2) and H^+ released in the corresponding solubility reactions, but gives no hint on the origin of the latter (either Pu^{4+} hydrolysis or deprotonation of –OH groups in HISA). It is the aim of this theoretical study to determine the degree of deprotonation of HISA and the number of the coordinated hydroxide ions to the Pu^{4+} center within the identified complexes. For this purpose, the stoichiometry of each species was systematically modified at a constant charge (either –1 or –2) and the resulting structures were optimized and characterized by means

Tab. 3: *Incorporation of U^{5+}/U^{6+} into magnetite (r in pm)*

.

EXAFS					
U-O	U-Fe_1	U-Fe_2	U-O	U-Fe_1	U-Fe_2
218	319	355			
Fe^{2+}/U^{5+} (oct)			Fe^{3+}/U^{5+} (oct)		
DFT					
215	317	362	215	318	360
DFT+U					
219	310	363	219	311	362
Fe^{3+}/U^{6+} (oct)			Fe^{3+}/U^{6+} (tet)		
DFT					
222	308	360	215	345	354

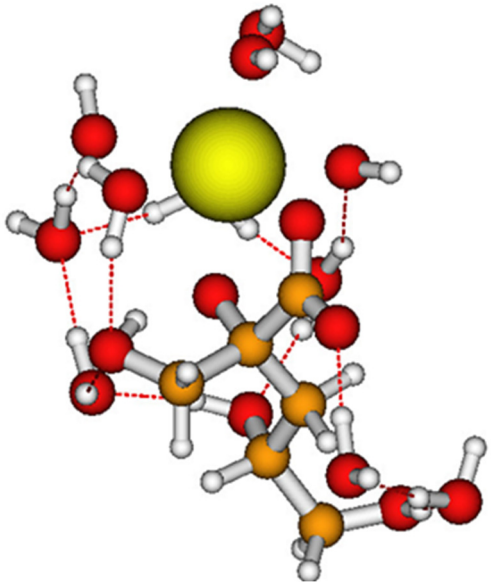

Fig. 3: *Optimized [Pu(OH)$_3$ISA$_{-H}$] complex*

of quantum chemical DFT calculations.

We used DFT(BP86/def2-SVP/ecpIVmwb-avdz) calculations with f-in core pseudopotentials (ecpIVmwb) and the corresponding GTO basis set at Pu^{4+}. This allows us to bypass any nondegeneracy of the ground state of the complex. The model system consisted of several water molecules and OH^- species around the metal ion and some additional water molecules at the acid. We found that a model system representing only the first water shell around the metal ion and the acid is sufficient for a realistic description of the system.

Complexes with the stoichiometries $Pu(OH)_3ISA_{-H}^-$ and $Pu(OH)_3ISA_{-2H}^{2-}$ were found to be the species with the lowest electronic energy for the charges –1 and –2, respectively. For the $Pu(OH)_3ISA_{-H}^-$ species, the optimized structure (see Fig. 3) showed three OH^- ions bound to the Pu^{4+} cation, whilst the coordinating OH–group of the ligand was deprotonated. Similarly, for the $Pu(OH)_3ISA_{-2H}^{2-}$ species the most stable structure indicates again the presence of three OH^- ions bound to the Pu^{4+} cation but with two OH–groups of HISA deprotonated. The insights gained by DFT calculations are incorporated in the chemical and thermodynamic models derived from solubility data (see section 4.1).

Fundamental understanding of An(III)/ Ln(III) separation with N-donor ligands

With the development of soft nitrogen based extracting ligands An(III) and Ln(III) can be separated efficiently reaching separation factors over 100. The origin of this separation as well as the failure of structurally similar ligands to accomplish separation is still a matter of controversy. Hence, we performed theoretical investigations of the ligands and their An(III)/Ln(III) complexes to shed further light on this origin.

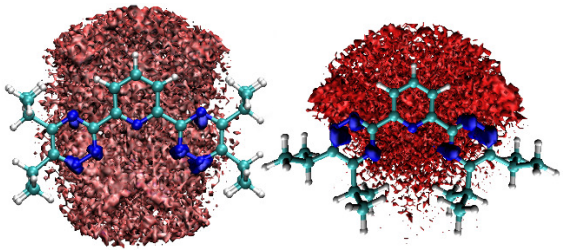

Fig. 4: *3D oxygen distribution function of the solvent molecules around iPr-BTP along the MD trajectory for cis/cis (left) and trans/trans (right) conformations within a 3.5 Å radius of the pyridin nitrogen.*

Before the formation of the metal-complex is modelled, a profound understanding of the ligand in solution is necessary in order to identify preorganization reactions and corresponding activation energies to transform the ligand into its conformation within the complex. These have been modelled by molecular dynamics (MD) simulations of the free iPr-BTP ligand in methanol/water mixtures of different molar fractions. Three different conformations of the triazine rings have to be taken into account, namely cis/cis, cis/trans and trans/trans. With increasing methanol concentration, the most favorable structures changes from cis/cis to trans/trans maximizing the accessible surface for lipophilic solvent molecules (see Fig. 4).

This is especially important for a deeper understanding of the processes during liquid-liquid extraction experiments. In upcoming simulations, the composition, width and shape of different liquid-liquid interfaces will be studied.

Considering metal-ligand complexes, a structural model is most important for further investigations. Especially the role of solvent molecules within the cluster formation is difficult to assess experimentally. Hence structure optimizations of possible Cm(III) complexes with two SO_3-Ph-BTBP ligands and 0, 1 and 2 water molecules have been performed using density functional theory. All three structures proved to be true minima in gas-phase (Fig. 5).

Analysis of the reaction energies of the successive intrusion of water molecules into the first coordination shell shows the presence of one or two water molecules (Table 4). Herein, both thermodynamic contributions $\mathbf{\Delta E_{vib}}$ as well as solvent contributions using the COSMO model have been included. For the latter, however, the explicit description of a full hydration shell would be necessary to shield the nega-

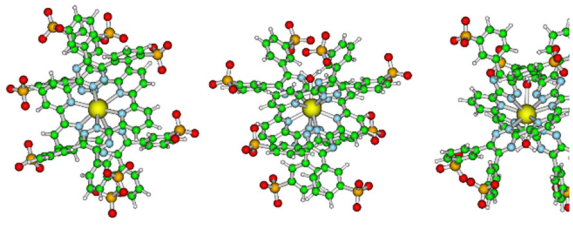

Fig. 5: *Optimized complex structures of [Cm(SO_3-Ph-BTBP)$_2$(H_2O)$_n$]$^{5-}$ (n=0,1,2).*

Tab. 4: *Calculated energy differences for the reactions (1) intrusion of a first water molecule and (2) intrusion of a second water molecule.*

	reaction (1) [kJ/mol]	reaction (2) [kJ/mol]
ΔE	-48.5	-7.4
ΔG	-57.4	-14.7
ΔE+ ΔE_{vib}	-35.9	15.7

tively charged sulfonyl groups from the COSMO-surface. Hence the **ΔE+ ΔE_{vib}** reaction energies should be preferred.

Experimental confirmation was provided by means of TRLFS and vibronic side-band (VSB) spectroscopy in H_2O and D_2O. Fluorescence life-times decrease from 173 µs in H_2O to 374 µs in D_2O. Corresponding vibronic side bands have been found proving the theoretical prediction of water molecule presence in the first hydration shell. [3]

Fundamental understanding of An(III) versus Ln(III) bonding

Many attempts have been pursued to qualitatively and quantitatively describe covalency in metal-ligand bonding. The main problem herein lies within the rather vague definition of the term "covalency" itself. Theoretical studies, which are commonly based on electron density deformation and orbital analysis cannot be directly compared to experimental data, for example from NMR studies. Hence our aim is directed towards a systematic theoretical study of An(III) and Ln(III) bonding that allows an experimental verification of the computed trends. Throughout the last years a force field approach, describing charge/charge, charge/dipole and dipole/dipole interactions classically has been presented [4,5]. The dipole polarizabilities can be calculated accurately using multi-reference methods and relativistic basis sets. Obtained values for the dipole polarizabilities from NEVPT2 calculations for all non-closed-shell An(III) and Ln(III) ions are presented in Fig. 6. With the 5f electrons being less shielded by 6s and 6p electrons in the actinide ions compared to their lanthanide 4f counterparts, it is not surprising, that the An(III) polarizabilities are higher by a factor of almost 2 throughout the whole series.

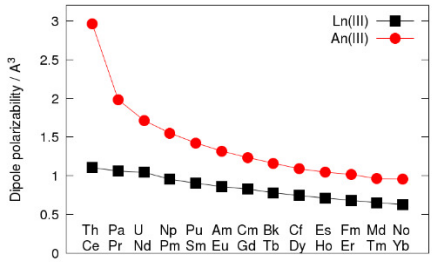

Fig. 6: *Dipole-polarizabilities of Ln(III) and An(III) ions computed with the NEVPT2 method.*

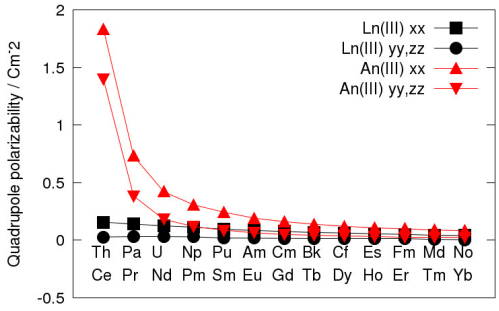

Fig. 7: *Quadrupole-polarizabilities of Ln(III) and An(III) ions computed with the NEVPT2 method.*

In order to clarify up to which order multipole moments are important in such an energy-decomposition scheme employed in force-field methods, it is necessary to consider quadrupole moments for these ions as well. Hence dipole-quadrupole- and quadrupole-polarizabilities have been computed for the same group of elements showing a similar trend with the actinide ions being more polarizable by a factor of up to 10 within the first half of the series (see Fig. 7). Future studies will quantify the implications of the An(III) versus the Ln(III) bond in detail.

References

[1] Pidchenko *et al.*, Environ. Sci. Technol., 2017, 51 (4), pp 2217–2225

[2] Glaus, M.A., et al., Environ. Sci. Technol., **42**, 2906-11, (2008).

[3] Trumm *et al.*, Dalton Trans., 2016, 45, 12308

[4] Trumm *et al.*, Mol Phys, 114, 876, 2016

[5] Réal *et al.*, J. Phys. Chem. B, 114, 15913, 2010

9 Radiochemical and elementary analysis

The scope of the INE radio-analytical group is a triad of R&D projects, third parties' collaborations and development of analytical methods and instrumentation. A pool of advanced analytical techniques for elemental and isotope analysis as well as for other routine analytical applications is available both in our radioactive controlled area as well as in cold labs. Our competences are in radio-analytical sample preparation, separation techniques, handling of radioactive material, technical skills and well-developed procedures. These capabilities enable us to cover a wide spectrum of analytical tasks and are, therefore, also requested by external clients, e.g., in the fields of decommissioning of nuclear installations, nuclear waste declaration or radiopharmaceuticals. A special focus is in mass spectrometry techniques that are adapted and improved for trace element analysis and speciation studies of actinides and fission products. The use of hyphenated techniques, like Sector Field (SF)-ICP-MS or Collision Cell Quadrupole CC-Q-ICP-MS coupled to species sensitive methods, e.g., to capillary electrophoresis (CE) or ion chromatography (IC), enables speciation of actinide, of fission product and iron redox states. Supersensitive determination of actinides below ppq levels and ^{99}Tc at the ppq levels in ground-, surface and seawater is achieved by accelerator mass spectrometry (AMS); see chapter 8.5 for further details. New separation methods are developed, e.g. for the simultaneous investigation of actinides and ^{99}Tc in groundwater samples from large-scale field experiments. Method development is also integrated in research projects, e.g. in the context of decommissioning. Furthermore, the analytical group supports the INE infrastructure, is involved in various teaching activities and is responsible for education of chemical laboratory assistants.

M. Plaschke, A. Bauer, M. Böttle, M. Brandauer, D. Fellhauer, M. Fuss, J. Gaona Martinez, C. Garcia, F.W. Geyer, S. Heck, S. Hilpp, F. Huber, A. Kaufmann, T. Kisely, M. Lagos, C.M. Marquardt, S. Moisei-Rabung, F. Quinto, F. Rinderknecht, E. Rolgejzer, T. Schäfer, J. Schepperle, D. Schild, A. Seither, W. Tobie, C. Walschburger, H. Geckeis

In co-operation with:

C.-O. Krauß[a]*, A. Heneka*[a]*, S. Gentes*[a]*, P. Steier*[b]

[a] Department of Deconstruction and Decommissioning of Conventional and Nuclear Buildings, Institute for Technology and Management in Construction (TMB), Karlsruhe Institute of Technology (KIT); [b] VERA Laboratory, Faculty of Physics, University of Vienna, Währinger Straße 17, A-1090 Vienna, Austria

Analytics for the INE R&D projects

At INE a pool of advanced analytical techniques, well-developed procedures and competences in radio-analytical sample preparation and separation, handling and technical skills are available. This includes core competences in elemental and isotope analysis, chromatographic methods and nuclear spectroscopic techniques. Our personnel is trained in handling of nuclear samples and in the operation and maintenance of instruments adapted to glove boxes. Several analytical techniques listed in Table 1 are available both in inactive and active labs. In the reporting period over twenty thousand samples were routinely analyzed providing the data mainly for the INE R&D projects but also for commercial analytical services.

For element and isotope analysis sensitive ICP optical emission and different types of mass spectrometers are available. For the trace concentration range, our ICP-MS equipment includes two quadrupole instruments (a Perkin Elmer Elan 6100 adapted to a glove-box, and a Thermo X-Series2 equipped with reaction/collision cell technology) and a sector field SF-ICP-MS (a Thermo Element XR/2 adapted to a glove box). Our routine instrumentation is continuously improved and modernized, e.g., in 2016 our box-adapted Q-ICP-MS was subject of major maintenance. The box was opened, decontaminated and parts of the sample introduction system were replaced.

SF-ICP-MS provides detection limits (DL) for transuranium elements as low as ~10^{-14} mol/L (lower ppq range) and elevated mass resolution (up to 10.000) which is beneficial for accurate determination of elements suffering from interfering species, e.g., Fe or Se. Even lower detection limits, down to 10^4 actinide atoms per sample, can be obtained by Acceleration Mass Spectrometry (AMS). For such ultra-trace determination, i.e. of actinides (An) and ^{99}Tc, new radiochemical separation methods are developed and close co-operations with the AMS community at national and international facilities are maintained (for more details cf. chapter 8.5).

Analytics for external clients

Commercial analytical service is offered to various clients on the basis of formal contract agreements. Data are recorded, documented and quality controlled according to the requirements of the clients.

Quality Control of Radiopharmaceuticals

A ^{223}Ra containing alpha-radiopharmaceutical (Xofigo®) is regularly analyzed with regard to toxic heavy metal trace impurities. ^{223}Ra acts as a calcium mimic and is indicated for patients suffering from bone metastases. Due to the short penetration of the alpha emitter, a highly-localized tumor cell killing is achieved with minimal damage to surrounding healthy tissue. We weekly analyze routine samples of the

radiopharmaceutical and additional samples from the methods development.

Nuclear Waste Treatment and Decommissioning of Nuclear Facilities (KTE-HDB)

We analyze routinely samples from the KTE-HDB (KTE since 2017 Kerntechnische Entsorgung Karlsruhe GmbH, previously Wiederaufarbeitungsanlage Karlsruhe GmbH, Hauptabteilung Dekontaminationsbetriebe, HDB). Samples are classified according to their origin as ashes (from an incineration facility), LAW liquid concentrates (from an evaporation plant), annually averaged samples (from different waste treatment facilities), samples from decommissioning of nuclear facilities (e.g., demolition waste) and others (e.g., wipe tests). Samples are processed by radioanalytical separation methods and analyzed using elemental, isotope and nuclear spectroscopic techniques in order to obtain isotope concentrations and vectors. The analyzed nuclides include neutron activation and fission products (^{55}Fe, ^{63}Ni, ^{90}Sr), as well as actinides (^{233,234,235,236,238}U, ^{238,239,240,241,242}Pu and $^{242,243+244}$Cm) as constituents of spent nuclear fuel. Starting fall 2016 Cm is determined additionally in all ash samples.

Analytics for decommissioning projects

For the deconstruction of a nuclear power plant, i.e. the reactor pressure vessel, waterjet abrasive suspension cutting technique is a promising cutting method providing intrinsic technical benefits. Accelerated by a waterjet, abrasive particles cut razor-sharp through, e.g. a steel material. During the cutting process, a mixture of abrasive particles (i.e., almandine garnet) and radioactive steel particles from the cut components is generated. However, by this process the amount of secondary waste is markedly increased compared to other cutting techniques. This is presently the major limitation for the application of this technique due to tremendous disposal costs.

Tab. 1: *Analytical techniques available at INE*

Elemental and Isotope Analysis
Quadrupole Inductively Coupled Mass Spectrometry (Q-ICP-MS)
Collision Cell Q-ICP-MS (CC-Q-ICP-MS)
Sector Field ICP-MS (SF-ICP-MS)
Inductively Coupled Optical Emission Spectrometry (ICP-OES)
Atomic Absorption Spectrometry (AAS)
Flame Atomic Emission Spectrometry (F-AES)
X-Ray Fluorescence Spectrometry (XRF)
Nuclear Spectroscopic Methods
Alphaspectrometry
Liquid Scintillation Counting (LSC, conventional/high sensitivity)
Gammaspectrometry (with auto-sampler)
Other Methods
Ion Chromatography (IC) for cations and anions
Gas Chromatography (GC)
Carbon Analysis (TOC, DOC, TIC, NPOC)
Specific Surface Area Analysis (BET)
Differential Thermal Analysis (DTA)
Dilatometry
Fusion and Microwave Digestions
Gravimetry and Titrations

The project MASK ("Magnetic Separation of granular mixtures from waterjet cutting to minimize secondary waste from the decommissioning of nuclear facilities", which is a follow-up of a previous project, as well funded by BMBF) starting in 2016 aims at the development and optimization of a separation technique of radioactive steel particles from inactive abrasive grains using a magnetic filter device, thus reducing drastically the amount of activated waste. For the quantification of the separation grade an analytical method based on inductively-coupled optical emission spectrometry (ICP-OES) was developed. Separated steel-grain fractions are leached with aqua regia and the steel content is quantified by the Ni content of the steel alloy. Using this method, the separation grade could be quantified and first conclusions for optimization of the separation process could be drawn. In the abrasive particle fraction after separation of the steel particles, a remaining contamination by tiny steel particles and steel adherence to abrasive grains and void fillings could be identified with scanning electron microscopy (cf. chapter 8.3) and subsequently quantified by elemental analysis. To further reduce the remaining steel content in the purified abrasive fraction further optimization and additional understanding of the separation process is still needed. For more details cf. chapter 7.

Analytics for large-scale field experiments

In the course of the Colloid formation and Migration experiment (CFM) a bentonite source was emplaced in the shear zone at the Grimsel Test Site (GTS) in May 2014 for better understanding of the real in-situ conditions in a bentonite-based geotechnical barrier (so-called **L**ong term **I**n situ **T**est, LIT). ^{45}Ca, ^{75}Se, ^{99}Tc, ^{137}Cs, ^{233}U, ^{237}Np, ^{241}Am and ^{242}Pu and the conservative tracer Amino-G are included in the source. Hydrogeological conditions are controlled in the CFM site via a mega-packer system and monitored constantly regarding volumetric flow velocity, pH, Eh, conductivity, bentonite swelling pressure and fluorescence of the effluent (conservative tracer). Water samples are taken from the outflow of the shear zone at the tunnel wall ("Pinkel" surface packer) and from an observation borehole close to the bentonite source (distance: ~10 cm). Effluent samples are analyzed at INE concerning colloid size and concentration (Laser Induced Breakdown Detection; LIBD), chemical (ICP-MS, IC) and radiochemical composition (ICP-MS, SF-ICP-MS, LSC, γ-spectroscopy, for the abbr. see Table 1). In parallel to the LIT experiment, a mock-up test is running at INE using the same compacted bentonite source, but instead of the natural fracture, a parallel plate Plexiglas setup with a 1 mm aperture is installed in an Ar glovebox.

Both the LIT experiment and the mock-up test reveal a release of the conservative tracer Amino-G from the radionuclide containing vials embedded in the compacted bentonite ring, clearly showing a direct contact of these vials with the water conducting feature. In the mock-up test, radionuclides included in

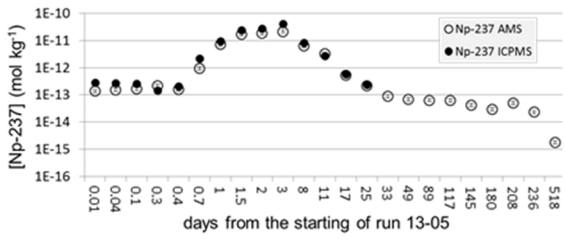

Fig. 1: *Concentrations of ^{237}Np measured with AMS (empty circles) and ICP-MS (black circles) in chosen samples of the breakthrough curve of run 13-05 until 660 days from the starting of the experiment. The last two data (at 518 and 660 days) refer to sampling at a different collection point (so-called "Pinkel").*

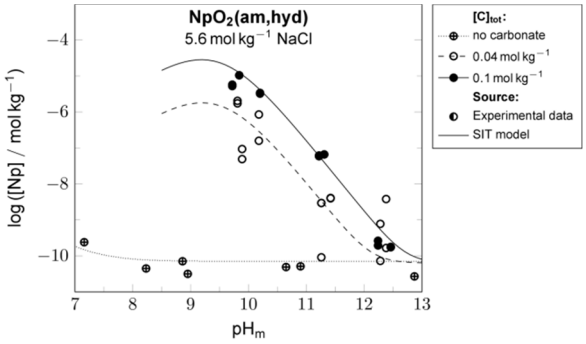

Fig. 2: *Solubility of NpO_2(am, hyd) in 5.6 m NaCl solutions in the absence and presence of carbonate. Solid lines calculated with thermodynamic and SIT activity models derived in the present work.*

the bentonite source with high oxidation states (^{99}Tc(VII), ^{237}Np(V),^{233}U(VI)) are released. In the LIT field experiment, a ^{99}Tc release at a very low concentration level could be assumed from SF-ICP-MS data. However, due to the isobaric interference on mass 99 from natural Ru in ICP-MS, additional accelerator mass spectrometry (AMS) measurements were necessary to quantify the exact amount of ^{99}Tc released (cf. chapter 8.5).

To test the complementarity of SF-ICP-MS and AMS for the analysis of [An] over a wide concentration range, selected samples from the previous CFM test run 13-05 (2013) have been analyzed using both techniques. While SF-ICPMS covers [An] levels from ~10 pg/g (~2×10^{10} atoms/g) and down to the DL of ~10 fg/g (~2×10^{7} atoms/g), AMS is capable to access concentration levels below 10 fg/g and down to ~10 ag/g (~2×10^{4} atoms/g). The AMS instrumental features also enabled us to develop a novel analytical method consisting in the simultaneous determination of several An without previous chemical separation from each other and with the use of non-isotopic tracers for the determination of ^{237}Np and ^{243}Am [2]. In Figure 1 a comparison of the breakthrough curve from run 13-05 of ^{237}Np determined both with SF-ICP-MS and AMS is depicted. The breakthrough curve is well-described by both analytical methods. While SF-ICP-MS provided a dense group of data limited to approx. one month from the injection, AMS allows for the long-term investigation of nearly two years. However, concentration values determined by AMS are generally lower than by SF-ICP-MS revealing an intrinsic difference in the results provided by the two analytical techniques. Possible sources of this systematic deviation will be further investigated.

Analytics for solubility studies

Carbonate minerals are ubiquitous in the natural environment, and therefore, dissolved CO_3^{2-} can be present in the groundwater horizon of a deep geological repository. Carbonate forms stable complexes with tetravalent actinides and can lead to enhanced An(IV) solubility. In a study performed in the frame of the ENTRIA project, the solubility of NpO_2(am, hyd) and PuO_2(am, hyd) is investigated in absence and presence of carbonate, in dilute to concentrated NaCl solutions with pH and [An] measured at regular time intervals until attaining equilibrium conditions. Because of the very low concentrations of Np and Pu in the absence of carbonate, and the high salt content in some of the solubility series investigated (up to 5.6 m NaCl), both LSC and SF-ICP-MS were used for the quantification of [An] in solution. Figure 2 exemplarily shows NpO_2(am, hyd) solubility data in 5.6 m NaCl solutions in the absence and presence of carbonate. Solid lines in the Figure 2 are calculated with the thermodynamic and activity models derived in the present work. The combination of highly sensitive analytical methods and advanced theoretical models enables us to better understand the actinide solution chemistry, further allowing to derive more reliable source terms for An(IV) under conditions relevant for nuclear waste disposal. For more details cf. chapter 4.1.

References

[1] Delos, A. et al., *Journal of Colloid and Interface Science,* **324(1-2)**, 212, (2008).

[2] Quinto, F. et al., *Analytical Chemistry*, **87**, 5766, (2015).

10 Radiation protection research

Radiation Protection Research at KIT-INE is focusing on assessing radiation exposures both by estimation of doses from external radiation fields and estimation of doses from intakes of radionuclides. The techniques applied for assessing radiation exposures are direct measurements and numerical simulation of radiation fields. During 2016, research activities have been focused on experimental and numerical simulations of the radiation field around a spent nuclear fuel cask as well as on assessment of uncertainties in biokinetic and dosimetric models by means of Monte Carlo simulations. Close collaborations are established with national and international partners in networks such as "Strahlung und Umwelt" in Competence Alliance Radiation Research KVSF and the European Radiation Dosimetry Group (EURADOS).

10.1 First-time operation of the neutron generator of the TU Dresden in the range of high-level nuclear waste neutrons at 2.5 MeV and neutron spectra determination after "POLLUX-type" materials

H. Saurí Suárez and F. Becker

in co-operation with:

A. Klix[a], T. Döring[b]

[a] KIT-INR; [b] IKTP/TU Dresden

Introduction

A proper and safe management of spent nuclear fuel (SNF) discharged from commercial nuclear power plants is a subject of societal concern. Certain working scenarios in the storage / disposal facilities might lead to an *enhanced* level of radiation exposure for workers. Hence, a realistic estimation of the personal dose during individual working scenarios is desired.
In previous work [1,2] the Monte-Carlo code MCNP6 [3] was employed to simulate the radiation fields and exposure in a final disposal in a rock salt and a clay stone repository. In both cases POLLUX® casks containing a mixture of spent PWR UOX and MOX fuel assemblies were investigated.

For the numerical simulations, the POLLUX® cask structure was simplified and composed of three layers: an internal stainless steel shielding layer, a neutron moderator layer (consisting mainly of polyethylene), and a modular cast iron external shielding layer.

However, to benchmark the MCNP6 simulations there is no POLLUX® cask with spent nuclear fuel available, so that measurements of the radiation field around a real POLLUX® are not feasible so far. Hence, to assess the modelling and simulation approaches applied in MCNP6, experiments with a setup consisting of materials similar to the POLLUX® were performed. Our simulations predict that for the POLLUX® containing UOX and MOX fuel assemblies the radiation field and dosimetry is dominated by neutrons.

For this reason, we have chosen a well-defined neutron source, which produce neutrons in the energy range close to neutrons emitted from spent nuclear fuel. The neutron generator of the TU Dresden (TUD-NG), located at Helmholtz Zentrum Dresden Rossendorf (HZDR), was selected for this purpose.

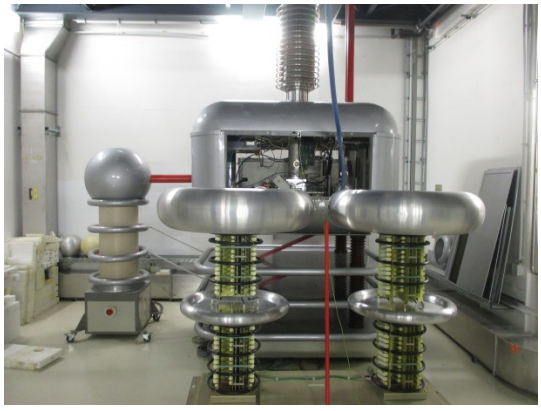

Fig. 1: *Deuterium accelerator at HZDR.*

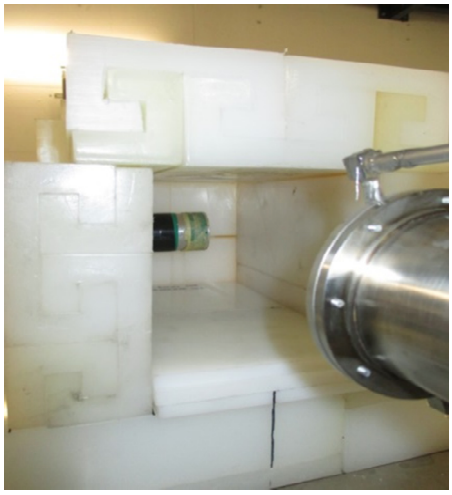

Fig. 2: *Experimental setup at the end of the beam line. The target was located in the beam line visible on the right; behind the beam line a polyethylene housing was mounted (white bricks) in which the NE213 detector (the scintillator position is indicated by the yellow/green tape) was placed.*

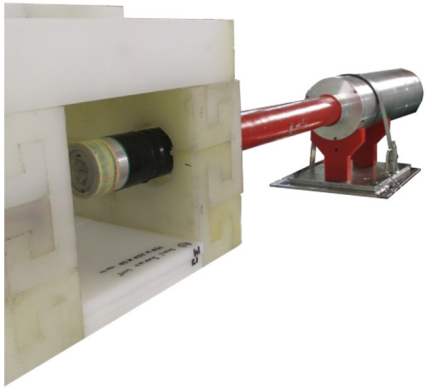

Fig. 3: *Experimental setup showing the NE213 detector. The picture was taken before the rear side of the PE house was closed. The scintillator position indicated by the yellow/green tape is inside the house while the light guide inside of the red tube and the adjacent photomultiplier in the metallic cylinder is located outside of the housing.*

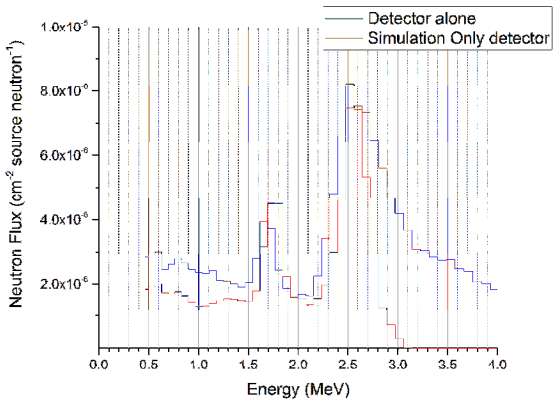

Fig. 4: *Measured and simulated spectra free-in-air.*

Experiment

As described by Klix et al. [4], the neutron generator is a Cockroft-Walton type deuterium accelerator (Fig. 1) with a terminal deuteron energy of 320 keV and a maximum current of 10 mA. Depending on the target, the generator can produce neutrons with different energies. So far the deuteron reaction of impinging on a tritiated titanium target, generating neutrons with energies of 14.1 MeV, was employed.

For the present investigation for the first time the TUD-NG was operated with a deuterated titanium target, so that neutrons of 2.5 MeV stemming from the reaction d + D → n + ^{3}He were produced.

The basic setup is displayed in Fig. 2. At the end of the beam line behind the target a polyethylene housing (PE house) was mounted. The scintillator of a NE213 detector [5], with the ability to measure both fast neutrons and gamma rays, was placed inside the housing (see Figures 2 and 3). This ensures a shielding of background radiation. The distance from the target to the detector amounted to 35.5 cm. The opening in the housing, empty in Fig. 2, was filled with different materials.

Four configurations were investigated:

- Detector free-in air (without polyethylene housing)
- polyethylene housing without material in the opening ("polyethylene house" configuration)
- polyethylene housing with a 10 cm polyethylene closure
- polyethylene housing with closure layers of 4 cm steel, 10 cm polyethylene, and 4 cm steel ("POLLUX-type" configuration)

The acquired raw pulse height spectra for the different configuration were unfolded according to the procedure given in [5].

Results and discussion

The Figures 4 to 7 show the resulting measured neutron spectra for the four configurations as well as the first simulation results of respective MCNP6 simulations. In all spectra two prominent peaks are observed. The one at a neutron energy of 2.5 MeV is in agreement with the expected neutron energy of the reaction d + D. The other one at 1.7 MeV is attributed to the inelastic scattering of 2.5 MeV neutrons on iron, one of the materials employed around the target position. According to the scattering reaction (n,n′γ) on ^{56}Fe, the gamma energy of the first excited state of ^{56}Fe would reduce the energy of the scattered neutrons to 1.7 MeV in agreement with the peak position in the spectra. Moreover, the enhancement of this peak in the "POLLUX-type" configuration (Fig. 7), with additional 4 cm steel in the entrance window, supports this explanation.

The effect of the shielding concept of the polyethylene housing can be recognized when comparing the configuration free-in-air (Fig. 4) with the configuration "PE house" (Fig. 5). A suppression of high energy neutrons above 3 MeV, stemming from background radiation, is observed. Hence the preliminary reflections of the experimental design concerning background shielding are confirmed to be successful.

When the opening on the target side of the PE house is closed, the shielding/moderation effect is visible in

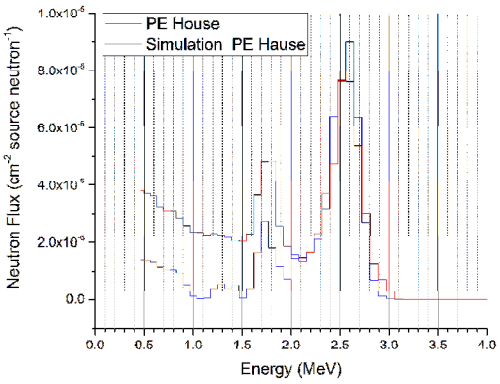

Fig. 5: *Measured and simulated spectra for the detector placed in the housing without material in the opening.*

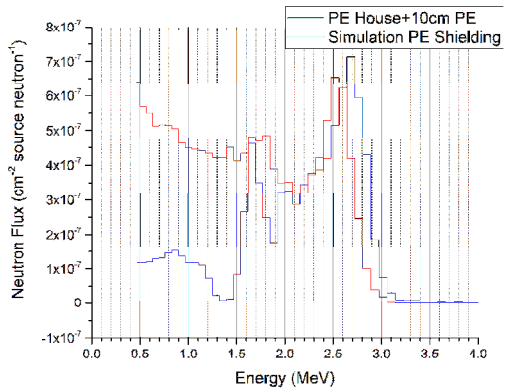

Fig. 6: *Measured and simulated spectra for the configuration polyethylene housing with a 10-cm polyethylene closure.*

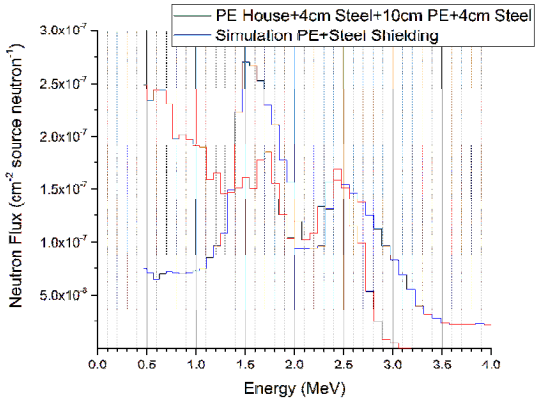

Fig. 7: *Measured and simulated spectra for the polyethylene-steel configuration ("POLLUX-type").*

the spectra, as the neutron flux is reduced (Fig. 6). When looking at the "POLLUX-type" configuration, the intensity of the 2.5 MeV peak is further reduced due to the larger amount of shielding material, but as stated before the iron in the neutron beam raises the respective inelastic scattering peak at 1.7 MeV.

Summary and conclusions

In the current study experiments at TUD-NG were performed, where for the first time, the reaction d + D was used to obtain 2.5 MeV neutrons. This complies with the energy range of neutrons in POLLUX® shielding casks loaded with UOX and MOX. As the radiation field is dominated by neutrons, we focused in this study on the neutron flux measurements and the corresponding MCNP6 simulations. The experiment for the first time realized at TUD-NG yielded straightaway comprehensive data. In general, the experimental and simulated results agree quite well, keeping in mind that the detector response and unfolding procedure is attributed with some uncertainties. Moreover, the simulations do not account for background neutrons e.g. stemming from cosmic radiation. The on-going data analysis and corresponding simulations will consider gamma-ray spectra too. In particular gamma rays from the scattering reaction (n,n′γ) on ^{56}Fe and other materials could be revealed more detailed in future.

Summarizing the first results of experiments at TUD-NG together with our modelling and simulation approaches applied in MCNP6 show that this methodology in promising to assess simulation scenarios with POLLUX® type casks containing a mixture of spent PWR UOX and MOX fuel.

Acknowledgements

We acknowledge the excellent support of the TU Dresden neutron generator laboratory. The work was partially financially supported by the German Federal Ministry of Education and Research (BMBF) in the context of the ENTRIA project (grant number 15S9082E).

References

[1] H. Saurí Suárez et al., Monte-Carlo calculations of the radiation field in a rock salt horizontal emplacement gallery of an underground nuclear waste disposal facility, *AMNT* (2015).

[2] B. Pang et al.; Individual Dosimetry in Disposal Repository of Heat-Generating Nuclear Waste, Radiation Protection Dosimetry **170**: 387 (2016)

[3] D. B. Pelowitz, MCNP6™ User's Manual, *LA-CP-13-00634*, (2013).

[4] A. Klix et al., Test facility for a neutron flux spectrometer system based on the foil activation technique for neutronics experiments with the ITER TBM, *Fusion Engineering and Design*, **86**: 2322 (2011).

[5] A. Klix et al., Blanket mock-up experiment with a LiAlPb assembly irradiated with 14 MeV neutrons in preparation of the HCLL-TBM neutronics experiment, Fusion Engineering and Design 83: 1813 (2008).

10.2 Studying uncertainties of internal doses due to variability in biokinetic models and dose coefficients by statistical modelling of parameter values

W. Klein

in co-operation with:

B. Breustedt[a]

[a] KIT-SUM

Introduction

Radiological doses after incorporation of radionuclides are assessed by applying biokinetic and dosimetric models to measured activity levels in the body, excreta, air or food samples. Biokinetic models are used to mathematically describe the distribution of the radionuclides after their intake in the body. They provide information about the activity which is retained in different parts of the body over time and can be used to infer the amount of activity that entered the body and to calculate the number of decays in a source region. Dosimetric models describe the energy deposition (and thus the final dose) in organs (target regions) by the radiation emitted following the decay of radionuclides in different parts (source regions) of the body. The two core quantities in the assessment of the dose are the number of nuclear disintegrations occurring in the body (or the organs) and the energy transfer per decay (S-coefficient). The former values are calculated by integration of the retention function from biokinetic models, the latter are calculated using Monte Carlo Simulation of Radiation Transport [1] in computational phantoms representing human anatomy [2]. Uncertainties in internal dose assessments include contributions from both biokinetic and dosimetric models.

Uncertainties in biokinetic models

Biokinetic models proposed by ICRP [3, 4, 5, 6] use the compartmental formalism to describe the transfer between different parts (compartments) of the body or to excretion from it. The parameters of the models (transfer coefficients) provided by ICRP are intended to describe a reference biokinetic behavior. True parameter values of individuals will surely differ from the reference values. These deviations will lead to uncertainties in the model predictions and thus finally in the doses assessed. It is barely possible to estimate sets of parameters for individuals because most of the parameters are not directly identifiable by the measurements. Uncertainties arising from applying reference parameter values are studied by interpreting parameter values as statistical distributions with the reference value of the parameter as median or mean value of the distribution [7, 8]. The results of calculations with biokinetic models will then also become distributions which are interpreted as uncertainties of the model prediction. By varying all parameters an uncertainty analysis can be performed. This will provide information on the overall uncertainties associated with the application of the biokinetic model in the dose assessment.

Dosimetric models are based on anatomic human voxel models with segmented volumes for source regions and target organs [2]. Depending on geometric position, tissue densities and compositions the energy deposition after the decay of radionuclides (S-coefficient) differs for individuals from the calculated value. According to the literature [9] only a small contribution to the total uncertainty of the assessed dose can be assumed. The uncertainty of S-coefficients can be estimated by using the variability of organ masses for the specific absorbed fraction (SAF-values) for alpha emitters, which are mainly depositing their energy in the organ, in which they are emitted.

For the uncertainty analysis C++ software was developed. It consists of a biokinetic and a dosimetric part. The compartment models for the biokinetic behavior can mathematically be described by first order differential equations systems. The software solves the differential equations systems by eigenvalue decomposition in matrix notation [7, 8, 10]. The number of nuclear disintegrations in the source tissues can be calculated by integration of the biokinetic retention curve. For analyzing the biokinetic of all the decay chain of U-238, U-235 and Th-232, the recent biokinetic models [11] for the daughter nuclides were connected to their mothers with the decay rate. The transfer rates within the biokinetic models are by 14 orders of magnitude bigger than the decay rate of the long-lasting nuclides. Thus, the algorithms used for solving the system of equations becomes numerically instable. For avoiding this instability, the decay was detached from the biokinetic models and considered by modification of the model input.

The uncertainties in these values are studied using Monte Carlo simulations with transfer coefficient matrices, which were sampled from distributions of the individual transfer coefficients. In order to take into account correlations of the parameters, the sampling algorithm which generates the individual values has been adapted. Values of parameters which describe the same transfers (for example in the lung model) for different nuclides are sampled once and all correlated parameters are set to identical values in the complete decay chain.

Uncertainties in dosimetric models

The second part of the software tool calculates the energy transfer per decay (S-coefficient) out of the nuclear disintegrations occurring in the body (or the organs). The S coefficients are calculated with the specific absorbed fractions (SAF values) that were obtained from simulations with Monte Carlo Transport Codes of voxel models of the human body. The energy dependent SAF values and nuclear decay data (particle types, energies, emission probabilities) for the relevant radionuclides are provided by ICRP [1, 12]. The software reads the data and calculates the nuclide-dependent S coefficients for the different combinations of source and target organs. A special feature is the organ "Other Tissues", in which several organs of the biokinetic models are summarized. The element-dependent definition of the compartments, which form the source region "Other Tissues", must be considered.

Various factors were compiled which led to uncertainties in the dose coefficients from the literature. Overall, there are few studies in the literature on the uncertainty of the S-coefficients. It is assumed that the uncertainty in the nuclear decomposition data for most nuclides provides almost no contribution to the overall uncertainty of the dose coefficient. The uncertainty in the SAF-values for alpha decay can be estimated in a first approximation with the variability of the organ masses.

References

[1] ICRP, *ICRP Publication* **133**. *Ann. ICRP* **45(2)**: 1–74, (2016).

[2] ICRP, *ICRP Publication* **109**. *Ann. ICRP* **39 (1),** (2009).

[3] ICRP, *ICRP Publication* **30 (1)**. *Ann. ICRP* **2 (3-4)**, (1979).

[4] ICRP, *ICRP Publication* **67**. *Ann. ICRP* **23 (3-4)**, (1993).

[5] ICRP, *ICRP Publication* **78**. *Ann. ICRP* **27 (3-4)**, (1997).

[6] ICRP, *Occupational Intakes of Radionuclides: Part* **1**. *ICRP Publication* **130**. *Ann. ICRP* **44 (2)**, (2015).

[7] W. Klein, *Dissertation*, (2011).

[8] W. Klein, *Abschlussbericht Verbundprojekt Strahlung und Umwelt,* (2012)

[9] NCRP, *NCRP Report No.*, **164,** Bethesda, MD, (2009).

[10] E. Polig, *Health Physics*, **81 (5)**: 492-501, (2001)

[11] A. Giussani, *private communication*, (2015)

[12] ICRP, *ICRP Publication* **107**. *Ann. ICRP* **38 (3)**, (2008).

11 Geoenergy

The Karlsruhe Institute of Technology has defined a broad research program on Enhanced Geothermal Systems (EGS) technology development following the necessity of a transdisciplinary approach. Research activities cover the whole process chain including system integration and span from fundamental to applied research across scales [1]. In this framework, geoenergy research at INE concerns mainly physical and chemical processes in the thermal water circuit and in fractured reservoir systems with special focus on EGS. Its technical feasibility was demonstrated in fractured crystalline basement at the Soultz-sous Forêts project (France). At the time, > 50 hydraulic experiments were performed in four wells at three different reservoir levels located between 2 and 5 km depth. These measures enhanced significantly the hydraulic yield of these reservoirs, in some instances by about two orders of magnitude, and provide a unique database for reservoir enhancement research. It was observed that hydraulic stimulation affects best hydrothermally altered fractures, i.e. comparably high permeable fractures with natural clay coating at the fracture surfaces [2]. With the aim to understand the formation of clay coating of fractures under natural flow condition, flow experiments with Na-illite have been carried out in simplified geometries and under low ionic and laminar groundwater flow conditions. In terms of process understanding, at Soultz, we identify cyclic injection in combination with circulation between wells reaching high hydraulic yield at comparatively low pressure. Furthermore, such hydraulic stimulations are accompanied by comparatively low number of seismic events and relatively low magnitudes [3]. In this context, new monitoring approaches addressing changes in hydraulic connectivity by electromagnetic methods have been successfully tested for EGS at Rittershoffen (France) [4]. It results that the electromagnetic response of the reservoir is different for production and injection and it is thus, not only dependent on the flow rate, but also on the reservoir pressure. Monitoring of continuous mud loss during drilling associated with localized seismicity and effects of long-term low flow rate injection in supercritical condition is currently tested in the IDDP2 well at Reykjanes (Iceland). To meet the evolving needs to carry out more EGS-specific experiments including monitoring in space and time, the condition of the southern Black Forest-Odenwald complex were investigated for a Geothermal Laboratory in Crystalline Basement (GeoLaB) [5]. This geothermal underground research infrastructure project is aimed as the first geothermal reservoir simulator for reservoir technology and borehole safety, in order to accomplish cutting-edge research in crystalline rock next to thermal hotspots.

Y. Abdelfettah, G. K. Darbha, N. Haaf, R. Haas-Nüesch, F. Huber, T. Schäfer, E. Schill, M. Stoll

In co-operation with:

N. Cuenot[a], E. Gaucher[b], A. Genter[c], J. C. Grimmer[b], T. Kohl[b], J. Meixner[b], C. Meller[b], I. Stober[b],

[a] GEIE "Exploitation Minière de la Chaleur", Kutzenhausen, France; [b] ÉS Géothermie, Strasbourg, France; [c] AGW, Karlsruhe Institute of Technology, Germany

Introduction

In central Europe, major geothermal resources are contained within deep fractured crystalline rock at high differential stresses. Economic viable projects require about 50 L s^{-1} of flow at temperature > 130°C. There are a number of scientific challenges along with an environmentally friendly development of deep geothermal energy in these geothermal fields. Key issues relate mainly to perceptible seismicity during enhancement of the reservoir performance and operation, as well as radioactive scaling.

The geothermal research at INE is embedded into Helmholtz Portfolio project *Environmentally friendly provision of local energy from georesources – Geoenergy* and the Helmholtz program *Renewable Energies*. In the view of economically viable condition and low environmental impact, fundamental research is carried out in particular on the relations between fluid circulation, hydro-mechanics, alteration and geophysical properties such as electric resistivity. To a large part, related phenomena are investigated at reservoir level. This concerns the investigation of hydraulic condition in natural geothermal systems and based on this, the understanding of reservoir engineering techniques for the crystalline basement. Furthermore, new monitoring techniques are developed to study processes related to reservoir engineering and operation. The Helmholtz research in these fields is completed in two EC H2020 projects:

1) Deployment of deep enhanced geothermal systems for sustainable energy business (DEEPEGS, www.deepegs.eu/)
2) Cooperation in Geothermal energy research Europe-Mexico for development of Enhanced Geothermal Systems and Superhot Geothermal Systems (GEMex, www.gemex-h2020.eu/)

Reflecting INE's strong expertise in radiochemistry, thermal circuit related issues such as scalings incorporating radioactive isotopes and corrosion are investigated at laboratory scale.

INE is strongly involved in the preparation of the large-scale research infrastructure *Geothermal Laboratory in the crystalline Basement (GeoLaB)*. GeoLaB is planned as large-scale underground research facility

Fig. 1: *Cataclased hydrothermally altered porphyroid granite of exploration well EPS-1 (K080 – bottom depth 1462.16 m).*

for controlled high flow-rate (CHFE) experiments in fractured, crystalline basement with the aim to investigate hydraulic, hydro-mechanic and heat transfer processes. It aims on closing the gap between geothermal researches on laboratory- and reservoir-scale.

Nano-particulate illite transport experiments using laser-induced breakdown-detection (LIBD)

Clay minerals in natural fractures, e.g. in EGS reservoirs, are known to reduce the frictional strength of the fracture's surface [6]. Notwithstanding the negative surface charges of both, clay colloids and fracture surfaces, clay colloids coat in hydrothermally altered fracture surfaces (Fig. 1). In order to understand the accumulation and mobilization of clay particles in hydraulically active fractures, the interaction of monodisperse carboxylated polystyrene [7] and polydisperse Na-illite colloids with cut granodiorite and acrylic surfaces was investigated. Colloid transport experiments are conducted in a cylindrical parallel plate type fracture flow cell with an aperture of 0.75 mm at pH 5 under overall unfavorable attachment conditions of low ionic strength (1 mM NaCl) and laminar flow (7 mL h^{-1}). The study focuses on the effect of residence time, colloid size, collector material, and fracture orientation on colloid retention. Long colloid residence times are achieved by stop-flow experiments.

LIBD measurements and SEM images show an illite colloid suspension sizes ranging from 35 - 350 nm in size. In continuous flow experiments the illite colloids show an earlier first arrival than the solute tracer and full colloid recovery. Similar to the 1000 nm and 25 nm carboxylated polystyrene, for the clay colloids a positive correlation was found between colloid retention and residence time. However, the recovery of the Na-illite colloids was significantly higher for long residence times (24 h). In case of monodisperse colloid suspensions the geometry of the fracture flow cell chosen gives the opportunity to observe the impact of fracture orientation and collector surface material on colloid retention. Despite a minor, less prominent double peak in the horizontal illite experiments for 24 h residence time, prominent features as observed in the break through curves of the carboxylated polystyrene were not detected. Thus, illite colloids show significant higher mobility.

Electromagnetic monitoring of reservoir processes

Changes in fluid pathways during hydraulic stimulation and operation of geothermal projects are typically inferred from micro-seismic monitoring. Microseismicity can provide information on the location and deformation mechanism of fractures, but hardly on fracture connectivity, while fluid flow through fractures causes electrokinetic effects. At INE, we aim at investigating the information value of electromagnetic monitoring of low volume, low flow rate and low-pressure fluid injection and production in a fractured reservoir. For this, data were collected at the ECOGI geothermal site of Rittershoffen that is located at about 10 km SE of the EGS reference project of Soultz-sous-Forêts. The site includes two wells, GRT1 and 2, reaching depths of 2526 m and 2693 m, respectively. The reservoir zone of Rittershoffen seems to be comparable to the Soultz EGS reference site with a characteristic low-resistivity anomaly at the top of the crystalline basement [8].

Magnetotelluric monitoring involves the acquisition of the natural electric and magnetic field components in XY and XYZ directions using non-polarizable electrodes and coil magnetometers. Electrical and magnetic components are acquired from the surface (Fig. 2) quasi-continuously at 512 Hz in a frequency range of 10^{-3} to 10^{2} Hz. Following the principle of skin depth, the frequency can be attributed to depth, i.e. the lower the frequency, the higher the contribution to the integral signal from depth.

Representative apparent resistivity variations calculated for three-day windows with period obtained after data processing were selected with respect to different operations ongoing at the site such as production from and injection into GRT2, injection in GRT1 and GRT2, and no ongoing operation (Fig. 3). Acceptable data uncertainties are obtained up to periods of about < 5 s for all days. Lowest uncertainty is obtained for the time window August 03 to 05, when

Fig. 2: *Installation of the magnetotelluric reference site for the IDDP2 monitoring in the framework of the EU-H2020 project DEEPEGS in Iceland.*

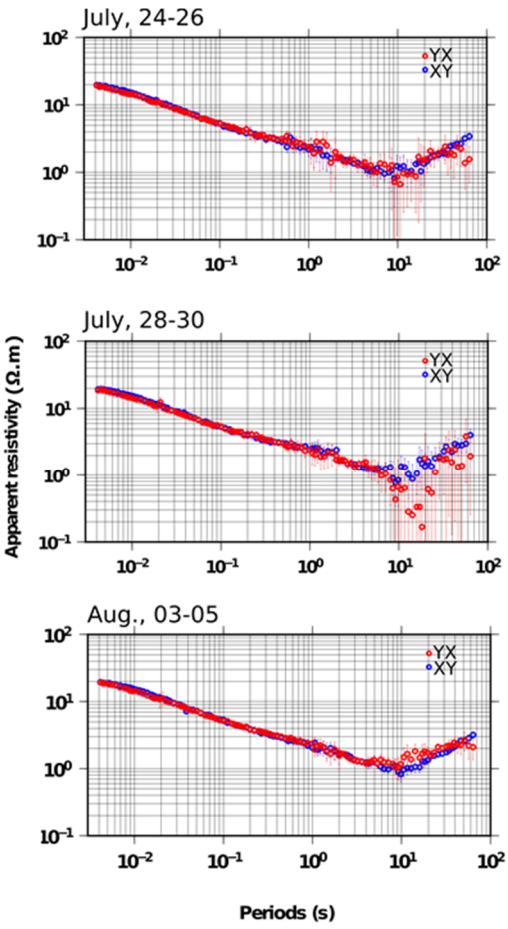

Fig. 3: *Apparent resistivities versus period obtained from robust processing including remote referencing of RITT station from representative three days for production from GRT2 (top), injection in GRT2 (center), and no operation (bottom).*

no operation was ongoing at the site. This window is used as reference. Uncertainties become significantly higher mainly at periods > 10 s for days when operation in the wells is ongoing. Note that they are significantly more prominent in the YX component that represents the direction of maximum horizontal stress (SH_{max}) and thus, the expected extension of the fractures controlling the reservoir. During production from GRT2, a moderate increase in uncertainty and decrease in smoothness is observed between 8 - 11 s for resistivity. In addition to this general increase of uncertainty and decrease of smoothness in this period range related to operation in the wells, we observe a strong decrease in resistivity by up to one order of magnitude between about 8 to 12 s during injection of fluid into GRT2.

GeoLaB

The geothermal underground research infrastructure project GeoLaB (Fig. 4) is aimed as the first geothermal reservoir simulator for reservoir technology and borehole safety. Real scale experiments and cutting-edge research in crystalline rock next to thermal hotspots will boost geothermal as renewable energy source.

In Central Europe, the largest geothermal potential resides in the crystalline basement rock with important hotspots in tectonically stressed areas. To better harvest this energy form under sustainable, predictable and efficient conditions, new focused, scientific driven strategies are needed. Similar to other geo-technologies, the processes for environmental sustainability in the subsurface need to be investigated in large-scale facilities.

The proposed new underground research laboratory GeoLaB will address the fundamental challenges of reservoir technology and borehole safety. The specific objectives of GeoLaB are

1) to perform controlled high flow rate experiments, CHFE, in fractured rock,
2) to integrate multi-disciplinary research to solve key questions related to flow regime under high flow rates, or higher efficiency in reservoir engineering,
3) risk mitigation by developing and calibrating smart stimulation technologies without creating seismic hazard, and
4) to develop save and efficient borehole installations using innovative monitoring concepts.

Planned experiments will significantly contribute to our understanding of processes associated with increased flow rates in crystalline rock. The application and development of cutting-edge tools for monitoring and analyzing will yield fundamental findings, which are of major importance for safe and ecologically-sustainable usage of geothermal energy and further subsurface resources. As an interdisciplinary and international research platform, GeoLaB will cooperate with research funding institutions, universities, industrial partners, and professional organizations to foster synergies and technological and scientific innovations.

GeoLaB is designed as a generic underground research laboratory in the crystalline rock adjacent to the Rhine Graben, one of the most prominent geothermal hotspots in Germany. A key aspect of the GeoLaB reservoir simulator is to conduct controlled, high flow rate experiments, CHFE, in fractured crystalline rock. This requires defining specific technical criteria that bring up clear differences to nuclear waste laboratories. They are:

1) Low complexity of the geology in terms of lithology changes in favor of a rather homogenous crystalline matrix. Fluid injection into high permeable zones such as faults or interconnected permeable natural fractures will keep fluid pressure low. This way, large-scale fracking will be prevented. Ambient hydraulic transmissivities in the order of 10^{-4} m s^{-1} similar to those of the Soultz reservoir are anticipated [3].
2) The hydraulic boundary conditions should represent ambient situations at far-field without infiltrating into artificial structures. As such, a "flooding" of other galleries would yield a safety issue

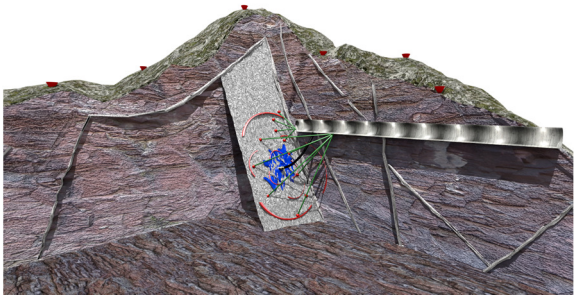

Fig. 4: *Possible layout of GeoLaB (not to scale) with an access tunnel to a fracture zone, observation wells (green) from the tunnel into the fracture zone. In addition to the monitoring stations (red cones), the main injection well (black) for controlled high-flow experiments (CHFE) targets the fracture zones. Possible CHFE with high flow rate injection from the surface into a fracture zone (blue volume) and related mechanical deformation indicated by red ring segments.*

but also would harm the total experimental results due to artificially imposed boundary conditions. Since extensive drainage may occur in old mining areas, minimum distances must be respected.

3) Injection into favorably oriented fractures for reactivation in the ambient stress field is an intrinsic pre-requisite of a geothermal URL implying differential stress magnitudes above approx. 3 - 5 MPa depending on the local stress field. Topography induced perturbations to the stress field should be minimized with maximum variations of 1 MPa to be tolerated.
4) Clay minerals are known to reduce the mechanical / frictional strength of fractures, i.e. the pressure required to cause shear during hydraulic stimulation [6]. Hydrothermal alteration products in the matrix and on the faults should cover the illite to smectite range.

GeoLaB is an analogue site representative of the world‘s most widespread geothermal reservoir rock, the crystalline basement. The first order suitability of a site for GeoLaB located in the Black Forest or the Odenwald is proven [5].

At the selected site, a two-km long gallery will be excavated, tapping individual caverns, from which controlled, high flow rate experiments will be conducted at depths of about 400 m. The experiments will be continuously monitored from multiple wells, drilled from the underground laboratory or from the surface. This will create a unique 4D-benchmark dataset of thermal, hydraulic, chemical and mechanical parameters. The experimental infrastructure GeoLaB is planned as a worldwide unique facility to specifically address the main challenges of EGS Systems:

- High flow experiments to better understand the fluid flow in fractured media – enhance the predictability of geothermal reservoir and towards a better modelling.
- Development and test of smart stimulation technologies – higher flow rates with reduced impact for the public.
- Real scale experiments for innovative well integrity schemes – double the security while reducing the costs by a factor of two.

Hence, GeoLaB will become a cornerstone for the target-oriented development of the enormous geothermal resource.

With its worldwide unique geothermal laboratory setting, GeoLaB allows for cutting-edge research, associating fundamental to applied research for reservoir technology and borehole safety, bridging laboratory to field scale experiments and connecting renewable energy research to social perception. GeoLaB comprises a novel approach that will shape research in earth science for the next generations of students and scientists.

References

[1] Meller, C., et al., *Energy Technology* 10.1002/ente.201600579 (2016)
[2] Evans, K. F., et al., *Geophysical Journal International* **160**, 1 (2005)
[3] Schill, E., et al., *Geothermics* (subm.).
[4] Abdelfettah, Y., et al., *Geothermics* (subm.).
[5] Schill, E., et al., *Geothermal Energy Journal* **4**, 7 (2016).
[6] Amitrano, D., J. Schmittbuhl, *Journal of Geophysical Research* **107**, 2375 (2002).
[7] Stoll, M. et al., *Journal of Colloid and Interface Sciences* **475**, 171-183 (2016).
[8] Geiermann, J., Schill, E., et al., *Comptes Rendue Geosciences* **342**, 587-599 (2010).

12 Publications

ISI/SCOPUS

[1] Adam, C.; Rohde, V.; Müllich, U.; Kaden, P.; Geist, A.; Panak, P. J.; Geckeis, H., *Comparative NMR study of nPrBTP and iPrBTP*, *Procedia Chemistry* **2016**, *21*, 38–45.

[2] Adushkin, V. V.; Chen, B. B.; Popel, S. I.; Weidler, P. G.; Friedrich, F.; Izvekova, Y. N., *Properties and origin of small particles in the atmosphere of Central Asia*, *Dokl Earth Sci* **2016**, *466*, 177-182.

[3] Amayri, S.; Fröhlich, D. R.; Kaplan, U.; Trautmann, N.; Reich, T., *Distribution coefficients for the sorption of Th, U, Np, Pu, and Am on Opalinus Clay*, *Radiochim Acta* **2016**, *104*, 33-40.

[4] Amgarou, K.; Paradiso, V.; Patoz, A.; Bonnet, F.; Handley, J.; Couturier, P.; Becker, F.; Menaa, N., *A comprehensive experimental characterization of the iPIX gamma imager*, *Journal of Instrumentation* **2016**, *11*, P08012.

[5] Banik, N. L.; Marsac, R.; Lutzenkirchen, J.; Diascorn, A.; Bender, K.; Marquardt, C. M.; Geckeis, H., *Sorption and Redox Speciation of Plutonium at the Illite Surface*, *Environ Sci Technol* **2016**, *50*, 2092-2098.

[6] Banik, N. L.; Vallet, V.; Real, F.; Belmecheri, R. M.; Schimmelpfennig, B.; Rothe, J.; Marsac, R.; Lindqvist-Reis, P.; Walther, C.; Denecke, M. A.; Marquardt, C. M., *First structural characterization of Pa(IV) in aqueous solution and quantum chemical investigations of the tetravalent actinides up to Bk(IV): The evidence of a curium break*, *Dalton T* **2016**, *45*, 453-457.

[7] Beele, B. B.; Skerencak-Frech, A.; Stein, A.; Trumm, M.; Wilden, A.; Lange, S.; Modolo, G.; Müllich, U.; Schimmelpfennig, B.; Geist, A.; Panak, P. J., *2,6-Bis(5,6-diisopropyl-1,2,4-triazin-3-yl)pyridine: a highly selective N-donor ligand studied by TRLFS, liquid-liquid extraction and molecular dynamics.*, *New J. Chem.* **2016**, *40*, 10389–10397.

[8] Breustedt, B.; Broggio, D.; Gomez-Ros, J. M.; Leone, D.; Marzocchi, O.; Poelz, S.; Shutt, A.; Lopez, M. A., *The Eurados-Kit Training Course on Monte Carlo Methods for the Calibration of Body Counters*, *Radiation protection dosimetry* **2016**, *170*, 446-450.

[9] Buerck, J.; Wadhwani, P.; Fanghaenel, S.; Ulrich, A. S., *Oriented Circular Dichroism: A Method to Characterize Membrane Active Peptides in Oriented Lipid Bilayers*, *Accounts of Chemical Research* **2016**, *49*, 184-192.

[10] Edwards, A. C.; Wagner, C.; Geist, A.; Burton, N. A.; Sharrad, C. A.; Adams, R. W.; Pritchard, R. G.; Panak, P. J.; Whitehead, R. C.; Harwood, L. M., *Exploring electronic effects on the partitioning of actinides(III) from lanthanides(III) using functionalised bis-triazinyl phenanthroline ligands*, *Dalton T* **2016**, *45*, 18102-18112.

[11] Fellhauer, D.; Altmaier, M.; Gaona, X.; Lutzenkirchen, J.; Fanghänel, T., *Np(V) solubility, speciation and solid phase formation in alkaline CaCl2 solutions. Part II: Thermodynamics and implications for source term estimations of nuclear waste disposal*, *Radiochim Acta* **2016**, *104*, 381-397.

[12] Fellhauer, D.; Rothe, J.; Altmaier, M.; Neck, V.; Runke, J.; Wiss, T.; Fanghaenel, T., *Np(V) solubility, speciation and solid phase formation in alkaline $CaCl_2$ solutions. Part I: Experimental results*, *Radiochim Acta* **2016**, *104*, 355-379.

[13] Ferrari, P.; Becker, F.; Carinou, E.; Chumak, V.; Farah, J.; Jovanovic, Z.; Krstic, D.; Morgun, A.; Principi, S.; Teles, P., *Monte Carlo study of the scattered radiation field near the eyes of the operator in interventional procedures*, *Journal of radiological protection* **2016**, *36*, 902–921.

[14] Finck, N.; Dardenne, K., *Interaction of selenite with reduced Fe and/or S species: An XRD and XAS study*, *J Contam Hydrol* **2016**, *188*, 44-51.

[15] Finck, N.; Lützenkirchen, J.; Hanna, K.; Rabung, T., *Comment on "Kinetics and thermodynamics of Eu(III) adsorption onto synthetic monoclinic pyrrhotite"*, *J. Mol. Liq.* **2016**, *224*, 1022-1024.

[16] Finck, N.; Nedel, S.; Dideriksen, K.; Schlegel, M. L., *Trivalent Actinide Uptake by Iron (Hydr)oxides*, *Environ Sci Technol* **2016**, *50*, 10428-10436.

[17] Finck, N.; Radulescu, I.; Schild, D.; Rothmeier, M.; Huber, F.; Lützenkirchen, J.; Rabund, T.; Heberling, F.; Schlegel, M. L.; Dideriksen, K.; Nedel, S.; Geckeis, H., *XAS signatures of Am(III) adsorbed onto magnetite and maghemite*, *Journal of physics / Conference Series* **2016**, *712*, 012085/012081-012085.

[18] Froehlich, D. R.; Trumm, M.; Skerencak-Frech, A.; Panak, P. J., *The Complexation of Cm(III) with Succinate Studied by Time-Resolved Laser Fluorescence Spectroscopy and Quantum Chemical Calculations*, *Inorg Chem* **2016**, *55*, 4504-4511.

[19] Geist, A.; Taylor, R.; Ekberg, C.; Guilbaud, P.; Modolo, G.; Bourg, S., *The SACSESS hydrometallurgy domain - an overview*, *Procedia Chemistry 21, 218–222.* **2016**, *21*, 218–222

[20] González-Robles, E.; Metz, V.; Wegen, D. H.; Herm, M.; Papaioannou, D.; Bohnert, E.; Gretter, R.; Müller, N.; Nasyrow, R.; de Weerd, W.; Kienzler, B., *Determination of fission gas release of spent nuclear fuel in puncturing test and in leaching experiments under anoxic conditions*, *J Nucl Mater* **2016**, *479*, 67-75.

[21] Grunwaldt, J.-D.; Hagelstein, M.; Rothe, J., *The 16th International Conference on X-ray Absorption Fine Structure (XAFS16)*, *Journal of physics / Conference Series* **2016**, *712*, 011001.

[22] Gyekye, P. K.; Becker, F.; Mensah, S. Y.; Emi-Reynolds, G., *Optimisation of scatter radiation to staff during CT-fluoroscopy: Monte Carlo studies*, *Radiation protection dosimetry* **2016**, *170*, 393-397.

[23] Heberling, F.; Paulig, L.; Nie, Z.; Schild, D.; Finck, N., *Morphology Controls on Calcite Recrystallization*, *Environ Sci Technol* **2016**, *50*, 11735-11741.

[24] Held, S.; Schill, E.; Pavez, M.; Diaz, D.; Munoz, G.; Morata, D.; Kohl, T., *Resistivity distribution from mid-crustal conductor to near-surface across the 1200 km long Liquine-Ofqui Fault System, southern Chile*, *Geophys J Int* **2016**, *207*, 1387-1400.

[25] Henry, C.; Norrfors, K. K.; Olejnik, M.; Bouby, M.; Luetzenkirchen, J.; Wold, S.; Minier, J.-P., *A refined algorithm to simulate latex colloid agglomeration at high ionic strength*, *Adsorption* **2016**, *22*, 503-515.

[26] Hoefener, S.; Trumm, M.; Koke, C.; Heuser, J.; Ekstrom, U.; Skerencak-Frech, A.; Schimmelpfennig, B.; Panak, P. J., *Computing UV/vis spectra using a combined molecular dynamics and quantum chemistry approach: bis-triazin-pyridine (BTP) ligands studied in solution*, *Phys Chem Chem Phys* **2016**, *18*, 7728-7736.

[27] Hofmann, S.; Voitchovsky, K.; Spijker, P.; Schmidt, M.; Stumpf, T., *Visualising the molecular alteration of the calcite (104) - water interface by sodium nitrate*, *Sci Rep* **2016**, *6*.

[28] Kamagate, M.; Luetzenkirchen, J.; Huber, F.; Hanna, K., *Comment on "Competitive Adsorption of Cd(II), Cr(VI), and Pb(II) onto Nanomaghemite: A Spectroscopic and Modeling Approach"*, *Environ Sci Technol* **2016**, *50*, 1632-1633.

[29] Kaufholz, P.; Modolo, G.; Wilden, A.; Sadowski, F.; Bosbach, D.; Wagner, C.; Geist, A.; Panak, P. J.; Lewis, F. W.; Harwood, L. M., *Solvent Extraction and Fluorescence Spectroscopic Investigation of the Selective Am(III) Complexation with TS-BTPhen*, *Solvent Extr Ion Exc* **2016**, *34*, 126-140.

[30] Kupcik, T.; Rabung, T.; Lützenkirchen, J.; Finck, N.; Geckeis, H.; Fanghänel, T., *Macroscopic and spectroscopic investigations on Eu(III) and Cm(III) sorption onto bayerite (beta-$Al(OH)_3$) and corundum (alpha-Al_2O_3)*, *J Colloid Interf Sci* **2016**, *461*, 215-224.

[31] Lee, S. S.; Heberling, F.; Sturchio, N. C.; Eng, P. J.; Fenter, P., *Surface Charge of the Calcite (104) Terrace Measured by Rb+ Adsorption in Aqueous Solutions Using Resonant Anomalous X-ray Reflectivity*, *J Phys Chem C* **2016**, *120*, 15216-15223.

[32] Li, S.; Leroy, P.; Heberling, F.; Devau, N.; Jougnot, D.; Chiaberge, C., *Influence of surface conductivity on the apparent zeta potential of calcite*, *J Colloid Interf Sci* **2016**, *468*, 262-275.

[33] McLachlan, F.; Greenough, K.; Geist, A.; McLuckie, B.; Modolo, G.; Wilden, A.; Taylor, R., *Nitric Acid Extraction into the TODGA/TBP Solvent*, *Solvent Extr Ion Exc* **2016**, *34*, 334-346.

[34] McLachlan, F.; Taylor, R.; Whittaker, D.; Woodhead, D.; Geist, A., *Modelling of innovative SANEX process maloperations*, *Procedia Chemistry 2016* **2016**, *21*, 109–116.

[35] Meixner, J.; Schill, E.; Grimmer, J. C.; Gaucher, E.; Kohl, T.; Klingler, P., *Structural control of geothermal reservoirs in extensional tectonic settings: An example from the Upper Rhine Graben*, *J Struct Geol* **2016**, *82*, 1-15.

[36] Meller, C. B., J.; Ankit, K.; Baur, S.; Bergfeldt, T.; Blum, P.; Canic, T.; Eiche, E.; Gaucher, E.; Hagenmeyer, V.; Heberling, F.; Held, S.; Herfurth, S.; Isele, J.; Kling, T.; Kuhn, D.; Mayer, D.; Müller, B.; Nestler, B.; Neumann, T.; Nitschke, F.; Nothstein, A.; Nusiaputra, Y.; Orywall, P.; Peters, M.; Sahara, D.; Schäfer, T.; Schill, E.; Schilling, F.; Schröder, E.; Selzer, M.; Stoll, M.; Wiemer, H.-J.; Wolf, S.; Zimmermann, M.; Kohl, T., *Integrated research as key to the development of a sustainable geothermal energy technology*, *Energy Technology* **2016**, *in press*.

[37] Misaelides, P.; Fellhauer, D.; Gaona, X.; Altmaier, M.; Geckeis, H., *Thorium(IV) and neptunium(V) uptake from carbonate containing aqueous solutions by HDTMA-modified natural zeolites*, *J Radioanal Nucl Ch* **2016**, *in press*, xx.

[38] Norrfors, K. K.; Marsac, R.; Bouby, M.; Heck, S.; Wold, S.; Lützenkirchen, J.; Schäfer, T., *Montmorillonite colloids: II. Colloidal size dependency on radionuclide adsorption*, *Applied clay science* **2016**, *123*, 292-303.

[39] Pang, B.; Becker, F., *Albedo Neutron Dosimetry in a Deep Geological Disposal Repository for High-Level Nuclear Waste [in press]*, *Radiation protection dosimetry* **2016**.

[40] Pang, B.; Becker, F.; Saurí Suárez, H., *Monte Carlo based investigation of a universal two-component albedo neutron dosimeter in a deep geological disposal system for high-level nuclear waste*, *Annals of nuclear energy* **2016**, *98*, 81-89.

[41] Pang, B.; Saurí Suárez, H.; Becker, F., *Individual dosimetry in disposal repository of heat-generating nuclear waste*, *Radiation protection dosimetry* **2016**, *170*, 387-392.

[42] Peterman, D.; Geist, A.; Mincher, B.; Modolo, G.; Galan, M. H.; Olson, L.; McDowell, R., *Performance of an i-SANEX System Based on a Water-Soluble BTP under Continuous Irradiation in a gamma-Radiolysis Test Loop*, *Ind Eng Chem Res* **2016**, *55*, 10427-10435.

[43] Pidchenko, I.; Heberling, F.; Kvashnina, K. O.; Finck, N.; Schild, D.; Bohnert, E.; Schäfer, T.; Rothe, J.; Geckeis, H.; Vitova, T., *Aqueous U(VI) interaction with magnetite nanoparticles in a mixed flow reactor system: HR-XANES study*, *Journal of Physics: Conference Series* **2016**, *712*.

[44] Podkovyrina, Y.; Pidchenko, I.; Pruesmann, T.; Bahl., S.; Soldatov, A.; Vitova, T., *Probing covalency in UO_3 polymorphs by U M4 edge HR-XANES*, *Journal of Physics: Conference Series, 16th International Conference on X-ray Absorption Fine Structure (XAFS16), Karlsruhe, Germany, 2016* **2016**, *712*.

[45] Poelz, S.; Breustedt, B., *Personalised Body Counter Calibration Using Anthropometric Parameters*, *Radiation protection dosimetry* **2016**, *170*, 221-224.

[46] Popa, K.; Prieur, D.; Manara, D.; Naji, M.; Vigier, J. F.; Martin, P. M.; Blanco, O. D.; Scheinost, A. C.; Prussmann, T.; Vitova, T.; Raison, P. E.; Somers, J.; Konings, R. J. M., *Further insights into the chemistry of the Bi-U-O system*, *Dalton T* **2016**, *45*, 7847-7855.

[47] Prieto, M.; Heberling, F.; Rodriguez-Galan, R. M.; Brandt, F., *Crystallization behavior of solid solutions from aqueous solutions: An environmental perspective*, *Prog Cryst Growth Ch* **2016**, *62*, 29-68.

[48] Ratnayake, S.; Schild, D.; Maczka, E.; Jartych, E.; Luetzenkirchen, J.; Kosmulski, M.; Makehelwala, M.; Weragoda, S. K.; Bandara, A.; Wijayawardana, R.; Chandrajith, R.; Indrarathne, S. P.; Weerasooriya, R., *A novel radiation-induced grafting methodology to synthesize stable zerovalent iron nanoparticles at ambient atmospheric conditions*, *Colloid Polym Sci* **2016**, *294*, 1557-1569.

[49] Reiche, T.; Noseck, U.; Schäfer, T., *Migration of Contaminants in Fractured-Porous Media in the Presence of Colloids: Effects of Kinetic Interactions*, *Transport Porous Med* **2016**, *111*, 143-170.

[50] Rothe, J.; Grunwaldt, J.-D.; Doyle, S., *XAFS16 at KIT: Five Days of Cutting-Edge X-ray Science in Karlsruhe*, *Synchrotron Radiation News* **2016**, *29*, 9.

[51] Sarri, S.; Misaelides, P.; Zamboulis, D.; Gaona, X.; Altmaier, M.; Geckeis, H., *Rhenium(VII) and technetium(VII) separation from aqueous solutions using a polyethylenimine-epichlorohydrin resin*, *J Radioanal Nucl Ch* **2016**, *307*, 681-689.

[52] Schill, E.; Meixner, J.; Meller, C.; Grimm, M.; Grimmer, J.; Stober, I.; Kohl, T., *Criteria and site assessment for the generic geothermal underground research laboratory, GeoLaB*, *Geothermal Energy Journal* **2016**, *4:1*, 1-30.

[53] Steudel, A.; Kleeberg, R.; Koch, C. B.; Friedrich, F.; Emmerich, K., *Thermal behavior of chlorites of the clinochlore-chamosite solid solution series: Oxidation of structural iron, hydrogen release and dehydroxylation*, *Applied clay science* **2016**, *132–133*, 626 - 634.

[54] Stoll, M.; Huber, F.; Darbha, G. K.; Schill, E.; Schäfer, T., *Impact of gravity, collector surface roughness and fracture orientation on colloid*, *J Colloid Interf Sci* **2016**, *475*, 171-183.

[55] Taylor, R.; Carrott, M.; Galan, H.; Geist, A.; Hères, X.; Maher, C.; Mason, C.; Malmbeck, R.; Miguirditchian, M.; Modolo, G.; Rhodes, C.; Sarsfield, M.; Wilden, A., *The EURO-GANEX process: current status of flowsheet development and process safety studies*, *Procedia Chemistry 2016* **2016**, *21*, 524–529.

[56] Teles, P.; Nikodemová, D.; Bakhanova, E.; Becker, F.; Knežević, Ž.; Pereira, M. F.; Sarmento, S., *A Review of Radiation Protection Requirements and Dose Estimation for Staff and Patients in CT Fluoroscopy [in press]*, *Radiation protection dosimetry* **2016**.

[57] Trumm, M.; Schimmelpfennig, B., *Towards the origin of effective An(III)/Ln(III) separation by tridentate N-donor ligands: a theoretical study on atomic charges and polarisabilities for Cm(III)/Gd(III) separation*, *Mol Phys* **2016**, *114*, 876-883.

[58] Trumm, M.; Wagner, C.; Schimmelpfennig, B.; Geist, A.; Panak, P. J., *A closer look on the coordination of soft nitrogen-donor ligands to Cm(III): SO_3-Ph-BTBP*, *Dalton T* **2016**, *45*, 12308-12311.

[59] Vanel, V.; Marie, C.; Kaufholz, P.; Montuir, M.; Boubals, N.; Wilden, A.; Modolo, G.; Geist, A.; Sorel, C., *Modelling and flowsheet design of an Am separation process using TODGA and H4TPAEN*, *Procedia Chemistry* **2016**, *21*, 223–230.

[60] Virtanen, S.; Bok, F.; Ikeda-Ohno, A.; Rossberg, A.; Lützenkirchen, J.; Rabung, T.; Lehto, J.; Huittinen, N., *The specific sorption of Np(V) on the corundum (α-Al_2O_3) surface in the presence of trivalent lanthanides Eu(III) and Gd(III): A batch sorption and XAS study*, *J Colloid Interf Sci* **2016**, *483*, 334–342.

[61] Wagner, C.; Muellich, U.; Geist, A.; Panak, P. J., *Selective Extraction of Am(III) from PUREX Raffinate: The AmSel System*, *Solvent Extr Ion Exc* **2016**, *34*, 103-113.

[62] Wagner, C.; Ruff, C.; Mullich, U.; Geist, A.; Panak, P. J., *The nephelauxetic effect of Eu(III)-N-donor compounds probed using fluorescence spectroscopy-further evidence for covalence?*, *New J Chem* **2016**, *40*, 9232-9237.

[63] Wallesch, M.; Verma, A.; Flechon, C.; Flugge, H.; Zink, D. M.; Seifermann, S. M.; Navarro, J. M.; Vitova, T.; Gottlicher, J.; Steininger, R.; Weinhardt, L.; Zimmer, M.; Gerhards, M.; Heske, C.; Brase, S.; Baumann, T.; Volz, D., *Towards Printed Organic Light-Emitting Devices: A Solution-Stable, Highly Soluble Cu-I-NHetPHOS Complex for Inkjet Processing*, *Chem-Eur J* **2016**, *22*, 16400-16405.

[64] Yalcintas, E.; Gaona, X.; Altmaier, M.; Dardenne, K.; Polly, R.; Geckeis, H., *Thermodynamic description of Tc(IV) solubility and hydrolysis in dilute to concentrated NaCl, $MgCl_2$ and $CaCl_2$ solutions*, *Dalton T* **2016**, *45*, 8916-8936.

[65] Yalçintaş, E.; Scheinost, A. C.; Gaona, X.; Altmaier, M., *Systematic XAS study on the reduction and uptake of Tc by magnetite and mackinawite*, *Dalton T* **2016**, *45*, 17874-17885.

[66] Yokosawa, T.; Tichelaar, F. D.; Zandbergen, H. W., *In-Situ TEM on Epitaxial and Non-Epitaxial Oxidation of Pd and Reduction of PdO at P=0.2-0.7 bar and T=20-650 degrees C*, *Eur J Inorg Chem* **2016**, 3094-3102.

[67] Zang, A.; Stephansson, O.; Stenberg, L.; Plenkers, K.; Specht, S.; Milkereit, C.; Schill, E.; Kwiatek, G.; Dresen, G.; Zimmermann, G.; Dahm, T.; Weber, M., *Fatigue hydraulic fracturing by cyclic reservoir treatment enhances permeability and reduces induced seismicity*, *Geophys J Int* **2016**, *xx*, xx.

[68] Zimina, A.; Dardenne, K.; Denecke, M. A.; Grunwaldt, J. D.; Huttel, E.; Lichtenberg, H.; Mangold, S.; Pruessmann, T.; Rothe, J.; Steininger, R.; Vitova, T., *The CAT-ACT Beamline at ANKA: A new high energy X-ray spectroscopy facility for CATalysis and ACTinide research*, *Journal of physics / Conference Series* **2016**, *712*, 012019.

Other referred publications

[69] Stability of compacted bentonite for radionuclide retardation – Experiments and modelling (Project Kollorado-e; Final Report), **2016**.

[70] Bouby, M., Organic matter (OM) stability at high ionic strengths (IS) in chloride media, Contribution to the HATT-2 final report, **2016**.

[71] Huber, F.; Noseck U.; Schäfer, T., Stability of compacted bentonite for radionuclide retardation – Experiments and modelling (Project Kollorado-e; Final Report), **2016**.

[72] Kaplan, U.; Bouby, M.; Rabung, T.; Kaden, P.; Schild, D.; Heck, S.; Schäfer, T., Characterization of natural organic matter (NOM) derived from different layers within the Boom clay formation and their radionuclide interaction, KIT-INE internal report number: 04/2016 **2016**.

[73] Quinto, F.; Lagos, M.; Plaschke, M.; Schäfer, T.; Steier, P.; Geckeis, H., Accelerator Mass Spectrometry (AMS) of Actinides in Ground-and Seawater: simultaneous Analysis of U, Np, Pu, Am and Cm isotopes below ppq levels, Stability of compacted bentonite for radionuclide retardation – Experiments and modelling (Project Kollorado-e; Final Report). Hrsg. F.M. Huber, **2016**

Invited talks

[74] Bahl, S.; Roth, G.; Weisenburger, S.; Vitova, T.; Geckeis, H.; Yano, T., Investigations of high U and Pu loaded boro- and alumosilicate glasses by advanced synchrotron based spectroscopic techniques – A cooperation with CEA Marcoule, 8th vitrification workshop, Tokyo, Japan, **2016**

[75] Bouby, M., Potential environmental impact of nanoparticles (NPs): the case of an underground nuclear waste repository, Journées Scientifiques de l'Université de Nantes, Colloque 12, 2ieme Journée Scientifique du G4F, Nantes, France, **2016**

[76] Gaona, X., Redox chemistry of Pu, Np and U under alkaline to hyperalkaline pH conditions, Plutonium Futures The Science, Baden-Baden, Germany, **2016**

[77] Geist, A., Plutonium and americium solvent extraction processes: recent development in Europe, Plutonium Futures – The Science, Baden-Baden, Germany, **2016**

[78] Martin, P.; Strach, M.; Prieur, D.; Bès, R.; Belin, R. C.; Manara, D.; Valot, C.; Vitova, T.; Prussmann, T.; Dardenne, K.; Rothe, J., Study of the 5f electronic states in uranium-plutonium mixed oxides using high resolution XANES, Plutonium Futures — The Science 2016, Baden-Baden, Germany, **2016**

[79] Metz, V., Radionuklid-Freisetzung gegenüber Rückhaltevermögen von Radionukliden in den Asse II Einlagerungskammern. , Seminar „Rückholung der Nuklearabfälle aus dem früheren Forschungsbergwerk Asse II bei Wolfenbüttel", KIT, Institut für Technikfolgenabschätzung und Systemanalyse, Karlsruhe, Germany, **2016**

[80] Panak, P., Speciation of actinides by time-resolved laser fluorescence spectroscopy, Ninth International Conference on Nuclear and Radiochemistry – NRC9, Helsinki, Finland, **2016**

[81] Quinto, F.; Lagos, M.; Plaschke, M.; Schäfer, T.; Steier, P.; Geckeis, H., Multi-Actinides analysis with AMS: a novel method for ultra-trace determination and small sample sizes, Plutonium Futures - The Science 2016, Baden-Baden, 18.- 22. September 2016, **2016**

[82] Quinto, F.; Lagos, M.; Plaschke, M.; Schäfer, T.; Steier, P.; Golser, R.; Geckeis, H., Multi-actinide analysis with AMS for ultra-trace determination and small sample sizes: advantages and drawbacks, Deutsche Physikalische Gesellschaft (DPG)-Frühjahrstagung, Hannover, Germany, **2016**

[83] Schill, E., EGS Soultz-sous-Forêts. Workshop on Reservoir Stimulation: Recent Field Practices, Monitoring Techniques and Theoretical/Laboratory Investigations, Geothermal Research Council, 40th Annual Meeting, Sacramento, USA, **2016**

[84] Steier, P.; Wallner, A.; Faestermann, T.; Feige, J.; Feldstein, C.; Knie, K.; Korschinek, G.; Kutschera, W.; Ofan, A.; Paul, M.; Quinto, F.; Rugel, G., From the stars through the ocean abyss: the long travel of super-nova Pu-244 into VERA's particle detector, Plutonium Futures - The Science 2016, Baden-Baden, 18.- 22. September 2016, **2016**

[85] Trumm, M., Molecular Dynamics applications, ThUL School in Actinide Chemistry Dresden-Rossendorf, Germany, **2016**

[86] Vitova, T., Structural investigations of actinides with high energy resolution X-ray absorption spectroscopy, Helmholtz-Zentrum Dresden-Rossendorf, Institute for Resource Ecology, 15.06.2016, **2016**

[87] Vitova, T., Structural properties of actinide materials revealed by high energy resolution X-ray absorption spectroscopy, 4th annual Carnival conference session, Universität Köln, Cologne, Germany, **2016**

[88] Vitova, T., Structural properties of plutonium systems revealed by high resolution XANES and RIXS techniques, Plutonium Futures — The Science 2016, Baden-Baden, Germany, **2016**

Proceedings

[89] Dardenne, K.; González-Robles, E.; Herm, M.; Kienzler, B.; Christill, G.; Müller, N.; Metz, V.; Rothe, J., XAFS and μ-XRF investigations of highly radioactive nuclear waste samples: spent nuclear fuel and zircaloy cladding segments, Plutonium Futures - the Science, Baden-Baden, Germany, **2016**

[90] González-Robles, E.; Herm, M.; Lagos, M.; Bohnert, E.; Müller, N.; Kienzler, B.; Metz, V., Matrix dissolution of spent nuclear fuel under H_2 overpressure in bicarbonate water, Materials Research Society, MRS Symposium: Scientific Basis for Nuclear Waste Management, Boston, USA, **2016**

[91] Herm, M.; González-Robles, E.; Böttle, M.; Müller, N.; Bohnert, E.; Dagan, R.; Papioannou, D.; Kienzler, B.; Metz, V.; Geckeis, H., C-14 and other activation/fission products present in irradiated Zircaloy-4 cladding and stainless steel: inventory and chemical form of C-14 after release, Materials Research Society, MRS Symposium: Scientific Basis for Nuclear Waste Management, Boston, USA, **2016**

[92] Kienzler, B.; Metz, V.; Valls, A., Proceedings of 7th EC FP – FIRST-Nuclides Final Workshop, KIT Scientific Reports **2016**, 7716, 276.

[93] Montoya, V.; ait Mouheb, N.; Schäfer, T.; Metz, V., Conceptual reactive transport model of low pH cement / clay interface processes, Proceedings of 1st Annual Workshop of CEBAMA project, Barcelona, Spain, **2016**

[94] Montoya, V.; Ait Mouheb, N.; Schäfer, T.; Metz, V., Modelling of radionuclides migration in the low pH cement/clay Interface, Subsurface Environmental Simulation Benchmarking Workshop V, A Coruna, E, October 13-15, 2016. Ed.: J. Samper, **2016**

Oral and poster presentations

[95] Abdelfettah, Y.; Sailhac, P.; Schill, E.; Larnier, H., Continuous magneto-telluric monitoring at Rittershoffen geothermal site, northern Alsace, 76. Jahrestagung der Deutschen Geophysikalischen Gesellschaft, Münster, Germany, **2016**

[96] Abdelfettah, Y.; Saillhac, P.; Schill, E.; Larnier, H.; Matthey, P.-D., Continuous MT monitoring for small fluid injection volume at Rittershoffen Geothermal Project, northern Alsace – France, 23rd Electromagnetic Induction Workshop, Chaing Mai, Thailand, **2016**

[97] Abdelfettah, Y.; Saillhac, P.; Schill, E.; Larnier, H.; Matthey, P.-D., Continuous and time-lapse geothermal monitoring at Rittershoffen EGS project, northern Alsace, using magnetotellurics, European Geothermal Congress, EGC, Strasbourg, France, **2016**

[98] Adam, C.; Kaden, P.; Beele, B. B.; Geist, A.; Müllich, U.; Panak, P. J., Evaluation of covalence in An(III) and Ln(III) complexes by NMR spectroscopy, ATALANTE 2016 (Nuclear Chemistry for Sustainable Fuel Cycles), Montpellier, France, **2016**

[99] Adam, C.; Rohde, V.; Müllich, U.; Kaden, P.; Geist, A.; Panak, P. J., Comparative NMR Study of nPrBTP and iPrBTP Complexes, ATALANTE 2016, Nuclear Chemistry for Sustainable Fuel Cycles, Montpellier, France, **2016**

[100] Adam, N.; Hinz, K.; Rieder, F.; Gaona, X.; Rabung, T.; Panak, P.; Altmaier, M.; Geckeis, H., Löslichkeit und Sorption von Actiniden bei Anwesenheit von relevanten Zementadditiven und ausgewählten organischem Modellsubstanzen, 3. Workshop des Verbundprojekts „Geochemische Radionuklidrückhaltung an Zementalterationsphasen (GRaZ)“ Heidelberg, Germany, **2016**

[101] Altmaier, M., Pitzer Database activity within NEA Salt Club: update on work on actinide-borate-interactions, NEA Salt Club meeting, Paris, France, **2016**

[102] Altmaier, M., Arbeiten am INE zur Actinid-Organik-Wechselwirkung 23. Koordinierungsgespräch KIT/INE – PSI/LES, Villigen, Switzerland, **2016**

[103] Altmaier, M.; Brandt, F.; Brendler, V.; Chiorescu, I.; Colase, E.; Curtius, H.; Endrizzi, F.; Franzen, C.; Gaona, X.; Grive, M.; Hagemann, S.; Koke, C.; Kulik, D. A.; Krüger, S.; Lee, J.-Y.; Maiwald, M.; Miron, G. D.; Panak, P. J.; Skerencak-Frech, A.; Steudtner, R.; Thoenen, T.; Tsushima, S., ThermAc, a collaborative project investigating aquatic chemistry and thermodynamics of actinides at elevated temperature conditions, Plutonium Futures – The Science 2016, Baden-Baden, Germany, **2016**

[104] Altmaier, M.; Brandt, F.; Brendler, V.; Chiorescu, I.; Colase, E.; Curtius, H.; Endrizzi, F.; Franzen, C.; Gaona, X.; Grive, M.; Hagemann, S.; Koke, C.; Kulik, D. A.; Krüger, S.; Lee, J.-Y.; Maiwald, M.; Miron, G. D.; Panak, P. J.; Skerencak-Frech, A.; Steudtner, R.; Thoenen, T.; Tsushima, S., ThermAc: a collaborative project on aquatic chemistry and thermodynamics of actinides at elevated temperature conditions, ISSP17 Conference, Geneva, Switzerland, **2016**

[105] Altmaier, M.; Costa, D.; Felmy, A.; Moog, H.; Pabalan, R.; Ragoussi, M.; Reed, D. T.; Runde, W.; Thakur, P.; Voigt, W., A state-of-the-art report within NEA-TDB to assess modeling and experimental approaches in aqueous high ionic-strength solutions relevant for nuclear waste disposal applications, ISSP17 conference, Geneva, Switzerland, **2016**

[106] Altmaier, M.; Costa, D.; Felmy, A.; Moog, H.; Pabalan, R.; Ragoussi, M.; Reed, D. T.; Runde, W.; Thakur, P.; Voigt, W., A state-of-the-art report within NEA-TDB to assess modeling and experimental approaches in aqueous high ionic-strength solutions, Plutonium Futures – The Science 2016, Baden-Baden, Germany, **2016**

[107] Altmaier, M.; Duro, L.; Montoya, V.; Valls, A.; Holt, E.; Claret, F.; Mäder, U.; Grambow, B.; Idiart, A., Overview on the Horizon2020 CEBAMA Project, 4th International Workshop on Mechanisms and Modelling of Waste / Cement Interactions, Murten, Switzerland, **2016**

[108] Altmaier, M.; Duro, L.; Montoya, V.; Valls, A.; Holt, E.; Claret, F.; Mäder, U.; Grambow, B.; Idiart, A., CEBAMA – a EC Horizon 2020 funded collaborative research project on cement-based-materials, 2nd Conference on Key Topics in Deep Geological Disposal, Cologne, Germany, **2016**

[109] Altmaier, M.; Gaona, X.; Fellhauer, D.; Yalcintas, E.; Metz, V., Thermodynamics in highly saline solutions, aquatic chemistry & activities in the OECD-NEA frame, Workshop „Geothermische Fluide in salinaren Systemen“ Karlsruhe, Germany, **2016**

[110] Altmaier, M.; Montoya, V.; Gaona, X., Thermodynamic key issues, CFM Partner Meeting, Karlsruhe, Germany, **2016**

[111] Altmaier, M.; Reed, D., Thermodynamic treatment of Actinide-borate interactions within the Pitzer approach (JIPD), NEA Salt Club Meeting, Arlington, Virginia, USA, **2016**

[112] Altmaier, M.; Schäfer, T.; Rothe, J.; Schimmelpfennig, B.; Geckeis, H., Lessons learnt from the EC ACTINET and TALISMAN projects performed at KIT-INE, 2nd Conference on Key Topics in Deep Geological Disposal, Cologne, Germany, **2016**

[113] Altmaier, M.; Yalcintas, E.; Felhhauer, D.; Gaona, X., Solubility and speciation of Uranium(VI) in dilute to concentrated sodium-chloride and magnesium-chloride solutions at 22°C, Workshop „Geothermische Fluide in salinaren Systemen“ Karlsruhe, Germany, **2016**

[114] Baumann, A.; Yalcintas, E.; Gaona, X.; Polly, R.; Altmaier, M.; Geckeis, H., Chemistry of technetium under repository-relevant conditions: solubility and carbonate complexation of Tc(IV), 9th International Conference On Nuclear And Radiochemistry – NRC9, Helsinki, Finland, **2016**

[115] Becker, F.; Pang, B.; Sauri Suarez, H.; Metz, V.; Geckeis, H., Entwicklung von Verfahren für individuelle Dosimetrie für Beschäftigte in Entsorgungsanlagen, Entria Transversalprojekt 4, Delemont, CH, 08.04.2016, **2016**

[116] Bès, R.; Kvashnina, K.; Martin, P.; Rothe, J.; Scheinost, A. C.; Solari, P. L.; Vitova, T., Actinide's valence states determination: benefits of HERFD-XAS in radioactive material dedicated beamlines, Ninth International Conference on Nuclear and Radiochemistry - NRC95, Helsinki, Finland, **2016**

[117] Borkel, C.; Schlieker, M.; Kienzler, B.; Metz, V., Degradation of real scale cemented simulated waste forms over 35 years in salt solutions, 4th International Workshop on Mechanisms and Modelling of Waste/Cement Interactions (CEMENT 2016), Murten, CH, May 22-25, 2016, **2016**

[118] Bouby, M.; Heck, S.; Geyer, F.; Hilpp, S.; Schäfer, T., Bentonite erosion experiments under dynamic conditions, BELBAR Project Final Workshop, Berlin, Germany, **2016**

[119] Bouby, M.; Heyrich, Y.; Heck, S.; Hilpp, S.; Schäfer, T., Influence of organic matter (fulvic acids, FA) on the (long term) stability of clay colloids prepared under different chemical conditions, BELBAR Project Final Workshop, Berlin, Germany, **2016**

[120] Bourg, S.; Geist, A.; Soucek, P.; Rhodes, C., SACSESS: three years of optimisation of safe actinide separation processes, Actinide and Fission Product Partitioning and Transmutation: 4th Information Exchange Meeting, San Diego, USA, **2016**

[121] Chevreux, P.; Tissandier, L.; Bahl, S.; Laplace, A.; Deloule, E., Uranium solubility in a molten reductive glas, NuMat2016: The Nuclear Materials Conference, Le Corum, Montpellier, France, **2016**

[122] Dardenne, K.; González-Robles, E.; Herm, M.; Kienzler, B.; Christill, G.; Müller, N.; Metz, V.; Rothe, J., XAFS and µ-XRF investigations of highly radioactive nuclear waste samples: spent nuclear fuel and zircaloy cladding segments, Plutonium Futures - The Science, Baden-Baden, Germany, **2016**

[123] Dardenne, K.; González-Robles, E.; Herm, M.; Kienzler, B.; Metz, V.; Müller, N.; Rothe, J., XAFS and µ-XRF investigation of highly radioactive nuclear waste samples at KIT/ANKA, 3rd International Workshop on Advanced Techniques in Actinide Spectroscopy (ATAS), Pacific Northwest National Laboratory, Richland, Washington, USA, **2016**

[124] Dardenne, K.; Rothe, J.; Pruessmann, T.; Vespa, M.; Vitova, T.; Geckeis, H., Radionuclide science at the KIT synchrotron facility ANKA – the INE-Beamline and the new ACT experimental station, Frontiers in Environmental Radioactivity, STFC Env-Rad-Net and RSC Radiochemistry Group, London, UK, **2016**

[125] Edwards, A. C.; Whitehead, R.; Sharrad, C.; Geist, A.; Harwood, L., Evaluating the extraction properties of electronically modified $CyMe_4$-BTPhen analogues, ATALANTE 2016 (Nuclear Chemistry for Sustainable Fuel Cycles), Montpellier, France, **2016**

[126] Endrizzi, F.; Gaona, X.; Marques Fernandes, M.; Baeyens, B.; Altmaier, M., Uranium(VI) Solubility and Hydrolysis in NaCl Solutions at Elevated Temperatures, Ninth international Conference on nuclear and Radiochemistry (NRC9), Helsinki, Finland, **2016**

[127] Fellhauer, D.; Gaona, X.; Dardenne, K.; Altmaier, M., Solubility and speciation of neptunium(V) in alkaline, dilute to concentrated NaCl, $MgCl_2$ and $CaCl_2$ solutions, 17th International Symposium on Solubility Phenomena and Related Equilibrium Processes (ISSP17), Geneva, Switzerland, **2016**

[128] Fellhauer, D.; Gaona, X.; Petrov, V.; Dardenne, K.; Altmaier, M., Solubility, hydrolysis and chloride complexation of Np(V) in alkaline, dilute to concentrated NaCl, $MgCl_2$ and $CaCl_2$ solutions, Plutonium Futures – The Science 2016, Baden-Baden, Germany, **2016**

[129] Fellhauer, D.; Montoya, V.; Gaona, X.; Schepperle, J.; Metz, V.; Altmaier, M.; Geckeis, H., Estimation of radionuclide source terms for generic nuclear waste disposal options within the ENTRIA project, 2nd Conference on Key Topics in Deep Geological Disposal - Challenges of a Site Selection Process: Society – Procedures – Safety, Cologne, Germany, **2016**

[130] Fellhauer, D.; Montoya, V.; Schepperle, J.; Metz, V.; Altmaier, M.; Geckeis, H., Radionuclide source term estimations for generic nuclear waste disposal options within the ENTRIA project, 17th International Symposium on Solubility Phenomena and Related Equilibrium Processes (ISSP17), Geneva, Switzerland, **2016**

[131] Galan, H.; Nunez, A.; Munzel, D.; Müllich, U.; Leoncini, A.; Verboom, W.; Cobos, J.; Geist, A., Development of partitioning processes for minor actinides to be applied at long term: Influence of gamma radiation on extraction systems based on diglycolamides and water soluble SO_3-Ph-BTP, ATALANTE 2016 (Nuclear Chemistry for Sustainable Fuel Cycles), Montpellier, France, **2016**

[132] Gaona, X.; Böttle, M.; Rabung, T.; Altmaier, M., Contribution of KIT-INE to WP2 (1st year): Solubility, hydrolysis and sorption of beryllium in cementitious systems, Cebama 1st Annual Workshop, Barcelona, Spain, **2016**

[133] Gaona, X.; Böttle, M.; Rabung, T.; Altmaier, M., Solubility, hydrolysis and sorption of beryllium in cementitious systems, 4th International Workshop on "Mechanisms and Modelling of Waste/Cement Interactions", Murten, Switzerland, **2016**

[134] Gaona, X.; Endrizzi, F.; Marques Fernandes, M.; Baeyens, B.; Lee, J.-Y.; Fellhauer, D.; Altmaier, M., Solution chemistry of radionuclides at elevated temperatures: the uranium case, Workshop „Geothermische Fluide in salinaren Systemen", Karlsruhe, Germany, **2016**

[135] Geist, A., An alternative approach to TALSPEAK chemistry using SO_3-Ph-BTP, 251st American Chemical Society National Meeting, San Diego, USA, **2016**

[136] Geist, A., An alternative approach to TALSPEAK chemistry using SO_3-Ph-BTP, 40th Annual Actinide Separations Conference, San Diego, USA, **2016**

[137] Geist, A.; Modolo, G.; Müllich, U.; Munzel, D.; Taylor, R.; Whittaker, D.; Wilden, A.; Woodhead, D., Equilibria involved in the extraction of An(III), Ln(III) and HNO_3 by a TODGA solvent, 40th Annual Actinide Separations Conference, San Diego, USA, **2016**

[138] Geist, A.; Taylor, R.; Ekberg, C.; Guilbaud, P.; Modolo, G.; Bourg, S., The SACSESS hydrometallurgy domain - an overview, ATALANTE 2016 (Nuclear Chemistry for Sustainable Fuel Cycles), Montpellier, France, **2016**

[139] Genter, A.; Baujard, C.; Cuenot, N.; Dezayes, C.; Kohl, T.; Masson, F.; Sanjuan, B.; Scheiber, J.; Schill, E.; Schmidtbuhl, J.; Vidal, J., Geology, Geophysics and Geochemistry in the Upper Rhine Graben: the frame for geothermal energy use, European Geothermal Congress, EGC, Strasbourg, France, **2016**

[140] Ginjaume, M.; Clairand, I.; Carinou, E.; Ciraj Bjelac, O.; Ferrari, P.; Sans-Merce, M.; Farah, J.; Becker, F.; Chumak, V.; Daures, J.; Domienik, J.; Jovanovic, Z.; Kopec, R.; Krstic, D.; Szumska, A.; Nikodemova, D.; Teles, P.; Principi, S.; Vanhavere, F.; Knezevic, Z.; Eurados, Overview of the activities on eye lens dosimetry within EURADOS WG 12 (Dosimetry in medical imaging), 14th Congress of the International Radiation Protection Association (IRPA), Cape Town, ZA, May 9-13, 2016, **2016**

[141] Gonzalez-Robles, E.; Herm, M.; Montoya, V.; Lagos, M.; Bohnert, E.; Müller, N.; Kienzler, B.; Metz, V., Study of the release of the fission gases (Xe and Kr) and the fision products (Cs and I) under anoxic conditions in bicarbonate water, Materials Research Society (MRS), Scientific Basis for Nuclear Waste Management XL, Boston, MA, November 28 - December 1, 2016, **2016**

[142] González-Robles, E.; Metz, V.; Wegen, D. H.; Herm, M.; Papaioannou, D.; Bohnert, E.; Gretter, R.; Müller, N.; Nasyrow, R.; de Weerd, W.; Wiss, T.; Kienzler, B., Determination of fission gas release of spent nuclear fuel in puncturing test and in leaching experiments under anoxic conditions, 28th Spent Fuel Workshop (SFW 16), Stockholm, S, May 3-4, 2016, **2016**

[143] Gonzalez-Siso, M. R.; Gaona, X.; Duro, L.; Altmaier, M.; Bruno, J., Hydrolysis and Solubility of Ni(II) under alkaline to hyperalkaline conditions and complex formation with ISA 17th International Symposium on Solubility Phenomena and Related Equilibrium Processes (ISSP-17), Geneva, Switzerland, **2016**

[144] Gonzalez-Siso, M. R.; Gaona, X.; Duro, L.; Schild, D.; Fellhauer, D.; Pidchenko, I.; Vitova, T.; Altmaier, M.; Bruno, J., Study of the interaction of Pu, U and Tc with iron corrosion products under highly alkaline conditions, 17th International Symposium on Solubility Phenomena and Related Equilibrium Processes (ISSP-17), Geneva, Switzerland, **2016**

[145] Grenthe, I.; Gaona, X.; Plyasunov, A.; Rao, L.; Runde, W.; Felmy, A.; Grambow, B.; Konings, R.; Smith, A. L.; Moore, E.; Spahiu, K.; Costa, D.; Ragoussi, M.-E., The OECD/NEA Update Book on the Chemical Thermodynamics of U, Np, Pu, Am and Tc, Plutonium Futures The Science, Baden-Baden, Germany, **2016**

[146] Gyekye, P. K.; Becker, F.; Emi-Reynolds, G., Investigations into Radiation Dose Distribution in a Computed Tomography Fluoroscopy Room: Monte Carlo Studies, 14th Congress of the International Radiation Protection Association (IRPA), Cape Town, ZA, May 9-13, 2016, **2016**

[147] Held, S.; Schill, E.; Pavez, M.; Diaz, D.; Morata, D., Effects of major fault zones on geothermal reservoirs – a case study at Villarrica Volcano, southern Chile, European Geothermal Congress, EGC Strasbourg, France, **2016**

[148] Herdzik-Koniecko, I.; Wagner, C.; Geist, A.; Panak, P. J.; Narbutt, J., On the formation of heteroleptic complexes in an innovative-SANEX system, Sustainable Nuclear Energy Conference, Nottingham, UK, **2016**

[149] Herdzik-Koniecko, I.; Wagner, C.; Geist, A.; Panak, P. J.; Rejnis, M.; Steczek, L.; Lyczko, M.; Narbutt, J., Use of TRLFS and ESI-MS methods for search and characterization of Cm(III) and Eu(III) complexes with SO_3-Ph-BTP and TODGA ligands in solvent extraction systems, ATALANTE 2016 (Nuclear Chemistry for Sustainable Fuel Cycles), Montpellier, France, **2016**

[150] Herm, M.; Gaona, X.; Fellhauer, D.; Metz, V.; Altmaier, M.; Geckeis, H., Formation, stability and solubility of ternary Nd(III)–OH–Cl(s) phases in dilute to concentrated Na–Mg–Ca–Cl solutions, ISSP17 conference, Geneva, Switzerland, **2016**

[151] Herm, M.; Gonzalez-Robles, E.; Böttle, M.; Müller, N.; Bohnert, E.; Dagan, R.; Papioannou, D.; Kienzler, B.; Metz, V.; Geckeis, H., Determination of 14C and other activation/fission products inventories in irradiated Zircaloy-4 cladding and a stainless steel plenum spring as well as the chemical form of ^{14}C after release from the studied materials, 28th Spent Fuel Workshop 2016, Stockholm, Sweden, **2016**

[152] Huber, F. M.; Totskiy, Y.; Montoya, V.; Enzmann, F.; Trumm, M.; Wenka, A.; Geckeis, H.; Schäfer, T., Modelling of Tc migration in an un-oxidized fractured drill core from Äspö, Sweden, 25. Tagung der Fachsektion Hydrogeologie in der DGGV 2016, Karlsruhe, Germany, **2016**

[153] Jovanovic, Z.; Dragana Krsric, D.; Ferrari, P.; Carinou, E.; Vadim Chumak, V.; Farah, J.; Principi, S.; Morgun, A.; Becker, F.; Teles, P., The study of the radiation scatter in interventional cardiology through Monte Carlo simulations: The EURADOS working group No.12, RAD Conference 2016, Nis, SRB, May 23-27, 2016, **2016**

[154] Lee, J.-Y.; Vespa, M.; Yalcintas, E.; Gaona, X.; Dardenne, K.; Rothe, J.; Rabung, T.; Altmaier, M.; Yun, J.-I., Complexation Behavior and Solubility of the Ternary Systems Ca/Mg-UO_2-CO_3 under Weakly Alkaline Conditions, Plutonium Futures – The Science 2016, Baden-Baden, Germany, **2016**

[155] Marie, C.; Vanel, V.; Duchesne, M. T.; Russello, E.; Kaufholz, P.; Wilden, A.; Modolo, G.; Carrott, M.; Taylor, R.; Geist, A.; Miguirditchian, M., Development of a selective americium separation process using TPAEN as a water-soluble stripping agent, ATALANTE 2016 (Nuclear Chemistry for Sustainable Fuel Cycles), Montpellier, France, **2016**

[156] Martin, P. M.; Prieur, D.; Bès, R.; Belin, R.; Strach, M.; Manara, D.; Valot, C.; Vitova, T.; Prüßmann, T.; Dardenne, K., Study of the 5f electronic states in uranium-plutonium mixed oxides using high resolution XANES, NuMat2016: The Nuclear Materials Conference, Le Corum, Montpellier, France, **2016**

[157] McLachlan, F.; Taylor, R.; Whittaker, D.; Geist, A., Modelling of innovative SANEX process maloperations, ATALANTE 2016 (Nuclear Chemistry for Sustainable Fuel Cycles), Montpellier, France, **2016**

[158] Metz, V., Zircaloy cladding properties under conditions of prolonged dry interim storage, 2nd Conference on Key Topics in Deep Geological Disposal - Challenges of a Site Selection Process: Society – Procedures – Safety, Cologne, Germany **2016**

[159] Montoya, V., Nuclear waste disposal in Germany – present situation and a 2050 perspective, 5. Jahrestagung des KIT-Zentrums Energie, Karlsruhe, Germany,

[160] Montoya, V.; Ait Mouheb, N.; Schäfer, T.; Metz, V., Modelling of radionuclides migration in the low pH cement/clay Interface, Subsurface Environmental Simulation Benchmarking Workshop V, A Coruna, E, October 13-15, 2016, **2016**

[161] Montoya, V.; Fellhauer, D.; Metz, V.; Geckeis, H., Reactive transport model in the near field of different generic spent nucelar fuel repository options: effect of the radionuclide source term, 2nd Conference on Key Topics in Deep Geological Disposal - Challenges of a Site Selection Process: Society – Procedures – Safety, Cologne, Germany, **2016**

[162] Norrfors, K. K.; Bouby, M.; Marsac, R.; Wold, S.; Finck, N.; Lützenkirchen, J.; Schäfer, T., Montmorillonite colloid Size heterogeneity effects on: I. Stability, II. Radionuclides sorption, III. Sorption reversibility, BELBAR Project Final Workshop, Berlin, Germany, **2016**

[163] Panak, P. J.; Altmaier, M.; Brandt, F.; Brendler, V.; Chiorescu, I.; Colas, E.; Curtius, H.; Endrizzi, F.; Franzen, C.; Gaona, X.; Grive, M.; Hagemann, S.; Koke, C.; Kulik, D. A.; Krüger, S.; Lee, J.-Y.; Maiwald, M.; Skerencak-Frech, A.; Steudtner, R.; Thoenen, T.; Tsushima, S., THERMAC – a joint project on aquatic actinide chemistry and thermodynamics at elevated temperature conditions, Ninth International Conference on Nuclear and Radiochemistry – NRC9, Helsinki, Finland **2016**

[164] Pang, B.; Saurí Suaréz, H.; Becker, F.; Metz, V.; Geckeis, H., Modelling of individual dosimetry in facilities for heat-generating waste: Spent nuclear fuel emplacement in a rock salt repository, 2nd Conference on Key Topics in Deep Geological Disposal - Challenges of a Site Selection Process: Society – Procedures – Safety, Cologne, Germany, **2016**

[165] Pidchenko, I.; Kvashnina, K. O.; Yokosawa, T.; Finck, N.; Schild, D.; Göttlicher, J.; Schäfer, T.; Rothe, J.; Geckeis, H.; Vitova, T., Speciation of U interacted with magnetite by high-energy resolution X-ray absorption spectroscopy, Ninth International Conference on Nuclear and Radiochemistry - NRC95, Helsinki, Finland, **2016**

[166] Polly, R.; Schimmelpfennig, B.; Pidchenko, I.; Geckeis, H.; Vitova, T., Quantum chemical investigation of incorporation of Uranium(V) into Magnetite: combining multi reference ab initio methods and density functional theory, 3rd International Workshop on Advanced Techniques in Actinide Spectroscopy. , EMSL Richland, Washington, USA,, **2016**

[167] Quinto, F.; Geyer, F.; Huber, F.; Lagos, M.; Plaschke, M.; Schäfer, T.; Steier, P.; Geckeis, H., Geochemistry and actinide monitoring in the geological formation: the Grimsel Test Site case, Helmholtz--Koordinierungstreffen 2016, Kalrsruhe, 12.-13. September 2016, **2016**

[168] Quinto, F.; Lagos, M.; Plaschke, M.; Schäfer, T.; Steier, P.; Geckeis, H., Multi-Actinides analysis with AMS: a novel method for ultra-trace determination and small sample sizes, 23. Koordinierungsgespräch KIT/INE - PSI/LES, Villigen, CH, July 13-14, 2016, **2016**

[169] Quinto, F.; Lagos, M.; Plaschke, M.; Schäfer, T.; Steier, P.; Geckeis, H., Simultaneous analysis of U, Np, Pu, Am and Cm isotopes at ultra-trace levels in groundwater samples with AMS and a comparison with SF-ICP-MS, 1st International Conference on Radioanalytical and Nuclear Chemistry (RANC-2016), Budapest, HU, April 10-16, 2016., **2016**

[170] Quinto, F.; Lagos, M.; Plaschke, M.; Schäfer, T.; Steier, P.; Geckeis, H.; Faestermann, T.; Gomez Guzman, J. M.; Hain, K.; Korschinek, G.; Ludwig, P., AMS measurements of actinides and technetium, CFM Partner Meeting, Karlsruhe, 29.-30. Juni 2016, **2016**

[171] Real, f.; Vallet, V.; Janicki, R.; Lindqvist-Reis, P., Unraveling the structure and the excited state dynamics of the aqueous cerium(III) ion by combined experimental and theoretical approaches, 46èmes Journées des Actinides (46th JdA), Alpes d'Huez, F, March 16-20, 2016, **2016**

[172] REED, D.; ALTMAIER, M., Chemistry/Thermodynamic database, 7th US/German Workshop on Salt Repository Research, Design, and Operation, Arlington, Virginia, USA, **2016**

[173] Renz, T.; Plaschke, M.; Quinto, F.; Lagos, M.; Bauer, A.; Taubald, H.; Geckeis, H., Development of an analytical procedure for the simultaneous determination of Np and Pu in clay samples, 1st International Conference on Radioanalytical and Nuclear Chemistry (RANC-2016), Budapest, HU, April 10-16, 2016., **2016**

[174] Saillhac, P.; Larnier, H.; Abdelfettah, Y.; Schill, E., Modelling the sensitivity of magnetotelluric monitoring data to geothermal fluids at depth in Northern Alsace, European Geothermal Congress, EGC, Strasbourg, France, **2016**

[175] Schepperle, J.; Fellhauer, D.; Gaona, X.; Altmaier, M.; Geckeis, H., Solubility, Hydrolysis and Carbonate Complexation of Pu(IV) and Np(IV) under Repository-Relevant Conditions, Plutonium Futures 2016, Baden-Baden, Germany, **2016**

[176] Stoll, M.; Darbha, G. K.; Huber, F.; Schill, E.; Schäfer, T., Particle retention on granite as a function of residence time and particle size using a synthetic fracture flow cell, 25. Tagung der Fachsektion Hydrogeologie in der DGGV 2016, Karlsruhe, Germany, **2016**

[177] Tasi, A. G.; Gaona, X.; Fellhauer, D.; Böttle, M.; Rothe, J.; Schild, D.; Graser, C.-H.; Grivé, M.; Bruno, J.; Källström, K.; Altmaier, M.; Geckeis, H., Solubility of Plutonium under alkaline to hyperalkaline reducing conditions: Redox chemistry and complexation with ISA, 4th International Workshop on "Mechanisms and Modelling of Waste/Cement Interactions, CEMENT, Murten, Switzerland, **2016**

[178] Taylor, R.; Carrott, M.; Galan, H.; Geist, A.; Hères, X.; Maher, C.; Mason, C.; Malmbeck, R.; Miguirditchian, M.; Modolo, G.; Rhodes, C.; Sarsfield, M.; Wilden, A., The EURO-GANEX process: current status of flowsheet development and process safety studies, ATALANTE 2016 (Nuclear Chemistry for Sustainable Fuel Cycles), Montpellier, France, **2016**

[179] Trumm, M.; Schimmelpfennig, B., Towards the origin of effective An(III)/Ln(III) separation by tridentate N-donor ligands: theoretical study on atomic charges and polarizabilities for Cm(III)/Gd(III) separation, Atalante Conference, Montpellier, France, **2016**

[180] Trumm, M.; Schimmelpfennig, B.; Panak, P. J.; Geist, A., Towards the origin of effective An(III)/Ln(III) separation by tridentate N-donor ligands: theoretical study on atomic charges and polarizabilities for Cm(III)/Gd(III) separation, Symposium für Theoretische Chemie, Bochum, Germany, **2016**

[181] Vanel, V.; Geist, A.; Wilden, A.; Modolo, G.; Marie, C.; Kaufholz, P.; Montuir, M.; Boubals, N.; Sorel, C., Modelling and flowsheet design of an Am separation process using TODGA and TPAEN, ATALANTE 2016 (Nuclear Chemistry for Sustainable Fuel Cycles), Montpellier, France, **2016**

[182] Wagner, C.; Mossini, E.; Macerata, E.; Mariani, M.; Iotti, N.; Arduini, A.; Casnati, A.; Geist, A.; Panak, P. J., Complexation of Cm(III) and Eu(III) with a novel i-SANEX/GANEX complexing agent, ATALANTE 2016 (Nuclear Chemistry for Sustainable Fuel Cycles), Montpellier, France, **2016**

[183] Yalcintas, E.; Baumann, A.; Gaona, X.; Altmaier, M.; Geckeis, H., New comprehensive thermodynamic model for the solubility of $TcO_2 \cdot xH_2O$(am) in the aqueous Tc^{4+}–Na^+–Mg^{2+}–Ca^{2+}–H^+–Cl^-–OH^- system, 17th International Symposium on Solubility Phenomena and Related Equilibrium Processes, Geneva, CH, July 24-29, 2016, **2016**

[184] Yalcintas, E.; Baumann, A.; Gaona, X.; Altmaier, M.; Geckeis, H., Tc(IV) solubility in repository-relevant systems, 4th International Workshop on Mechanisms and Modelling of Waste/Cement Interactions (CEMENT 2016), Murten, CH, May 22-25, 2016, **2016**

[185] Yalcintas, E.; Baumann, A.; Gaona, X.; Altmaier, M.; Geckeis, H., Thermodynamic model for the solubility of tetravalent $TcO_2 \cdot xH_2O$(am) in the aqueous Tc^{4+}–Na^+–Mg^{2+}–Ca^{2+}–H^+–Cl^-–OH^- system, 2nd Conference on Key Topics in Deep Geological Disposal, Cologne, September 26-28, 2016, **2016**

[186] Yalcintas, E.; Gaona, X.; Altmaier, M., Solubility of tetravalent UO_2(am,hyd) in alkaline carbonate solutions, 17th International Symposium on Solubility Phenomena and Related Equilibrium Processes, Geneva, CH, July 24-29, 2016, **2016**

Others

[187] Gaona, X.; Tasi, A.; Fellhauer, D.; Böttle, M.; Grivé, M.; Colàs, E.; Bruno, J.; Altmaier, M., Redox behavior, solubility and sorption of Pu(III/IV) in the absence and presence of ISA and cement; WP2. Binary system Pu-ISA, SKB-Pu-ISA, WP2. Final report, **2016**.

[188] Gaona, X.; Yalcintas, E.; Altmaier, M., Thermodynamic data selection for the system Tc(VII)–Na–K–Mg–Ca–OH–Cl–H_2O at 298.15 K, THEREDA Technical Paper, **2016**.

[189] Kienzler, B.; Borkel, C.; Metz, V.; Schlieker, M., Long-Term Interactions of Full-Scale Cemented Waste Simulates with Salt Brines, KIT Scientific Report Vol. 7721, **2016**.

190] Kienzler, B., 50 Jahre Forschungs- und Entwicklungsarbeiten zu Endlagerung im KIT, KIT Scientific Report Vol. 7723, **2016**.

[191] Metz, V., in In Smeddinck, U., Kuppler, S. und Chaudry, S. (eds.), „Inter- und Transdisziplinarität in der Entsorgungsforschung“, Interdisziplinäre Analysen von Entsorgungsoptionen für radioaktive Reststoffe – der Beitrag geochemisch-basierter Analysen, Springer Vieweg Verlag, Wiesbaden, **2016**, pp. 17-23

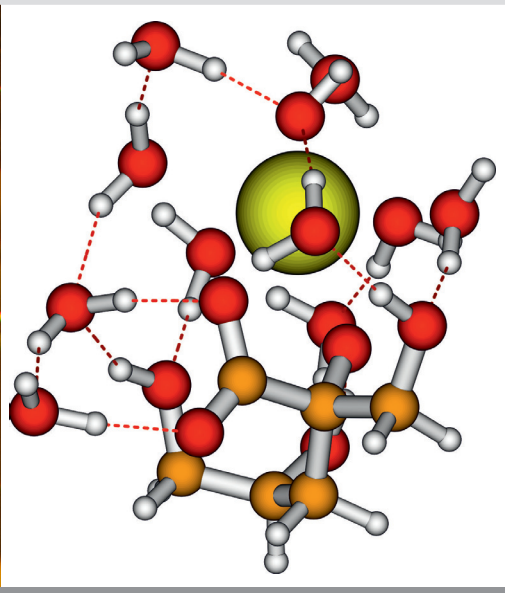

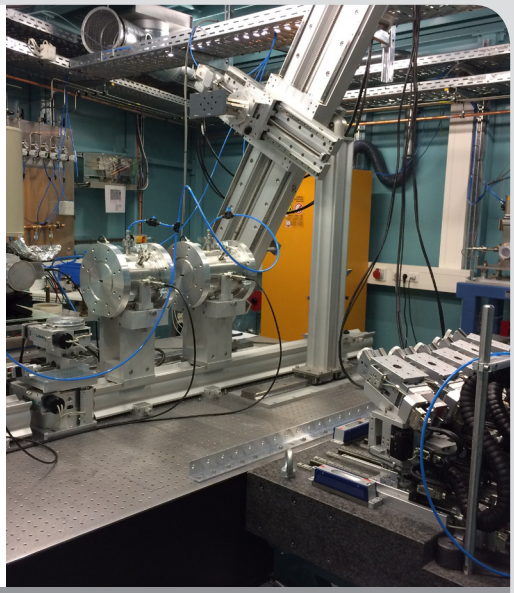

ISSN 1869-9669